BOEING

AD 734235

DDC
RECEIVED
DEC 29 1971
D

Reproduced by
NATIONAL TECHNICAL
INFORMATION SERVICE
Springfield, Va. 22151

249

Best
Available
Copy

Unclassified

Security Classification

DOCUMENT CONTROL DATA - R & D

(Security classification of title, body of abstract and indexing annotation must be entered when the overall report is classified)

1. ORIGINATING ACTIVITY (Corporate author)	2a. REPORT SECURITY CLASSIFICATION
Vertol Division The Boeing Company P. O. Box 16858, Philadelphia, PA 19142	Unclassified
	2b. GROUP N/A

3. REPORT TITLE

Four Prop Tilt Wing with Cyclic Pitch Propellers: Results of Full Span Wind Tunnel Test/Phase I

4. DESCRIPTIVE NOTES (Type of report and inclusive dates)

Contractor Test Report (May-July 1970)

5. AUTHOR(S) (First name, middle initial, last name)

Kolesar, Charles
Kassianides, G, and Andrews, J

6. REPORT DATE	7a. TOTAL NO. OF PAGES	7b. NO. OF REFS
Oct 1970	243	3

8a. CONTRACT OR GRANT NO.	9a. ORIGINATOR'S REPORT NUMBER(S)
F33615-70-C-1000 b. PROJECT NO. 698BT c. Task Area Number: 02 d. Work Unit Number: 005	Boeing Vertol Document D170-10038-1 9b. OTHER REPORT NO(S) (Any other numbers that may be assigned this report) AFFDL TR 71-91, Reference 3

10. DISTRIBUTION STATEMENT

Approved for public release; distribution unlimited.

11. SUPPLEMENTARY NOTES	12. SPONSORING MILITARY ACTIVITY
	Air Force Flight Dynamics Laboratory Wright-Patterson AFB, Ohio 45433

13. ABSTRACT

This report presents the results of wind tunnel test BVWT 061 (Phase I test of two phase test program) performed in the Boeing-Vertol V/STOL wind tunnel on a powered four prop tilt wing full span model equipped with cyclic pitch propellers for longitudinal control. Items evaluated include cyclic pitch control in hover (in and out of ground effect), yaw control in performance, plus basic longitudinal stability and control throughout transition with a high horizontal tail.

Propeller hub pitching moment and normal force were also measured during this test so that in conjunction with a previous isolated propeller test, the influence of the wing/flaps/fuselage on the propeller forces and moments could be determined. ( )

DD FORM 1 NOV 68 1473

I

Unclassified

Security Classification

14. KEY WORDS	LINK A		LINK B		LINK C	
	ROLE	WT	ROLE	WT	ROLE	WT
Cyclic Pitch Propellers						
Descent Capability						
Double Slotted Flaps						
Hover						
Longitudinal Stability/Control						
Propeller Hub Pitching Moment						
Propeller Normal Force						
Slats						
Tilt Wing Aircraft						

REV LTR

THE BOEING COMPANY

VERTOL DIVISION · PHILADELPHIA, PENNSYLVANIA

CODE IDENT. NO. 77272

NUMBER D170-10038-1

TITLE FOUR PROP TILT WING WITH CYCLIC PITCH PROPELLERS: RESULTS OF FULL SPAN WIND TUNNEL TEST/PHASE I

ORIGINAL RELEASE DATE Oct. 1970. FOR THE RELEASE DATE OF SUBSEQUENT REVISIONS, SEE THE REVISION SHEET. FOR LIMITATIONS IMPOSED ON THE DISTRIBUTION AND USE OF INFORMATION CONTAINED IN THIS DOCUMENT, SEE THE LIMITATIONS SHEET.

MODEL _____ CONTRACT F33615-70-C-1000

ISSUE NO. _____ ISSUED TO: _____

DDC
RECEIVED
DEC 29 1971
D

PREPARED BY George Kassianides. Chas E. Kolesar, Jr. Andrews DATE 10/27/70

APPROVED BY Charles E. Kolesar DATE 10/27/70
C.E. Kolesar

APPROVED BY D. Bevan DATE 10/27/70
D. Bevan, Unit Chief, V/STOL Aero

APPROVED BY K.B. Gillmore DATE 10/27/70
K.B. Gillmore, Mgr., V/STOL Technology

APPROVED BY G.P. Kapinski DATE 10/27/70
W.L. Kapinski, Program Manager

DISTRIBUTION STATEMENT A
Approved for public release;
Distribution Unlimited

LIMITATIONS

This document is controlled by V/STOL Aerodynamics, Org. 7481

All revisions to this document shall be approved by the above noted organization prior to release.

ACTIVE SHEET RECORD

SHEET NUMBER	REV LTR	ADDED SHEETS				SHEET NUMBER	REV LTR	ADDED SHEETS			
		SHEET NUMBER	REV LTR	SHEET NUMBER	REV LTR			SHEET NUMBER	REV LTR	SHEET NUMBER	REV LTR
i						39					
ii						40					
iii						41					
iv						42					
v						43					
vi						44					
1						45					
2						46					
3						47					
4						48					
5						49					
6	A					50					
7						51					
8						52					
9						53					
10						54					
11						55					
12						56					
13						57					
14						58					
15						59					
16						60					
17						61					
18						62					
19						63					
20						64					
21						65					
22						66					
23						67					
24						68					
25						69					
26						70					
27						71					
28						72					
29						73					
30						74					
31						75					
32						76					
33						77					
34						78					
35						79					
36						80					
37						81					
38						82					

ACTIVE SHEET RECORD

SHEET NUMBER	REV LTR	ADDED SHEETS				SHEET NUMBER	REV LTR	ADDED SHEETS			
		SHEET NUMBER	REV LTR	SHEET NUMBER	REV LTR			SHEET NUMBER	REV LTR	SHEET NUMBER	REV LTR
83						127					
84						128					
85						129					
86						130					
87						131					
88						132					
89						133					
90						134					
91						135					
92						136					
93						137					
94						138					
95						139					
96						140					
97						141					
98						142					
99						143					
100						144					
101						145					
102						146					
103						147					
104						148					
105						149					
106						150					
107						151					
108						152					
109						153					
110						154					
111						155					
112						156					
113						157					
114						158					
115						159					
116						160					
117						161					
118						162					
119						163					
120						164					
121						165					
122						166					
123						167					
124						168					
125						169					
126						170					

ACTIVE SHEET RECORD

SHEET NUMBER	REV LTR	ADDED SHEETS				SHEET NUMBER	REV LTR	ADDED SHEETS			
		SHEET NUMBER	REV LTR	SHEET NUMBER	REV LTR			SHEET NUMBER	REV LTR	SHEET NUMBER	REV LTR
171						215					
172						216					
173						217					
174						218					
175						219					
176						220					
177						221					
178						222					
179						223					
180						224					
181								225	A		
182								226	A		
183								227	A		
184								228	A		
185								229	A		
186								230	A		
187								231	A		
188								232	A		
189								233	A		
190								234	A		
191								235	A		
192								236	A		
193								237	A		
194											
195											
196											
197											
198											
199											
200											
201											
202											
203											
204											
205											
206											
207											
208											
209											
210											
211											
212											
213											
214											

REVISIONS			
LTR	DESCRIPTION	DATE	APPROVAL
A	Appendices A and B incorporated into report	11/30/70	CEM RLK

ABSTRACT

This report presents the results of wind tunnel test BVWT 061 (Phase I test of two phase test program) performed in the Boeing-Vertol V/STOL wind tunnel on a powered four prop tilt wing full span model equipped with cyclic pitch propellers for longitudinal control. Items evaluated include cyclic pitch control in hover (in and out of ground effect), yaw control in hover with differential flaps and spoilers, low speed descent performance, plus basic longitudinal stability and control throughout transition with a high horizontal tail.

Propeller hub pitching moment and normal force were also measured during this test so that in conjunction with a previous isolated propeller test, the influence of the wing/flaps/fuselage on the propeller forces and moments could be determined.

KEY WORDS

Cyclic Pitch Propellers

Descent Capability

Double Slotted Flaps

Hover

Longitudinal Stability/Control

Propeller Hub Pitching Moment

Propeller Normal Force

Slats

Tilt Wing Aircraft

NOMENCLATURE

The following nomenclature was used for Model VRO68Q in BVWT 061. Additional nomenclature is included in the Data Reduction section of this report.

Symbol		
A_p	Propeller disc area	$ft.^2$
α_F	Fuselage angle of attack relative to freestream	degrees
$\alpha_{W_{EFF}}$	Effective wing angle of attack	degrees
B_1	Fuselage	
b	Wing span	ft.
c	Mean aerodynamic wing chord	ft.
γ	Cyclic angle (positive ~ nose down pitching moment)	degrees
D	Propeller diameter	ft.
δ_F	Flap angle	degrees
F_1	Wing fence configuration	
f_1	Basic double slotted flaps	
$\theta_{.75}$	Propeller blade pitch angle at .75R	degrees
H_1	Horizontal tail	
h	Height of outboard propeller plane to ground plane in hover	inches
i_w	Wing incidence angle	degrees
J	Propeller advance ratio, $\frac{V}{nD}$	
L	Aircraft lift	lbs.
M	Aircraft pitching moment (positive ~ nose up)	ft.lbs.

N_1	Nacelle configuration	D170-10038-1
n	Propeller rotational speed	rps
P_1	Collective hubs	
P_2	Cyclic hubs	
Q	Shaft torque	ft-lbs
Q_1	Basic slat configuration	
q	Freestream dynamic pressure	lbs/ft^2
q_s	Slipstream dynamic pressure, $q+T/A_p$	lbs/ft^2
R	Propeller blade radius	ft.
r	Radial station along blade	ft.
ρ	Density	$slugs/ft^3$
S	Wing area	$ft.^2$
i_s	Horizontal stabilizer incidence relative to waterline	degrees
T	Propeller thrust	lbs.
T_j	Jet thrust from air motor	lbs.
V	Velocity	ft/sec.
V_F	Full scale aircraft velocity	knots
V_1	Vertical tail	
W_1	Wing	
X	Aircraft longitudinal force, positive forward	lbs.
x	Longitudinal distance	ft.
z	Vertical distance	ft.

Superscripts - (Superscripts are in sequence, left wing tip to fuselage centerline)

f^{60}	Flap at 60°
$p^{1,1}$	Both propellers turning down inboard
$p^{1,2}$	Both propellers turning down between nacelles
Q^{10}	Slat setting, see notes
Q^{*}	Slat setting, see notes.

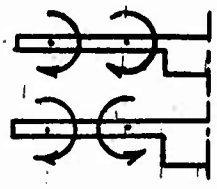

NOTES: 1) According to the notation used, slat setting $Q^{10,10,10,*}$ indicated that all slat segments inboard of the wing tip were set at Q^{10} position with the exception of the segment inboard of the inboard nacelle which was set at Q^{*} position.

TABLE OF CONTENTS

TABLE OF CONTENTS

1.0 INTRODUCTION

Wind tunnel test BVWT 061 was performed in the 20ft x 20ft test section of the Boeing-Vertol V/STOL wind tunnel on a full span (9.04ft) model of the Model 170 four propeller tilt wing aircraft that utilizes cyclic pitch propellers for low speed longitudinal control. Installation of the sting mounted model (VRO68Q) commenced on July 14 for the Phase I test of a two phase test program. This air motor powered model incorporated an internal six component strain gage fuselage balance and a six component strain gage balance mounted in each nacelle between the propeller/hub assembly and the air motor. Two separate sets of propeller hubs were used: collective hubs and cyclic pitch hubs. An identical 2.143 ft. diameter propeller/cyclic pitch hub/nacelle balance/air motor assembly was tested during May 1970 as a part of the contract (Reference 1).

The primary objectives of this Phase I test were:

a. Pitch Control in Hover
Determine the effectiveness of cyclic propeller pitch for longitudinal control in hover using two propeller rotation arrangements.

b. Yaw Control in Hover
Determine the effectiveness of double slotted flaps, opposite wing flap up travel, and spoilers for yaw control in hover, and establish the yaw control capability of a combined flap/spoiler configuration. Evaluate the effect on hover yaw control of the alternate inboard propeller rotation and of cyclic pitch.

c. Low Speed Descent Performance
Determine the basic power-off lift/drag characteristics with several flap deflections. Establish the rate of sink capability with selected flap angles, and the effect of cyclic pitch on descent performance.

d. Longitudinal Stability and Control in Transition
Establish the tail-off longitudinal characteristics with selected combinations of wing incidence, flap angle, and slipstream thrust coefficient. Determine the aircraft stability and trim capability with a high horizontal tail. Evaluate the effectiveness of cyclic pitch for trim and its effect on stability. Determine the influence of ground proximity in take-off and landing configurations on longitudinal characteristics.

During cyclic pitch running on August 21, 1970, the aft radial

Lamiflex bearings in the left inboard cyclic pitch hub assembly were damaged. Since the collective pitch runs planned for the Phase I test were largely complete, a decision was made to end Phase I and perform the remainder of the planned cyclic pitch runs during the Phase II test later in the year. This delay will enable the Lamiflex bearing design to be re-examined, modifications to the cyclic hubs to be incorporated as required, and testing to be resumed within the contract schedule.

Four prop Model VRO68Q utilizes a 9.23 aspect ratio tapered wing with a straight leading edge, propellers overlapped 7% in diameter, full span slats and full span large chord double slotted flaps that incorporate a movable fore flap which "nests" when the flap is retracted. Longitudinal and vertical location of the propeller hub centerlines with respect to the wing leading edge were chosen to maximize descent capability, using as a basis the data acquired in mid-1969 during a Boeing-Vertol wind tunnel test of a semispan four prop tilt wing model, the primary objective of which was to investigate the effect of propeller hub location on descent performance with overlapped propellers. The slat and double slotted flap configurations used on Model VRO68Q were also established from data acquired during the 1969 Boeing-Vertol four prop tilt wing wind tunnel test program, that included investigations of single vs double slotted flaps and full span slats vs Kruger leading edge flaps for the purpose of maximizing descent performance.

Two wing fences per wing, one at the fuselage side and the other, 18% of a propeller diameter outboard, were used to contain the stall occurring on the wing center section.

2.0 MODEL DESCRIPTION AND INSTALLATION

The general arrangement and geometry of full span Model VR068Q and wind tunnel installation details are presented in this section. Figure 1 is a photograph of this model as installed in the Boeing-Vertol V/STOL wind tunnel for the subject test.

2.1 WING GEOMETRY (See Figure 2)

The model utilizes a tapered wing with the following geometry:

Span	9.036 ft.
Root chord	1.263 ft.
Tip chord	0.696 ft.
Mean Aerodynamic Chord (MAC)	1.007 ft.
Taper ratio	0.551
Area	8.850 ft.^{2}
Aspect ratio	9.225
Wing 1/4c sweep	1.6° fwd.
Dihedral	0°
Wing pivot position	
X-Axis	42.56% MAC aft of wing L.E.
Z-Axis	11.67% MAC below w.c.p.
Basic Wing Sections	
Root	NACA 64_4221
Tip (actually 1.047 b/2)	NACA 64_2215
Inboard Nacelle Wing Chord/Prop Diameter	0.492
Outboard Nacelle Wing Chord/Prop Diameter	0.376
Slats (from wing tip to body centerline)	15% basic wing chord

Double Slotted Flaps	39% basic wing chord (when retracted) 23.5% chord Fowler action

Slats

The Model VRO68Q tapered wing incorporated a 15% chord full span leading edge slat of the design illustrated in Figure 3. Figures 4 and 5 show the slat positioned at tip and root sections, respectively. The slat, which extended spanwise across the fuselage to the body centerline (wing root), was attached to the basic wing leading edge with preset brackets,and were arranged in nine spanwise segments (wing tip to wing tip). One segment per wing extended from the wing tip to the outboard nacelle; the slat between the nacelles was divided into two equal span segments; one segment extended from the side of the inboard nacelle to the fuselage; and finally, one segment covered the entire width of the fuselage. This arrangement enabled the slats to be set differentially according to the direction of rotation of the propeller blades in front of each slat segment.

The slat angle, gap and trailing edge location used for this test were based on previous Boeing-Vertol tilt wing testing that was conducted for the purpose of maximizing descent capability. In general, the Q^{10} slat setting shown in Figures 3 and 4 was used behind a "down-going" propeller blade and the Q* setting was used behind an "up-going" propeller blade.

Flaps

The large chord double slotted flaps used in test BVWT 061 are shown in Figures 6 and 7, which present the arrangement of the flaps for the 40°, 50°, and 60° deflections. Figures 6 and 7 depict tip and root sections, respectively. Nacelle length precluded extending the flaps behind the nacelles, thus splitting the flaps into three spanwise segments: outboard, midspan, and inboard. The lengths of these segments were as follows:

Flap Segment	Length
Outboard	STA 54.215" (tip) to STA 45.789"
Midspan	STA 41.789" to STA 21.875"
Inboard	STA 17.875" to STA 7.145" (side of body)

The flaps were 39% chord in the retracted position. In this position, the fore flap "nests" against the main flap as shown in Figure 8. During the initial portion of the flap extension,

the "nested" fore flap/main flap assembly is moved aft 23.5% of the basic wing chord. This value represents the Fowler action. For the first 20° of flap deflection, the fore flap remains "nested" as shown in Figure 9. As the flap is deflected to a higher angle, the main flap moves away from the fore flap, resulting in an extended flap chord of 49% at the 40° flap angle. The geometric relationship between the fore flap and main flap was held constant between 40° and 60° flap angle (the maximum angle tested). Gaps and locations used for the double slotted flaps were determined from previous test data.

Yaw control in hover is provided by flap down-travel on one wing, plus spoiler and flap up-travel on the opposite wing. The arrangement of the flap in the up-travel position for hover is illustrated in Figure 9.

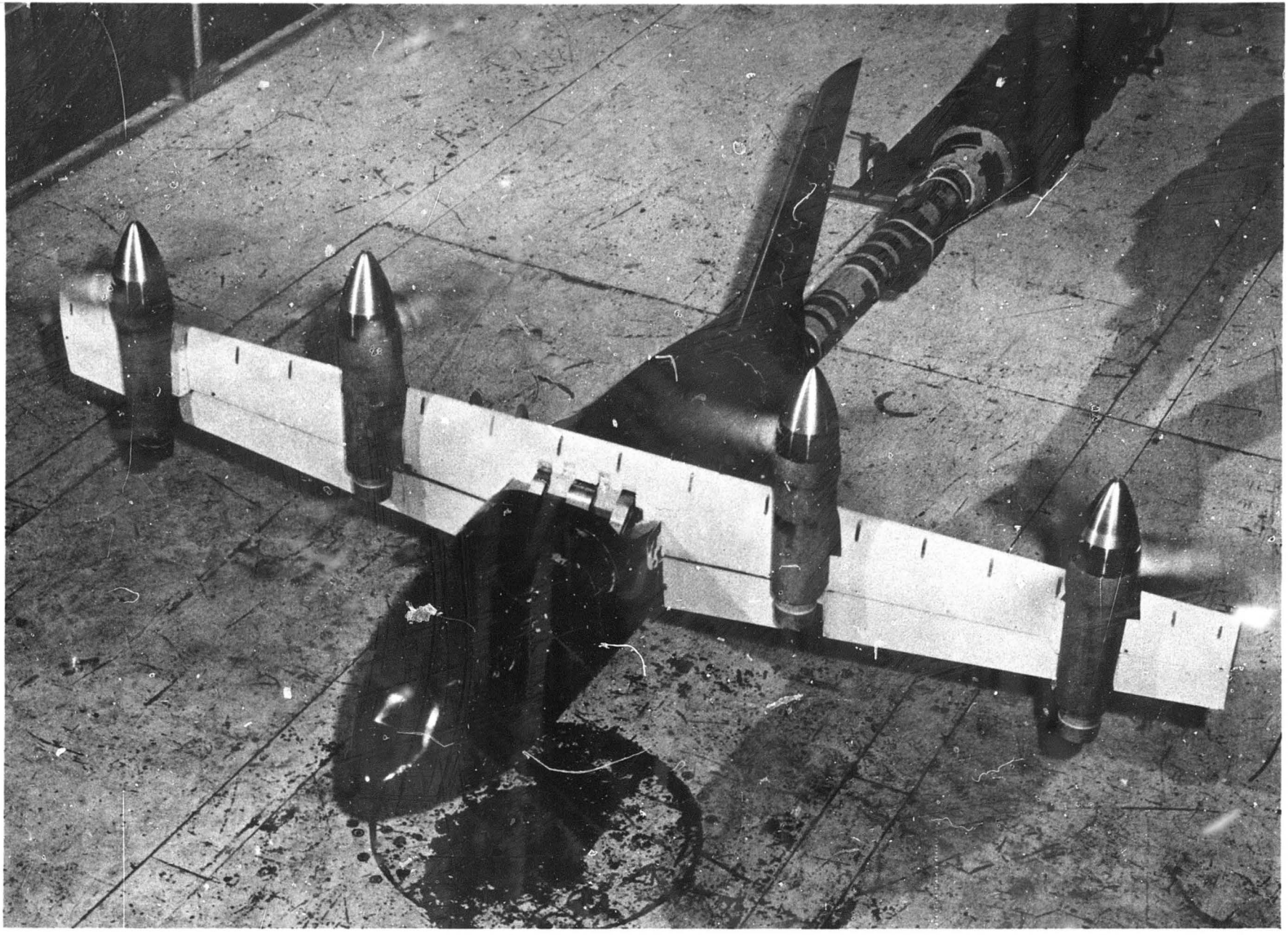

FULL SPAN MODEL VRO68Q
INSTALLATION IN BOEING-VERTOL
V/STOL WIND TUNNEL

Figure 1

Figure 2

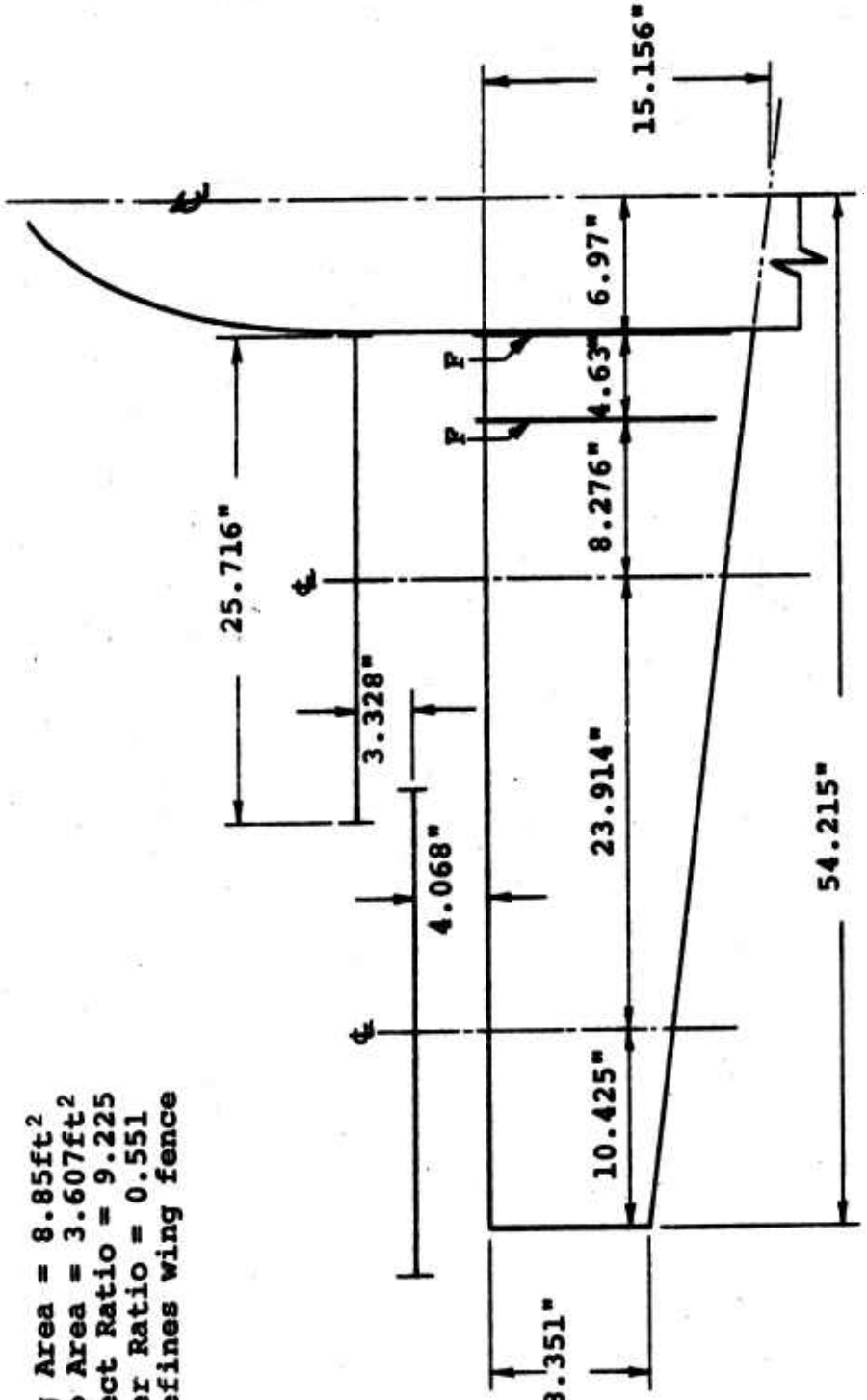

NOTES:
1. Wing Area = 8.85ft²
2. Prop Area = 3.607ft²
3. Aspect Ratio = 9.225
4. Taper Ratio = 0.551
5. F defines wing fence

MODEL VR068Q
BASIC WING GEOMETRY
AND PROPELLER LOCATION

Figure 3

MODEL VR068Q
SLAT DESIGN
5° T.E. ANGLE
SLAT T.E.
NACA 64$_2$215 Section Shown
15% C
WING CHORD LINE
22.7°
29.5° for
NACA 64$_4$221
Root Section
SLAT CHORD LINE
38 C
0% C
Slat Chord
Along
Slat Chord Line
16.3%C
17.3%C
Wing
Sta.
Tip
Root
C: Basic Wing Chord

Figure 4

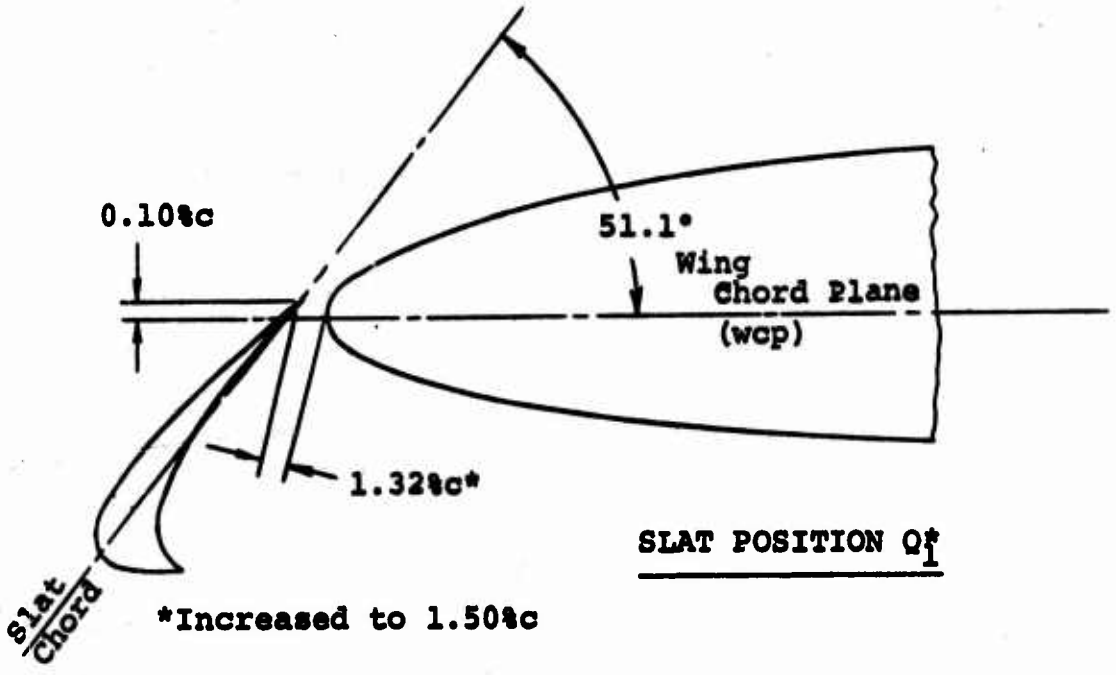

SLAT POSITION Q_1^*

*Increased to 1.50%c

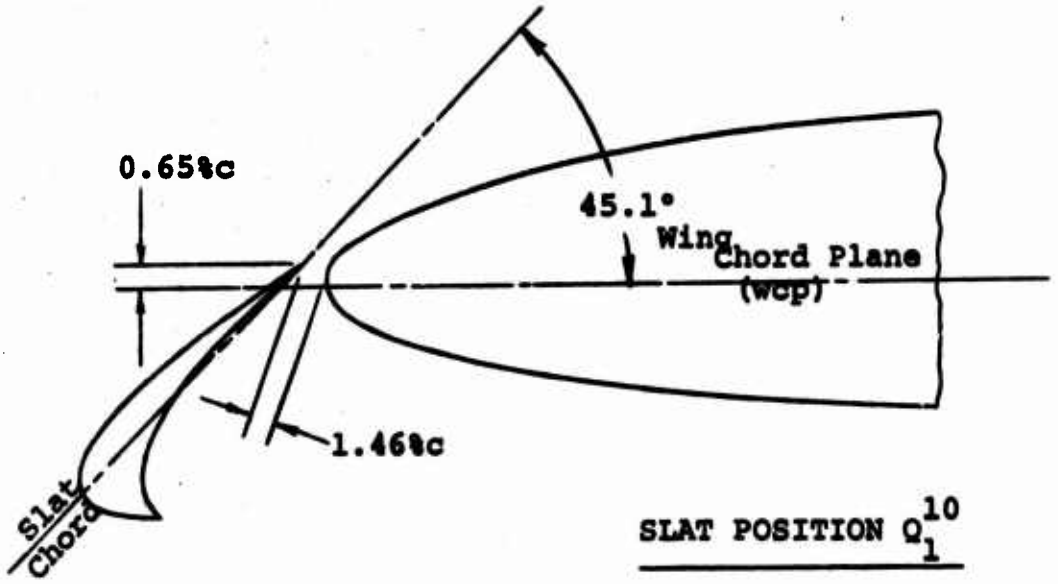

SLAT POSITION Q_1^{10}

MODEL VRO68Q
SLAT POSITIONS
TIP SECTION

Figure 5

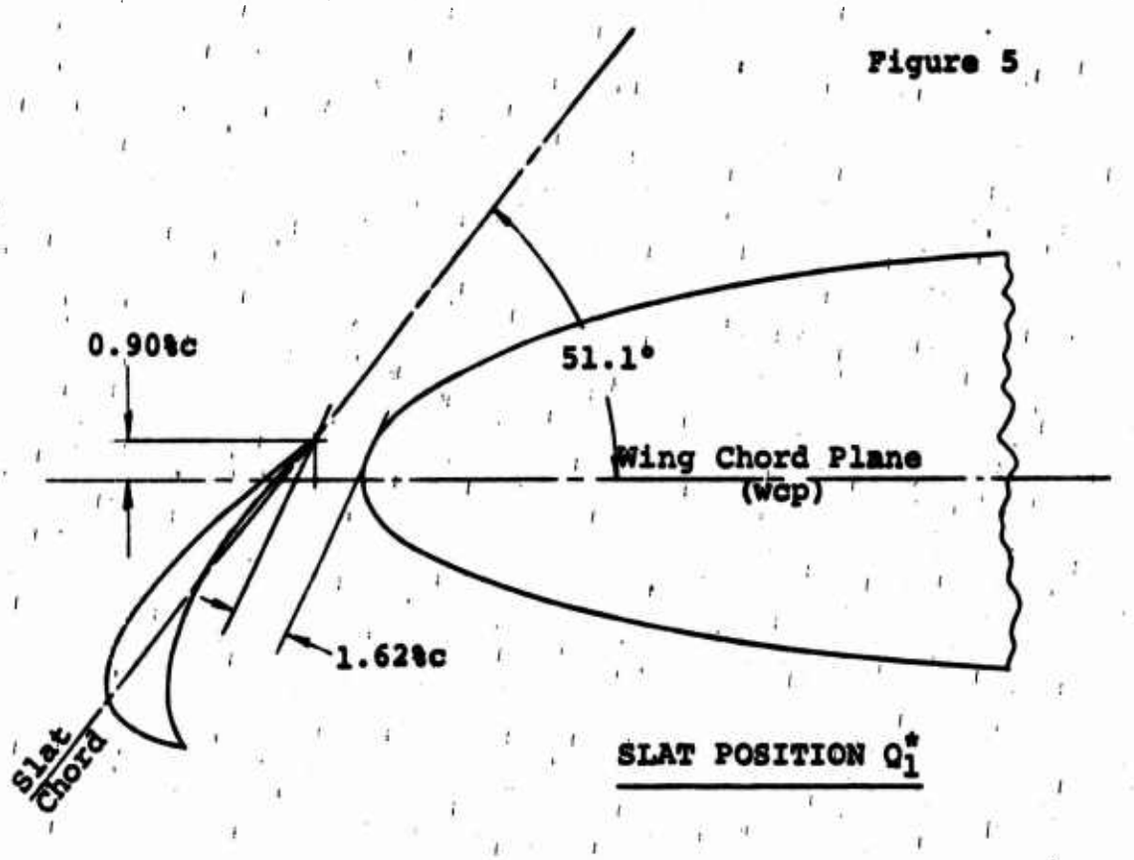

SLAT POSITION Q_1^*

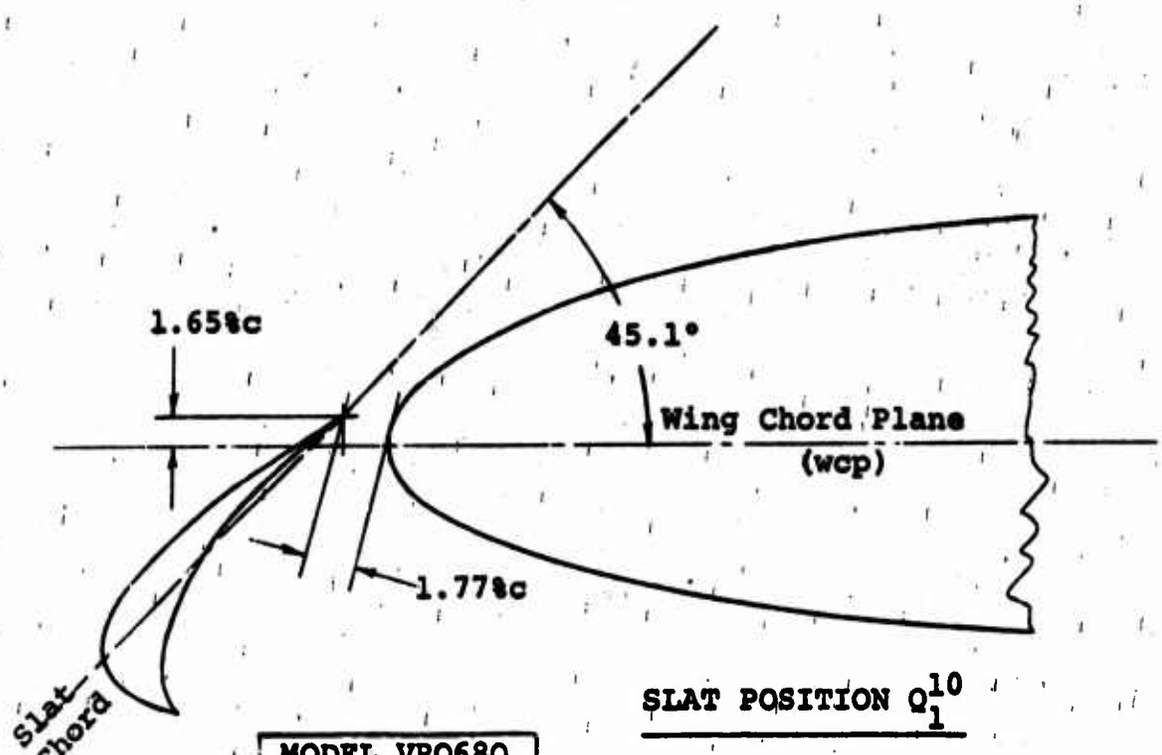

SLAT POSITION Q_1^{10}

MODEL VR068Q
SLAT POSITIONS
ROOT SECTION

Figure 6

MODEL VR068Q
DOUBLE SLOTTED FLAP GEOMETRY
40°, 50°, & 60° POSITIONS
TIP SECTION

Main Flap Chord: 34.6%c
Fore Flap Chord: 15.4%c

Flap Angle	G_1		X_1	
60°	1.51%c	.126"	.25%c	.021"
50°	1.51%c	.126"	.75c	.063"
40°	1.51%	.126"	1.63%c	.136"

c: Basic Wing Chord

*30° angle between main flap chord line and fore flap chord is for section from outboard nacelle to wing tip. 32° angle for section between nacelles.

Figure 7

Fore Flap Chord: 15.4%c
Main Flap Chord: 34.6%c
C: Basic Wing Chord

Flap Angle	G_1		X_1	
60°	1.40%c	.227"	.52%c	.079"
50°	1.50%c	.227"	1.17%c	.178"
40°	1.76%c	.267"	1.65%c	.250"

*34° angle between main flap chord line and fore flap chord line is for section from root to inboard nacelle. 32° angle for section between nacelles.

Figure 8

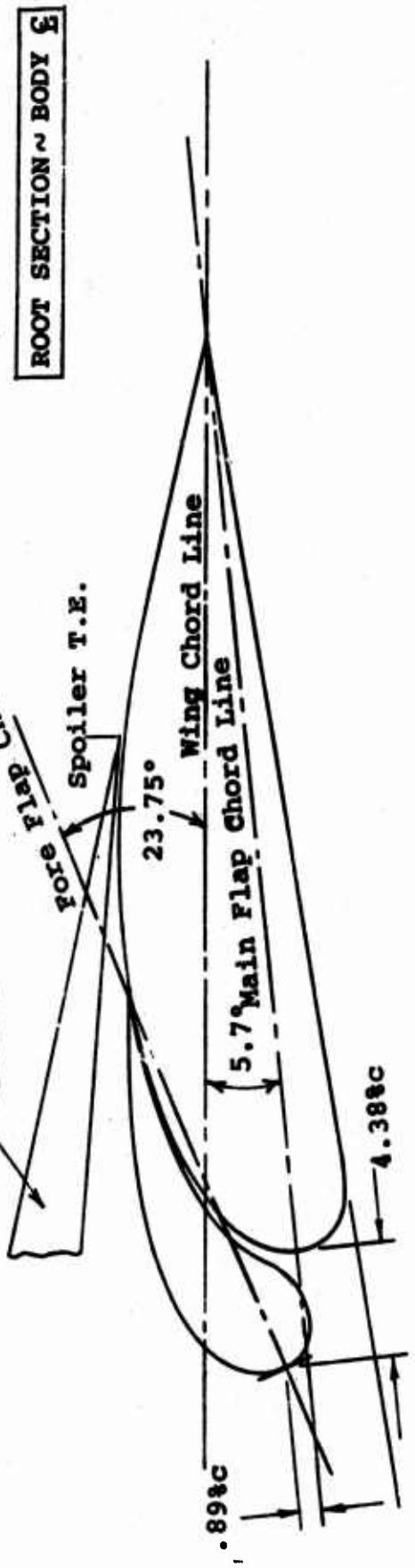

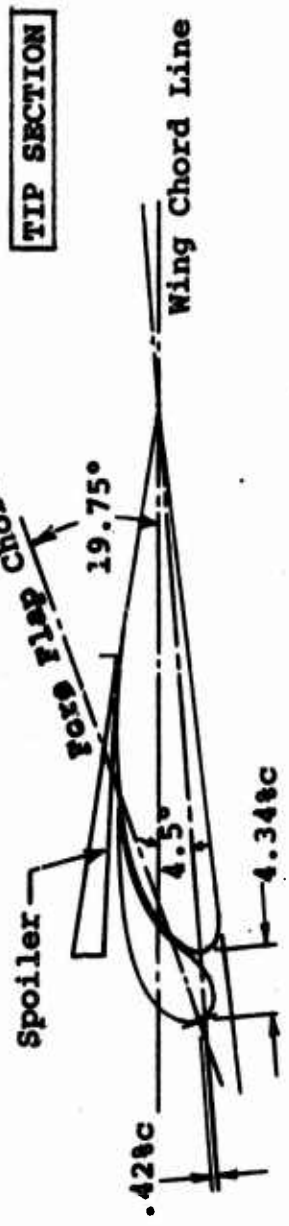

MODEL VR068Q
DOUBLE SLOTTED FLAP GEOMETRY
RETRACTED POSITION

Figure 9

MODEL VRO68Q

DOUBLE SLOTTED FLAP GEOMETRY
20° AND UP-FLAP POSITIONS

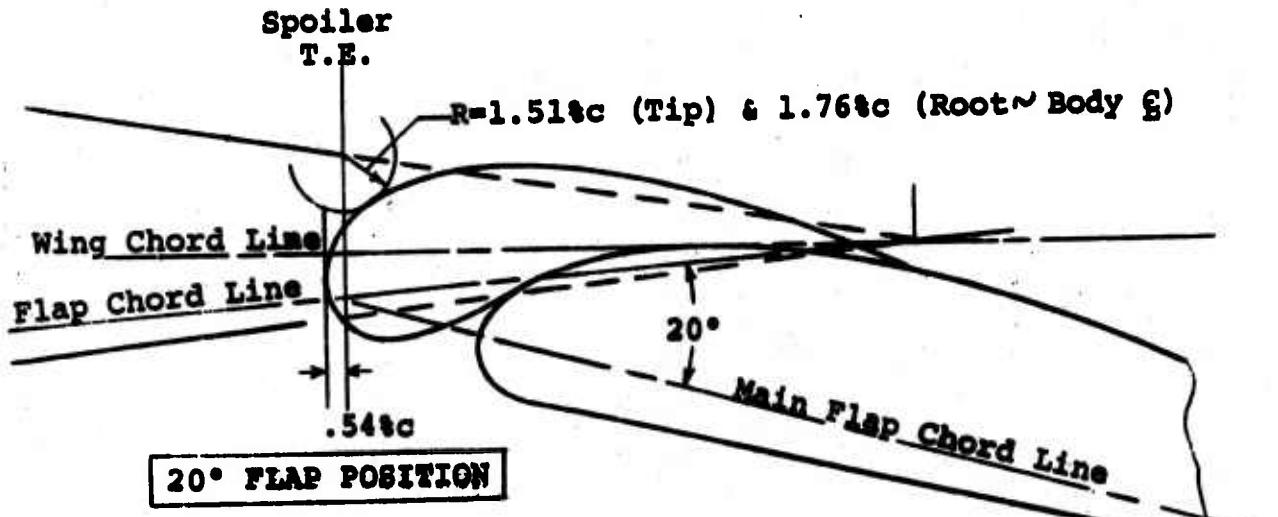

20° FLAP POSITION

c: Local Wing Chord

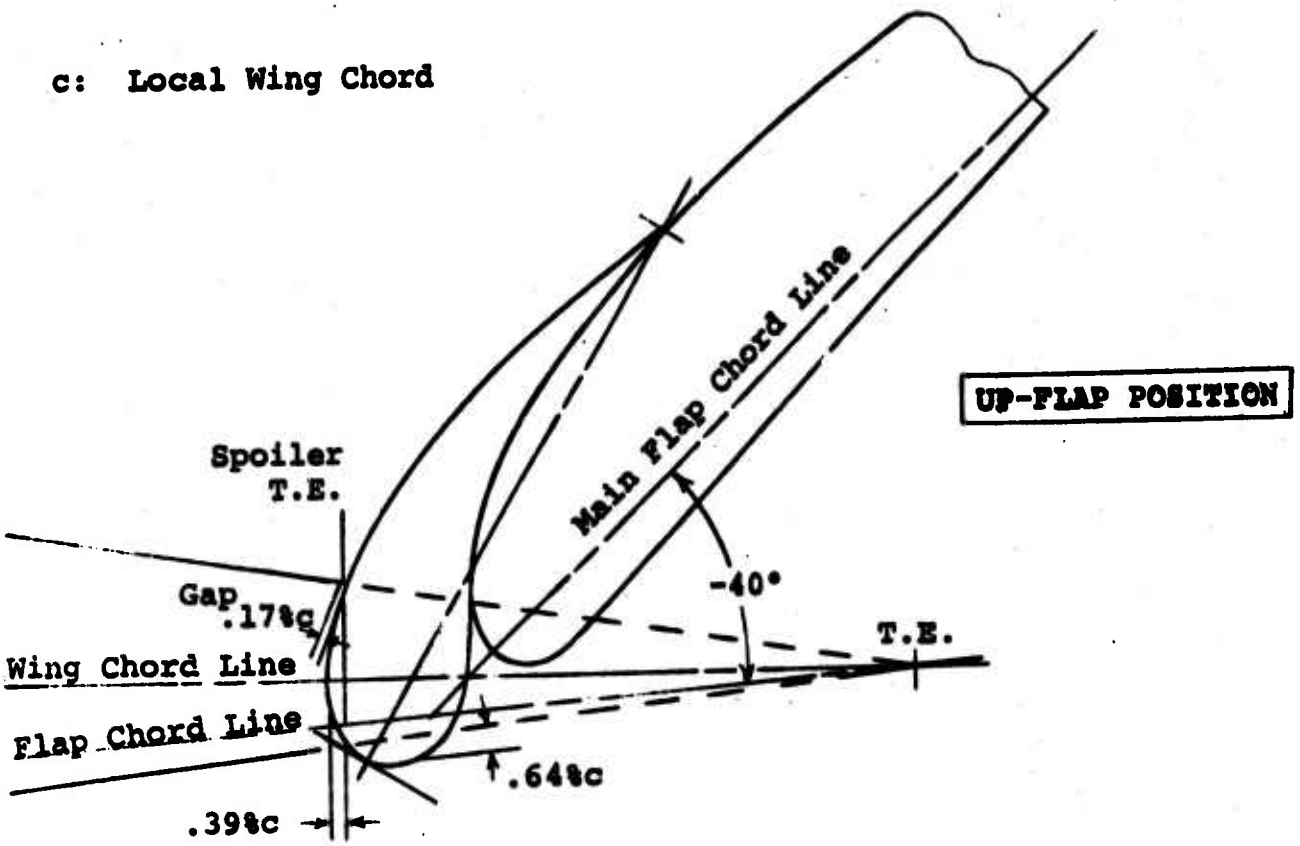

UP-FLAP POSITION

2.2 PROPELLER, HUB GEOMETRY

Geometric characteristics of the propeller blade used in this test are shown in Figure 10. The variation with radial station, of blade chord, design lift coefficient, thickness ratio and blade twist are presented in this plot. Figure 11 depicts the blade planform. Note that the blade pivots for manual collective settings about the 35% chord line.

Three-way collective hubs were used during the non-cyclic portion of the test. These were replaced with three-way cyclic hubs, using identical propeller blades, when cyclic pitch was required. Both propeller collective and cyclic angles were manually adjusted.

Figure 12 is a photograph of the 4.80 in. diameter cyclic hub. This hub employed a swashplate mounted on a cyclic stack fixed to the front of the six component nacelle balance. The outer annulus of the swashplate was driven by scissors mounted on the rear face of the hub. Cyclic pitch was applied to the blades through a set of pitch links. Elastomeric (Lamiflex) bearings were used in the hub for blade retention and blade angle motion.

Principal dimensional information and airfoil designations for the propellers are listed below:

Diameter	2.143 ft
Disc area	3.61 ft^2
Root chord (at .2r/R)	3.20 in.
Tip chord	2.32 in.
Root section	NACA 64A030
Tip section	NACA 64A306
Activity Factor	160 per blade
Overall Blade Twist	33.5°

NO. 340DR-MP DIETZGEN GRAPH PAPER
MILLIMETER

EUGENE DIETZGEN CO.
MADE IN U. S. A.

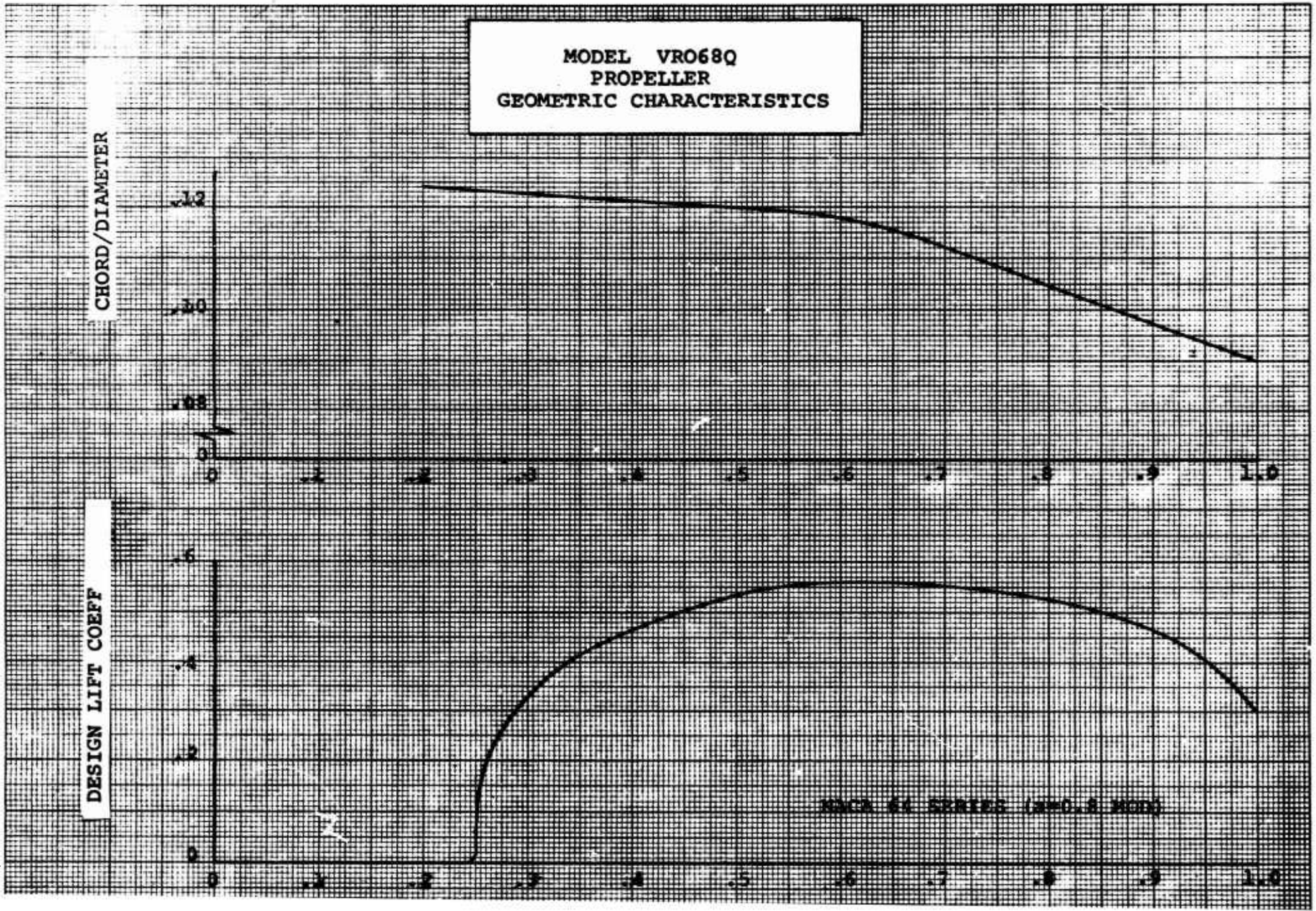

(a)-22

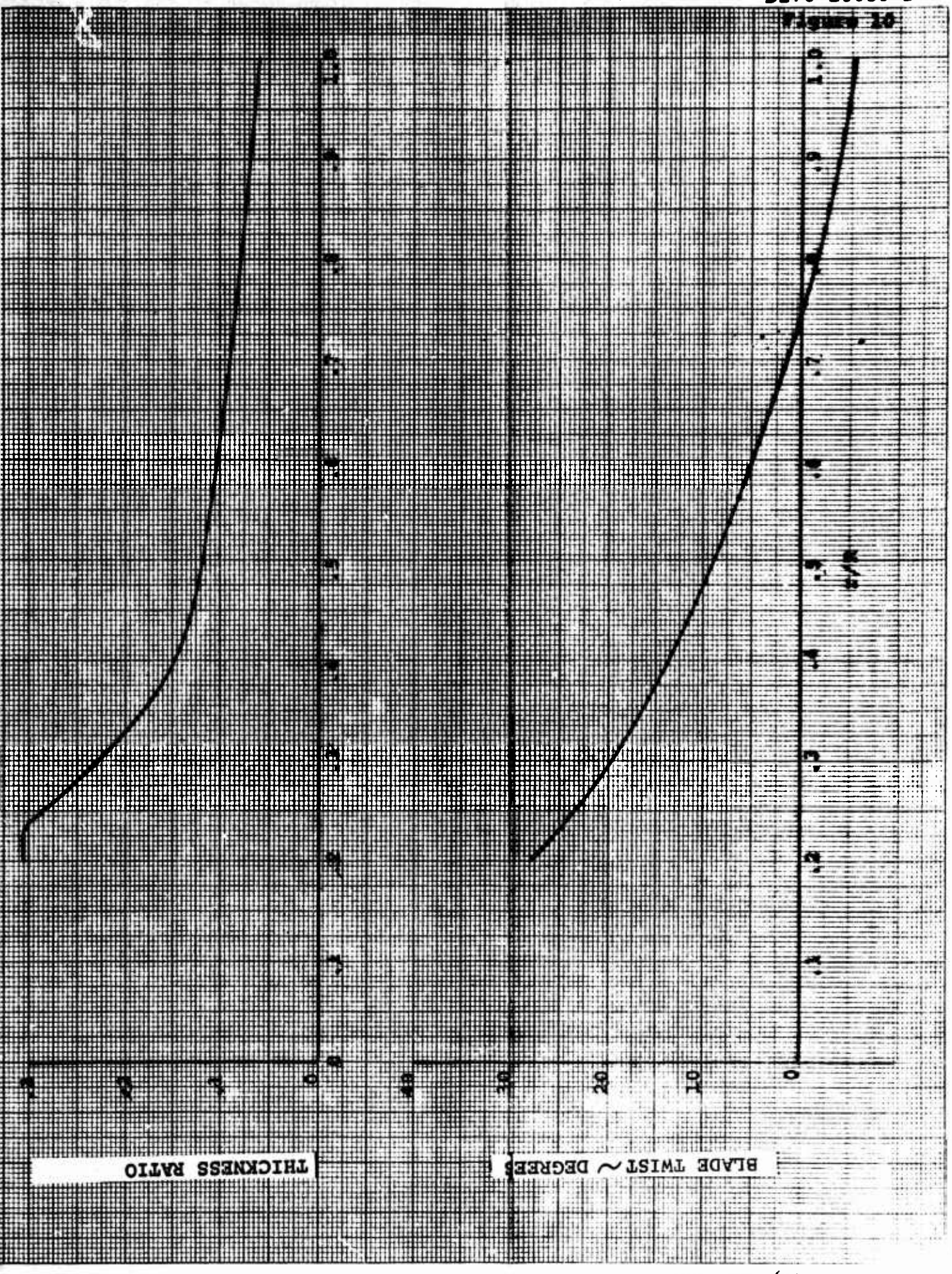
THICKNESS RATIO
BLADE TWIST ~ DEGREES

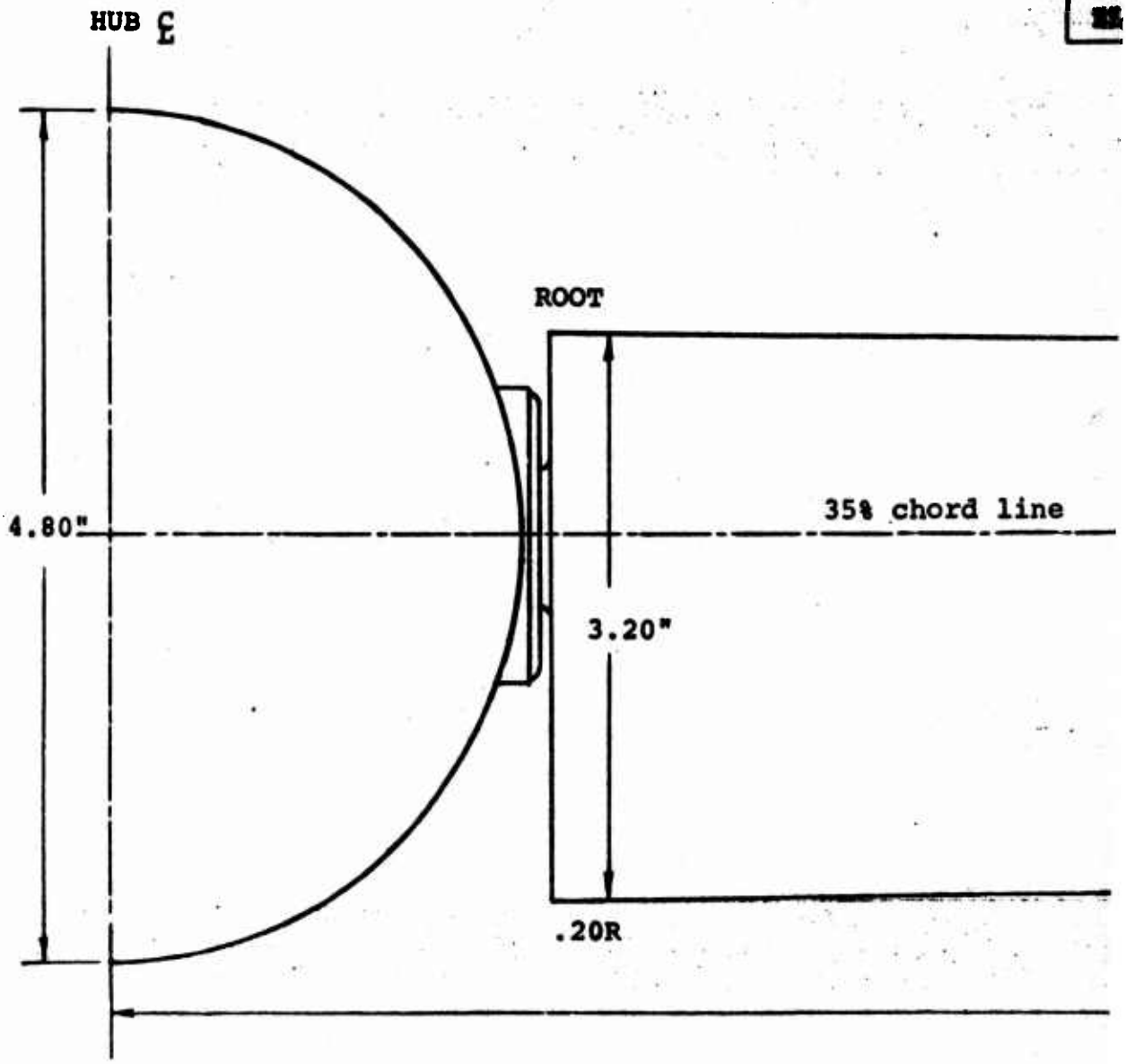

SCALE: FULL

NOTE: Actual Dimensions (Untwisted)

FORM 13910 (6/66)

Figure 11

L VRO68Q
PELLER
PLANFORM

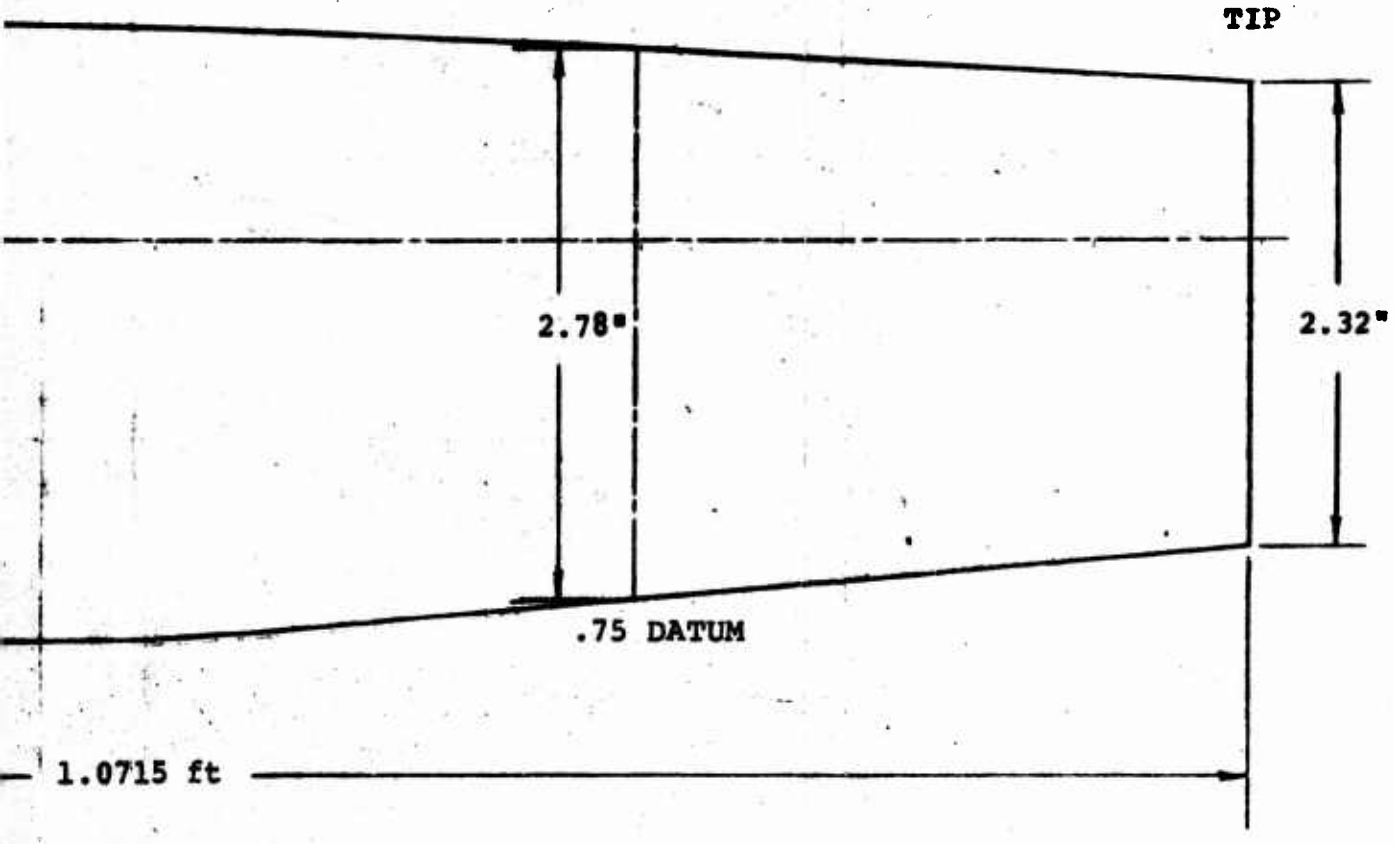

Figure 12

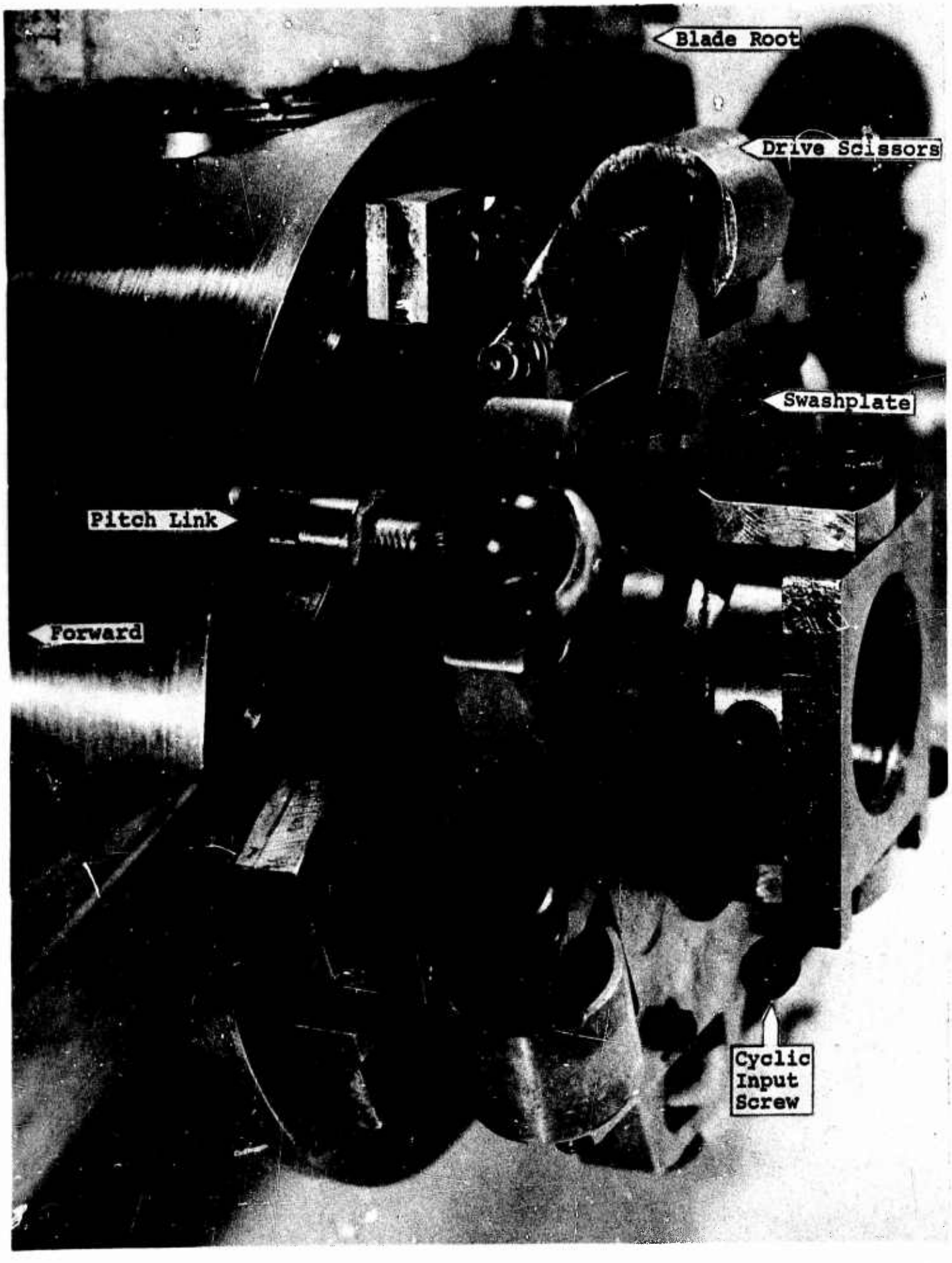

Details of Cyclic Hub Mechanism

2.3 NACELLE DESCRIPTION

A schematic drawing showing the arrangement of the propeller hub, swashplate, slip ring, strain gage internal balance, and air motor in the inboard nacelle along with the geometric relationship of the wing with the nacelle and hub center is presented in Figure 13. Similar information is depicted for the outboard nacelle in Figure 14. Not shown in the two sketches is the flexible bellows coupling that joined the propeller shaft to the air motor drive shaft. This coupling, located 1.875 in. aft of the nacelle balance center, isolated propeller forces and moments.

The air motor power source, which utilizes a four stage turbine, is designed to deliver 90 shaft horsepower at 9000 RPM. At this design point, approximately 2 lb/sec of air flow is required. Compressed air was individually ducted out to the inboard and outboard air motors from the wing root thru parallel 1.125 inch diameter air passages located internally in the basic wing structure. A 90° bend was used to introduce the air into the top of the inboard motor plenum in front of the first stage turbine. The lack of sufficient wing spar material at the outboard nacelle as a result of the relatively high thrust line (See Figure 14) necessitated stopping the internal wing air passage short of the outboard nacelle and angling the air into the outboard motor plenum (45° from vertical) via a short air passage drilled into a wedge shaped piece of material which was bolted to the lower surface of the wing inboard of the outboard nacelle.

A diverging nozzle with eight straightening vanes for eliminating exhaust swirl was attached to the rear end of each motor.

The location of the propeller thrust line with respect to the wing chord plane, and the prop plane location with respect to the wing leading edge in terms of percentage of local wing chord, can be determined from the information presented in Figures 13 and 14. These values are listed below.

Prop Hub ℄	Distance below wing chord plane	Distance ahead wing leading edge
Inboard	.218 z/c	.584 x/c
Outboard	.181 z/c	.421 x/c

The above ratios were established using data obtained during a 1969 Boeing-Vertol semispan wind tunnel test of a four prop tilt wing model. In this test, various prop hub centerline locations with respect to the wing were evaluated to determine the effect on descent capability.

Figure 13

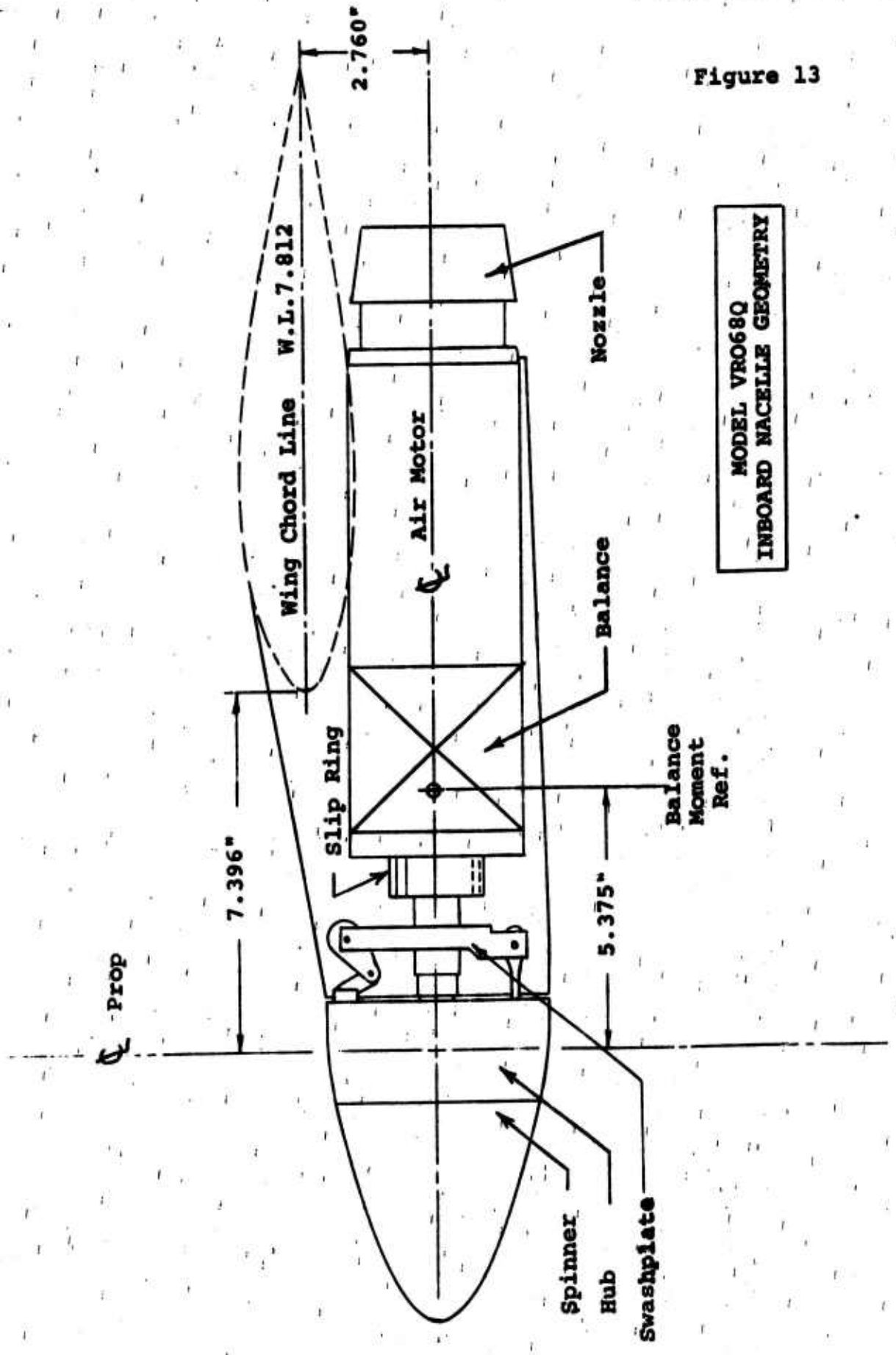

MODEL VRO68Q
INBOARD NACELLE GEOMETRY

D170-10038-1

Figure 14

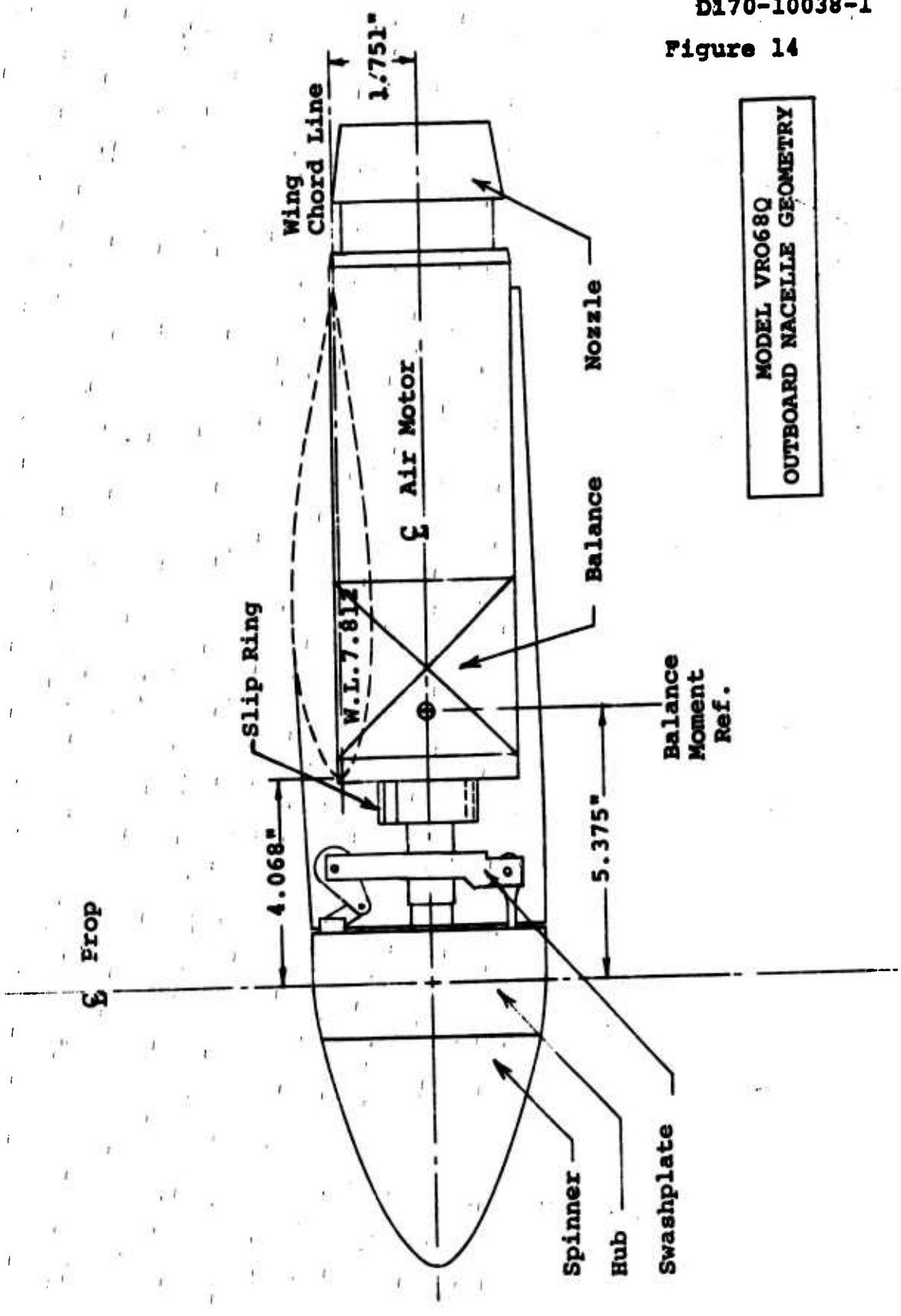

2.4 FUSELAGE GEOMETRY

The fuselage used on Model VRO68Q, as shown in Figure 15, had a shape generally representative of a four propeller tilt wing transport-type aircraft designed for rear ramp loading. Body cross section was generally oval with flattened top, bottom, and sides in the vicinity of the wing. Principal dimensions of the fuselage are as follows:

Length	79.88 in.
Maximum width	13.94 in.
Maximum depth	14.85 in.

Locations of the wing and empennage are also illustrated in Figure 15. The wing was essentially buried in the down position, protruding only slightly above the fuselage crown line. At the rear of the wing center section over the fuselage, a spring loaded fairing was located. This fairing, hinged at its aft end to the top of the fuselage, was designed to slide along the top surface of the wing as the wing was tilted.

With the wing down, zero wing tilt, the fuselage/wing junctures were smoothly contoured. A fuselage cut-out was provided at the leading edge of the wing to enable the slat to extend over the wing center section as the wing was tilted.

Figure 15 shows the vertical and longitudinal locations of the fuselage balance with reference to the fuselage and wing. Note that the balance was located directly below the wing pivot.

2.5 HORIZONTAL TAIL POSITION AND GEOMETRY

The horizontal tail was positioned high on the fin as illustrated in Figure 15. An additional horizontal tail position, mid-fin, was available, however, this tail height was not utilized during Phase I test BVWT061.

Figure 16 depicts the geometry of the horizontal tail. This tail pivoted for stabilizer angular motion about a line perpendicular to the aircraft axis of symmetry and passing through the quarter chord point of its mean aerodynamic chord is shown in Figures 15 and 16. Stabilizer angles from +45° to -15° were available in 5° increments. Note in Figure 15, that with the maximum stabilizer angle of +45°, the leading edge of the root "unported" slightly.

Primary geometry characteristics of the horizontal tail are listed below.

Tail area, S_H	2.764 ft.^{2}

Taper ratio	0.609
Aspect ratio	4.646
Tail arm, ℓ_H	4.288ft.
Tail volume coefficient, $V_H = \frac{S_H \ell_H}{Sc}$	1.330
Dihedral	0°

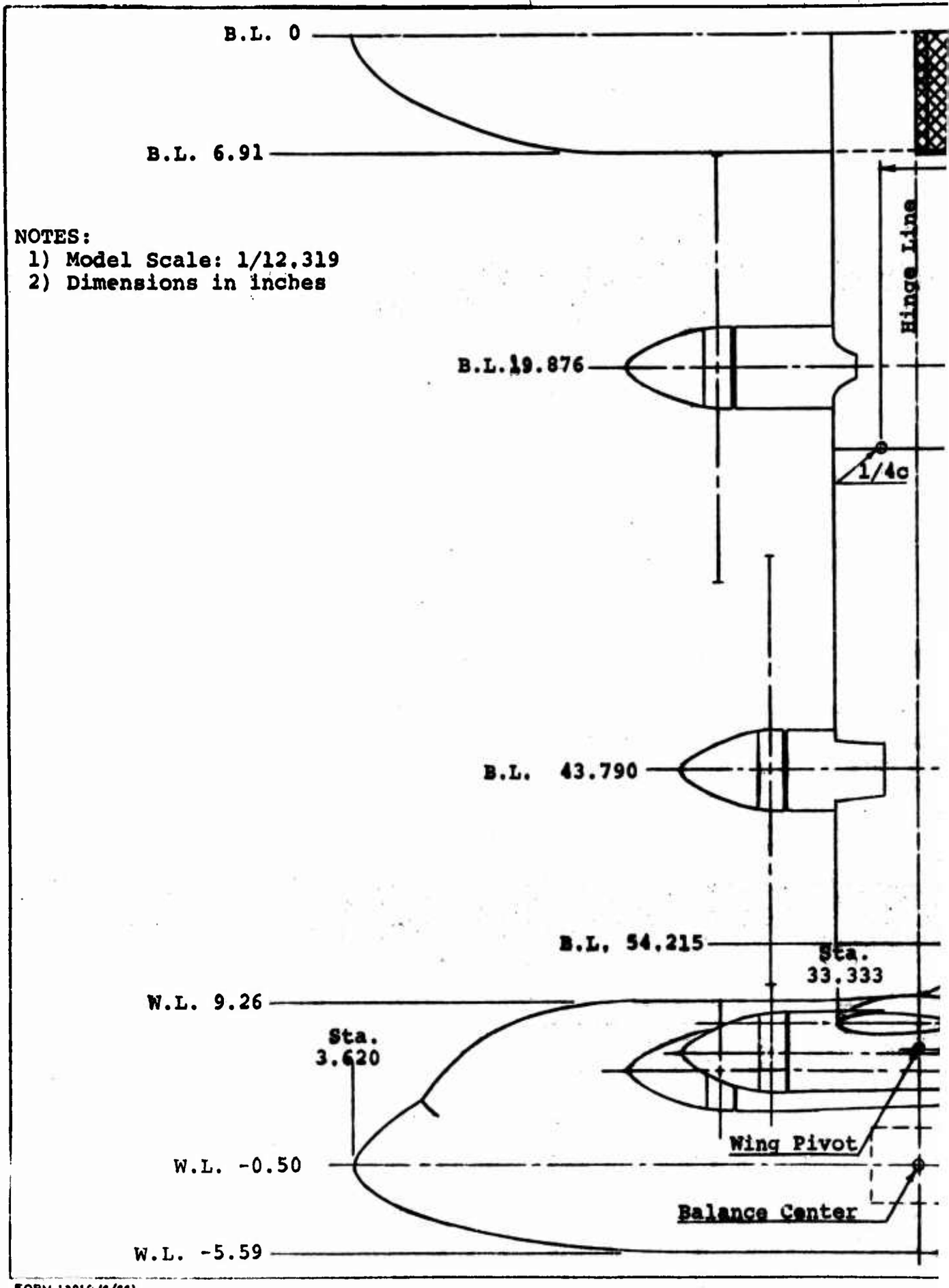

FORM 13910 (6/68)

1 B

D170-10038-1

Figure 15

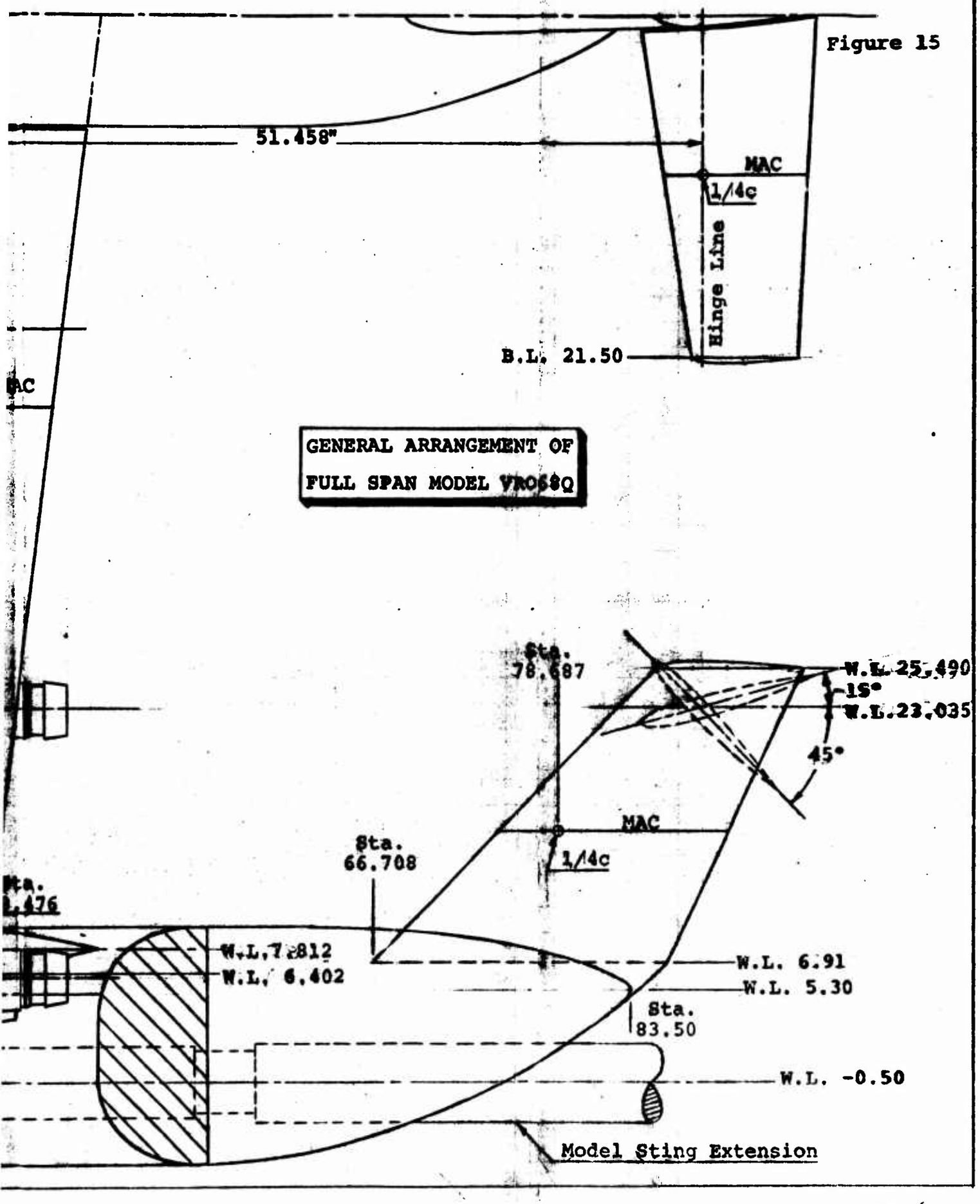

Figure 16

MODEL VRO68Q
HORIZONTAL TAIL GEOMETRY

NOTES:

1) No anhedral or dihedral

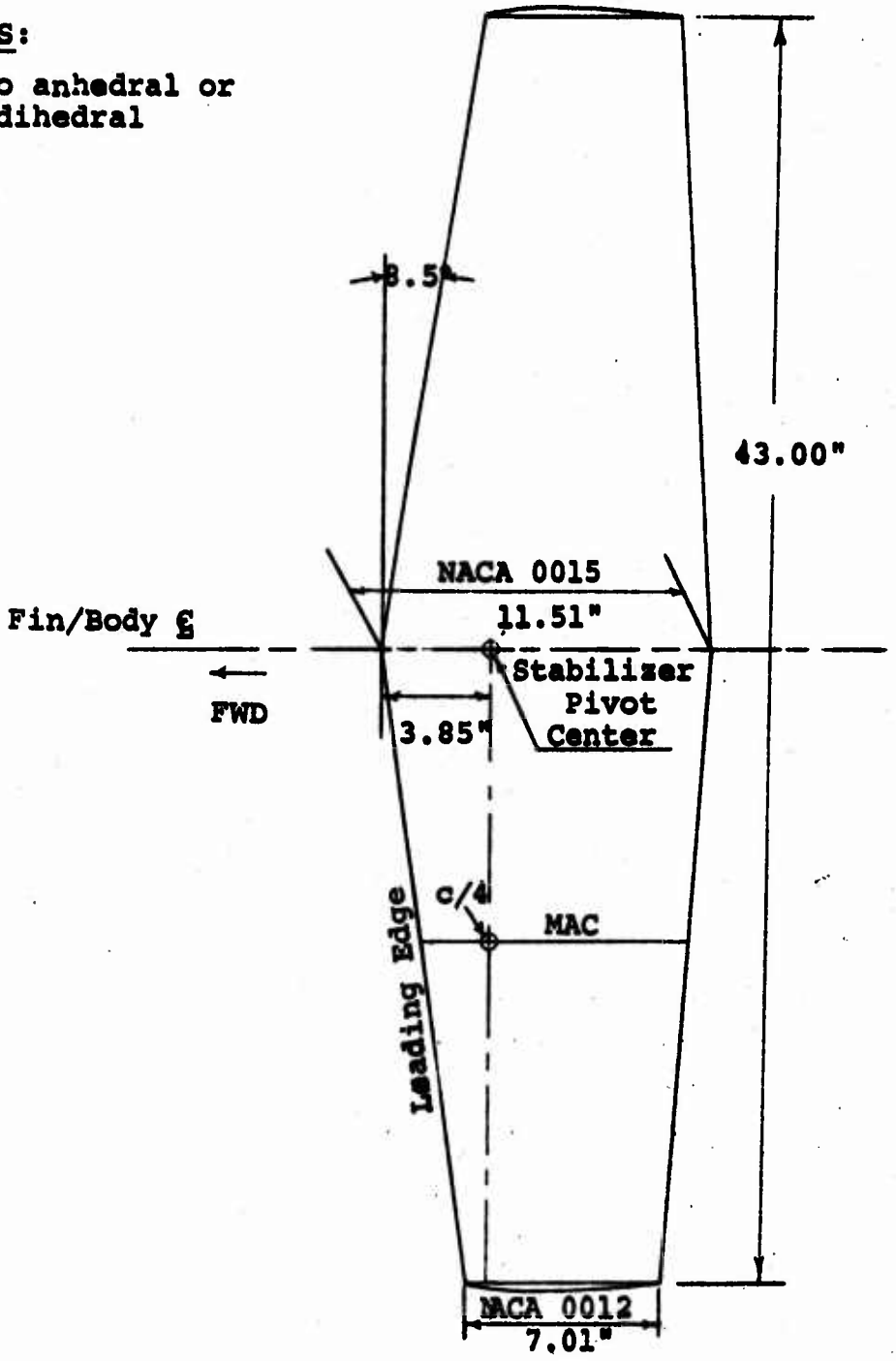

2.6 MODEL INSTALLATION

A schematic drawing of the model air supply system for powering the four pneumatic motors of Model VRO68Q is shown in Figure 17. High pressure air enters the model through the hollow sting extension. Interactions of the model air supply system on the fuselage balance measurements were minimized by ducting the air symmetrically past the balance from the forward section of the sting via dual ducts (one per fuselage side) and thence into a plenum chamber located forward of the balance in the frontal portion of the fuselage. A set of internal flexible bellows were used to connect the dual ducts to the plenum chamber structure.

Air for each air motor was individually ducted forward from the front wall of the plenum chamber, through separate motor control valves, and then aft over the top of the plenum chamber via four pipes which were connected to a hollow segmented air pivot joint. Four internal wing spanwise air ducts (one per motor) were used to direct the air outboard from the wing pivot joint into the forward portion of the air motors bolted directly to the wing.

Mass flow into each motor was remotely controlled by the four individual motor control valves used in conjunction with the main tunnel compressor system controls which established the plenum chamber pressure.

Model VRO68Q utilized the main tunnel hydraulically driven sting support system. The 16 ft. long sting pivots, for model angle of attack motion, about its attachment point on a vertical moving strut, which enables the model to be retained near the center of the test section as the model is pitched. A "yaw adapter" that provides pure yawing motion for selected angles of attack, was attached to the forward end of the main sting. This "yaw adapter" also incorporates a horizontal pivot and pin arrangement for manually setting the desired "pre-bend" angle between the fuselage centerline of the model and the centerline of the main sting.

The desired wing angle of attack range for a prescribed combination of wing tilt angle and thrust coefficient was achieved by selecting the proper "pre-bend" angle. With zero "pre-bend", the available fuselage angle of attack range is -20° to +12°. The -20° angle is the limit imposed by the maximum up-travel of the vertical strut (contact with the tunnel ceiling). The maximum positive angle of the sting with respect to the tunnel centerline (+12°) results from the limit imposed by the minimum bend radius of the 3 inch diameter (I.D.) braided steel model air hose passing up the vertical strut, through the main sting and "yaw adapter", and into the tilt wing model sting extension which is bolted to the forward end of the yaw adapter.

Selection of a positive 10° "pre-bend" angle provides a fuselage angle of attack range of -10° to +22°, for example.

A

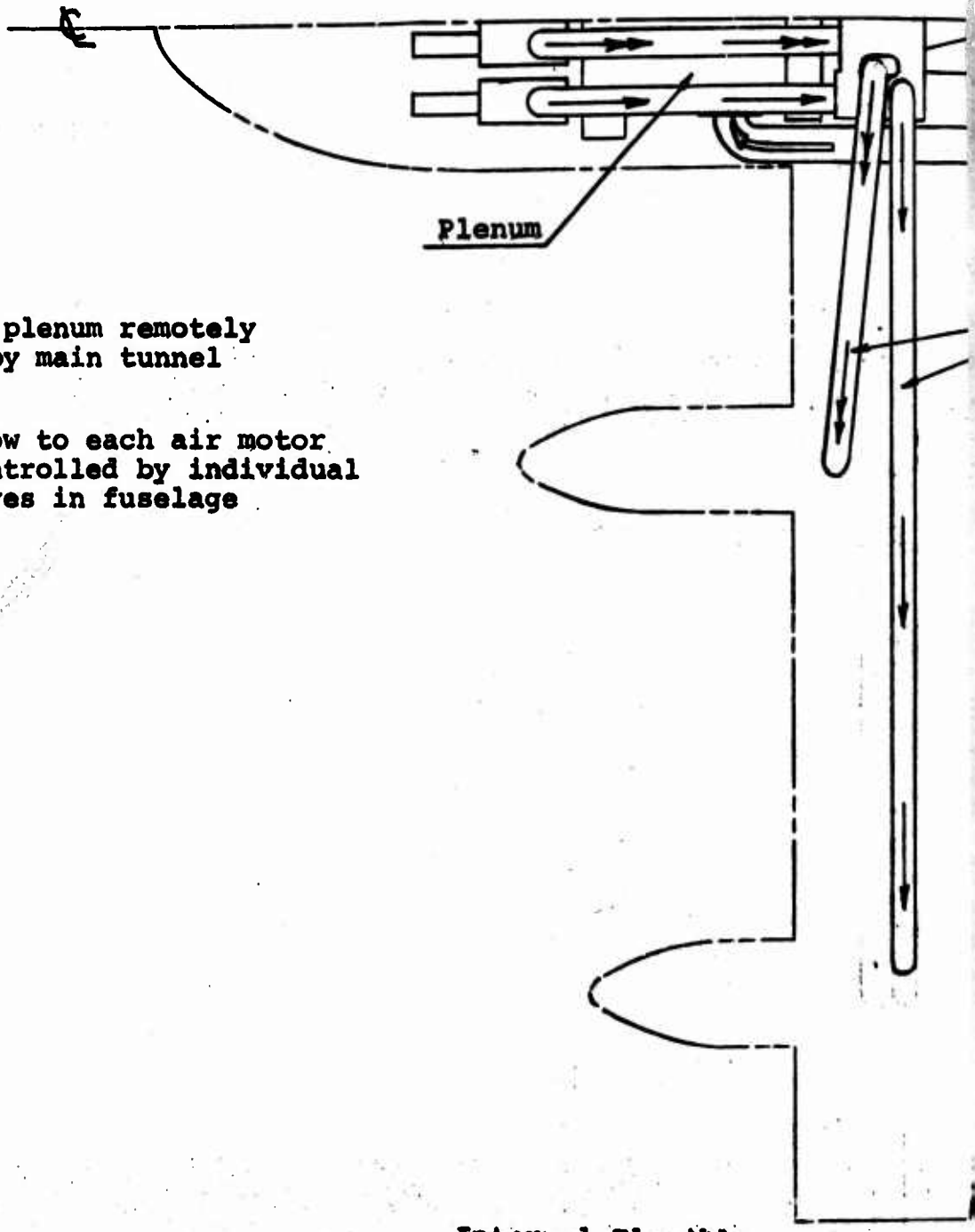

NOTES:

1) Pressure to plenum remotely controlled by main tunnel air valve

2) Mass air flow to each air motor remotely controlled by individual control valves in fuselage

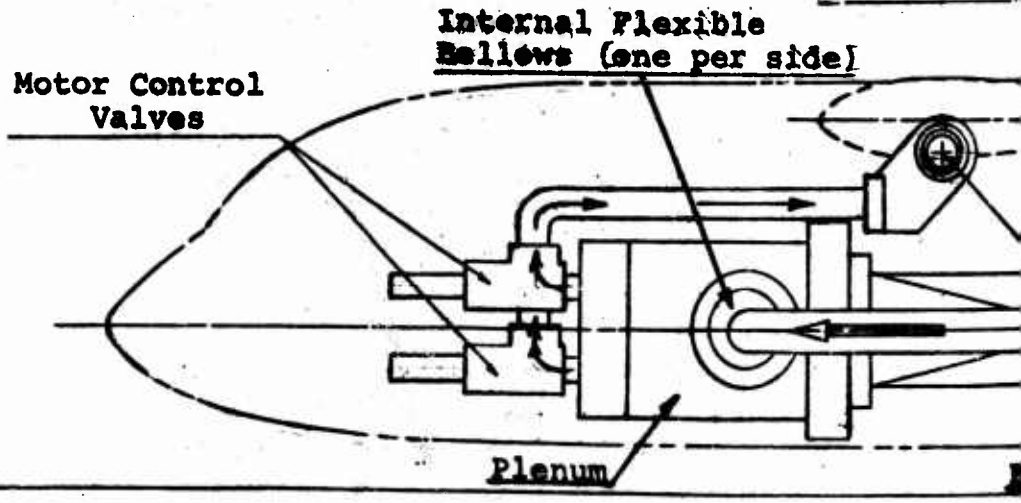

FORM 13910 (6/66)

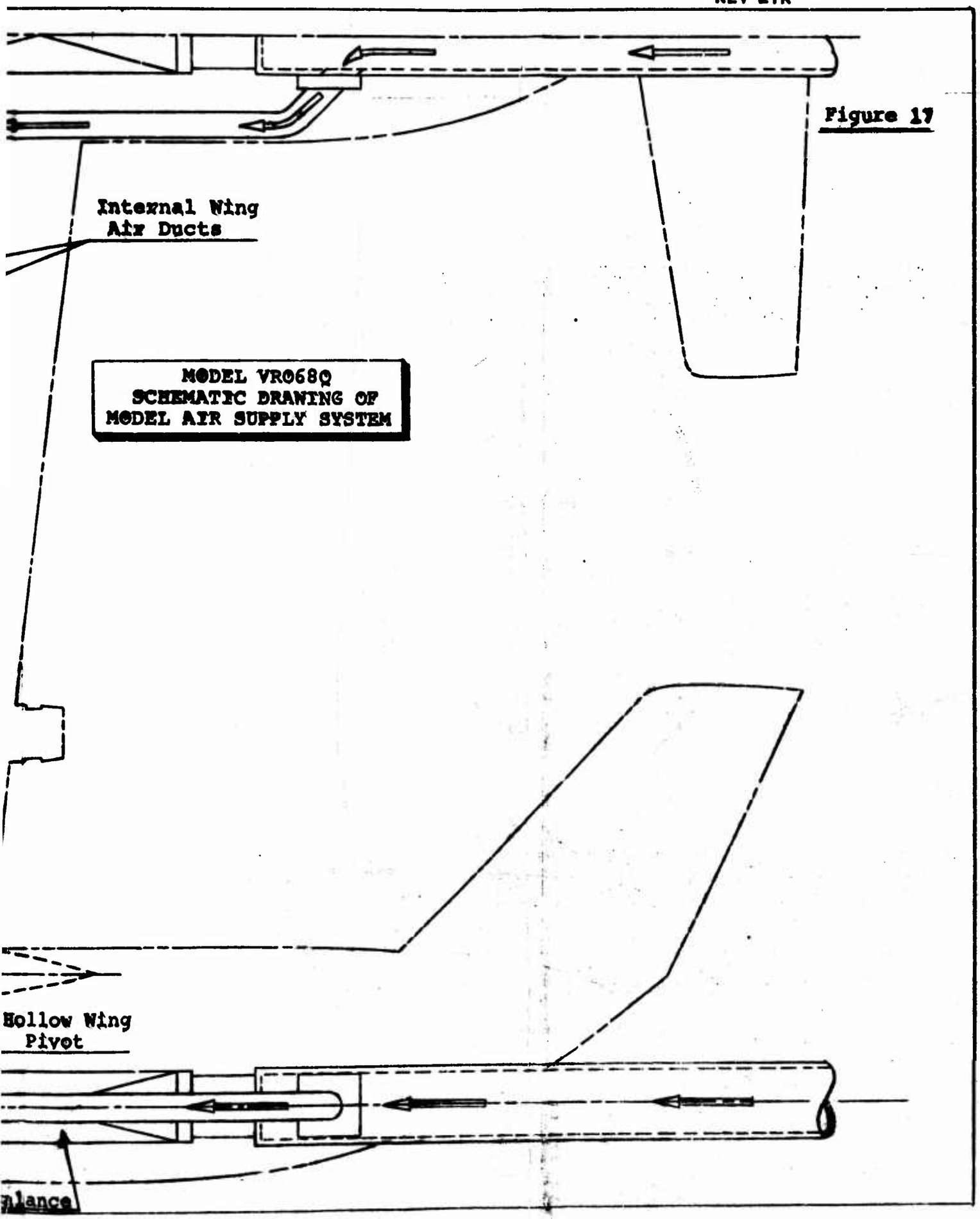

Figure 17

MODEL VR068Q
SCHEMATIC DRAWING OF
MODEL AIR SUPPLY SYSTEM

2.7 TEST FACILITY

As mentioned previously, the test was conducted in the 20 ft high x 20 ft wide x 29 ft long test section of the Boeing-Vertol V/STOL wind tunnel. A schematic view of this facility is presented in Figure 18.

The slotted throat test section configuration was used for the transition or forward flight portion of the test. This tunnel configuration is obtained by removing covers from slots built into the test section walls, floor, and ceiling.

During the hover phase of the test, the 29 ft long x 20 ft high test section walls were removed and lowered into pits. The raising of the test section ceiling to the top of the 67 ft diameter plenum chamber that surrounds the test section provided a hover test area with a height, as measured from the solid test section floor used as a ground plane, of approximately 50 ft.

The auxiliary air for powering the four nacelle pneumatic motors was supplied by a 20 pound per second, 1000 psi compressor system.

Figure 18

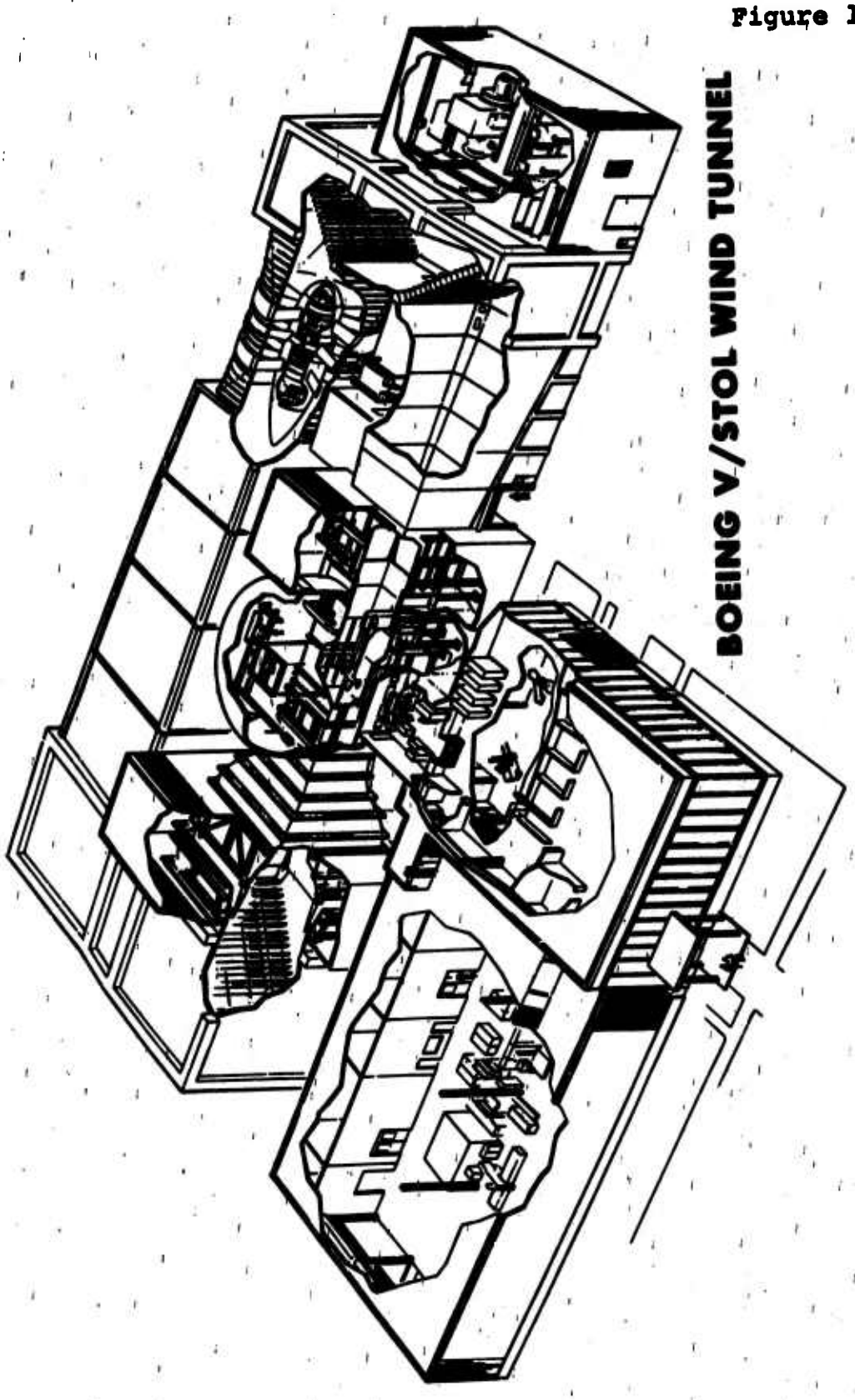

BOEING V/STOL WIND TUNNEL

3.0 INSTRUMENTATION AND EQUIPMENT

3.1 MODEL INSTRUMENTATION

Model instrumentation consisted of the following items:

a) Six Component Strain Gage Fuselage Balance

Total aircraft normal force, axial force, pitching moment, yawing moment, rolling moment, and side force were measured by this balance, that was located with its longitudinal axis parallel to the body centerline and with the balance center directly below the wing pivot as shown in Figure 15.

b) Six Component Strain Gage Balance in Each Nacelle

Identical balances were used in the outboard and inboard nacelles and were similarly located as shown in Figures 13 and 14. Each balance measured propeller thrust, pitching moment, normal force, yawing moment, side force, and rolling moment. The rolling moment in this case was the friction torque produced by the bearings and cyclic pitch mechanism. In addition to measuring steady values, normal force, pitching moment, and propeller thrust from selected nacelles were displayed on oscilloscopes so that dynamic loads in the balance flexures could be monitored to prevent exceeding the fatigue allowables.

c) Strain Gaged Propeller Drive Shafts

Each nacelle assembly incorporated a high speed slip ring assembly for the purpose of transmitting electrical signals from the strain gage bridges measuring torque.

d) Tachometers

The rotational speed of each propeller was measured by a tachometer, installed internally behind the front bearing of the air motor. This type of tachometer worked on the pulse generator principle (thirty pulses per cycle). Four digital voltmeters were used for direct readouts following amplification of the signals.

e) Wing Tilt Angle Potentiometer

Wing tilt angle was measured using a precision potentiometer. A gearing arrangement was used to prevent potentiometer slippage due to model motions.

f) Bearing Temperature Thermocouples

Each propeller shaft thrust bearing, located in the nacelle

stack, was instrumented. The four bearing temperatures were displayed on the control panel for model condition monitoring purposes.

g) Air Passage Metering Valve Position Indication

Mass flow into each air motor was individually controlled by a metering valve. The position of these four valves was displayed on the control panel as an aid to the operation of the four air motors.

3.2 DATA ACQUISITION SYSTEM

The flow diagram of the wind tunnel data system used in this test is shown in Figure 19. This data system can accept up to 120 channels from a model and the tunnel itself. These signals are routed as illustrated to an IBM 1800 computer for processing and data reduction. The computed results are tabulated by a line printer and selected quantities are plotted by the X-Y plotters. Final data is stored on magnetic tape.

A digital display of any nine channels is also available during testing for monitoring purposes. Dynamic data of six quantities can be continuously displayed on oscilloscopes. This provides assistance in preventing balance or structural limits from being exceeded.

A choice of sampling rates in terms of samples per channel/sec. and in sampling time periods is available. The sampling process is accomplished with channel switching devices called multiplexers.

Figure 19

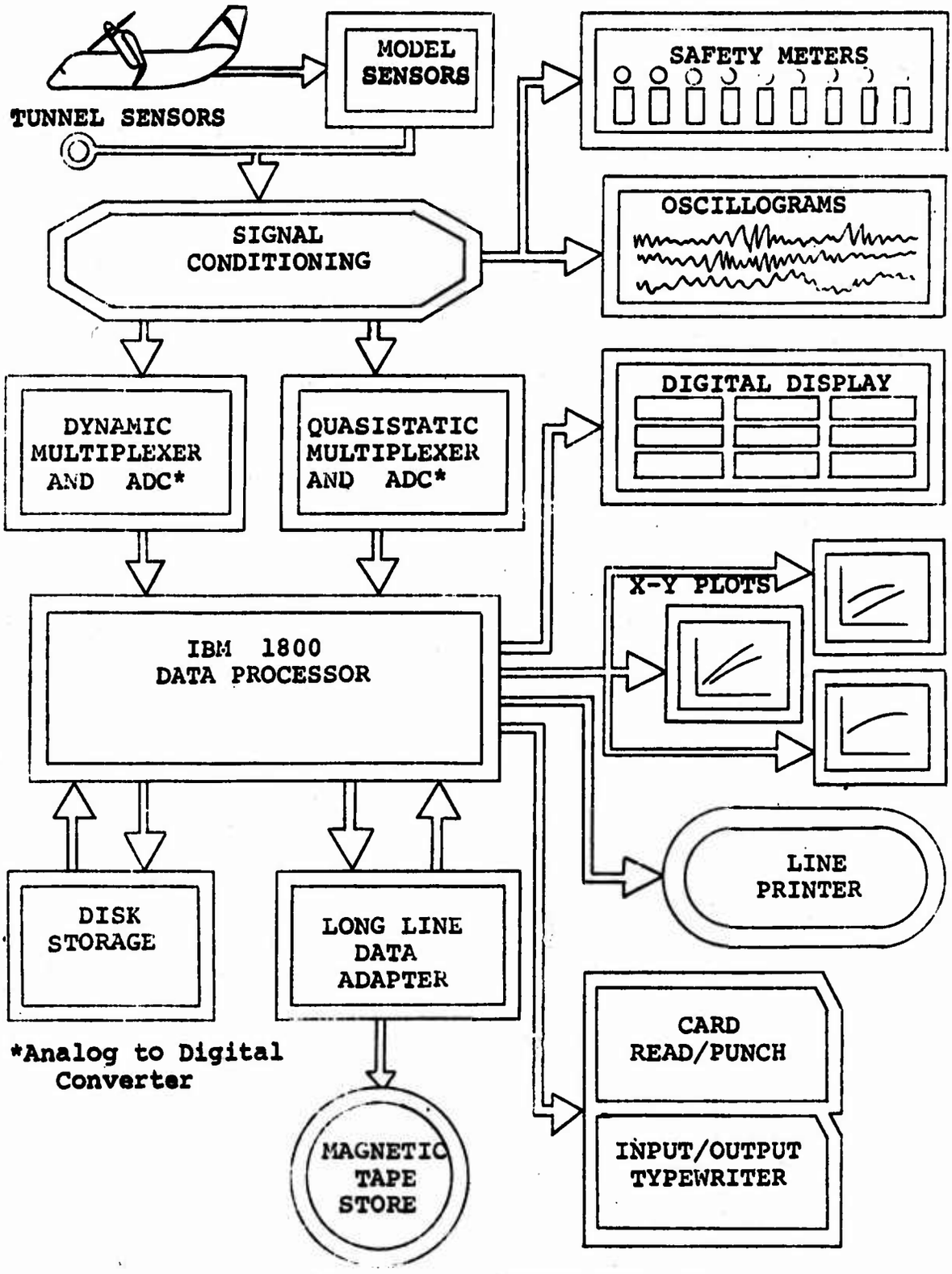

DATA ACQUISITION SYSTEM

4.0 DATA REDUCTION

At each test point, measurements were taken for computing and printing out on-line the quantities listed below.

Air supply line pressure	psi
Density, ρ	slugs/ft^3
Freestream dynamic pressure, q	lb/ft^2
Fuselage angle of attack, α_F (correction applied for sting deflection)	degrees
Model height, h	inches
Propeller speed (each propeller)	RPM
Shaft torque (each propeller)	ft.lbs.
Tunnel velocity, V	ft/sec
Wing tilt angle, i_w	degrees

The following aircraft forces and moments were measured by the fuselage balance.

Normal force (positive:up)	lbs.
Axial force (positive:forward)	lbs.
Pitching moment (positive:nose up)	ft.lbs.
Yawing moment (positive: nose right)	ft.lbs.
Rolling moment (positive:right wing down)	ft.lbs.
Side force (positive:to the right)	lbs.

Balance interaction corrections to these measured forces and moments were calculated and applied on-line using the balance interaction matrix incorporated into the data program. Static pressure tares, resulting from the high pressure model air supply lines extending forward from the model sting extension into the plenum chamber located in the frontal portion of the fuselage, were also applied on-line. The static pressure tare curves inserted into the data program were linear and of the following magnitude at 300 psi, a typical operating line pressure.

Normal force: -4 lbs.

Axial force: -10 lbs.

Pitching moment: -1 ft.lb.

Yawing moment: +1 ft.lb.

Rolling moment: +2 ft.lbs.

Side force: -2.5 lbs.

At each test point, the value of jet thrust produced by each air motor was established by entering the jet thrust correction "look-up" tables incorporated into the computer program as a function of shaft torque. The components of jet thrust inherent in the measured values of aircraft normal force, axial force, and pitching moment were extracted on-line, as a function of wing tilt angle.

Finally, model weight tare values for a particular wing tilt/fuselage angle combination and model configuration were determined and applied on-line using the appropriate weight tare equations inserted into the data program.

Aircraft normal force and axial force from the fuselage balance were resolved on-line into the wind axis system in order to compute

Lift, L lbs.

Longitudinal force, X(positive forward) lbs.

Aircraft pitching moment measured by the fuselage balance was transferred on-line to the wing pivot for runs wherein wing tilt angle was varied (fuselage angle was held constant) and to an aircraft c.g. position representative of the wing tilt angle for runs wherein fuselage angle was varied (wing tilt angle held constant)or yaw angle was varied.

Aircraft forces and moments were reduced on-line to the following coefficient form based on slipstream dynamic pressure.

Lift coefficient, $C_{L_s} = \frac{L}{q_s S}$

Longitudinal force coefficient, $C_{X_s} = \frac{X}{q_s S}$

Pitching moment coefficient, $C_{M_s} = \frac{M}{q_s c S}$

(where c=MAC of tapered wing)

Side force coefficient, $C_{y_s} = \frac{\text{Side force}}{q_s S}$

Yawing moment coefficient, $C_{n_s} = \frac{\text{Yawing moment}}{q_s S b}$

Rolling moment coefficient, $C_{\ell_s} = \frac{\text{Rolling moment}}{q_s S b}$

Aircraft lift, longitudinal force and pitching moment were also reduced on-line into the following non-dimensional form.

$\frac{L}{qb^2}$, $\frac{D}{qb^2}$ (positive aft for drag), $\frac{M}{qb^2c}$

Each of the four internal nacelle balances measured the following forces and moments.

Thrust, T (positive:forward)	lbs.
Prop normal force (positive:up)	lbs.
Prop pitching moment (positive:nose up)	ft.lbs.
Prop side force (positive:to the right)	lbs.
Prop yawing moment (positive: nose right)	ft.lbs.
Prop rolling moment (same as friction torque)	ft.lbs.

A balance interaction matrix for each nacelle balance, as developed from the static calibration, was incorporated into the on-line computer program. Interaction corrections to the measured propeller forces and moments were calculated and applied using the appropriate nacelle interaction matrix. Weight tares due to the weight of the propeller/hub assembly were then calculated and corrections applied on-line.

Pitching moment and yawing moment that were measured about the balance center were transferred to the hub ℄ so that hub moment coefficients could be calculated at the plane of the propeller. The following propeller-type coefficients were computed and printed out on-line for each of the four propellers.

Advance ratio, $J = \frac{V}{nD}$

Thrust coefficient, $C_T = \frac{T}{\rho n^2 D^4}$

Prop pitching moment coefficient,

$$C_{M_p} = \frac{\text{Prop pitching moment}}{\rho n^2 D^5}$$

Prop shaft power coefficient, $C_p = \frac{\text{Shaft power}}{\rho n^3 D^5}$

$$= \frac{2\pi(\text{Shaft torque})}{\rho n^2 D^5}$$

Prop normal force coefficient, $C_{NF_p} = \frac{\text{Prop normal force}}{\rho n^2 D^4}$

Prop side force coefficient, $C_{SF_p} = \frac{\text{Prop side force}}{\rho n^2 D^4}$

Prop yawing moment coefficient, $C_{YM_p} = \frac{\text{Prop yawing moment}}{\rho n^2 D^5}$

Friction power coefficient, $C_{p_F} = \frac{2\pi(\text{Balance rolling moment})}{\rho n^2 D^5}$

Coefficients of prop thrust, prop pitching moment, and prop normal force in slipstream notation were also calculated and printed out on-line for each propeller per the following listing.

Thrust coefficient, $C_{T_s} = \frac{T}{q_s A_p}$

Prop pitching moment coefficient, $C_{MP_s} = \frac{\text{Prop pitching moment}}{q_s S c}$

Prop normal force coefficient, $C_{NF_s} = \frac{\text{Prop normal force}}{q_s S}$

where $q_s = q + T/A_p$

Full scale aircraft rate of descent in ft/min and velocity in knots were computed on-line at each test point by the following equations inserted in the data program.

$$R/D = 60\left(\frac{D}{qb^2}\right) \cdot \sqrt{\frac{2W}{\rho b^2}} \cdot \sqrt{\frac{1}{\left[\left(\frac{L}{qb^2}\right)^2 + \left(\frac{D}{qb^2}\right)^2\right]^{3/2}}}$$

$$V_F = .592\sqrt{\left(\frac{2W}{\rho b^2}\right)\left(\frac{qb^2}{L}\right)}$$

The weight term used in the above equations was commensurate with a typical full scale tilt wing aircraft operating at its maximum gross weight in the "V" mode which corresponded to a wing loading (W/S) of 66 lb/ft^2. This value was increased to 73.5lb/ft^2 to account for the difference between the average tunnel density used in the above equations (ρ=.00228 slugs/ft^3) and the typical atmospheric design conditions of 3000ft/90°F (ρ=.00204 slugs/ft^3) for a full scale tilt wing.

The following equation was used in the data program to compute propeller induced velocity, w, in ft/sec.

$$w^4 + w^3\ 2V \cos i_w + w^2V^2 = \left(\frac{T}{2\rho A_p}\right)^2$$

The above parameter was used to determine the effective wing angle of attack, $\alpha_{W_{EFF}}$, at buffet onset. This angle is defined as the angle between the wing chord and the resultant velocity at the wing. The resultant velocity was obtained by adding vectorially, the tunnel velocity and the induced velocity at the leading edge of the wing, assuming full contraction of the propeller wake at the wing leading edge.

Three wind tunnel X-Y plotters were used to produce on-line plots of the following during pitch sweeps.

Force polars in terms of C_{L_s} vs C_{X_s}

or L/qb^2 vs D/qb^2

Lift curves in terms of C_{L_s} vs α_f

or L/qb^2 vs i_w

Pitching moment curves in terms of M/qb^2c vs i_w

or C_{M_s} vs α_F

No tunnel wall corrections were applied to the data.

5.0 TEST PROCEDURE AND TEST CONDITIONS

5.1 TEST PROCEDURE

The fuselage and four nacelle strain gage balances were check calibrated statically with the model built-up and installed in the test section (i.e., plumbing was installed and the nacelles were assembled) by applying known forces and moments on each balance. The resultant calibrations compared favorably with those obtained previously from the bench calibration of the same balances. Balance interaction matrices utilized in the on-line computer program were developed from the bench calibration data.

The installed model was then statically pressurized in increments to determine the effect on the measured forces and moments from the fuselage balance, of the high pressure air lines extending forward from the sting, across the fuselage balance, and into the plenum chamber located in the nose of the fuselage. Static pressure tares developed from this calibration were incorporated into a look-up routine in the data program so that corrections could be applied on-line to forces and moments sensed by the fuselage balance.

Sting deflections due to the net vertical force (lift minus model weight) acting on the model were established by hanging known weights on the model and measuring the true fuselage angle of attack with an inclinometer. The resultant correction curve,showing incremental fuselage angle of attack as a function of net vertical force, was inserted into the computer program so that the indicated fuselage and wing angle of attack could be adjusted on-line to true values.

Due to the different resultant stiffnesses of the inboard and outboard nacelle when mounted on the model, it was necessary to dynamically balance each of the propeller/hub assemblies (cyclic plus collective hubs) in place on the wing. The balancing target in each case was +10% of the allowable fatigue load for nacelle balance pitching moment and normal force, which were monitored during the test.

The jet thrust produced by each air motor was determined by individually running each motor in place on the model with a cylindrical cross section "propeller" installed and zero tunnel q. This tubular "propeller" was utilized so that the air motor torque could be absorbed without the simultaneous production of propeller thrust. The calibration curves as obtained from resolving fuselage balance yawing moment are presented in Figure 20, as a function of shaft torque. These curves were incorporated into the computer program so that the jet thrust produced by each motor could be extracted on-line from the forces and moments measured by the fuselage balance.

Prior to performing the actual data runs with a particular set of propeller hub assemblies installed (collective or cyclic hubs), it was necessary to balance the thrusts from the four propellers. This procedure was straightforward in the hover portion of the test, wherein the collective blade angle of each propeller was manually adjusted until the maximum thrust difference between propellers was within 1% of the total thrust from the four propellers. The total propeller thrust varied from approximately 450 lb. with collective hubs (6800 RPM and 14° average blade angle ~0.75 blade radius) to 230 lb. with cyclic hubs (5000 RPM and 12.5° average blade angle). During the forward flight portion of the test, it was necessary to examine the thrust balance at the tunnel dynamic pressures and representative wing tilt angles for which data was to be acquired and adjust the collective settings accordingly.

Weight tares were taken for each significant model configuration. Subsequent to the incorporation of the weight tare data into the on-line data program, wind-off data points were acquired at a couple of model angles to ensure that the weight tare routine was accurately functioning.

As mentioned previously, test BVWT 061 was performed using two different tunnel test section configurations: (1) walls/ceiling removed and solid floor for the hover portion and (2) slotted walls/ceiling/floor for the forward flight portion. In the hover runs, ground height was varied, with the wing tilt angle being held constant at 90° and fuselage angle at zero degrees. Five values of model height above the tunnel floor were preselected, with the height measured vertically from the plane of the outboard propeller. These heights corresponded to 4.0, 2.0, 1.5, 1.25, and 1.0 propeller diameters.

A dynamic problem was experienced on sting mounted Model VR068Q operating in the hover mode with the wing tilted at 90°, that resulted in a scatter of the yawing and pitching moment data. The distance from the center of the fuselage balance to the tunnel sting pivot on the vertical strut was over 25 ft. This problem, which manifested itself in a long period random-type model oscillation (approximately 10 second period), was largely circumvented by increasing the time period for data sampling to 10 seconds and averaging the moments from a minimum of three data points at the most dynamically critical test conditions.

All hover runs were performed at constant RPM: 5000 RPM with cyclic hubs and 6800 RPM with collective hubs.

Two separate test procedures were used during the forward flight portion of the test: (1) wing tilt angle pitch sweeps with the fuselage level for the descent performance runs, and

(2) fuselage angle pitch sweeps with a fixed wing tilt angle for the longitudinal stability and control runs. These transition runs were conducted with a constant tunnel q and propeller RPM (except the zero thrust coefficient, C_{T_s}, runs, wherein propeller RPM was reduced as the model was pitched to maintain zero propeller thrust).

Maximum tunnel dynamic pressure utilized during test BVWT 061 (approximately 30q) occurred during the zero thrust runs. The lowest tunnel q used (1.0q) was that that could be achieved with reasonable accuracy. This q value established the maximum test value of C_{T_s}. Tunnel dynamic pressures between these two extremes were selected to achieve the desired spread of C_{T_s} values.

Throughout the test, dynamic loads as measured by the nacelle balances (pitching moment and normal force from the four propellers and thrust of two of the propellers) were continuously monitored via oscilloscope presentations to ensure that fatigue loads inside the four nacelles were not exceeded. The drive shaft bearing temperatures in each of the nacelles were also continuously monitored to prevent running with overheated bearings.

5.2 TEST CONDITIONS

Tabulations on the following pages summarize the data runs performed during the subject test (BVWT 061)in terms of key test variables. The runs have been arranged in sets according to test objectives. Air motor jet thrust calibration runs and thrust balancing runs required for "setting-up" the model, have been deleted from the listings. All data runs were performed with the $P^{1,2}$ prop rotation (props turning down between the nacelles).

The tabulations on the following pages do not include two runs (Runs 101 and 102) that were performed to investigate the effect of propeller RPM on the forces and moments measured by the fuselage balance.

Ranges of propeller thrust, slipstream thrust coefficient, and slipstream q as attained during the runs to determine descent capability are plotted in Figures 21 through 23 and Figures 24 through 26 as a function of wing incidence angle for runs with collective hubs and cyclic pitch hubs, respectively. The range of slipstream thrust coefficient evaluated during the forward flight longitudinal stability testing varied from zero C_{T_s} to a maximum C_{T_s} of 0,97. This testing was phased so that the longitudinal stability and trim with the smaller wing tilt angles (0° and 15°) was examined at the low end of the C_{T_s} spectrum and large wing tilt angles (up to 70°)were examined at the high end.

A check was made in Run 31 to establish the variation of propeller thrust with $(RPM)^2$. This was of concern since a flexible coupling (with a thin wall to reduce centrifugal stiffening) was used to isolate propeller forces and moments. Centrifugal stiffening of the coupling would result in a low measurement of propeller thrust. If Mach number and Reynolds number effects on lift curve slope were negligible, along with coupling effects, the thrust would vary linearly with $(RPM)^2$. The data presented in Figure 27 shows that the propeller thrust varies linearly up to 5500 RPM and 2.5% beyond linear at the highest propeller speed (7400 RPM), thus indicating only small effects due to the flexible coupling.

Figure 20

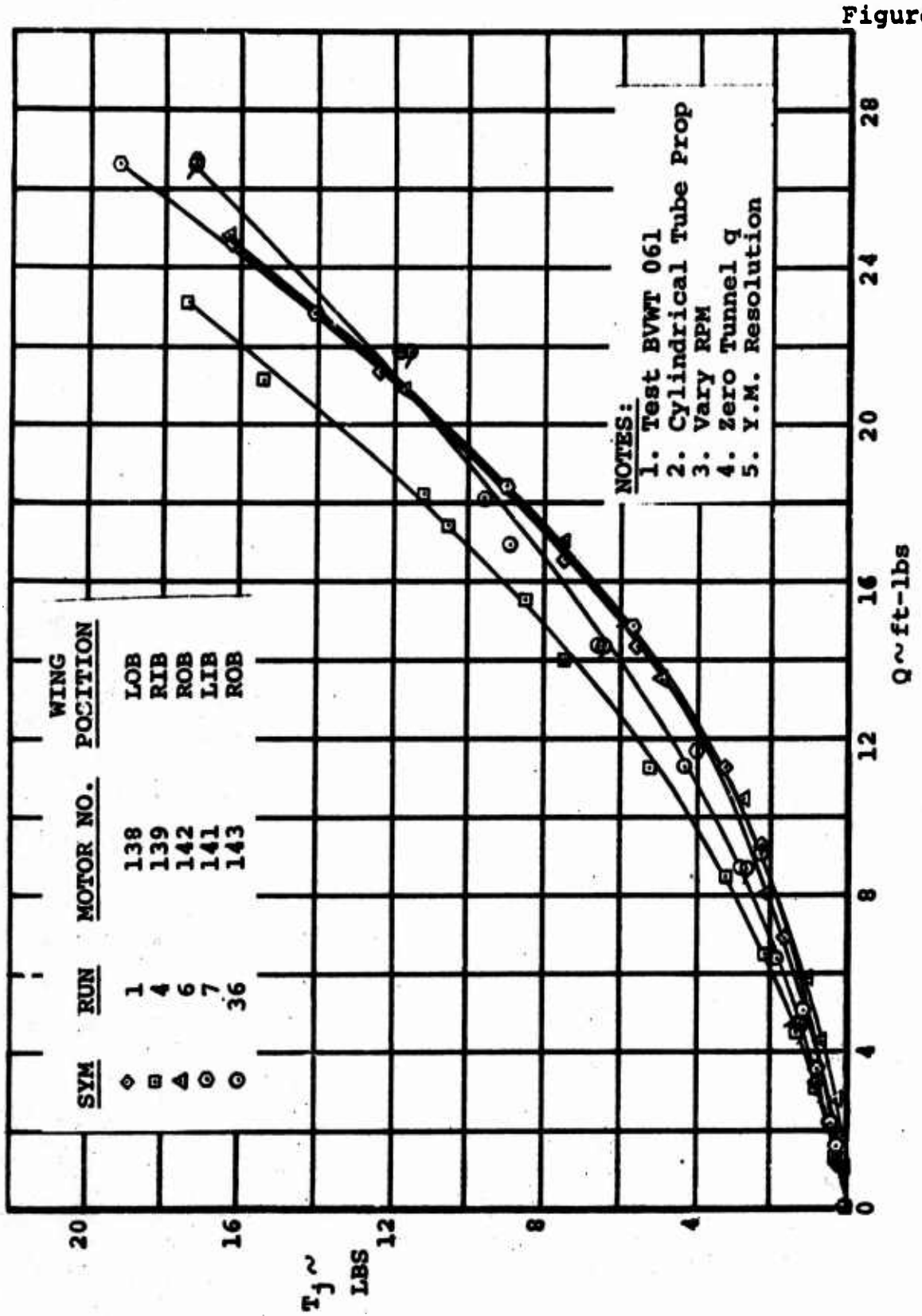

AIR MOTOR JET THRUST CALIBRATIONS

BVWT 061
RUN SUMMARY
HOVER

RUNS	HUBS	CYCLIC ANGLE	RPM	FLAP ANGLE LEFT/RT WING/WING	SPOILER ANGLE LEFT/RT WING/WING	OBJECTIVE
17	Cyclic	0°	5000	0/0	0/0	Cyclic Pitch Control
18/21	↓	+4°	↓	↓	↓	↓
22		+6°				
23		+8°				
24		-4°				
25		-6°				
26	↓	-8°	↓	↓	↓	↓
34	Coll.	---	6800	0/0	0/0	Yaw Control
40	↓	↓	↓	0/40	↓	↓
41				0/50		
42				0/60		
43				-40/60		
44				-40/0	↓	
45				0/0	40/0	
46	↓	↓	↓	0/0	60/0	↓

NOTES:

1. Wing tilt angle: 90°
2. Ground height varied for each run
3. Average collective setting with cyclic hubs: 12.5°
4. Average collective setting with collective hubs: 14°

BVWT 061
RUN SUMMARY
FORWARD FLIGHT (TRANSITION)

RUNS	HUBS	CYCLIC ANGLE	RPM	FLAP ANGLE	SLAT POSITION	C_{T_s}	OBJECTIVE
48	Coll.	---	Vary	0	0	0	Low Speed Descent Capability
49	↓	↓	✓	20°	Q10,10,10,*	✓	↓
54	↓	↓	6800	60°	↓	.85	↓
55/57	↓	↓	↓	↓	↓	.75	↓
56	↓	↓	↓	↓	↓	.64	↓
57/58	↓	↓	↓	↓	↓	.43	↓
59	↓	↓	↓	50°	Q*,10,10,*	.85	↓
60	↓	↓	↓	↓	↓	.75	↓
61	↓	↓	↓	↓	↓	.64	↓
62	↓	↓	↓	↓	↓	.43	↓
113	↓	↓	Vary	40°	↓	0	↓
133	↓	↓	✓	60°	↓	✓	↓
158	Cyclic	0°	4750	↓	↓	.85	↓
159	↓	↓	↓	↓	↓	.75	↓
160	↓	↓	↓	↓	↓	.58	↓
161	↓	↓	↓	↓	↓	.37	↓
162	↓	+4°	↓	↓	↓	.85	↓
163	↓	✓	↓	↓	↓	.75	↓

NOTES:

1. Wing tilt angle sweeps
2. Average collective setting with collective hubs: 14°
3. Average collective setting with cyclic hubs: 13°

BVWT 061
RUN SUMMARY
FORWARD FLIGHT (TRANSITION)

RUNS	HUBS	RPM	FLAP ANGLE	i_w	STAB. ANGLE	C_{T_s}	OBJECTIVE
63-65	Coll.	6800	60°	30°	---	.55,.70,.81	Tail Off
66-68	↓	↓	↓	↓	+20°	.81,.70,.55	Long. Stab.
69-71	↓	↓	↓	↓	+15°	↓	Horiz.Tail
72-74	↓	↓	↓	↓	+10°	↓	Effective-
75	↓	↓	↓	↓	+25°	.81	ness and
80-82	↓	↓	↓	15°	--	.70,.50,.30	Trim
83-86	↓	↓	↓	↓	+10°	↓	↓
87-89	↓	↓	↓	↓	+15°	↓	↓
90-92	↓	↓	↓	↓	+5°	↓	↓
93/94	↓	↓	↓	↓	+20°	.70,.50	↓
95/97	↓	↓	40°	0°	---	.50,.30	↓
98-100/112	↓	6000	↓	↓	---	.50,.30,0	↓
103-105	↓	↓	↓	↓	-5°	↓	↓
106-108	↓	↓	↓	↓	0°	↓	↓
109-111	↓	↓	↓	↓	-10°	↓	↓
114/115	↓	↓	0°	↓	---	.30,0	↓
116/117	↓	↓	↓	↓	-5°	↓	↓
118/119	↓	↓	↓	↓	-10°	↓	↓
120/121	↓	↓	↓	↓	0°	↓	↓
122/123	↓	↓	60°	45°	---	.92,.81	↓
124/125	↓	↓	↓	↓	+35°	↓	↓
126/127	↓	↓	↓	↓	+30°	↓	↓
128/129/131	↓	↓	↓	↓	+25°	↓	↓
130	↓	↓	↓	↓	+20°	.81	↓
132	↓	↓	↓	55°	---	.94	↓
134	↓	↓	↓	↓	+45°	↓	↓
135	↓	↓	40°	↓	---	↓	↓
136	↓	↓	↓	70°	---	.97	↓
137-139	↓	↓	↓	30°	---	.81,.70,.55	↓
140-142	↓	↓	↓	↓	+15°	↓	↓
143-145	↓	↓	↓	↓	+20°	↓	↓
147-149	↓	↓	↓	↓	+25°	↓	↓
150/151	↓	↓	↓	↓	+10°	.70,.55	↓
152/153	↓	↓	60°	↓	+20°	↓	Check at lower RPM
154/155	↓	↓	✓	↓	✓	↓	Center slat removed

NOTES:
1. Fuselage angle sweeps
2. Average collective setting: 14.25°
3. Slat setting: 0*, 10,10,*
4. RPM actually varied during zero C_{T_s} runs to maintain zero thrust.

Figure 21

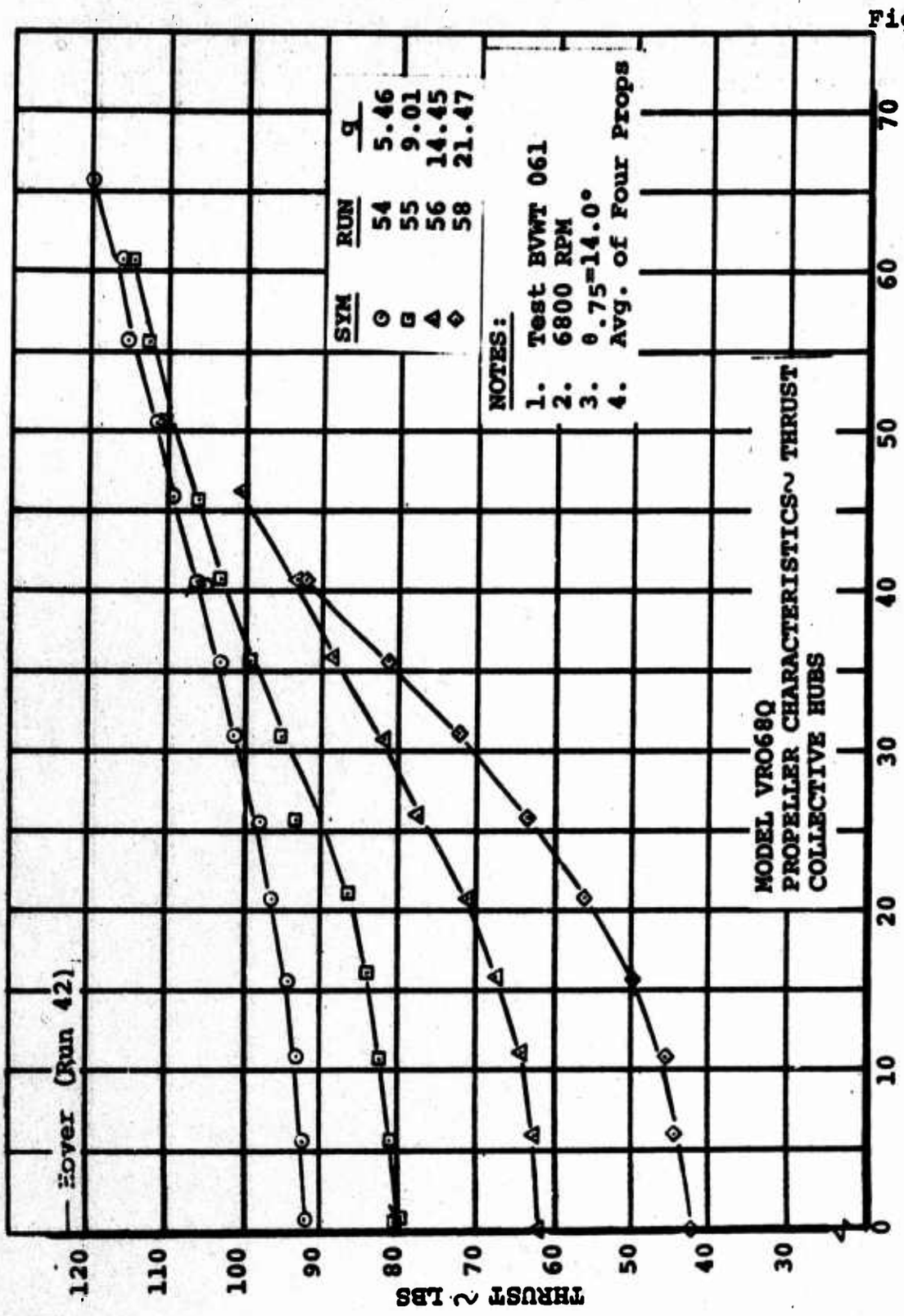
MODEL VR068Q
PROPELLER CHARACTERISTICS - THRUST
COLLECTIVE HUBS
NOTES:
1. Test BVWT 061
2. 6800 RPM
3. θ.75=14.0°
4. Avg. of Four Props
SYM RUN q
54 5.46
55 9.01
56 14.45
58 21.47
Hover (Run 42)
THRUST - LBS
WING INCIDENCE ANGLE, i_w, DEGREES

Figure 22

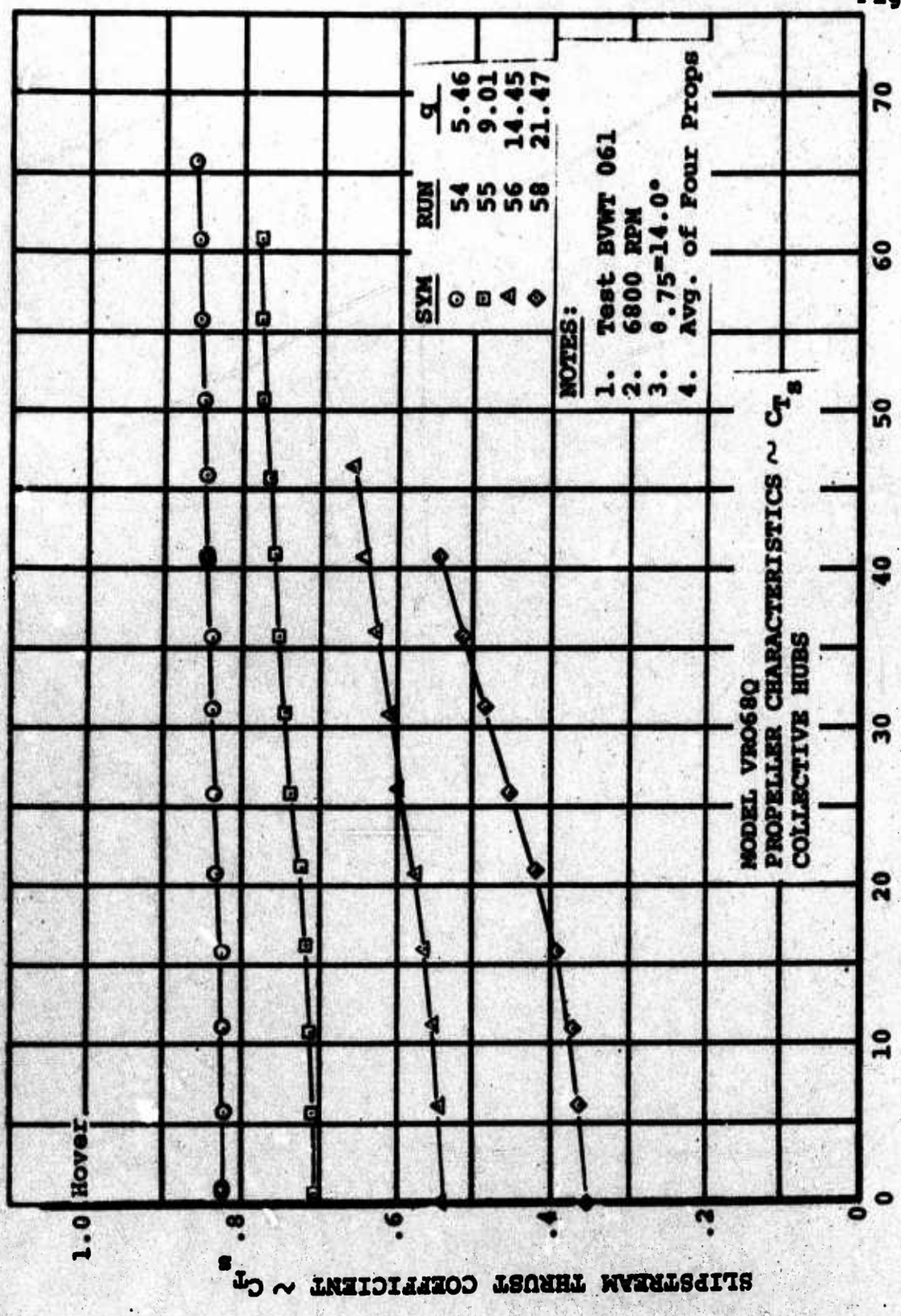
MODEL VR068Q
PROPELLER CHARACTERISTICS ~ C_{T_s}
COLLECTIVE HUBS
NOTES:
1. Test BVWT 061
2. 6800 RPM
3. θ.75=14.0°
4. Avg. of Four Props
SYM RUN q
54 5.46
55 9.01
56 14.45
58 21.47
Hover
1.0
.8
.6
.4
.2
0
10
20
30
40
50
60
70
SLIPSTREAM THRUST COEFFICIENT ~ C_{T_s}
WING INCIDENCE ANGLE, i_w ~ DEGREES

Figure 23

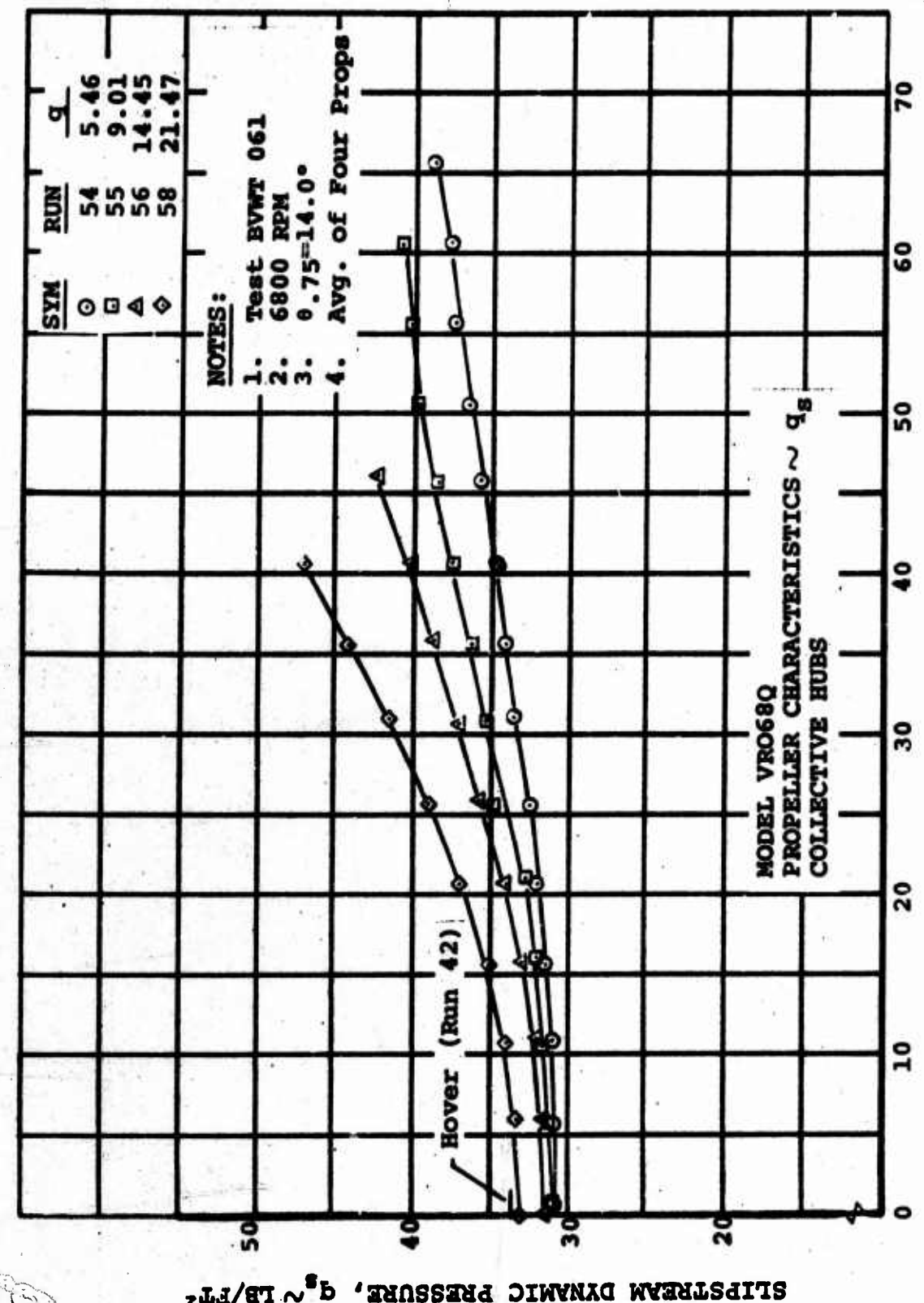
SYM
RUN
q
54 5.46
55 9.01
56 14.45
58 21.47
NOTES:
1. Test BVWT 061
2. 6800 RPM
3. 0.75=14.0°
4. Avg. of Four Props
MODEL VR068Q
PROPELLER CHARACTERISTICS ~ q_s
COLLECTIVE HUBS
Hover (Run 42)
SLIPSTREAM DYNAMIC PRESSURE, q_s~ LB/FT²
WING INCIDENCE ANGLE, i_w~ DEGREES
50
40
30
20
0
10
20
30
40
50
60
70

Figure 24

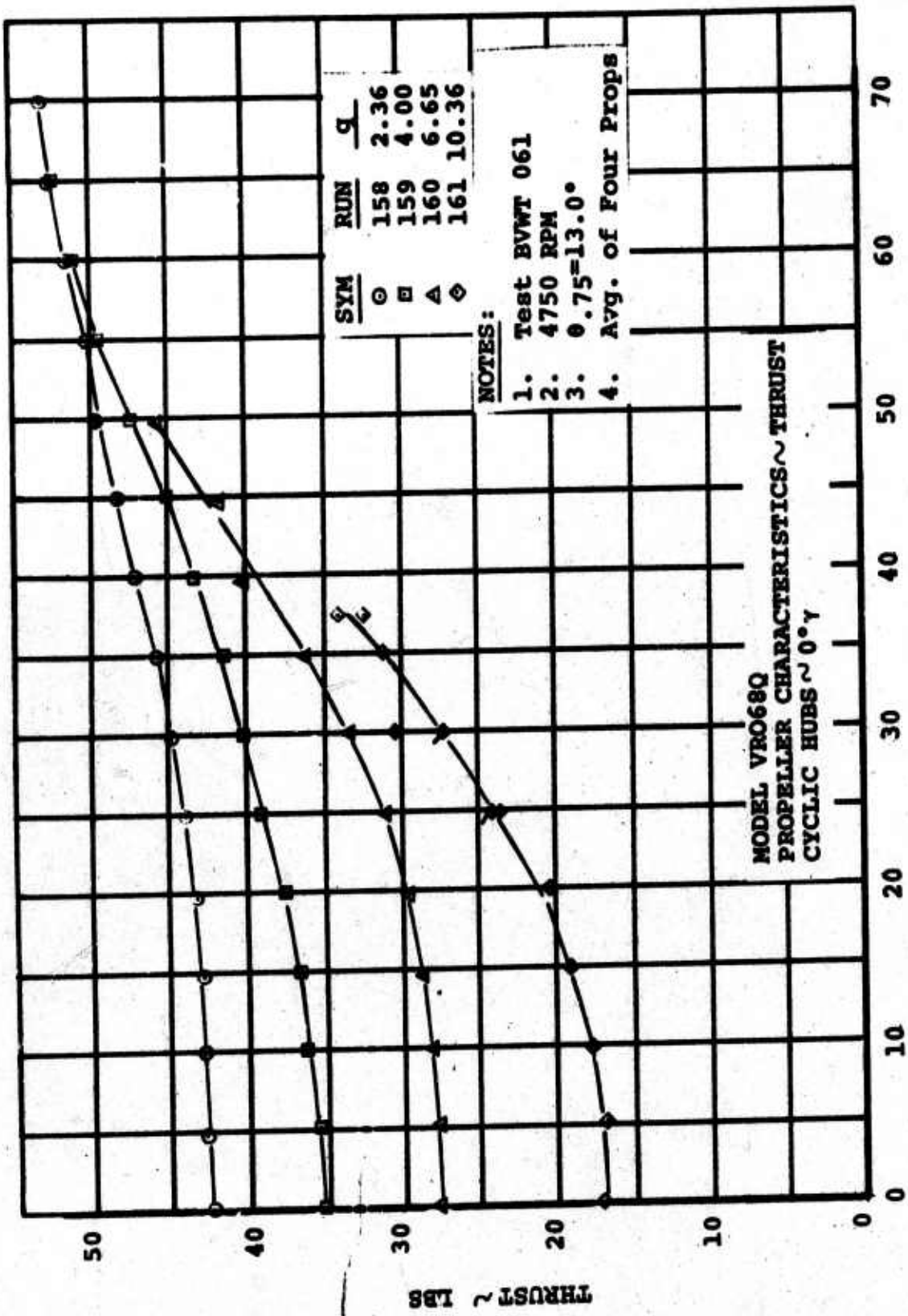
MODEL VR068Q
PROPELLER CHARACTERISTICS ~ THRUST
CYCLIC HUBS ~ 0°γ
NOTES:
1. Test BVWT 061
2. 4750 RPM
3. 0.75=13.0°
4. Avg. of Four Props
SYM RUN q
158 2.36
159 4.00
160 6.65
161 10.36
THRUST ~ LBS
WING INCIDENCE ANGLE, i_w ~ DEGREES
0
10
20
30
40
50
60
70

Figure 25

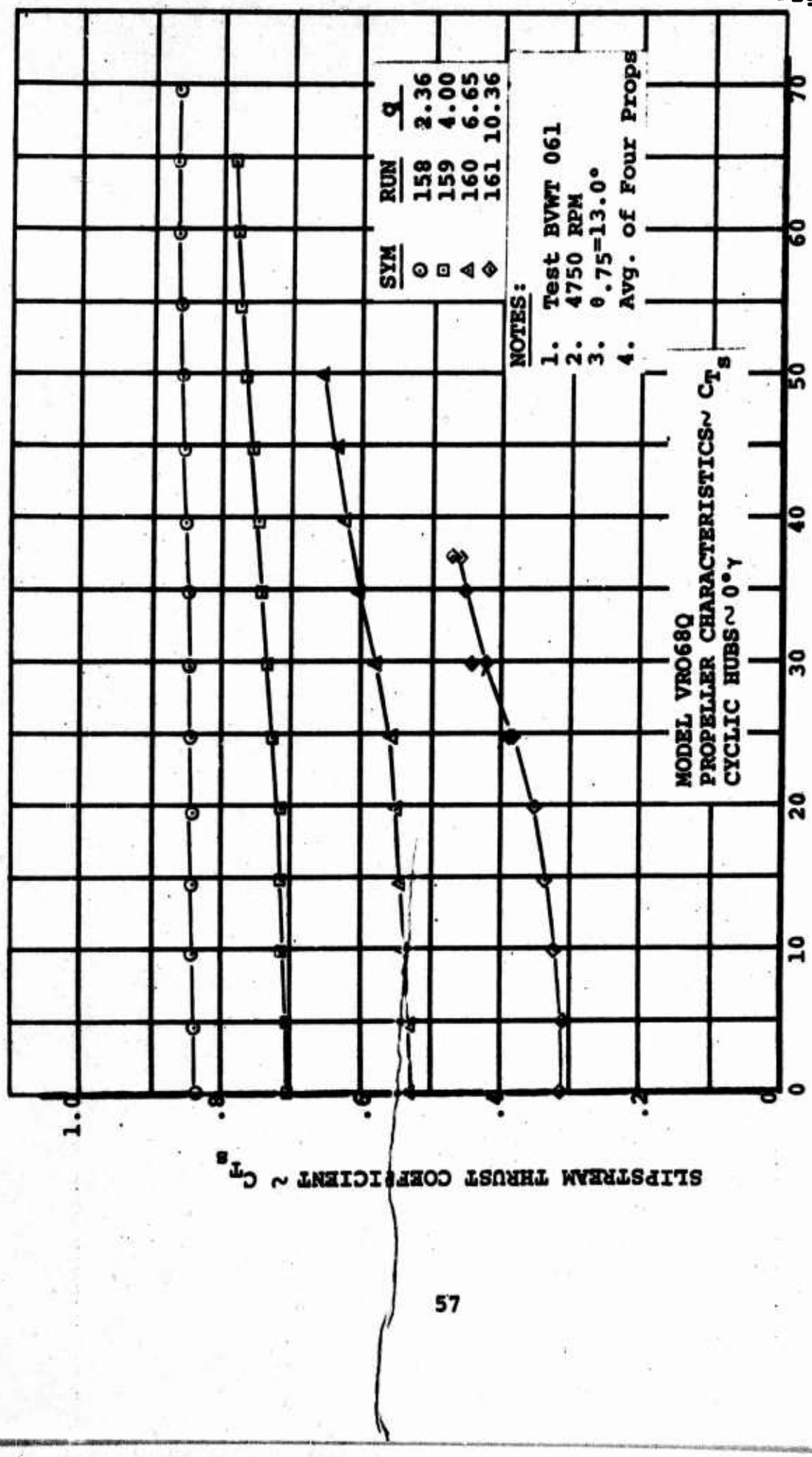
MODEL VRO68Q
PROPELLER CHARACTERISTICS, C_{T_s}
CYCLIC HUBS ~ 0°
NOTES:
1. Test BVWT 061
2. 4750 RPM
3. θ.75=13.0°
4. Avg. of Four Props
SYM RUN q
158 2.36
159 4.00
160 6.65
161 10.36
SLIPSTREAM THRUST COEFFICIENT, C_{T_s}
WING INCIDENCE ANGLE, i_w, DEGREES

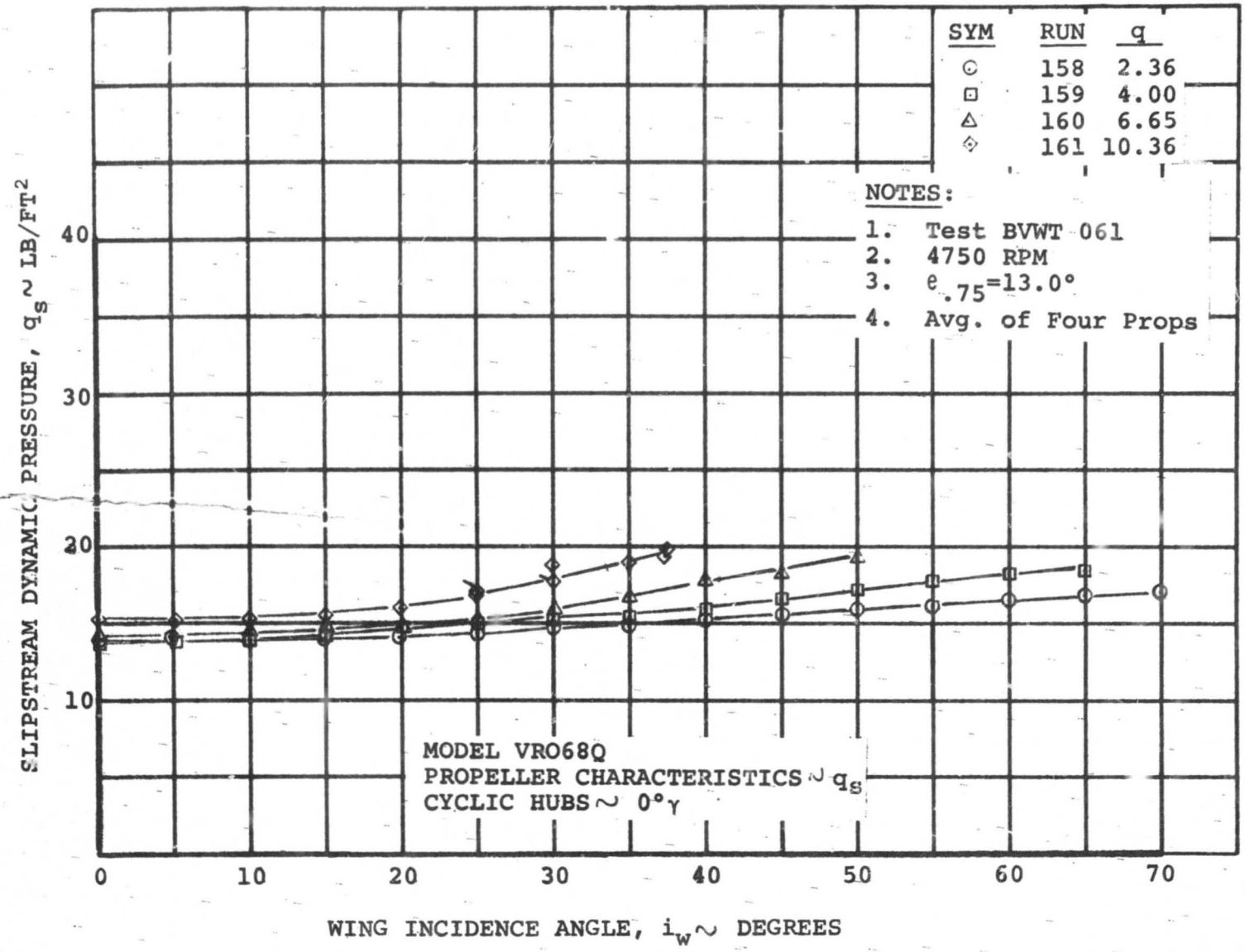

Figure 26

D170-10038-1

Figure 27

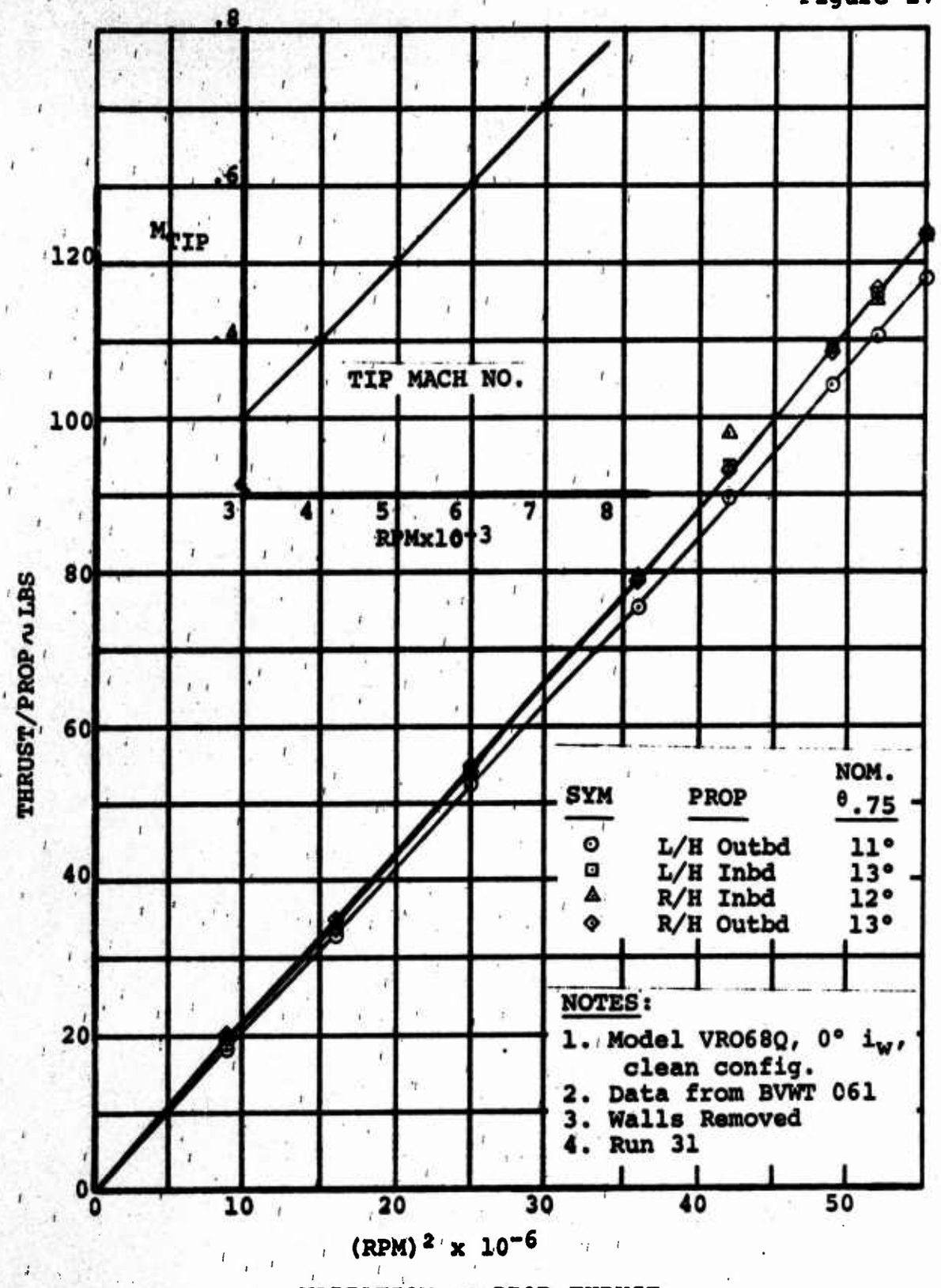

VARIATION OF PROP THRUST WITH $(RPM)^2$

6.0 TEST RESULTS AND DISCUSSION

The primary objectives of this Phase I test of the full span four prop tilt wing Model VRO68Q, which was equipped with cyclic pitch propellers for low speed longitudinal control, were outlined in the Introduction and consisted of the following four major topics.

a. Cyclic Pitch Control in Hover
b. Yaw Control in Hover
c. Low Speed Descent Performance
d. Longitudinal Stability and Control in Transition

In addition to the above listed objectives, the data from the subject test can be used in conjunction with the data acquired during the isolated prop test of an identical prop/hub/nacelle assembly (Reference 1) to determine the effect of the wing on propeller forces and moments.

As mentioned previously, in the Introduction, the damage to the aft radial Lamiflex bearings in the left inboard cyclic pitch hub assembly that occurred during cyclic pitch running on August 20, 1970 (Run 163), resulted in the remainder of the cyclic pitch runs planned for Phase I and not performed, to be rescheduled for completion during the later Phase II test.

6.1 CYCLIC PITCH CONTROL IN HOVER

The effectiveness of the propellers in producing aircraft pitching moment when cyclic pitch is applied was investigated in the hover mode with a clean configuration (no flaps or slats extended/horizontal tail removed) and the wing tilted to 90°. Data was acquired at five preselected ground heights which varied from an h/D of 4.0 to an h/D of 1.0. The parameter h/D, has been defined as the ratio of the distance between the outboard propeller plane and ground plane to the propeller diameter. For clarification purposes, other key model height relationships are compared below to the parameter chosen.

If h(outboard prop plane)/D = 1.0
h(inboard prop plane)/D = 1.129
h(wing pivot point)/D = 0.642

Presented in Figure 28 is the measured variation of aircraft pitching moment (about the wing pivot) with cyclic angle for the ground heights tested. The variation is found to be linear over the range of cyclic pitch angles evaluated (-8° to +8°) and the aircraft pitching moment is seen to be essentially invariant with ground height, however, there is an indication of a "fall-off" in pitching moment at h/D's of 1.5 and 1.25 for cyclic angles of +6° and +8°. Since the same trend was not exhibited with negative cyclic angles, the noted "fall-off" is probably data scatter. The following check was made to assure that the positive aircraft pitching moment measured with zero cyclic angle resulted largely from the moment produced by the propeller thrustlines being located below the wing pivot.

$$\frac{M}{D \cdot T} = \frac{Z_{INBD} + Z_{OUTBD}}{2D}$$

Z_{INBD}, distance from inbd prop thrustline to wing pivot
Z_{OUTBD}, distance from outbd prop thrustline to wing pivot
D, prop diameter

$$\frac{M}{D \cdot T} = \frac{1.35" + .341"}{2(25.72")} = .033 \text{ (noted on Figure 28)}$$

Figure 29 is an equivalent presentation for the left inboard prop as measured by the nacelle balance. The hub pitching moment is linear over the cyclic angle range tested and does not vary to any extent with ground height.

Depicted in Figure 30 is a comparison for the h/D=4.0 case of the hub pitching moment variation with cyclic pitch angle for the four propellers. No major difference (beyond a value of 10% favoring the outboard props) can be ascertained between the ability of the inboard props and outboard props to

produce hub pitching moment upon application of cyclic pitch. The average value of hub pitching moment coefficient per degree of cyclic ($\Delta C_{M_p}/\Delta\gamma$=.00205) agrees well with the corresponding value measured ($\Delta C_{M_p}/\Delta\gamma$=.00215) during the isolated propeller test reported in Reference 1. Thus, it appears that there is no influence of the wing and fuselage on the cyclic pitch effectiveness in hover.

Incremental aircraft pitching moment (about the wing pivot) due to cyclic as measured by the fuselage balance is compared in Figure 31 for the h/D=4.0 case, to the averaged prop hub moment as measured by the four nacelle balances. It can be noted that the aircraft pitching moment produced by cyclic is 27% greater than that contributed by the four propeller hubs. The positive difference is attributed to the prop normal force acting about the wing pivot.

Figure 32 examines the variation of prop normal force with cyclic pitch and ground height. This figure shows that the change in prop normal force with cyclic is in the correct direction, i.e. with positive cyclic a negative increment in prop normal force is produced that in turn produces a negative pitching moment about the wing pivot. The following calculation was made to evaluate the magnitude of aircraft pitching moment resulting from prop normal force.

$$\left(\frac{\Delta M}{D \cdot T}\right)_{PIVOT} = \frac{\Delta C_{NF_{P_{OUTBD}}} \left(x_{OUTBD}\right) + \Delta C_{NF_{P_{INBD}}} \left(x_{INBD}\right)}{2D \cdot C_T}$$

$\Delta C_{NF_{P_{OUTBD}}}$ = .0143 for 8° of cyclic

x_{OUTBD} = .768 ft., distance from prop plane to pivot

$\Delta C_{NF_{P_{INBD}}}$ = .0178 for 8° of cyclic

x_{INBD} = 1.045 ft., distance from prop plane to pivot

C_T = .171, average prop thrust coefficient

$$\left(\frac{\Delta M}{D \cdot T}\right)_{PIVOT} = \frac{.0178(1.045)+.0143(.768)}{(2)(2.143)(.171)}$$

=.04 for 8° of cyclic (noted in Figure 31)

The average value of prop normal force coefficient per degree of cyclic ($\Delta C_{NF_p}/\Delta\gamma$=.0160/8=.002) measured during this test can be noted to be over twice that measured during the isolated prop test of Ref 1. This difference requires more investigation.

Effect of Cyclic Pitch on Thrust

Figure 33 depicts the small changes in average thrust coefficient that occurred as cyclic pitch was applied and the distance of the model from the ground was decreased. For this figure, the average thrust coefficient was chosen to be presented in lieu of individual propeller thrust coefficients, as a result of the small differences in thrust that existed between propellers. Figure 33 shows a 4% decrease in thrust coefficient upon application of 8° of cyclic pitch for a propeller operating at constant RPM and collective, whereas, the isolated prop data reported in Reference 1, indicates a 4% increase for the comparable hover test condition.

Effect of Cyclic Pitch on A/C Longitudinal Force

The variation in longitudinal force with ground height and cyclic pitch angle is presented in Figures 34 and 35 for negative cyclic angles and positive cyclic angles, respectively. Longitudinal force is expressed in terms of the ratio of fore and aft force to total propeller thrust and consequently, represents fore and aft aircraft acceleration in hover. Figures 34 and 35 show that as the aircraft approaches the ground (h/D=1.0 and zero cyclic pitch) more of the propeller slipstream is turned forward than aft, resulting in a net aft longitudinal force acting on the aircraft $\left(\frac{-X}{T}\right)$. The effect of cyclic pitch control application, when in the proximity of the ground, is to increase the net aft longitudinal force with negative cyclic angles and decrease the net aft longitudinal force with positive cyclic angles.

Noted on Figures 34 and 35 are the incremental amounts of prop normal force for 8° of cyclic as determined by the nacelle balances and the following calculation.

$$\Delta X/T = \Delta C_{NF_p}/C_T$$

ΔC_{NF_p} = .016 for 8° of cyclic, average four props

C_T = .171, average prop thrust coefficient

$$\Delta X/T = \frac{.016}{.171}$$

= .093, positive for positive cyclic

It appears that when cyclic pitch is utilized out-of-ground effect, the X force generated on the wing by the propeller slipstream is in the opposite direction to the prop normal force and tends to offset it.

Effect of Cyclic Pitch on Shaft Power

The effect of cyclic pitch on propeller shaft power (includes the friction losses in the cyclic hub assembly) at the different hover heights evaluated is presented in Figures 36 and 37. Shaft power for the inboard props is shown in Figure 36. Corresponding information for the outboard props is shown in Figure 37. A line has been drawn in each of these figures to represent the average variation of shaft power with cyclic pitch for the h/D=4.0 case, that is the average power variation considering both positive and negative cyclic angles. Proximity of the ground can be noted to exert only a small influence on the power requirements.

The average shaft power curves (h/D=4.0) of Figures 36 and 37, reduced to the form of $C_p/C_{p_{\gamma=0}}$, are compared in Figure 38 to to the corresponding curve obtained during the isolated prop test reported in Reference 1. Shaft power increase due to cyclic as measured during the isolated prop test is seen to be essentially an average of that measured on the outboard and inboard props of the subject test.

The outboard props exhibit higher power requirements than the inboard props. This is probably a result of the overlapping, whereby the outboard props have been placed in the direct influence of the inboard props. However, the difference in power requirements between the outboard and inboard props appears to be excessive.

Noted in Figure 38 is the friction power increment as measured by the rolling moment components of the six component nacelle balances. The difference between the shaft power curve and the friction power is the aerodynamic power required by the cyclic pitch action.

Figure 28

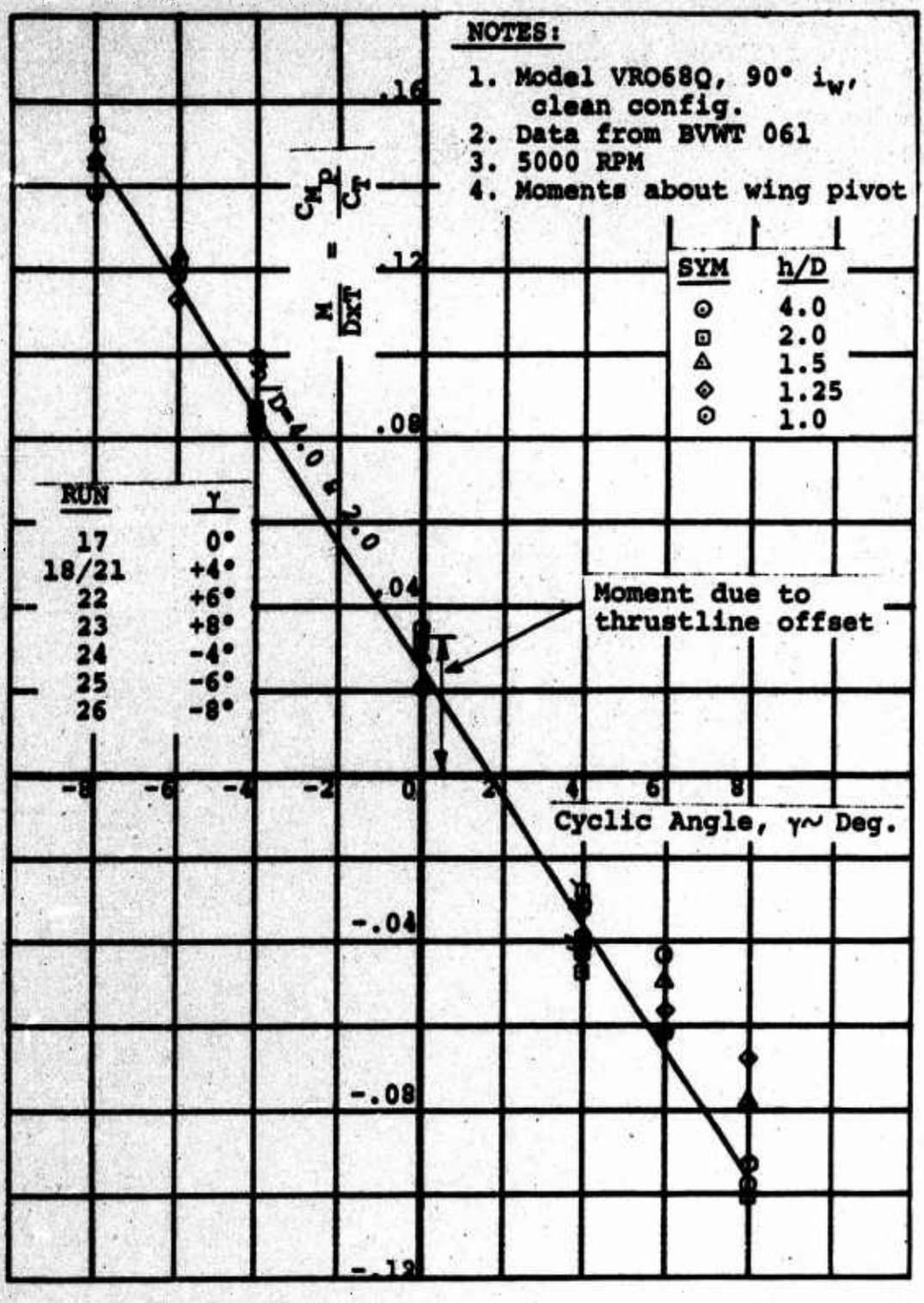

A/C PITCHING MOMENT DUE TO CYCLIC IN HOVER
VARYING GROUND HEIGHT

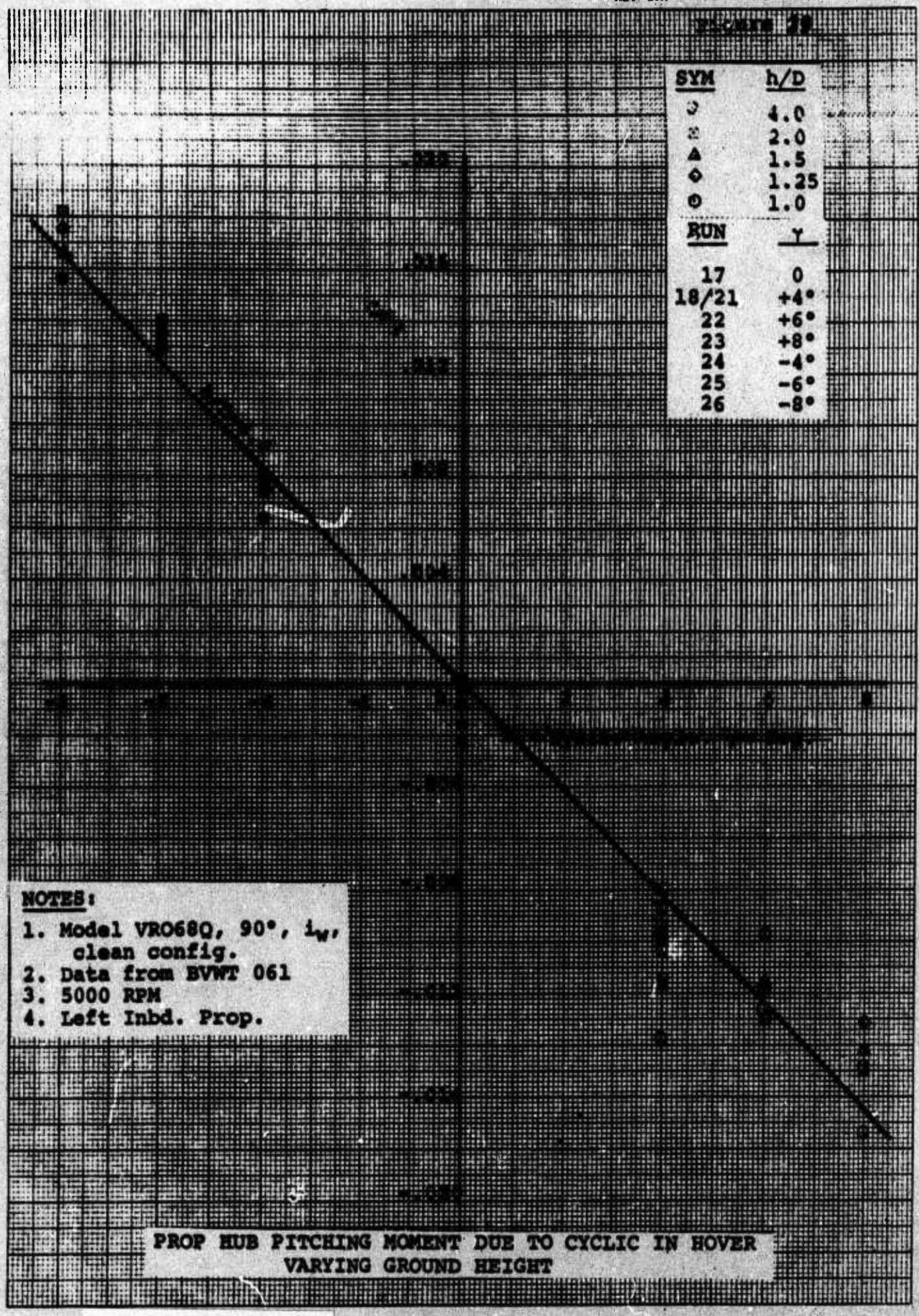

PROP HUB PITCHING MOMENT DUE TO CYCLIC IN HOVER
VARYING GROUND HEIGHT

EUGENE DIETZGEN CO.
MADE IN U. S. A.
NO. 340R-HP DIETZGEN GRAPH PAPER
MILLIMETER

NOT REPRODUCIBLE

Figure 30

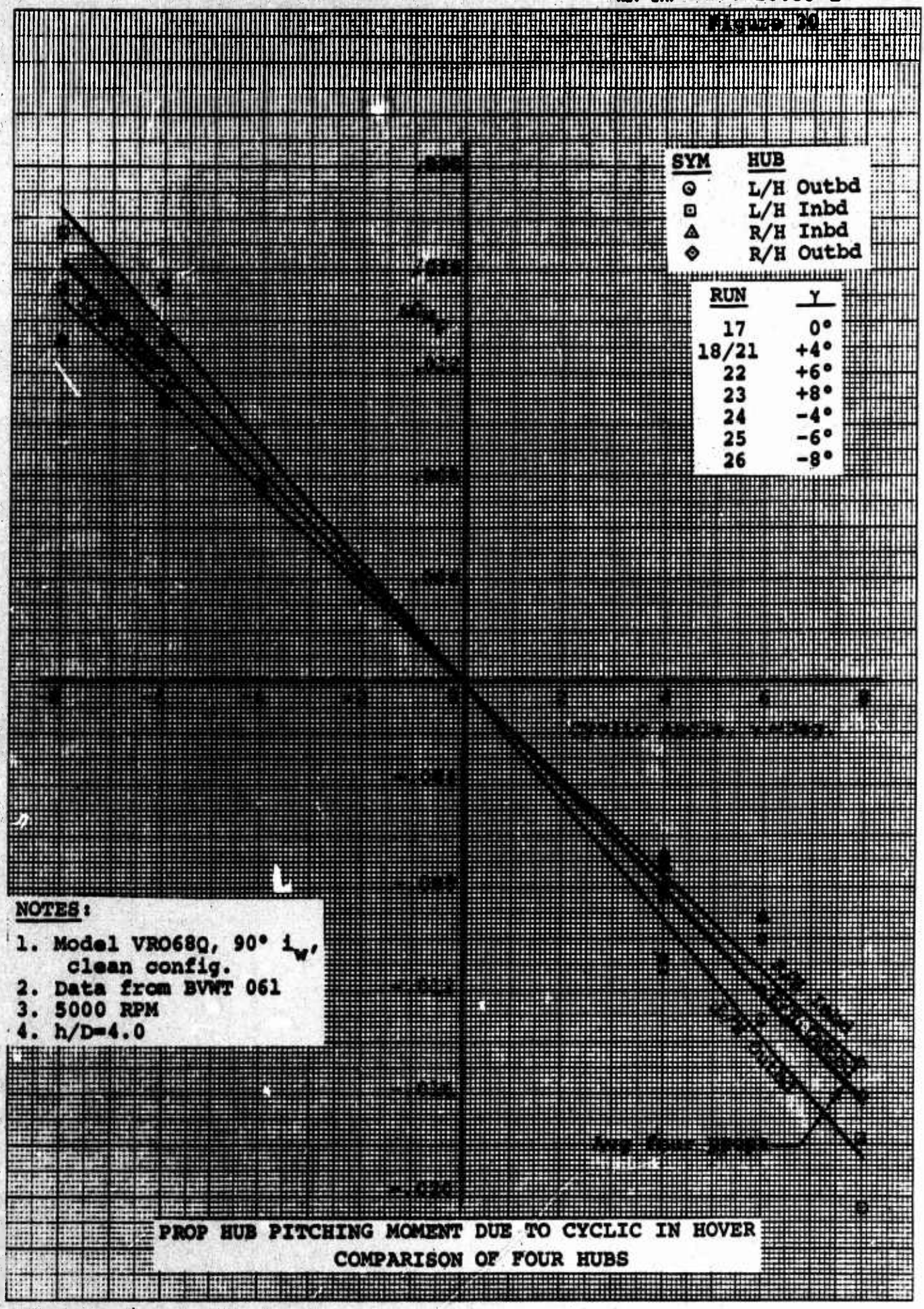

PROP HUB PITCHING MOMENT DUE TO CYCLIC IN HOVER
COMPARISON OF FOUR HUBS

NO. 340R-MP DIETZGEN GRAPH PAPER
MILLIMETER
MADE IN U. S. A.

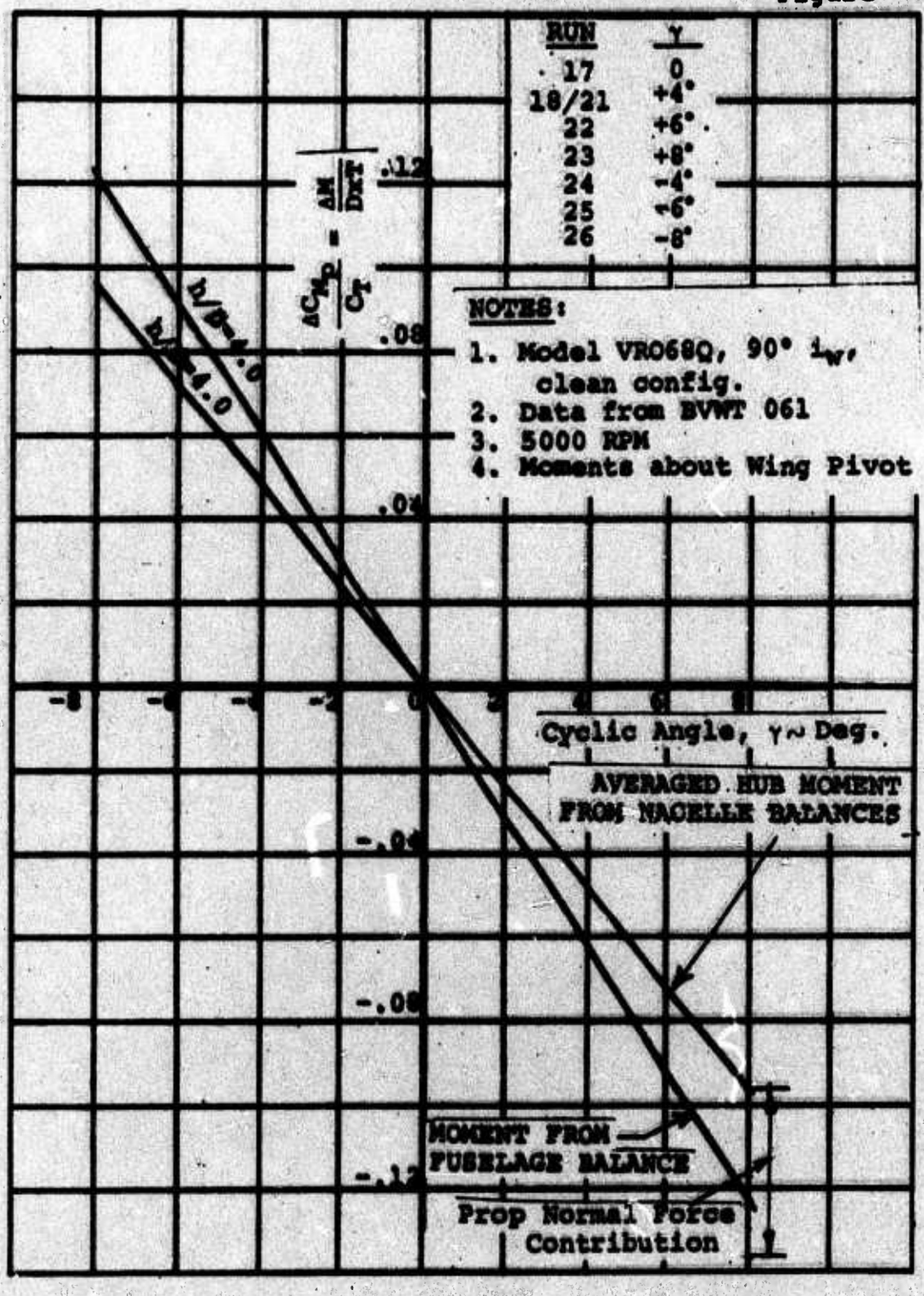

COMPARISON OF A/C PITCHING MOMENT DUE TO CYCLIC WITH HUB PITCHING MOMENT HOVER

Figure 34

SYM	h/D
○	4.0
□	2.0
△	1.5
◇	1.25
⊙	1.0

RUN	γ
17	0
18/21	+4°
22	+6°
23	+8°
24	-4°
25	-6°
26	-8°

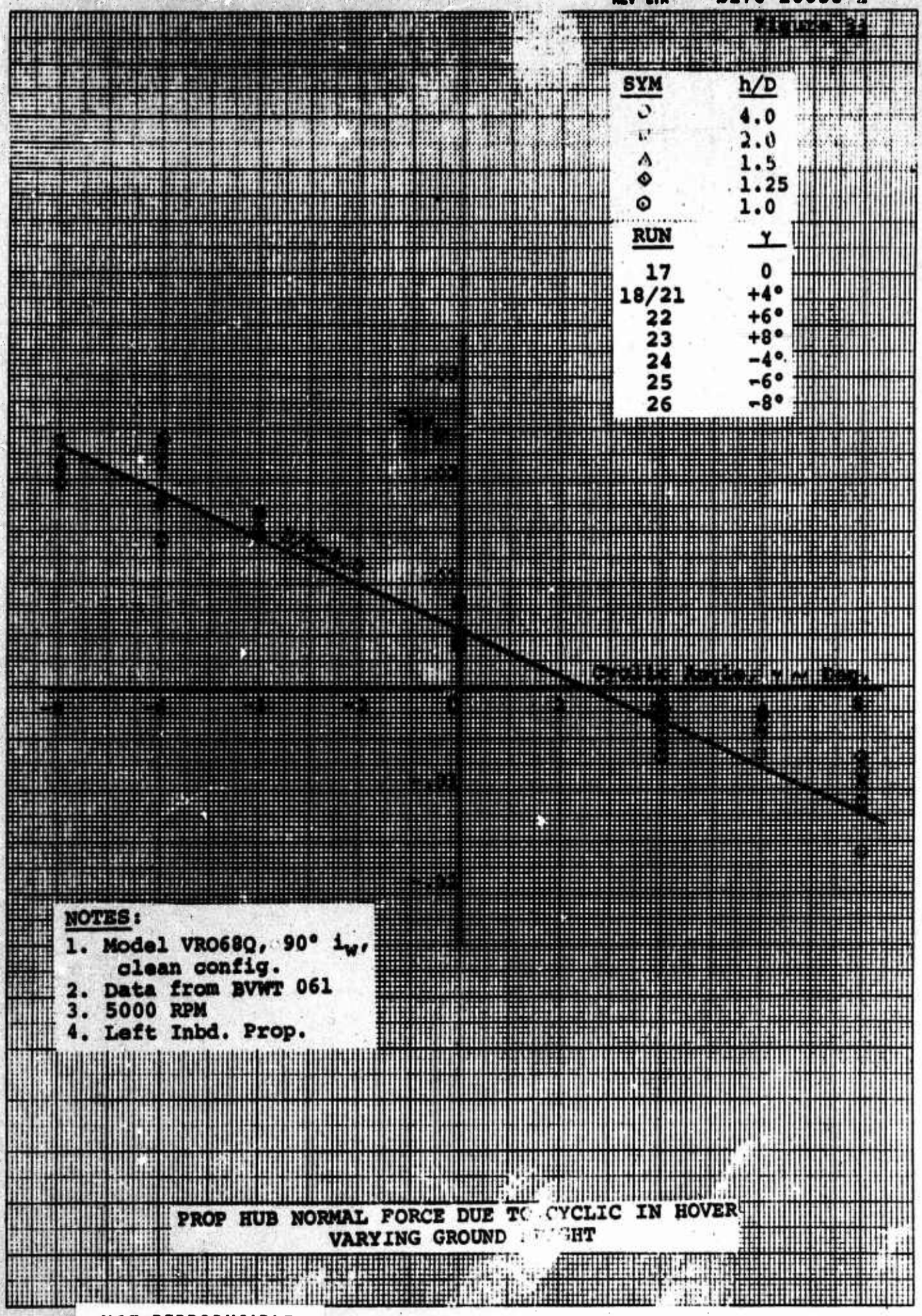

NOTES:
1. Model VRO68Q, 90° i_w, clean config.
2. Data from BVWT 061
3. 5000 RPM
4. Left Inbd. Prop.

PROP HUB NORMAL FORCE DUE TO CYCLIC IN HOVER
VARYING GROUND HEIGHT

NOT REPRODUCIBLE

EUGENE DIETZGEN CO.
MADE IN U.S.A.
NO. 340R-MP DIETZGEN GRAPH PAPER
MILLIMETER

Figure 33

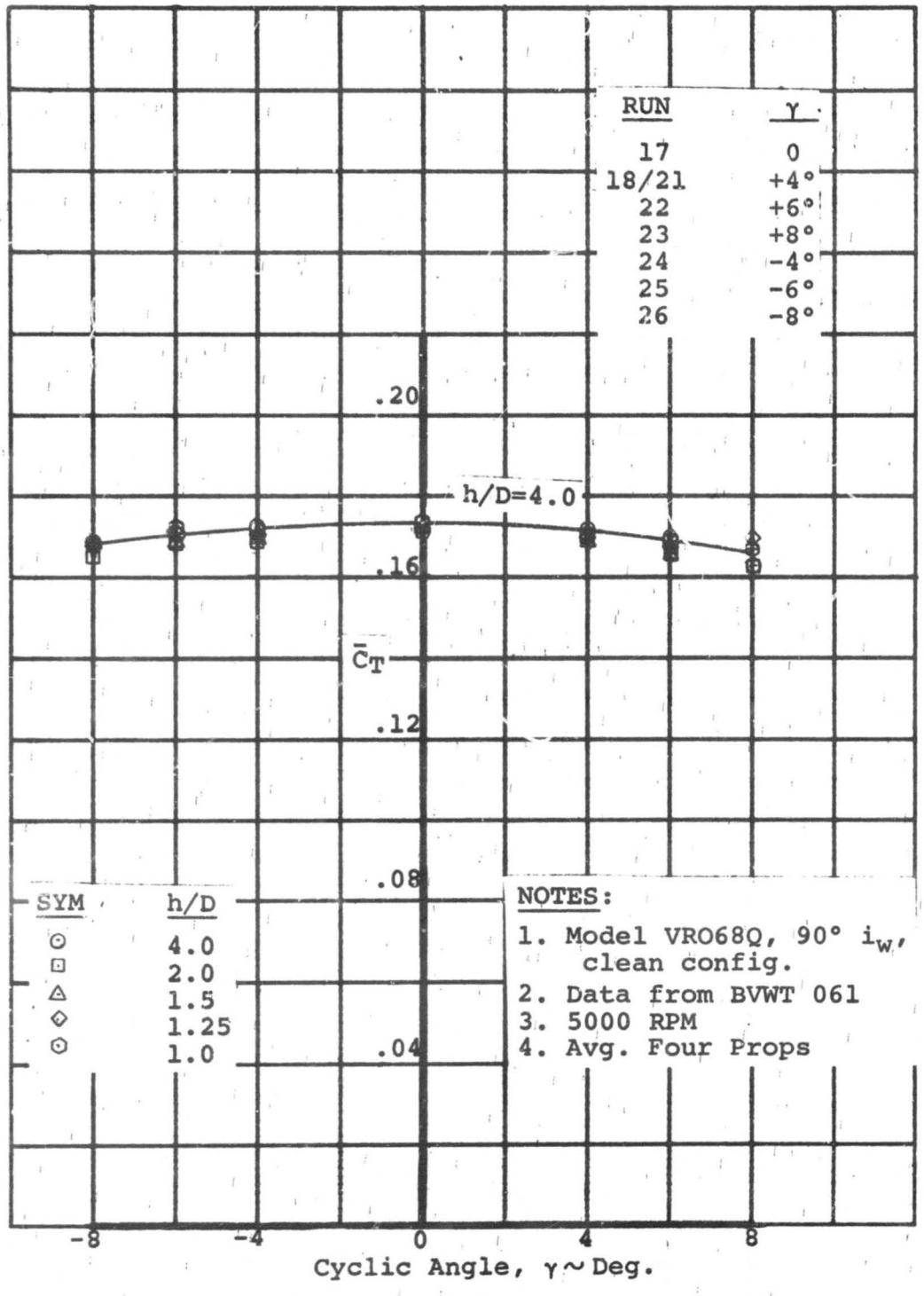

VARIATION OF THRUST WITH CYCLIC IN HOVER
VARYING GROUND HEIGHT

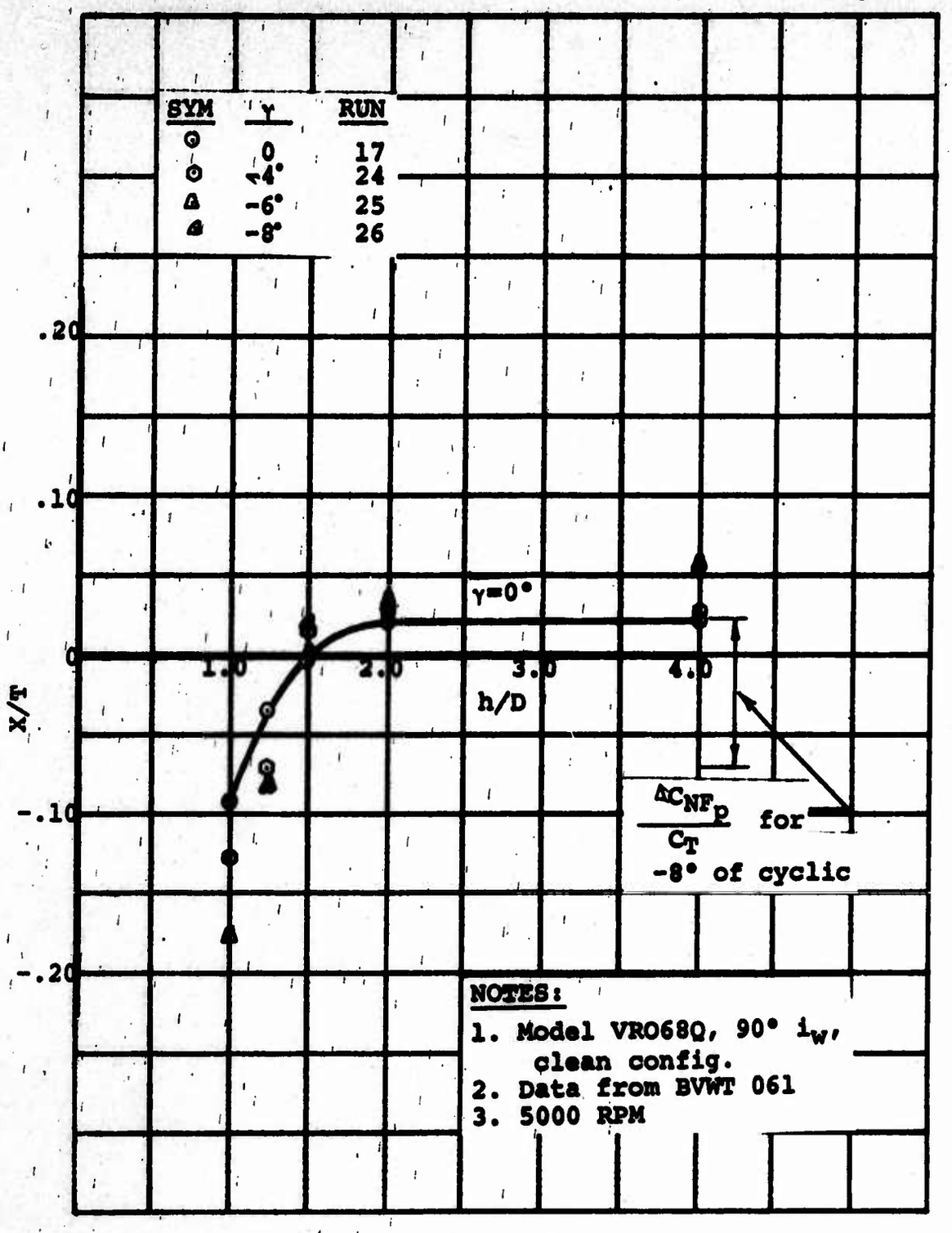

VARIATION OF X FORCE WITH HOVER GROUND HEIGHT
NEGATIVE CYCLIC PITCH

Figure 35

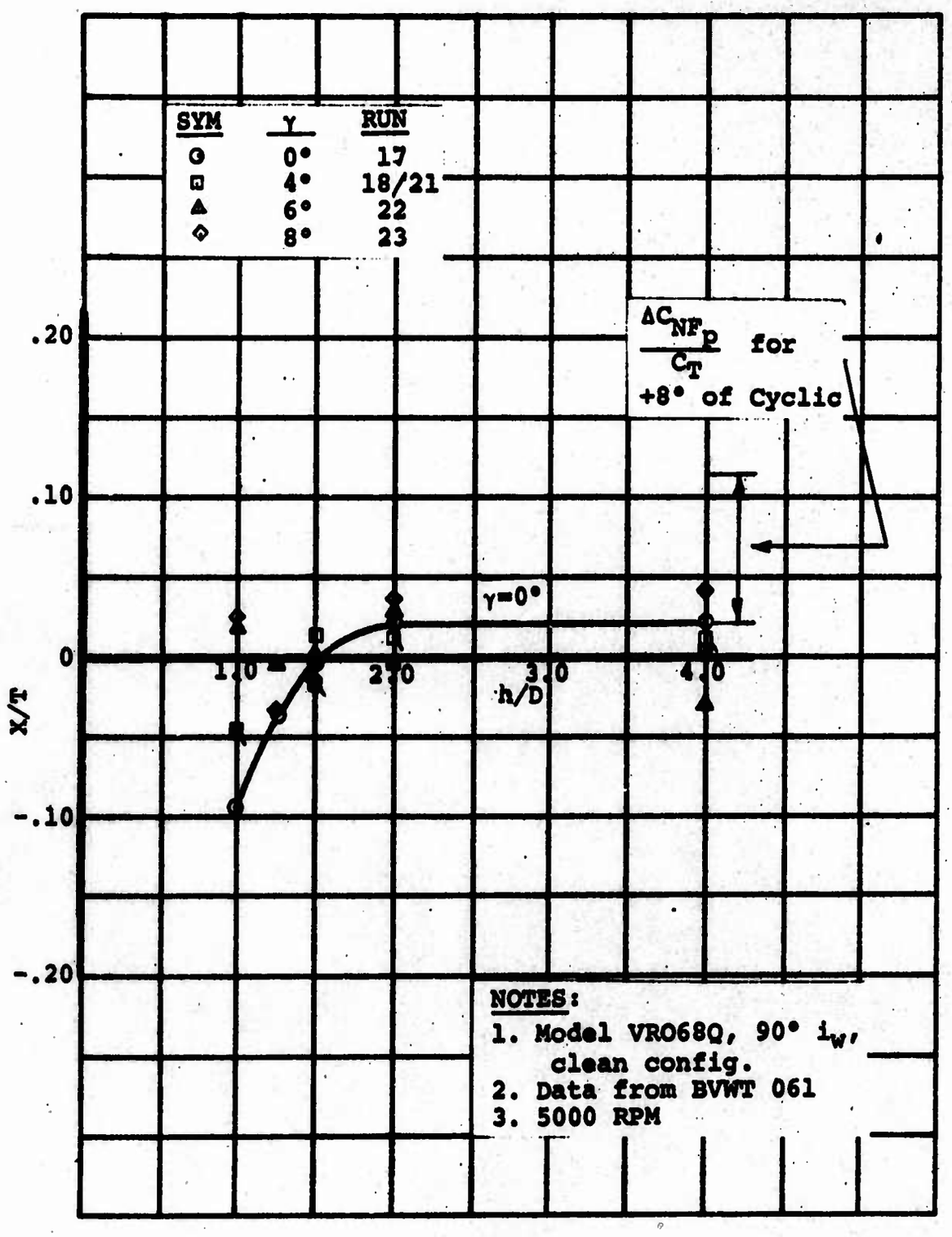

VARIATION OF X FORCE WITH HOVER GROUND HEIGHT
POSITIVE CYCLIC PITCH

Figure 36

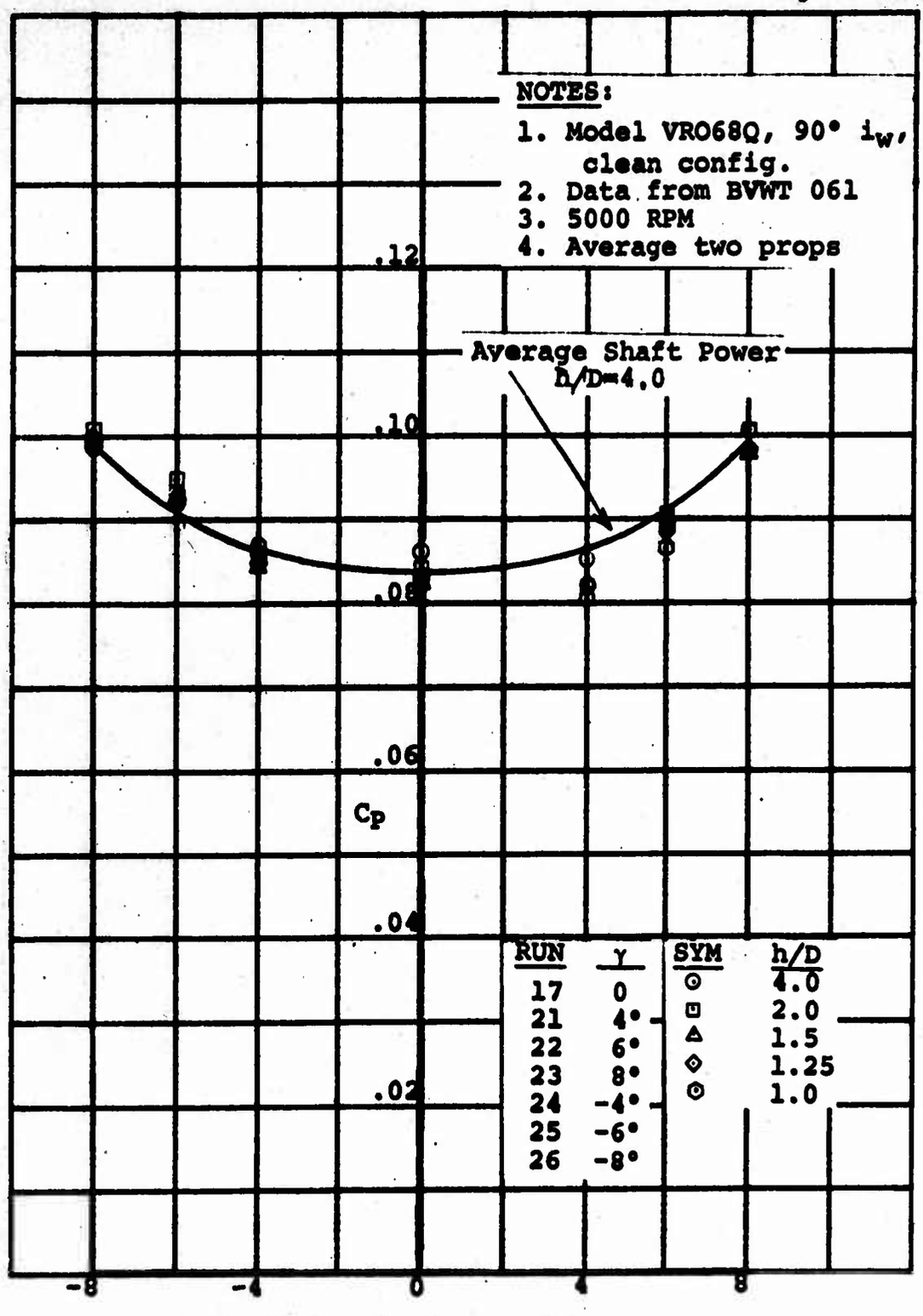

EFFECT OF CYCLIC AND HOVER GROUND HEIGHT ON SHAFT POWER - INBD PROPS

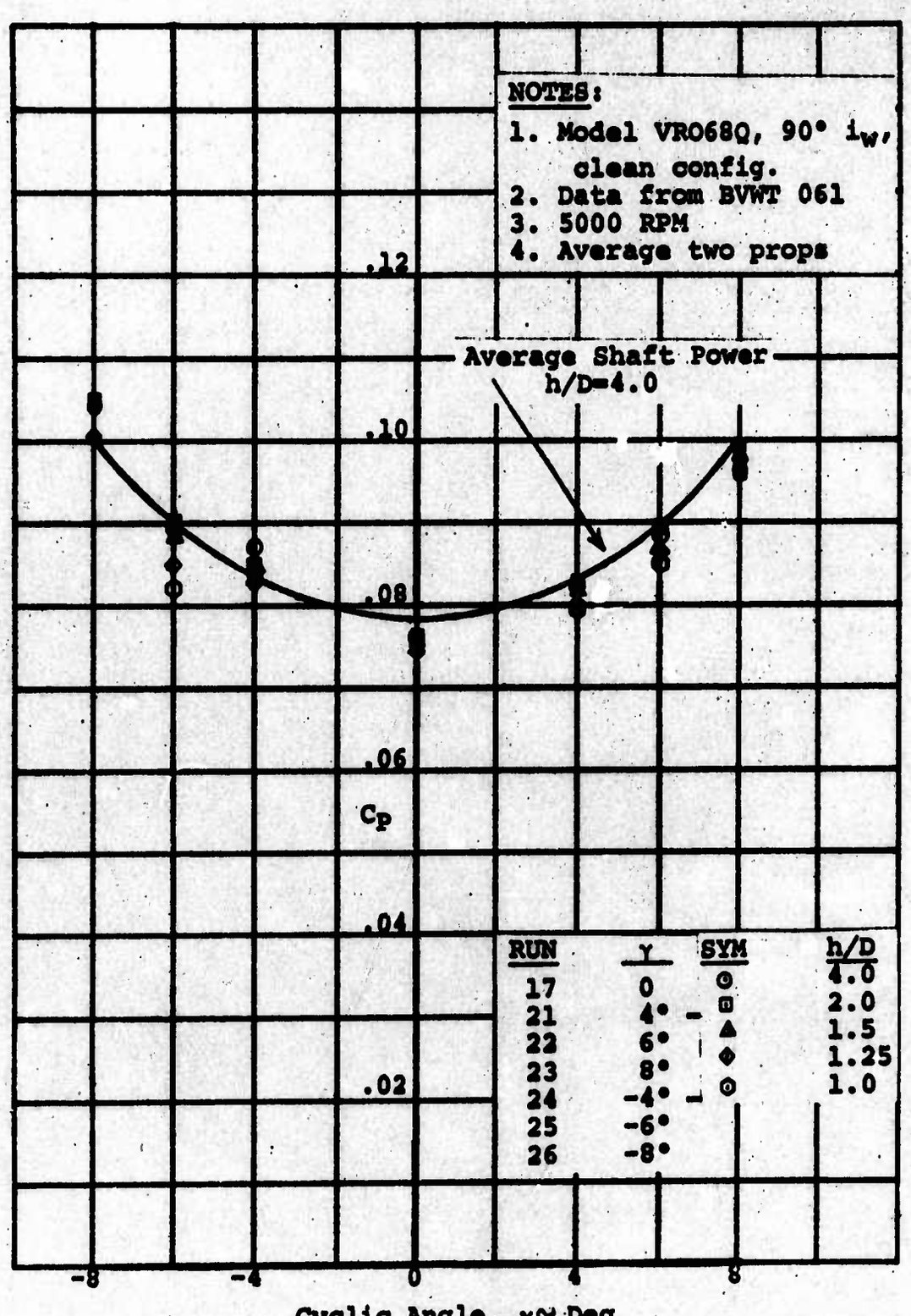

EFFECT OF CYCLIC AND HOVER GROUND HEIGHT ON SHAFT POWER - OUTBD PROPS

Figure 38

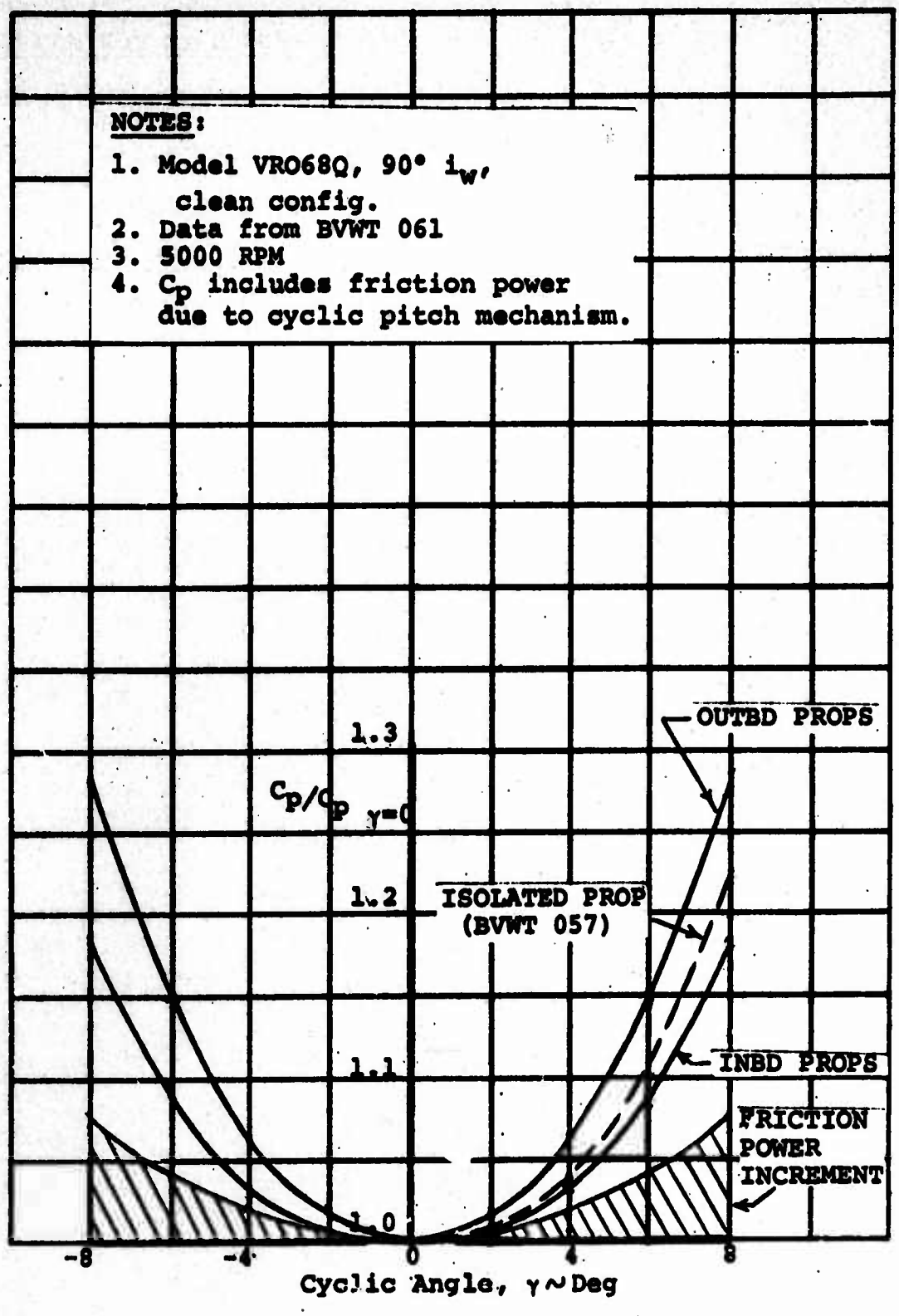

INCREASE IN SHAFT POWER DUE TO CYCLIC HOVER AT h/D=4.0

6.2 YAW CONTROL IN HOVER

Yaw control in hover is achieved by differential wing surface control deflections, that is, the double slotted flaps are deflected down on one wing and both the flaps and spoilers are deflected up on the opposite wing. The flap arrangement for the downward flap deflections tested on the right wing is depicted in Figures 6 and 7. Figure 9 shows the up-flap position tested on the left wing.

The hover mode yaw control testing accomplished during Phase I test BVWT 061 was conducted with the leading edge slats retracted, a wing tilt angle of 90°, horizontal tail removed, the $P^{1,2}$ prop rotation (both props turning down between the nacelles), and a propeller speed of 6800 RPM, which resulted in a hover disc loading of 34 lb/ft^2 with the collective blade angle setting of 14°. Data was acquired at the same five preselected ground heights used for the cyclic pitch control testing, namely, h(height of outboard prop plane to ground plane)/D values that ranged from 4.0 to 1.0. Results of this hover yaw control testing are presented in terms of the non-dimensional yawing moment parameter Y.M./ℓT, wherein

Y.M.,	aircraft yawing moment	ft.lbs.
ℓ,	average distance from inboard and outboard propeller ℄'s to fuselage ℄ (2.653 ft. on the model)	ft.
T,	propeller thrust (total)	lbs.

Hover yaw control power available with the double slotted flaps was measured incrementally, that is, separate runs were performed with the following yaw control configurations.

a. Double slotted flaps deflected down on the right wing, clean left wing.

b. Up-flap deflection on the left wing, clean right wing.

c. Differential flap deflection, flaps down on the right wing and up on the left wing.

Yaw Control with Downward Flap Deflection

Non-dimensional yawing moment essentially varied linearly with flap angle over the angle range evaluated (40°, 50° and 60°) and ground height ratios tested as shown in Figure 39. Note that the lines were drawn to intersect the abscissa at 5° of flap angle.

Flap angle on Model VR068Q was defined as the angle between the main flap chord line in the retracted position and the main flap chord line in the extended position. See Figures 6 and 7 for sketches of the deflected flap. The relatively high wing thickness ratio (21% t/c at the body ℄ to 15% t/c at the tip) in combination with the large flap Fowler action results in the flap being tilted down in the retracted position. See Figure 8. If in the initial portion of the flap extension process, the flap is moved aft along its own chord line (main flap chord line), the flap would be deflected at a net negative angle. As a consequence, the effective zero position for the flap was chosen as 5° δ_F, which is the average angle between the main flap chord line and the wing chord line. This angle varies from 5.7° at the body ℄ to 4.5° at the tip.

Figure 40 illustrates the variation in non-dimensional yawing moment with h/D for the various downward flap deflections tested. At ground heights less than a value corresponding to an h/D of 1.50, the yawing moment capability decreases at a relatively high rate.

Run 42 (δ_F=60°) was used in conjunction with Run 34 (δ_F=0°) to calculate the slipstream turning angle, θ, for the out-of-ground effect conditions (h/D=4.0 and 2.0). In this calculation, it was assumed that the forces acting on the right wing were independent of those acting on the left wing.

$$\theta = \tan^{-1} \frac{\text{net X force on right wing}}{\text{net L (lift) on right wing}}$$

$$= \tan^{-1} \frac{-80.9 \text{ lbs.(Run 42)} - 5.5 \text{ lbs.(Run 34)}}{439 \text{ lbs.(total~ Run 42)} - 239.4 \text{ lbs.(left wing L)}}$$

$$= \tan^{-1} \frac{-86.4}{199.6}$$

$$= .433 \text{ or } 23.4°$$

This number agrees well with the value that would be predicted using Section 9.2 of DATCOM (Reference 2) for a double slotted flap of comparable flap chord to diameter ratio, $C_{F/D}$.

$$C_{F/D} = C_{F/c} \ (c/D)$$

$C_{F/c}$ = .49 (ratio extended flap chord to wing chord ~ constant percentage for wing)

c/D = .45 (ratio of average wing chord to diameter)

$C_{F/D}$ = .221

DATCOM indicates a max turning angle of 24° for this ratio.

Yaw Control with Differential Flap Deflections

Figure 41 shows the yaw control available with the flap deflected differentially: 60° down on the right wing and 40° up on the left wing. Data is also presented in this figure from the runs performed with the individual flap motions. It is shown by the dashed line on the plot, that the yawing moment achieved with the individual motions is directly additive, i.e. the same total value of Y.M./ΔT was obtained when the up and down flaps were operated simultaneously on opposite wings as for the summation of the individual contributions. Noted in Figure 41 is the h/D ratio that corresponds to the aircraft hovering in-ground-effect with wheels two ft. off the ground.

Since an out-of-ground effect condition exists at h/D's greater than 2.0, it would be expected that the measured yawing moment would not change, especially decrease between values of h/D of 2.0 and 4.0. This was not reflected in the test data from Model VRO68Q as Figure 41 clearly shows, but was indicative, however, of the hover yaw control data acquired during the four prop tilt wing testing that Boeing-Vertol conducted in 1969 in the same wind tunnel. It should be pointed out that the 1969 tests were performed on a model that was power limited to a hover disc loading that was approximately only 1/3 of that achieved in the subject test.

During the BVWT 061 hover testing, long wool tufts were placed around the model such as on the open railing located at the sides of the ground plane, to check for recirculation. No tuft movement of any magnitude could be discerned at model heights of 4.0 and 2.0 h/D. The tufts were not placed in a position, though, that could completely check whether some flow was being induced through the tunnel circuit. This will be accomplished during the Phase II test to help resolve the data inconsistency noted.

Model dynamics is another factor that could be contributing to this problem. The necessity for data sampling over a ten second time period to reduce data scatter was discussed previously in the Test Procedure write-up. During the hover runs, it was observed that the dynamics problem, which largely manifested itself in data scatter was more critical at some model heights than at others.

Yaw Control with Spoilers

Figures 42 and 43 present the yawing moment capability with spoilers alone for two different angles of deflection, 40° and 60°. Effectiveness at the 60° angle was still in the linear range as shown in Figure 42. One characteristics of the spoiler, when utilized for hover yaw control, is that the decrease in yawing moment capability with ground height is not as

large percentagewise as with trailing edge flaps. Compare Figures 43 and 40.

Hover Download due to Yaw Control

Figures 44 thru 46 present the loss in vertical lifting capability associated with the use of wing control surfaces for hover yaw control. The download shown in these figures, was calculated as a percentage of the total propeller thrust as measured at each data point.

$$\text{Hover Download, } \%T = \left(1 - \frac{\text{Normal Force}}{T}\right) 100$$

Figures 44 thru 46 show the download as a function of ground height for the following configurations, respectively: down flaps on one wing alone, differential flaps, and spoilers deflected on one wing alone. In each case tested, the download varies from a maximum for the out-of ground effect condition to a net upload at the lowest model height evaluated (h/D=1.0). This upload is probably a result of the positive pressures being generated on the bottom of the fuselage.

As would be expected the maximum download measured (11.7%) was recorded with the differential flap configuration (60° flaps deflected down on the right wing and 40° flaps deflected up on the opposite wing). Of this 11.7% value, an increment of 1.7% was measured with the clean wing.

Effect of Hover Yaw Controls on Thrust

The table in Figure 47 lists the total propeller thrust measured during each hover yaw control run. Each thrust has been normalized with respect to the clean wing run (Run 34). The normalized numbers listed, indicate that the deflection of the hover yaw control devices reduced the overall thrust by 1.0 to 1.5%.

Figure 48 illustrates the small change in total propeller thrust that occurred with ground height.

Longitudinal Force Due to Hover Yaw Control Deflections

Figure 49 shows that the differential flap configuration of 60° down on one wing and 40° up on the opposite wing produces a net aft acting force. This occurred as a result of the positive or forward force produced by the 40° up flap being too small in magnitude to offset the larger negative or aft force generated by the 60° down flap.

Aircraft Pitching Moment due to Hover Yaw Control Deflections

In hover, the aircraft pitching moment about the wing pivot with the yaw control devices undeflected, is nose-up of the magnitude shown in Figure 50. This nose-up moment, which is essentially invariant with ground height, is a result of the propeller thrust lines being located below the wing pivot as illustrated earlier in the report (Figure 28). The net effect of deflecting the flaps differentially is to reduce the magnitude of the nose-up moment.

A cyclic pitch angle of 1.1° would be required to trim out the pitching moment producing by the differential flap action ($.017 \frac{M}{D_i T}$ increment between clean wing curve and-40°/60° flaps extended curve in Figure 50.).

Yaw Hover Control Requirement

The necessary value of the non-dimensional parameter Y.M./ℓT is 0.293 for a representative tilt wing transport-type aircraft hovering at its design "V" gross weight of 86,930 lbs. and meeting a 0.5 radian/sec^2 yaw angular acceleration level. The value 0.293 was developed from the following calculation.

$$\frac{Y.M.}{\ell T} = \frac{\ddot{\psi} I_{zz}}{\ell T}$$

$\ddot{\psi}$ = 0.5 radian/sec^2, yaw angular acceleration

I_{zz} = 1.66(10^6) slug ft^2, yaw moment of inertia

ℓ = 32.53 ft (full scale aircraft)

T = 86,930 lbs (assuming T/W=1.0)

$$\frac{Y.M.}{\ell T} = \frac{0.5(1.66)10^6}{(32.53)(86,930)} = 0.293$$

The maximum value recorded in the test was 0.28. See Figure 41.

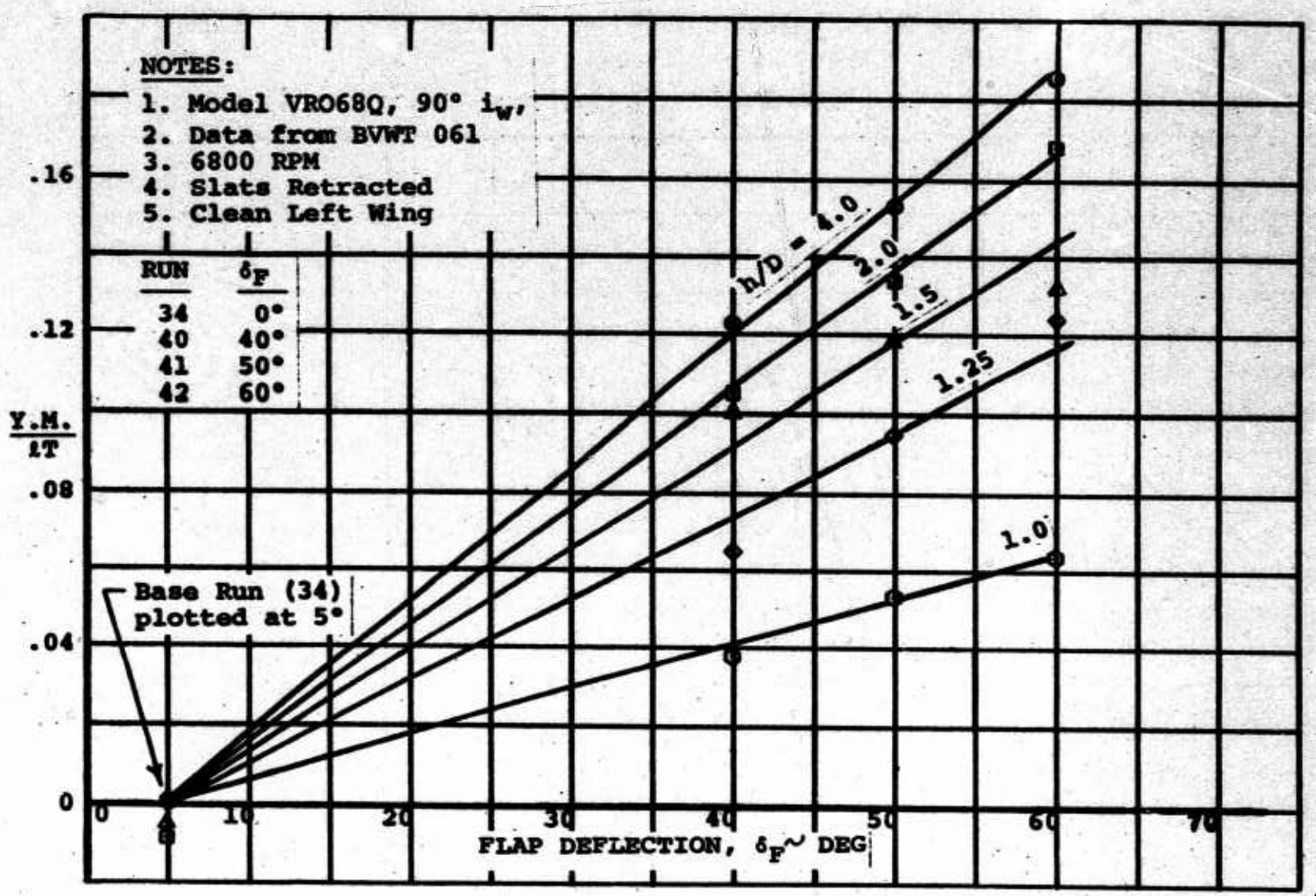

VARIATION OF HOVER YAW CONTROL WITH FLAP DEFLECTION
DOWN FLAP ~ RIGHT WING

Figure 39

D170-10038-1

Figure 40

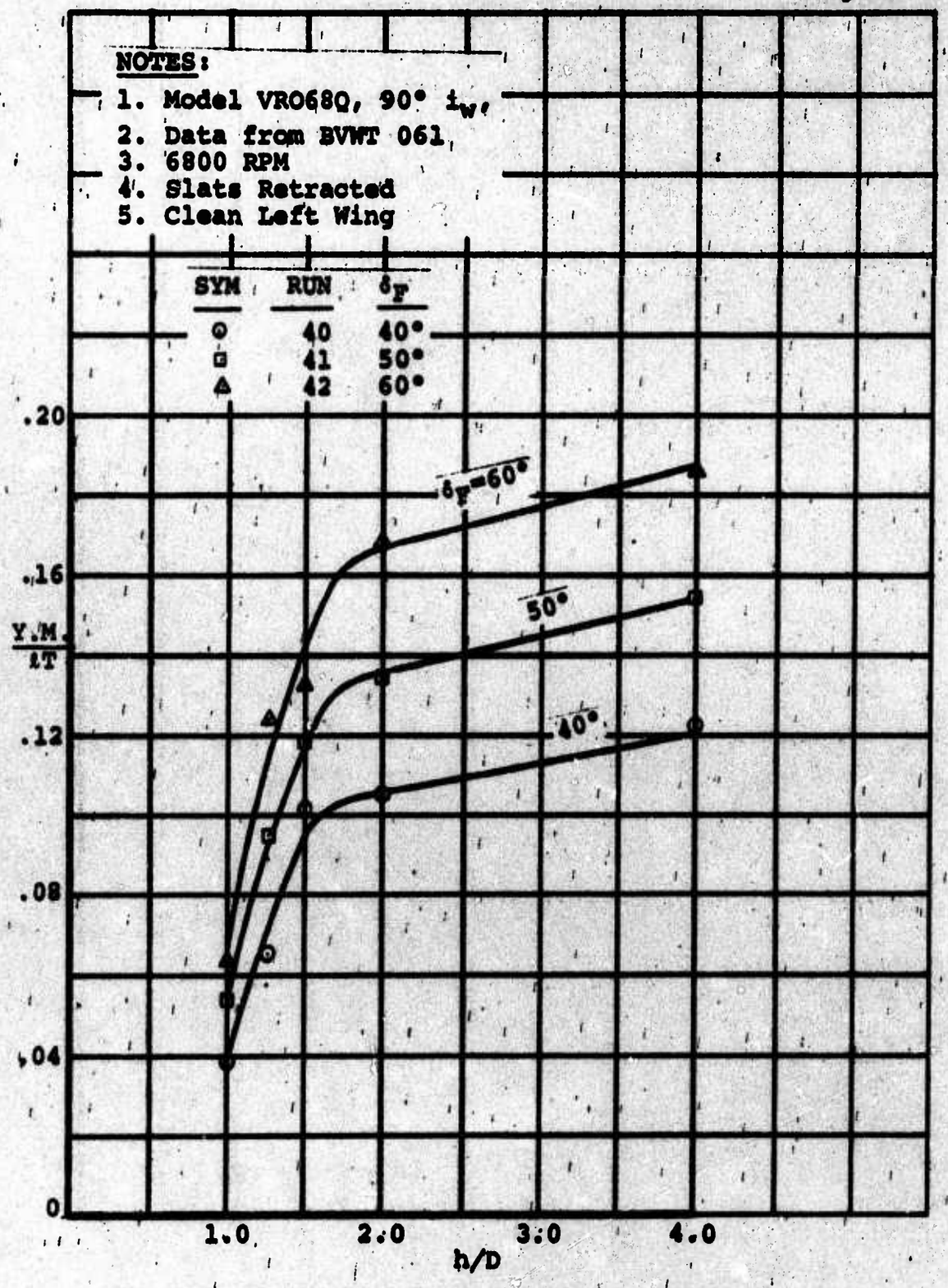

EFFECT OF GROUND HEIGHT ON HOVER YAW CONTROL
DOWN FLAP ~ RIGHT WING

Figure 41

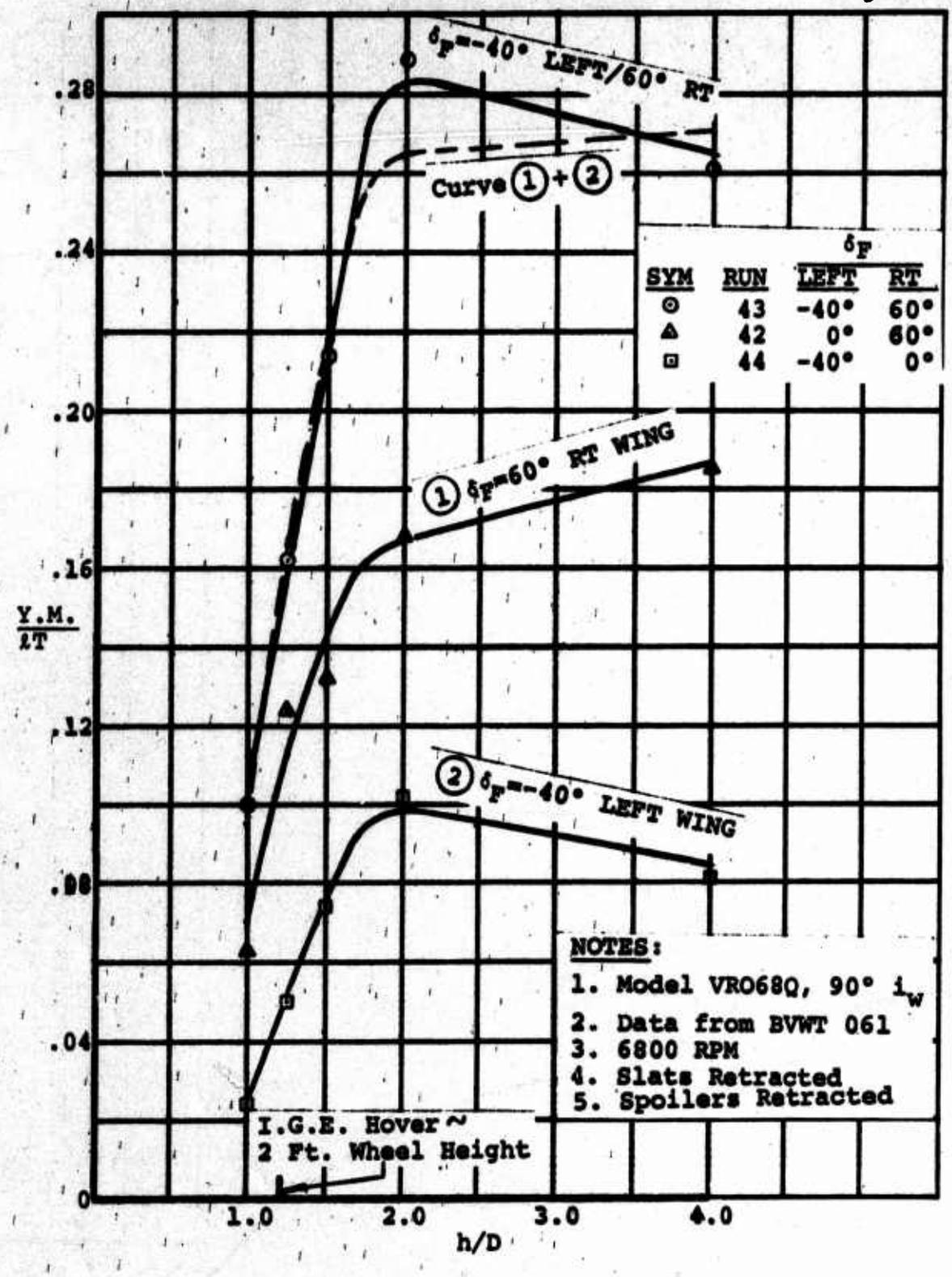

HOVER YAW CONTROL WITH
DIFFERENTIAL FLAP DEFLECTIONS

Figure 42

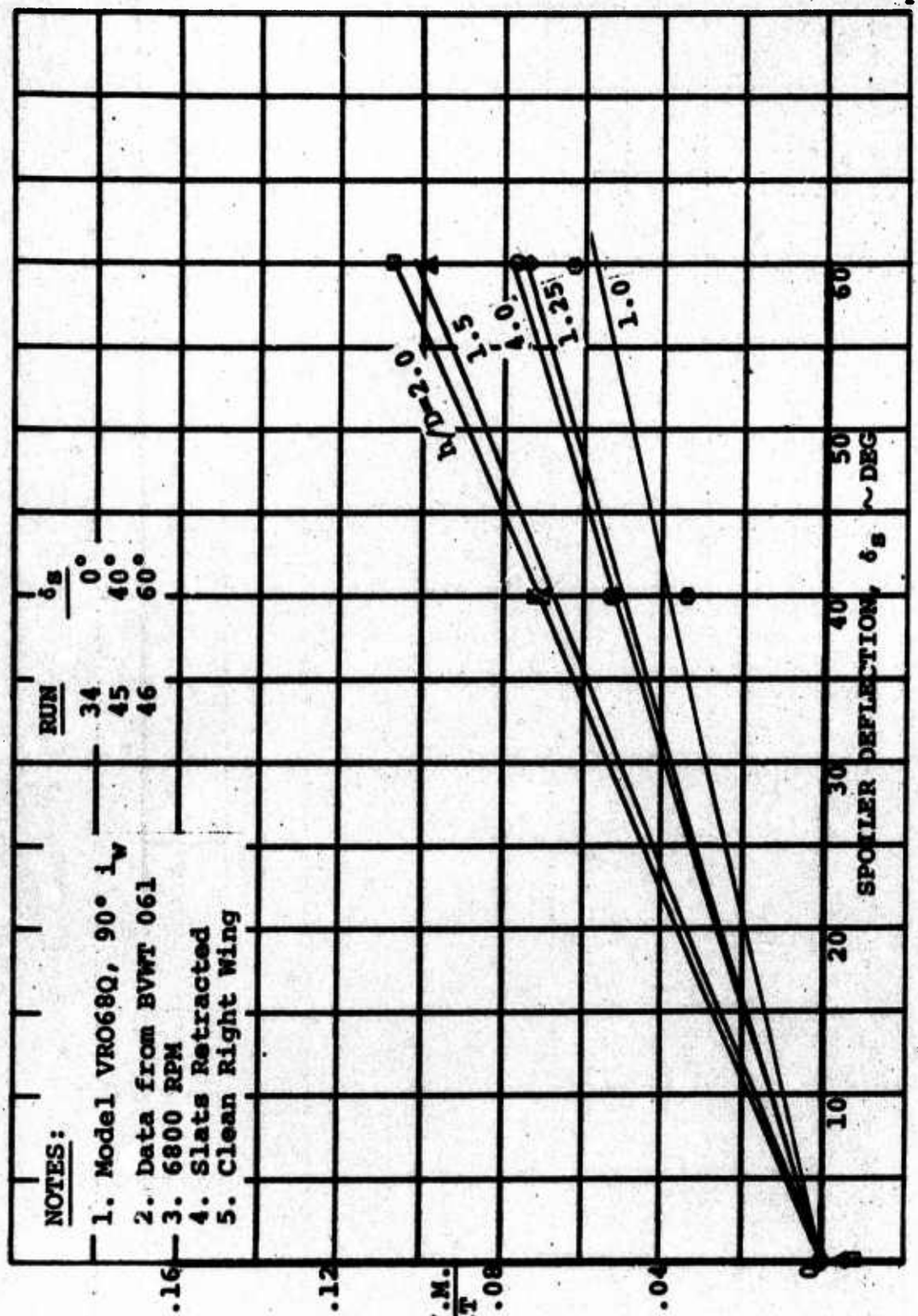

VARIATION OF HOVER YAW CONTROL
WITH SPOILER DEFLECTION

Figure 63

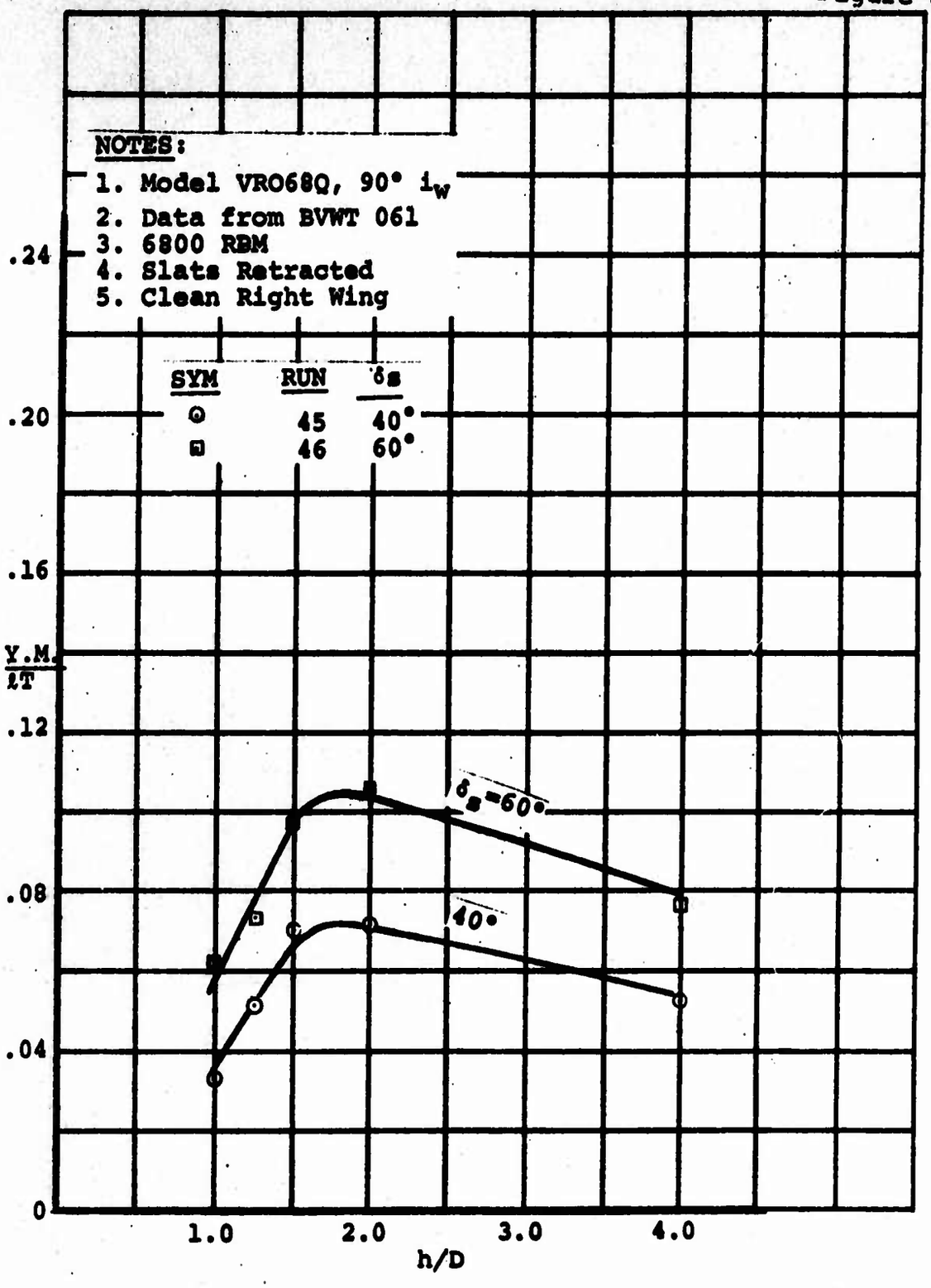

EFFECT OF GROUND HEIGHT ON HOVER YAW CONTROL
SPOILERS DEFLECTED~LEFT WING

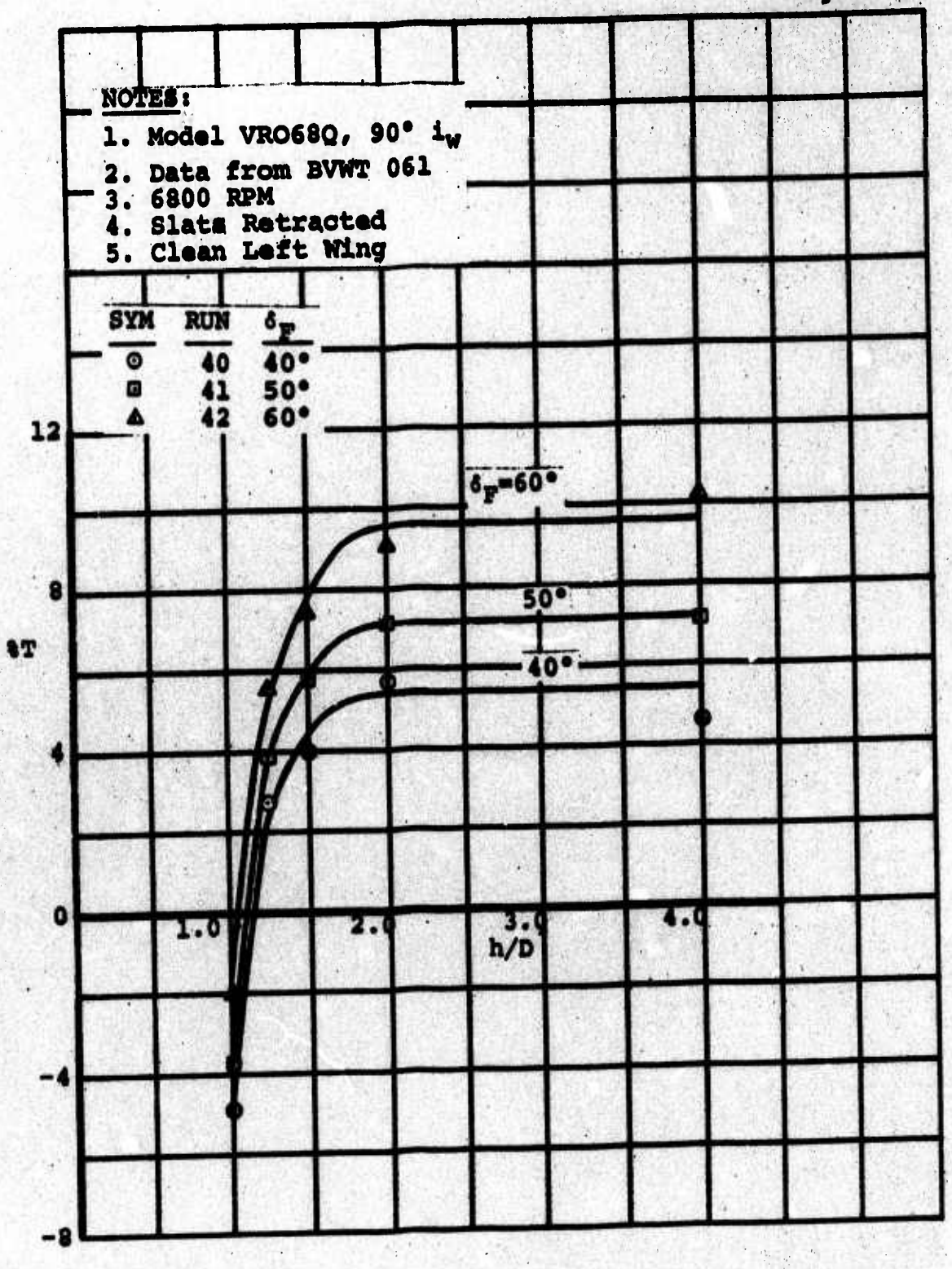

HOVER DOWNLOAD DUE TO FLAPS
DOWN FLAP~RIGHT WING

Figure 45

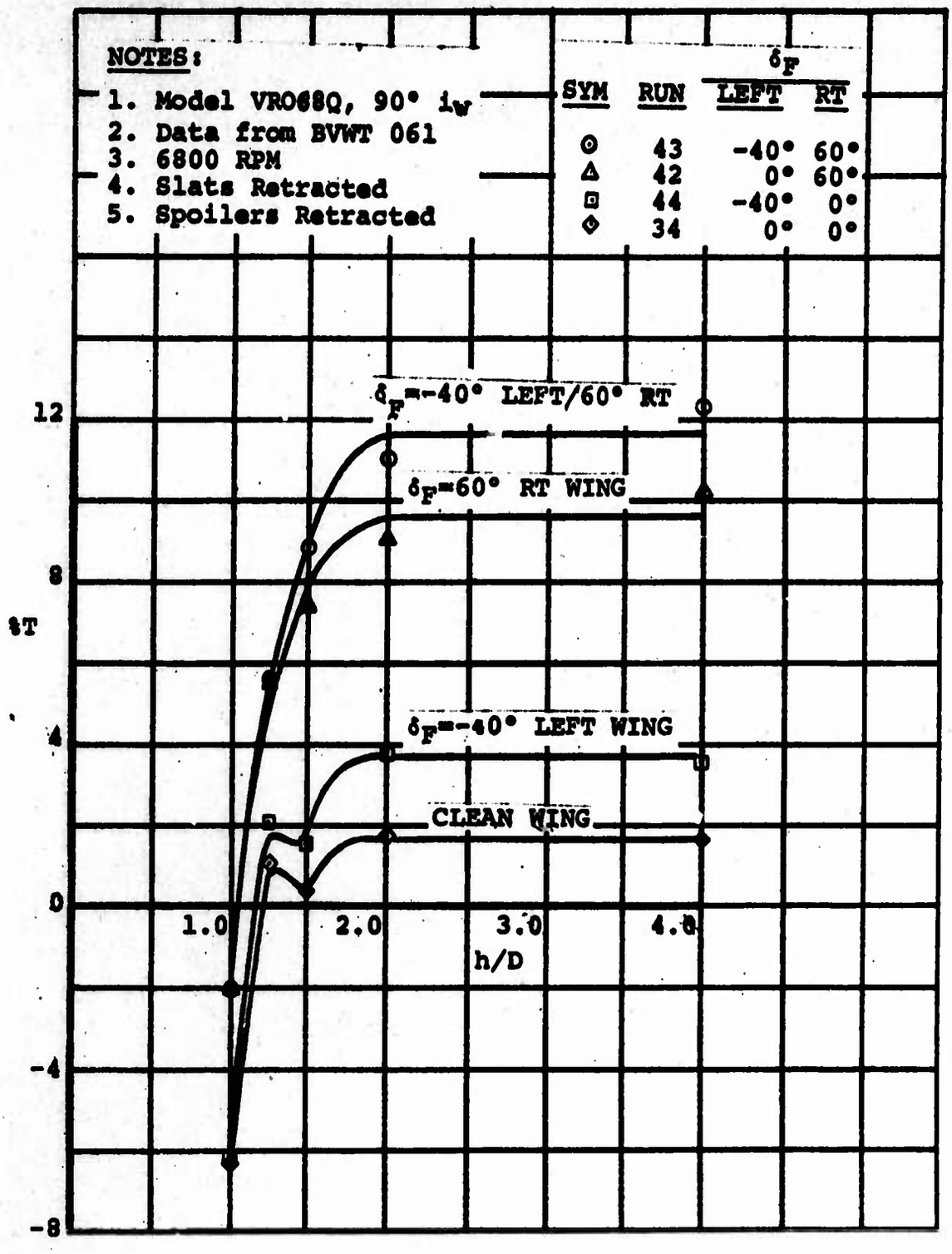

HOVER DOWNLOAD DUE TO
DIFFERENTIAL FLAP DEFLECTIONS

Figure 46

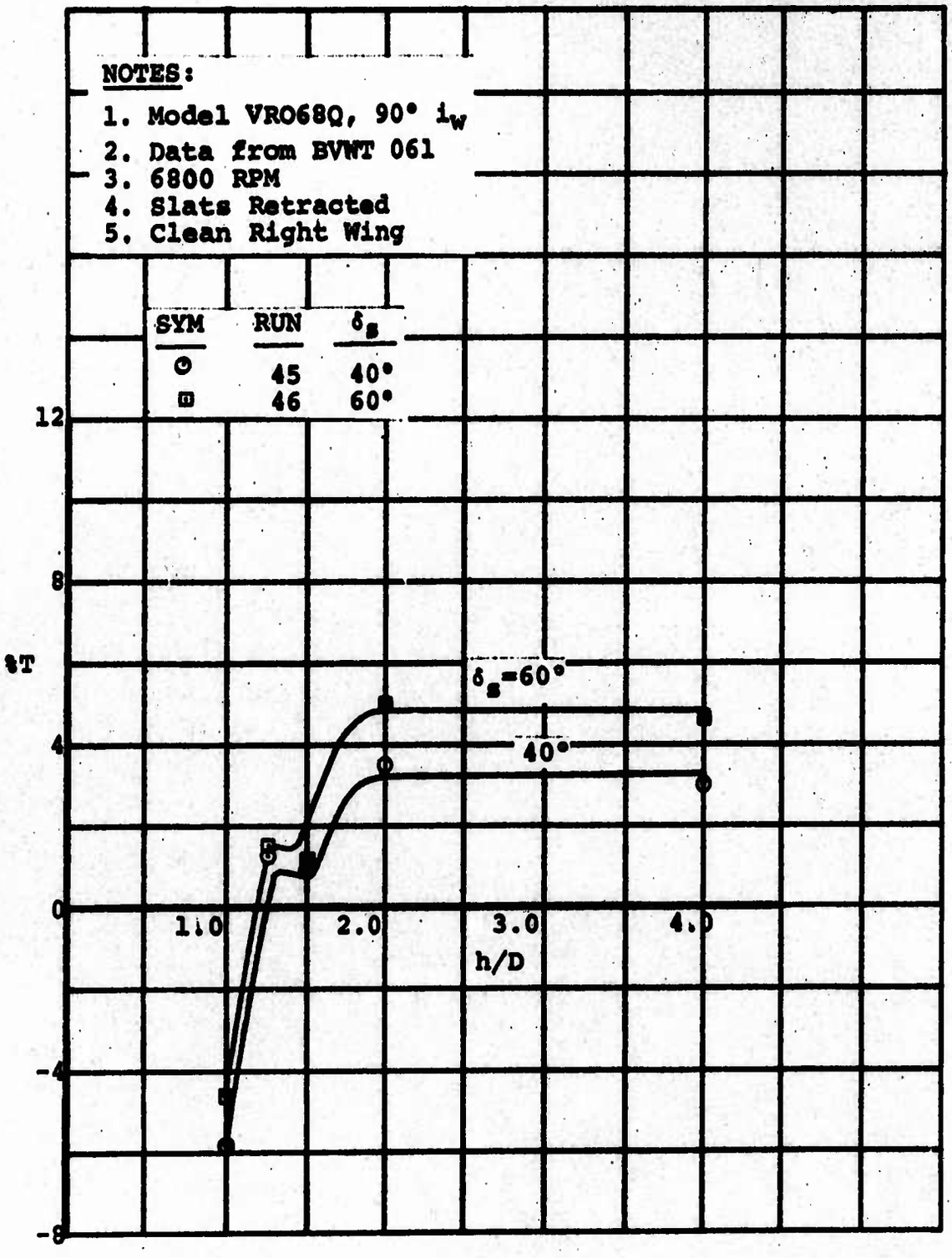

HOVER DOWNLOAD DUE TO SPOILERS
SPOILERS DEFLECTED ~ LEFT WING

Figure 47

VARIATION IN TOTAL THRUST WITH HOVER YAW CONTROL DEFLECTIONS

RUN	δ_F LEFT	δ_F RT	δ_s LEFT	δ_s RT	TOTAL T	$T/T_{RUN\ 34}$
34	0°	0°	0°	0°	488.4 lbs.	1.000
40	0°	40°	0°	0°	480.9	.985
41	0°	50°	0°	0°	487.6	.998
42	0°	60°	0°	0°	486.0	.995
44	-40°	0°	0°	0°	476.5	.976
43	-40°	60°	0°	0°	482.1	.987
45	0°	0°	40°	0°	473.2	.969
46	0°	0°	60°	0°	476.6	.976

NOTES:

1. Out-of-ground effect, h/D=4.0 and 2.0 average.
2. Average collective setting, $\theta_{.75}$=14.0°
3. 6800 RPM
4. Run 34 adjusted for tunnel density

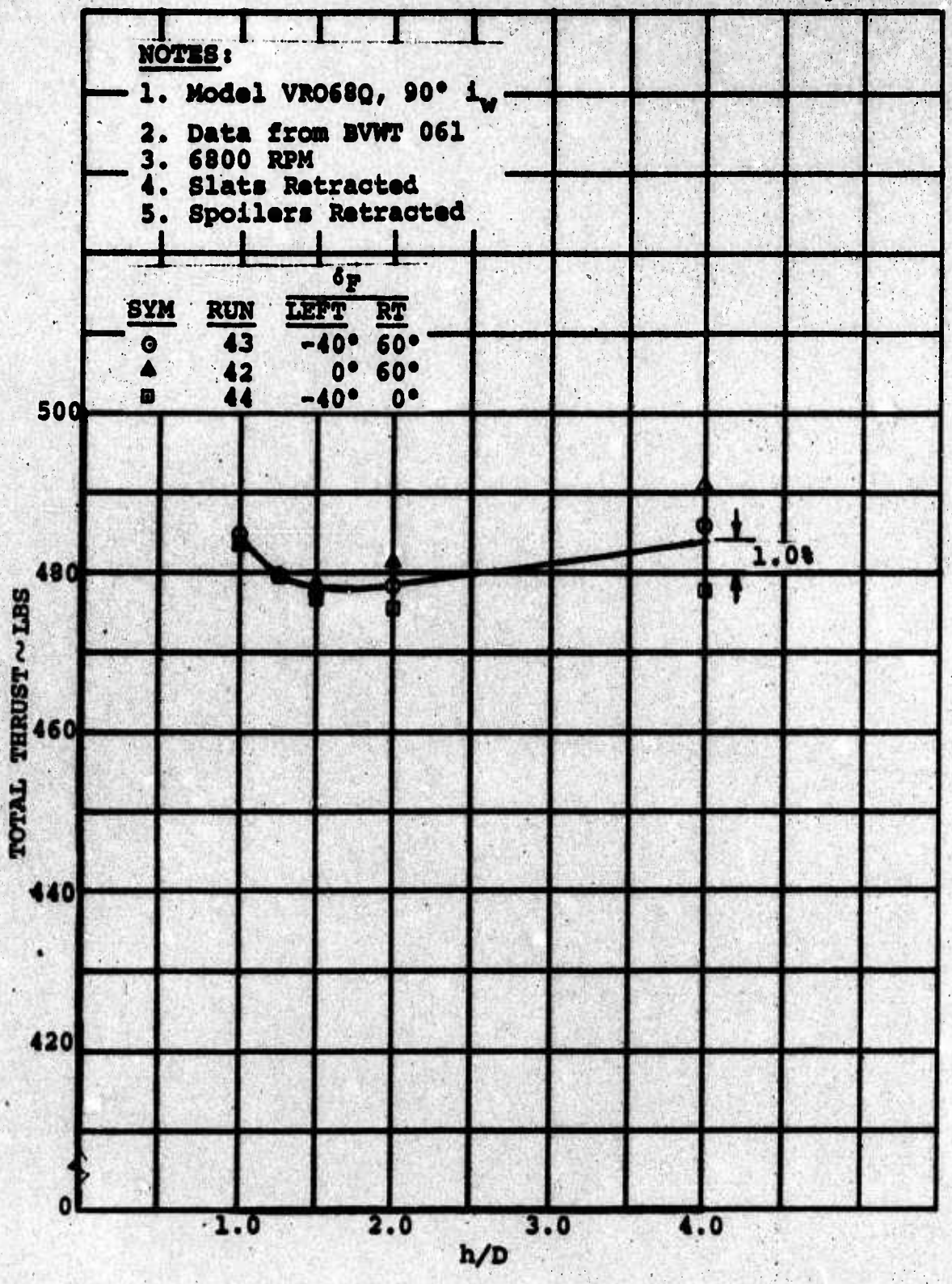

VARIATION OF THRUST WITH GROUND HEIGHT

Figure 49

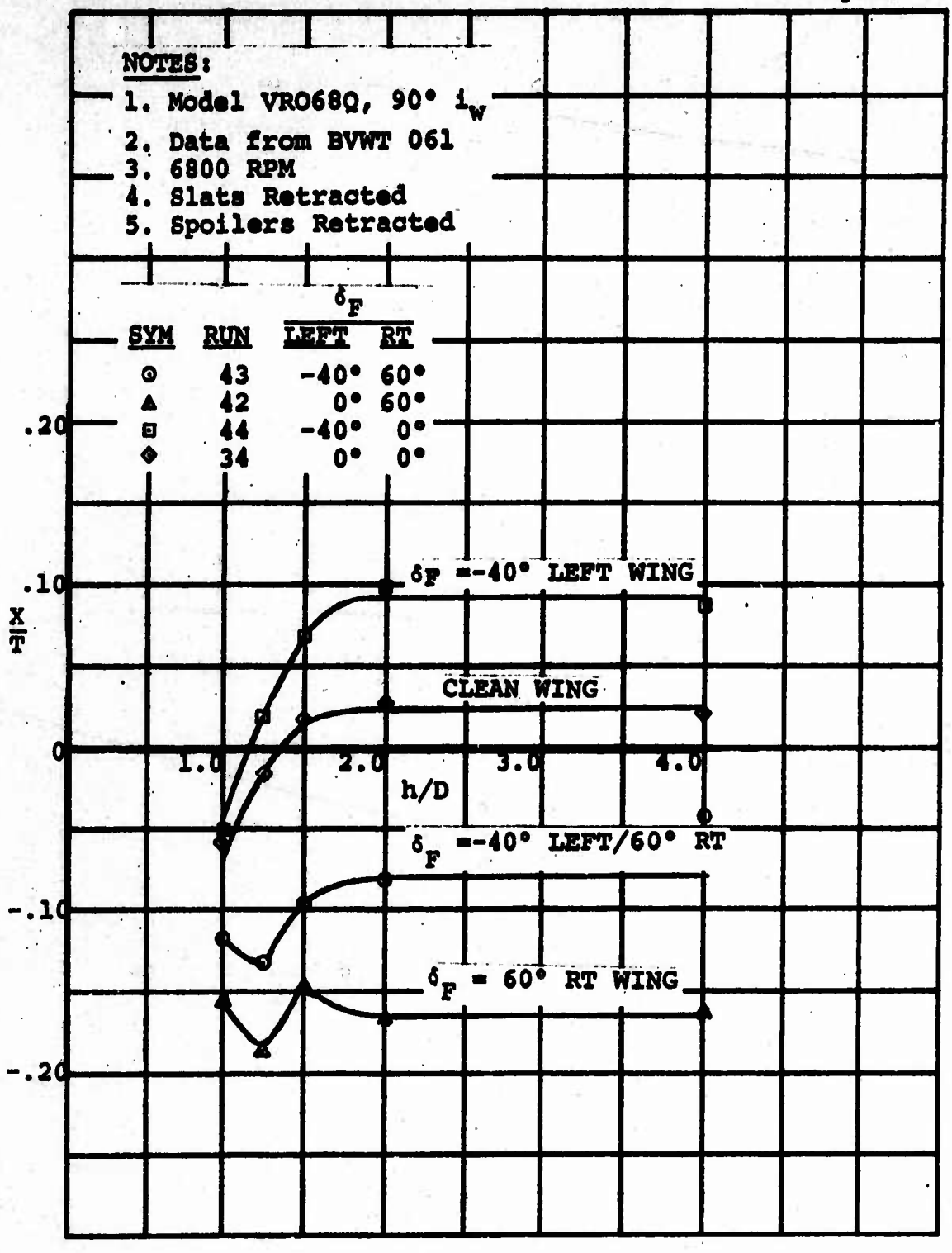

CHANGE IN A/C LONGITUDINAL FORCE
WITH HOVER YAW CONTROL DEFLECTIONS

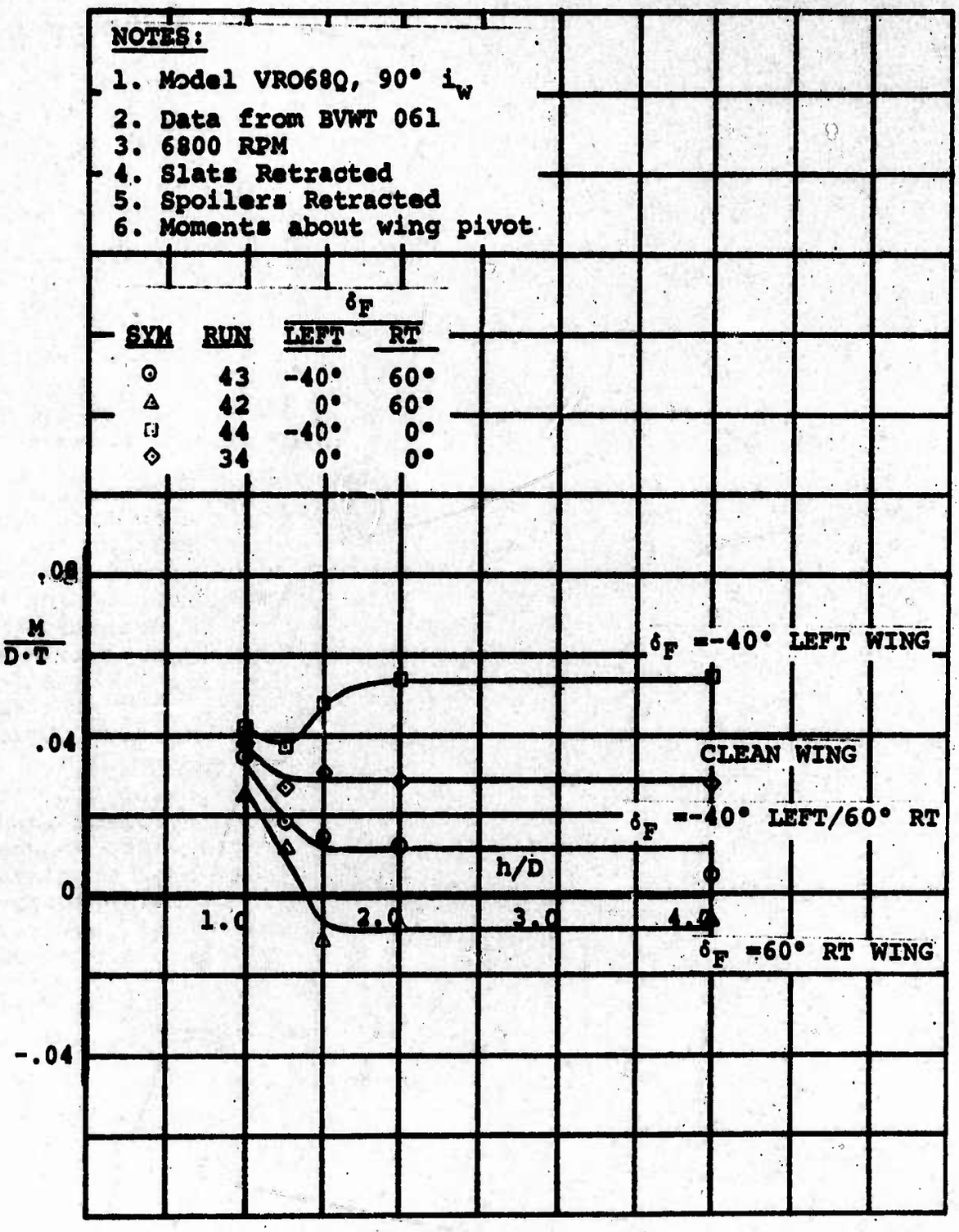

CHANGE IN A/C PITCHING MOMENT
WITH HOVER YAW CONTROL DEFLECTIONS

6.3 LOW SPEED DESCENT PERFORMANCE

One of the critical design items for a tilt wing aircraft is the low speed descent capability. (Boeing-Vertol has been using as a design goal, a minimum descent rate of 800 fpm up to a flight speed of 42.5 kt and a descent angle of 12° at higher speeds.)

The leading edge slat and double slotted flap configurations utilized on Model VRO68Q, were developed during the 1969 Boeing-Vertol wind tunnel test program of a four prop tilt wing aircraft as a means of meeting the descent rate goal. In the same test program, the placement of the propeller hub ℄'s with respect to the wing leading edge, was investigated with regard to maximizing descent performance. The results were incorporated into the design of Model VRO68Q.

During the subject test, the low speed descent capability was evaluated with slats extended, double slotted flaps deflected to 50° and 60°, the $P^{1,2}$ prop rotation (props turning down between the nacelles), and a propeller speed (without cyclic pitch) of 6800 RPM so that descent data could be acquired at a Reynolds number per foot of approximately 1.2×10^6 (corresponds to a slipstream q of 38.5 psf at the appropriate wing incidence angles). The $P^{1,2}$ prop rotation direction was selected on the basis of previous wind tunnel tests to maximize descent performance.

Previous Boeing-Vertol tilt wing wind tunnel testing has shown that, positive cyclic pitch angles (nose-down pitching moment) reduces descent capability by primarily reducing the slipstream turning effectiveness. This is indicated in Reference 3. An investigation of the effect of cyclic pitch on descent capability was planned for the Phase I test of Model VRO68Q, however, the damage to the Lamiflex radial bearings in the left inboard cyclic pitch hub which occurred during these runs (discussed previously in the Introduction) necessitated delaying the completion of this investigation to the Phase II test.

Data was also acquired for establishing the basic flaps down lift/drag characteristics. This data was obtained in zero thrust runs ($C_{T_s}=0$) with flap settings of 20°, 40°, and 60°.

6.3.1 Rate of Descent Capability

The descent capability of each configuration tested was determined by establishing the wing incidence angle at which initial stall or separation occurred on the wing outboard of the inboard set of fences i.e., outboard of the region between fences shown in Figure 2. Inboard areas where stall was tolerated comprise the area between fences, the area behind the gap

between the propeller tip and fuselage side, and the wing center section over the fuselage - in summary, sections over which the low freestream q or less than full slipstream q prevail and where roll disturbances are minimal.

In choosing the buffet onset angle, observer written comments and tuft photographs were studied in conjunction with the corresponding force polars. Analysis of previous tilt wing tests indicated that buffet onset angle choice was aided when the force polars were presented in terms of L/qb^2 vs D/qb^2 rather than C_{L_s} vs C_{X_s}.

Another curve that has been found useful in determining the descent performance is the variation with C_{T_s} of the effective wing angle of attack, $\alpha_{W_{EFF}}$, at buffet onset. (The latter parameter is described in the Data Reduction section.) This curve and the companion plot of wing incidence angle at buffet onset vs C_{T_s} should be reasonably smooth and consistent.

The descent data is presented as plots of rate of descent, R/D, vs full scale aircraft velocity, V_F. As discussed in the Data Reduction section, V_F was calculated using a wing loading of 73.5 psf and test section atmospheric conditions.

Figure 51 shows the descent rate capability measured for 60° and 50° of flap angle. The corresponding curves of effective wing angle of attack at stall are presented in Figure 52. The descent capability runs performed first (60° flap angle) utilized a slat setting of $Q^{10,10,10,*}$. It was apparent, via tuft observations made during these four runs, that initial stall occurred on the wing tip panel in each run. As a consequence, the slat segment was steepened at the wing tip panel to the Q* setting (Figure 4 describes the setting) for the subsequent four runs with 50° flap angle. The net result was an increase in descent capability for the 50° flap/$Q^{*10,10,*}$ slat configuration.

Buffet onset angles and the corresponding descent performance with 60° of flap were re-evaluated with the higher angle setting on the tip panel slat (Q* setting) during fuselage pitch sweep Runs 63 thru 65. These runs were performed with a constant 30° of wing incidence as a portion of the tail off longitudinal stability runs. The steepened tip slat segment increased the buffet onset angle as shown in Figure 52 and substantially improved the descent capability with the 60° flap angle as illustrated in Figure 51. The data indicates that the resultant descent performance with 60° of flap as compared to that provided by 50° of flap is better at speeds higher than 47 kts.

Figure 53 shows a comparison between the rate of descent capability obtained with the collective hubs operating at 6800 RPM and cyclic hubs operating at 4750 RPM, all other model configuration items being identical: 60° flap, Q_1*,10,10,*slat setting, and zero cyclic. Since the two different prop/hub sets were geometrically similar any difference in descent performance could be attributed to disc loading and Reynolds number effects. The rate of descent measured with 4750 RPM was less by an average of 50 fpm than that obtained at the test conditions commensurate with 6800 RPM, even though the data indicated a small increase in buffet onset angle for the 4750 RPM case (Figure 54).

Figure 53 also shows the loss in descent performance for 4° of nose-down cyclic pitch. This decrease must be associated with a decrease in slipstream turning effectiveness as a result of the 4° nose-down cyclic not reducing the buffet onset angle (Figure 54). The 50 fpm loss in descent rate per positive degree of cyclic compares to a value of 100 fpm/deg positive cyclic measured in Reference 3.

Note that both Figure 52 and 54, which present data from wing sweep runs with the fuselage set at 0°, express buffet onset angles in terms of wing incidence angle plus fuselage angle ($i_w+\alpha_f$). This was necessary in order to account for the incremental wing angle of attack being produced by the upward deflection of the model on the sting due to the high lift forces generated. The increment in angle of attack from sting deflection is accounted for by a calculation routine in the data reduction program.

Figures 55 thru 67 present the basic data from the runs that were conducted for the purpose of determining the low speed descent capability. The data is presented as plots of L/qb^2 vs X/qb^2 (force polars), L/qb^2 vs i_w (lift curves), and M/qb^2c vs i_w (moment curves). Marked off on each force polar plot are the selected buffet onset points and a .3g deceleration line (corresponds to 16.7° descent angle) for reference purposes.

Figure 51

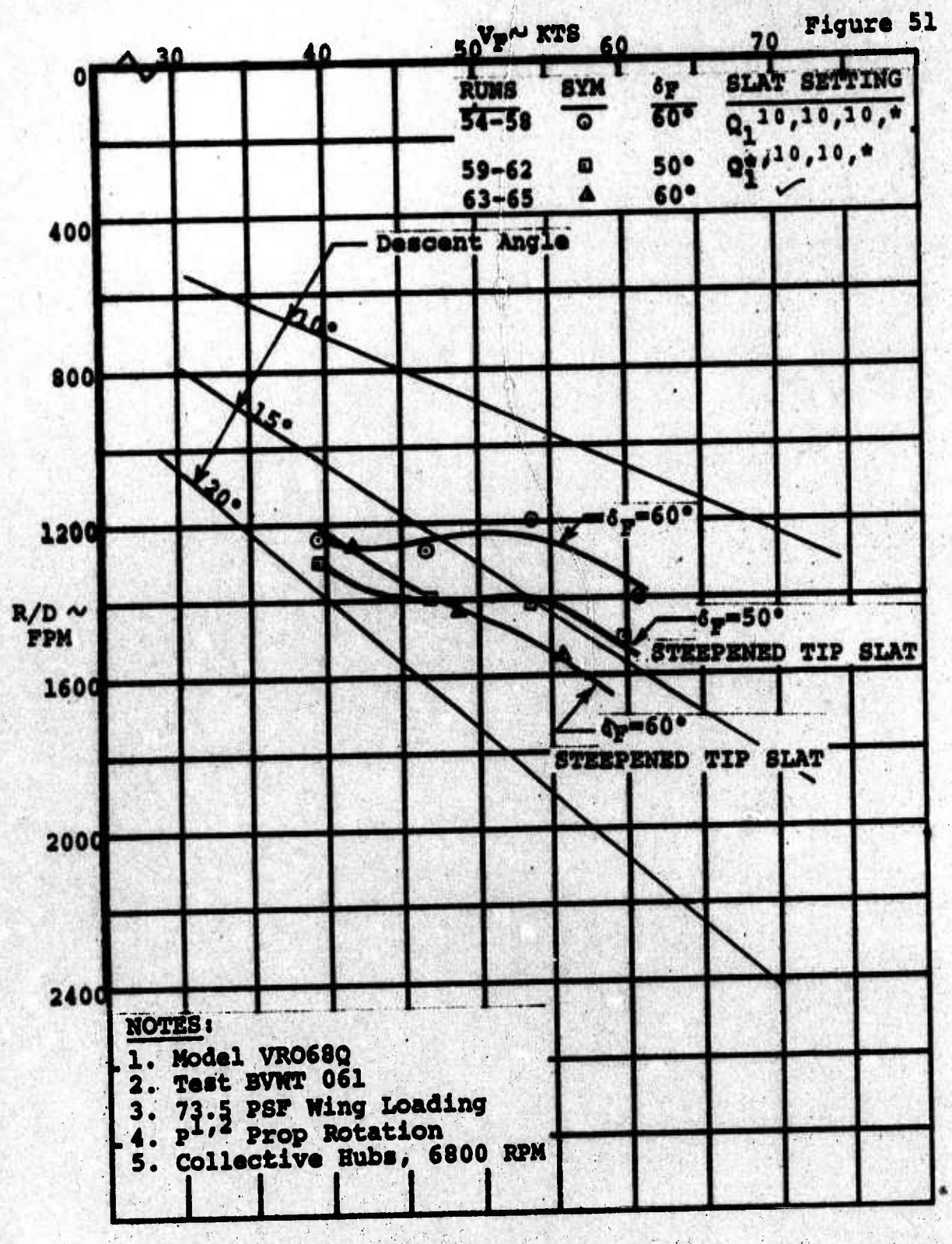

EFFECT OF FLAP ANGLE
AND SLAT SETTING ON DESCENT RATE

Figure 52

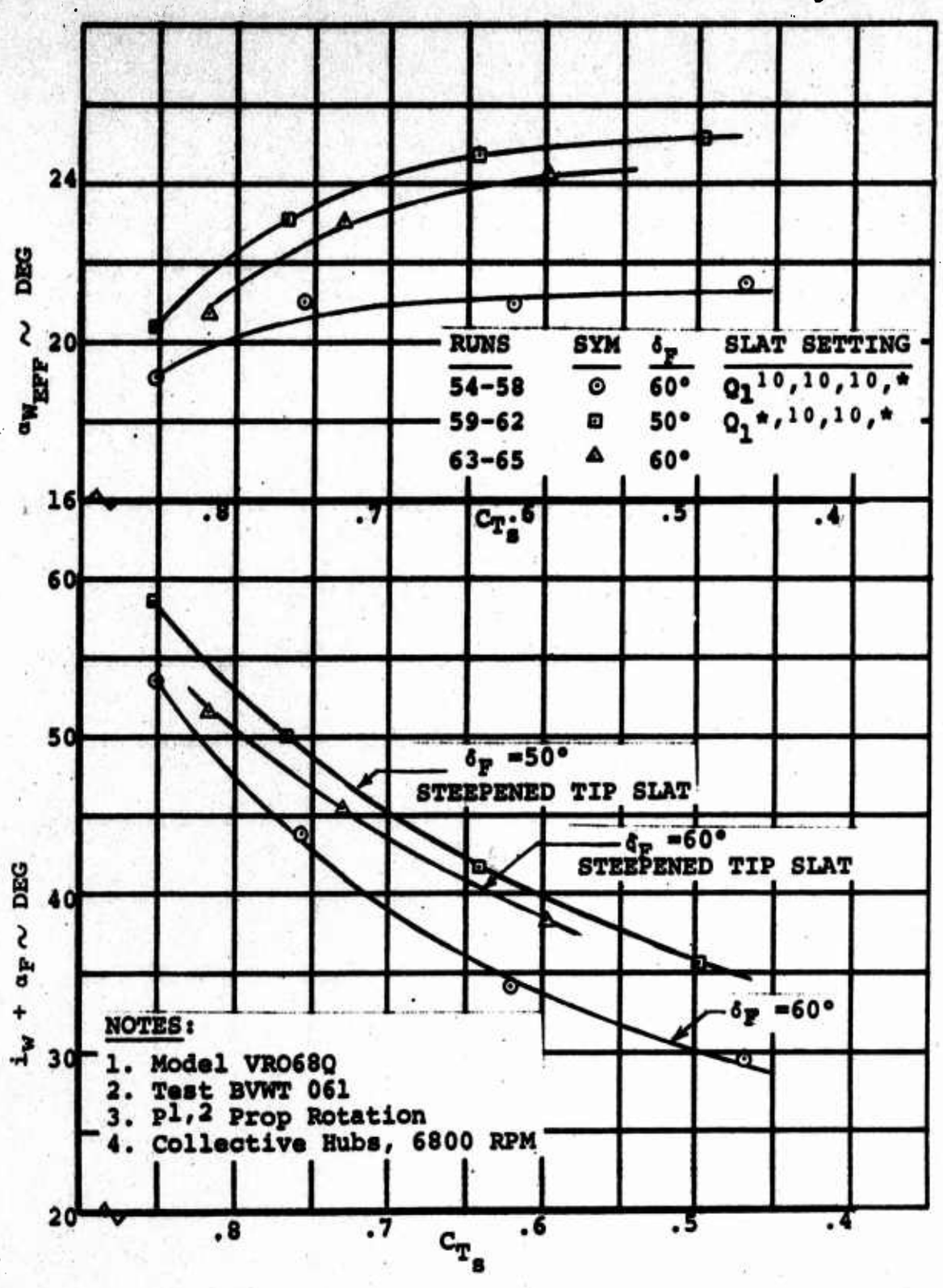

EFFECT OF FLAP ANGLE
AND SLAT SETTING ON BUFFET ONSET ANGLE

Figure 53

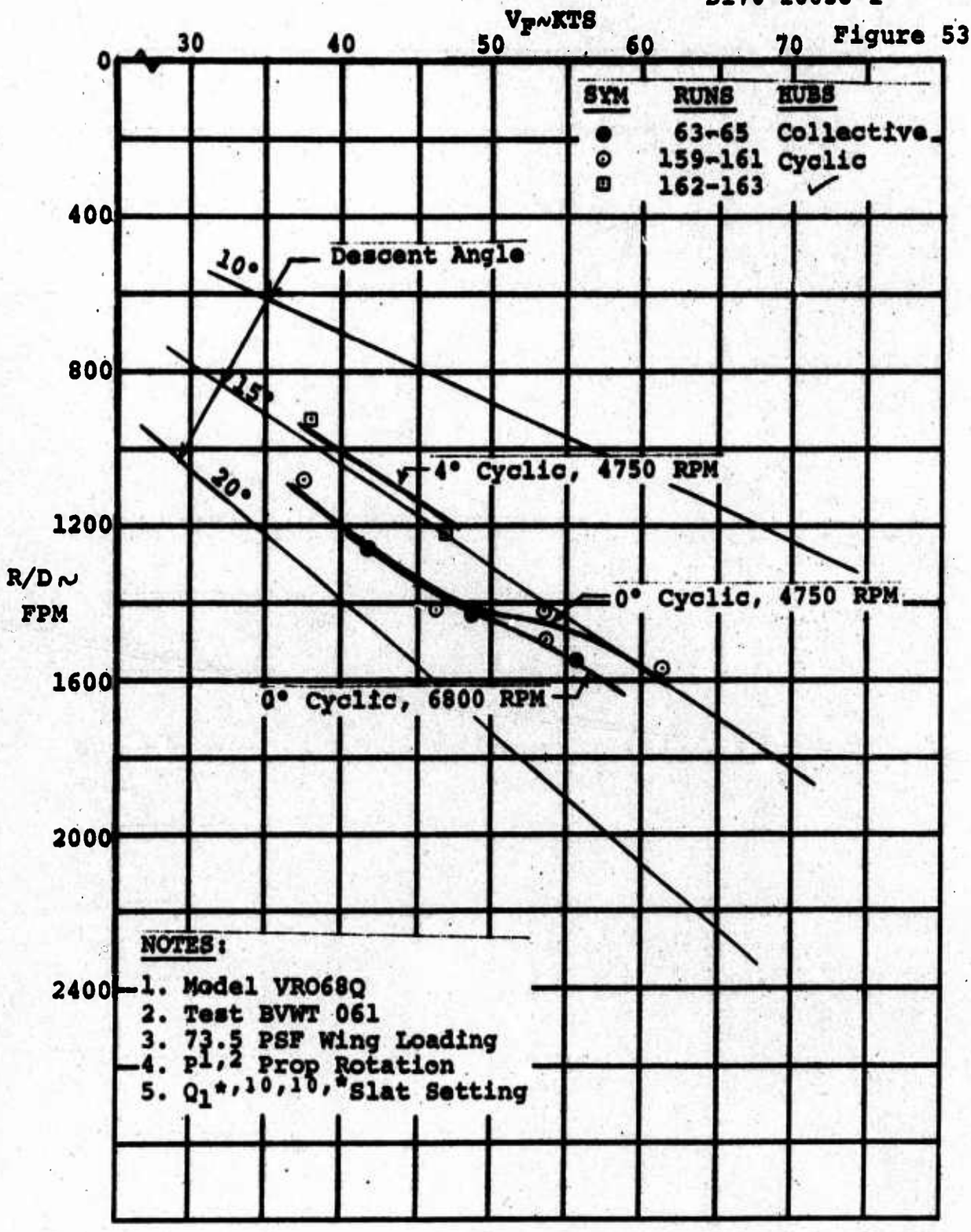

EFFECT OF RPM AND CYCLIC ANGLE
ON DESCENT RATE
60° FLAP ANGLE

Figure 54

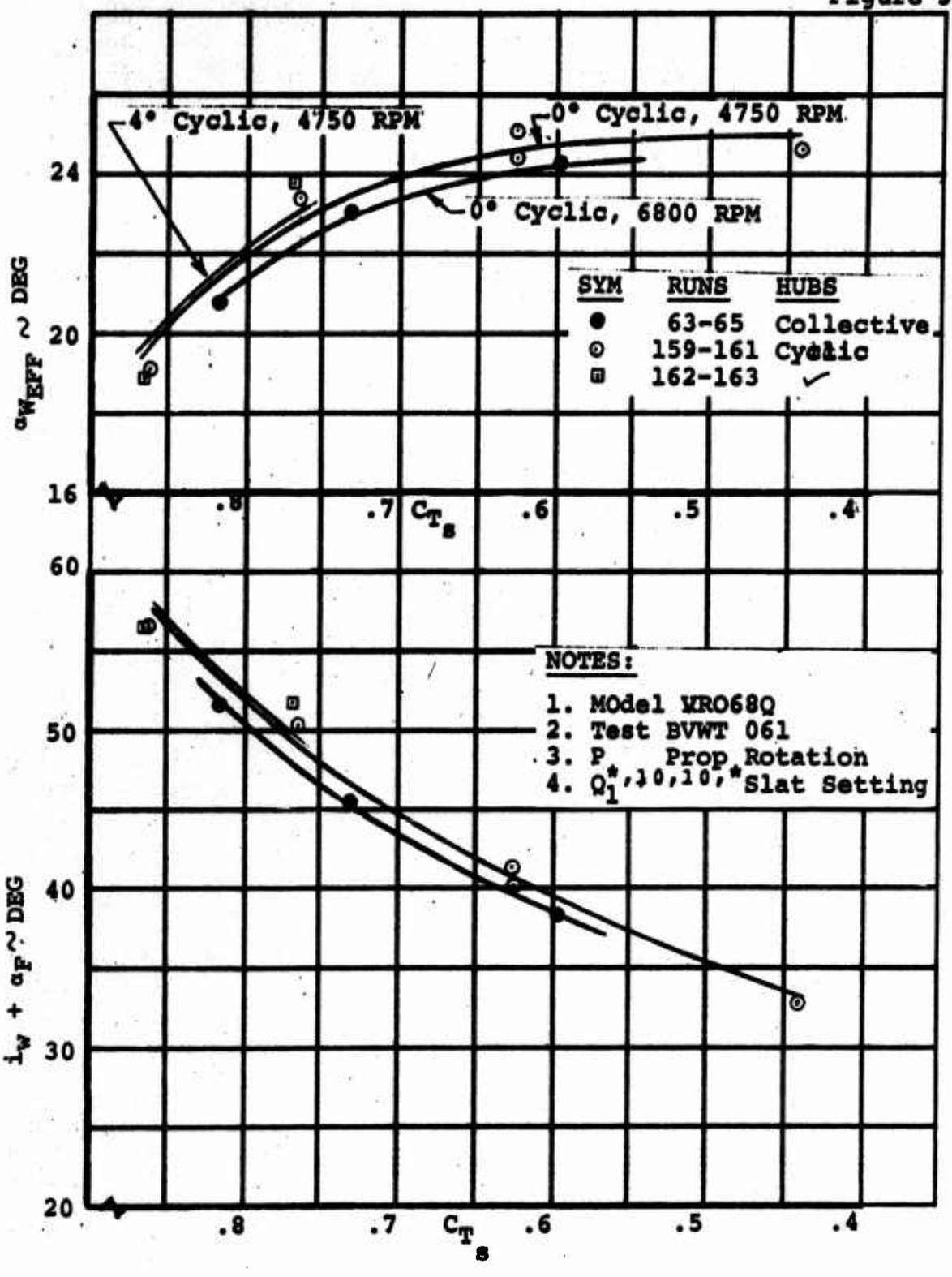

EFFECT OF RPM AND CYCLIC ANGLE
ON BUFFET ONSET ANGLE
60° FLAP ANGLE

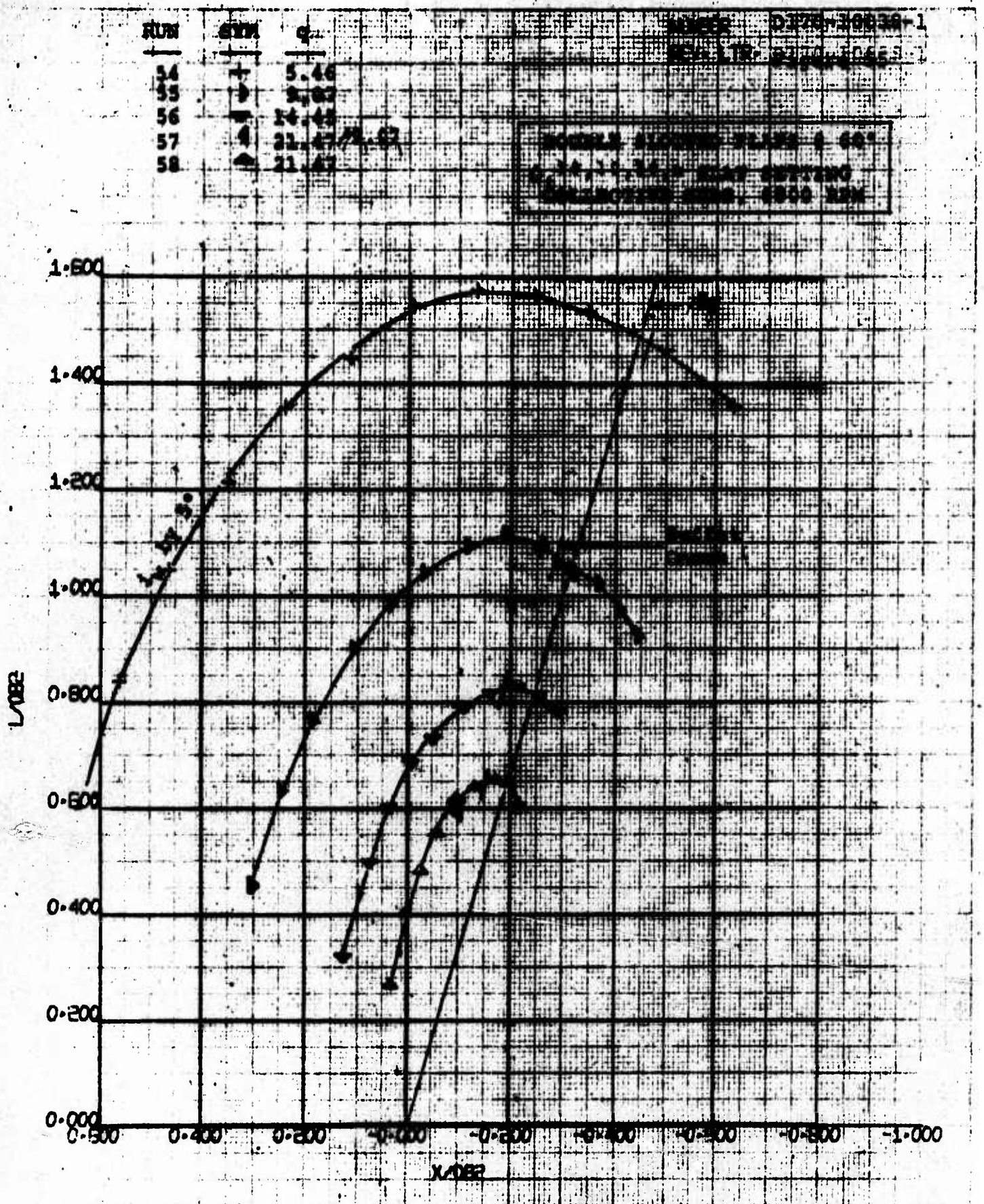

4-PROP TILT WING MODEL V806BD (FULL SPAN) L/QB2 VS X/QB2	BWT 61 7/22/70

NOT REPRODUCIBLE

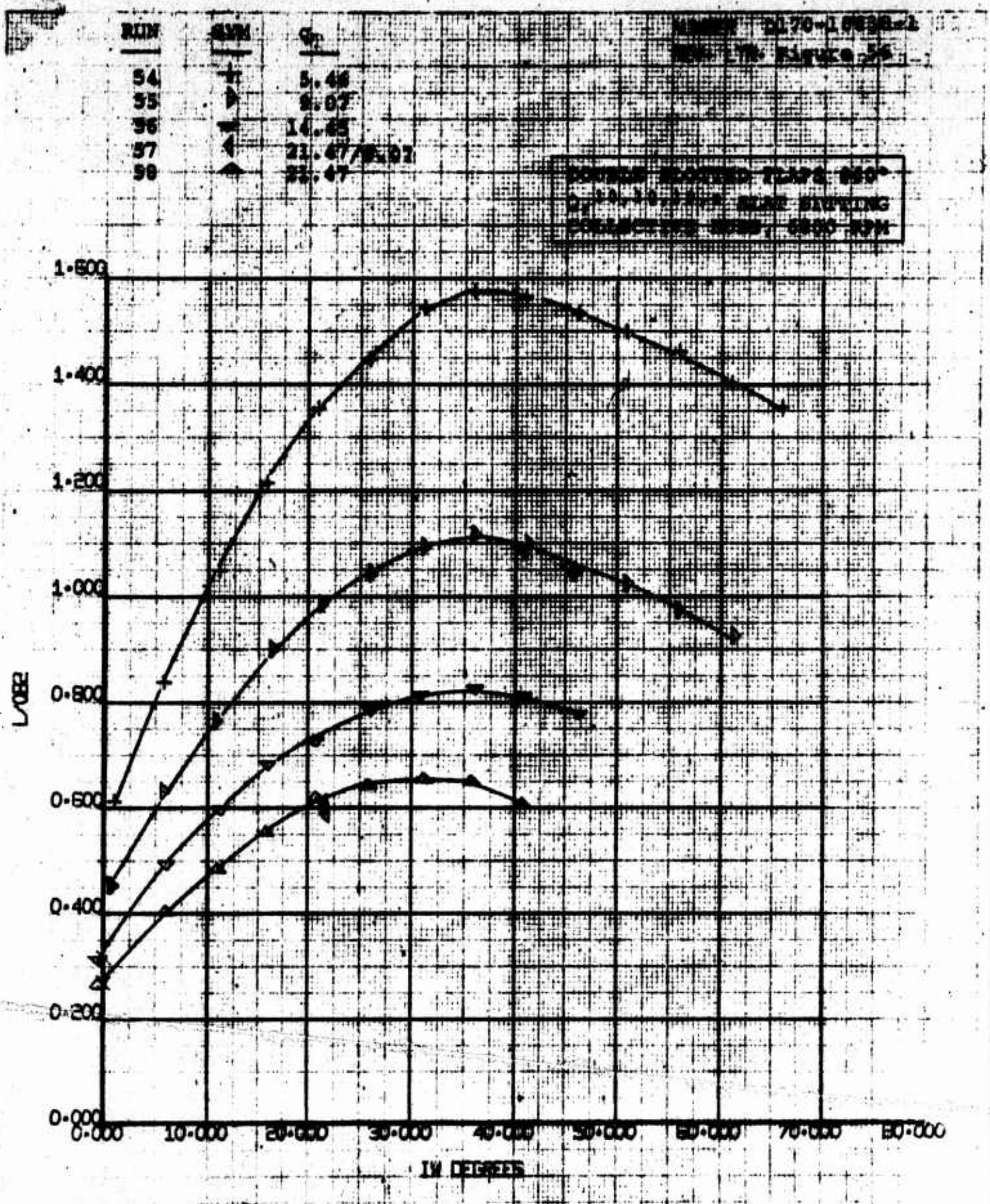

4-PROP TILT WING MODEL VROSED (FULL SPAN) L/QBP VS IW	BWT 61 7/22/70

NOT REPRODUCIBLE

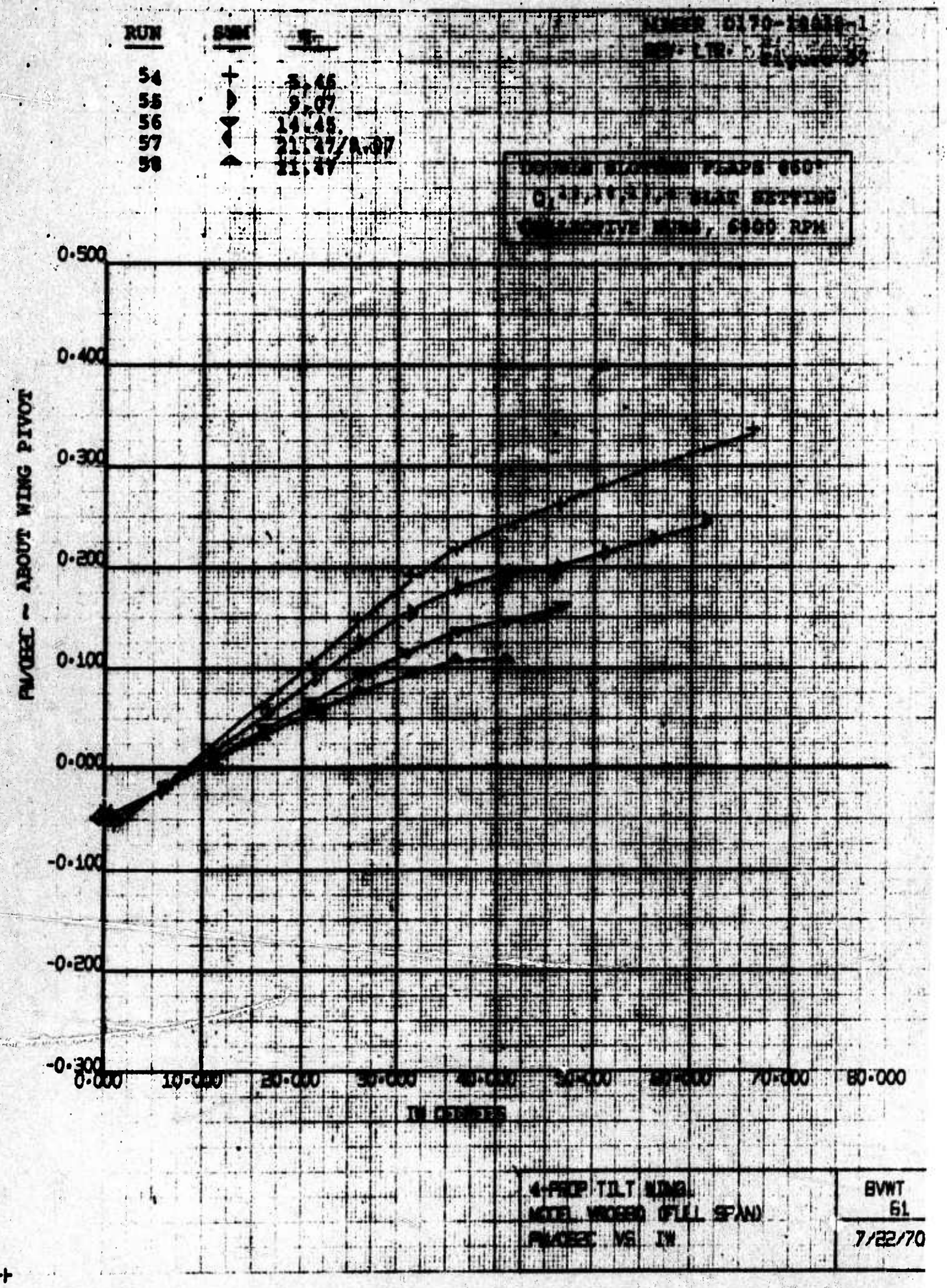
RUN
SYM
54
55
56
57
58
0·500
0·400
0·300
0·200
0·100
0·000
-0·100
-0·200
-0·300
0·000
10·000
20·000
80·000
70·000
4-PROP TILT WING.
MODEL MOUNTED (FULL SPAN)
BVWT
61
7/22/70

RUN	BOM	q_∞
58	+	5.46
60	▲	9.82
61	▼	14.45
62	◆	21.47

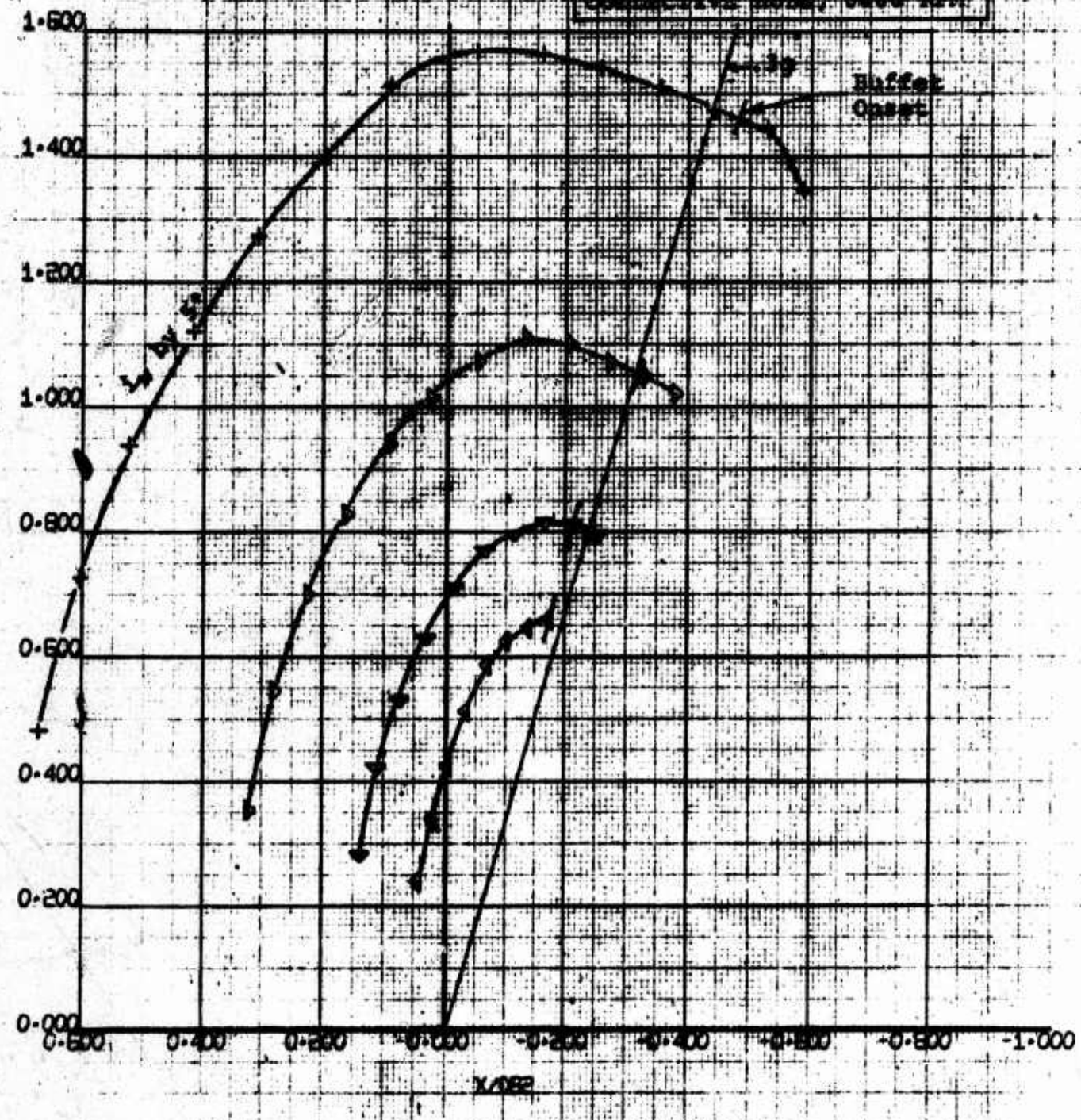

4-PROP TILT WING MODEL YROSS (FULL SPAN) L/QB2 VS X/QB2		BWT 61 7/22/70

NOT REPRODUCIBLE

RUN	SYM	q_∞
59	+	5.46
60	▷	9.01
61	▽	14.45
62	◁	21.47

NUMBER D170-10038-1
REV. LTR. Figure 58

DOUBLE SLOTTED FLAPS @ 50°
CONFIG 1.1.4 SLAT SETTING
COLLECTIVE MIN. 6800 RPM

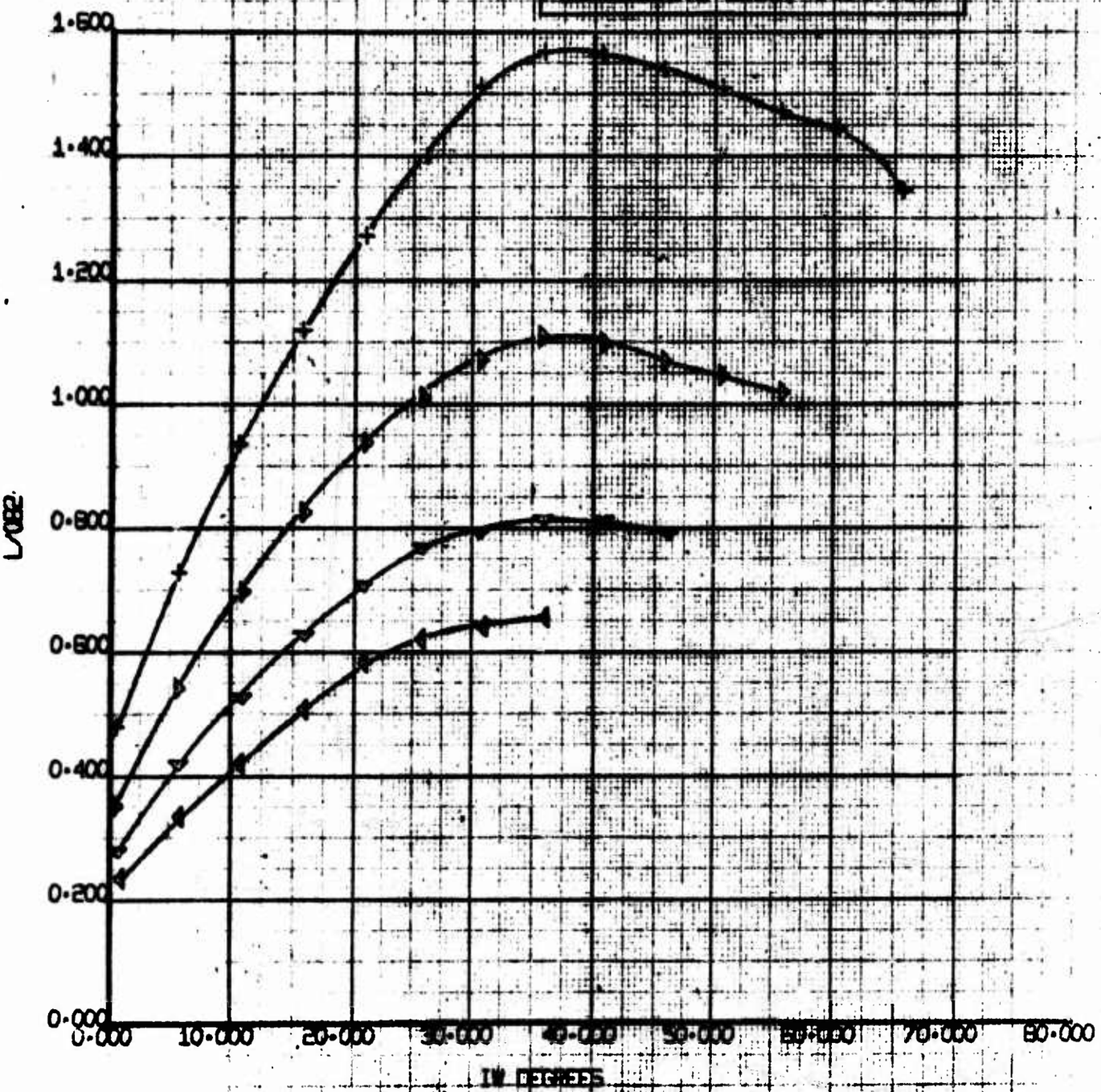

4-PROP TILT WING MODEL VROBBO (FULL SPAN) L/QB2 VS IW	BWT 61 7/22/70

RUN	SYM	q
59	+	5.46
60	▶	9.01
61	▼	14.45
62	◀	21.47

DOUBLE SLOTTED FLAPS @ 50°
$\delta_{e_{10,10}}$ SLEF SETTING
COLLECTIVE RUNS, 6900 RPM

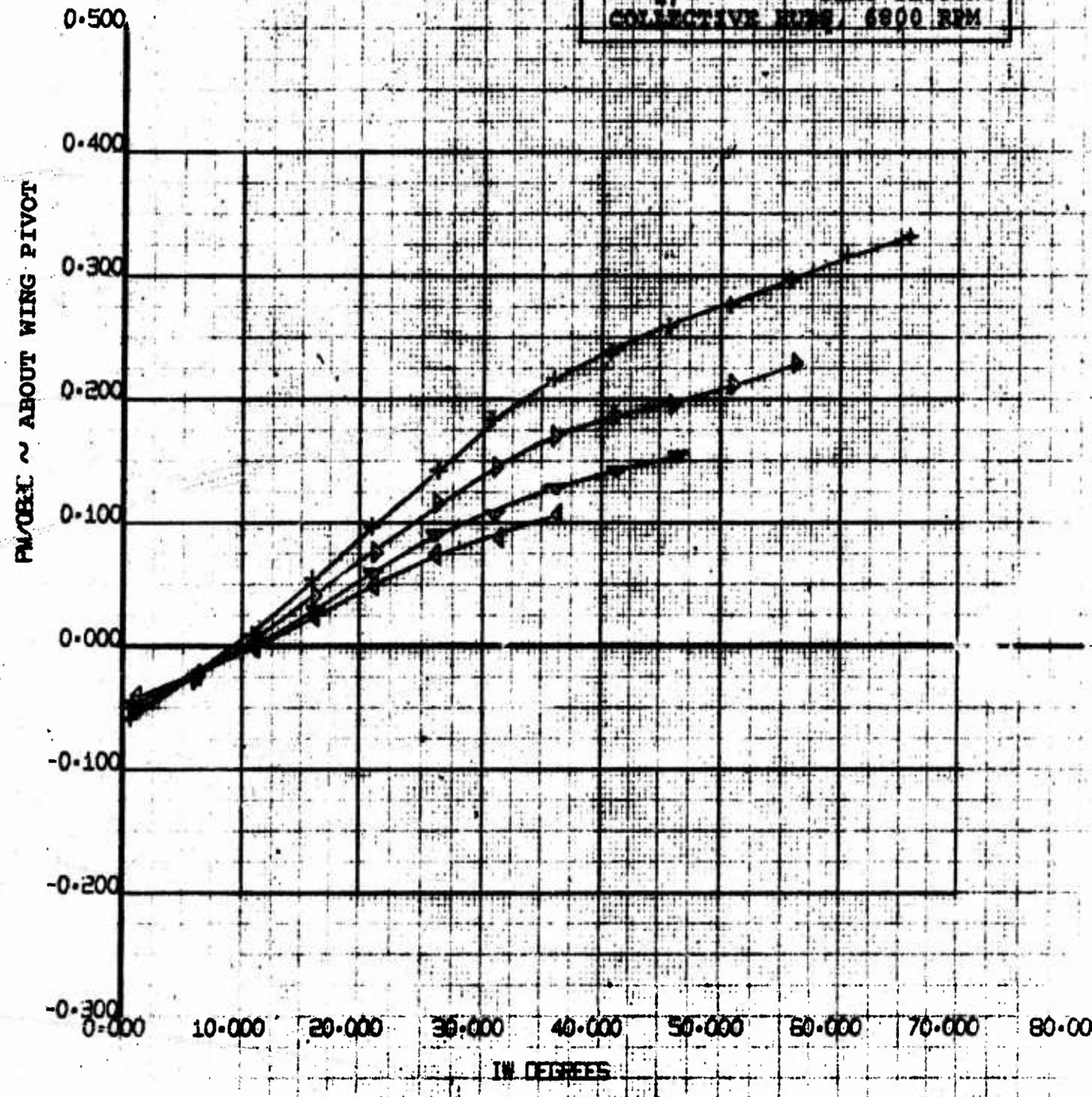

4-PROP TILT WING MODEL VRO680 (FULL SPAN) PM/OBIC VS IW	BVWT 61 7/22/70

+

NOT REPRODUCIBLE

RUN	SYM	q
65	+	15.34
64	b	10.57
63	▼	6.80

DOUBLE SLOTTED FLAPS 60°
[illegible] SPOIL SETTING
[illegible] 6000 RPM

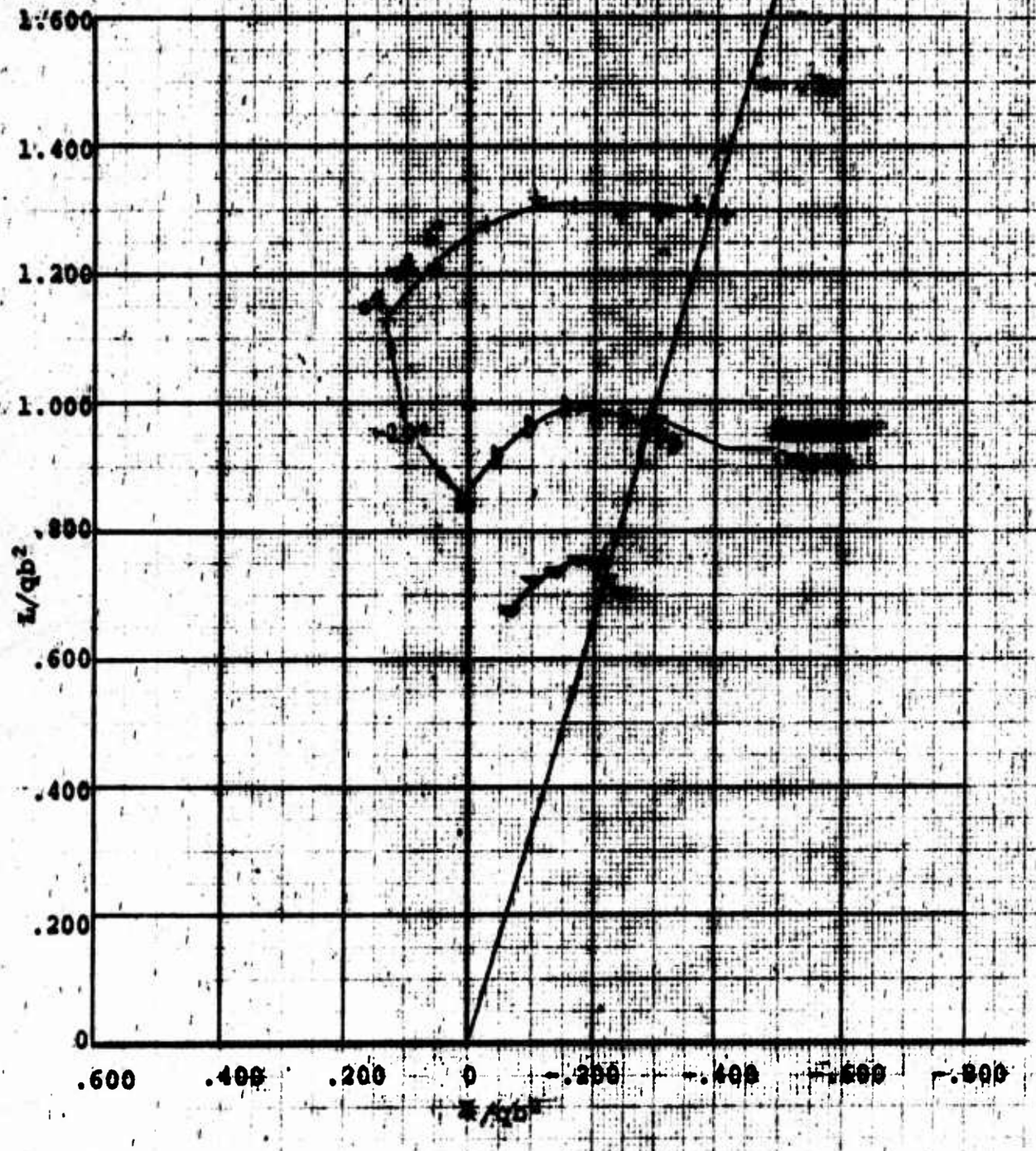

4-PROP TILT WING MODEL WRONSKIAN (FULL SPAN) [illegible] vs α/qb²	BVWT 61 8/19/70

RUN	SYM	q_f
158	+	3.36
159	◇	4.00
160	◁	4.65
161	◁	10.36

DOUBLE SLOTTED FLAPS 65°
δ_e -5, 10, +10, +5° BEAT SETTING
ZERO CYCLIC, 6750 RPM

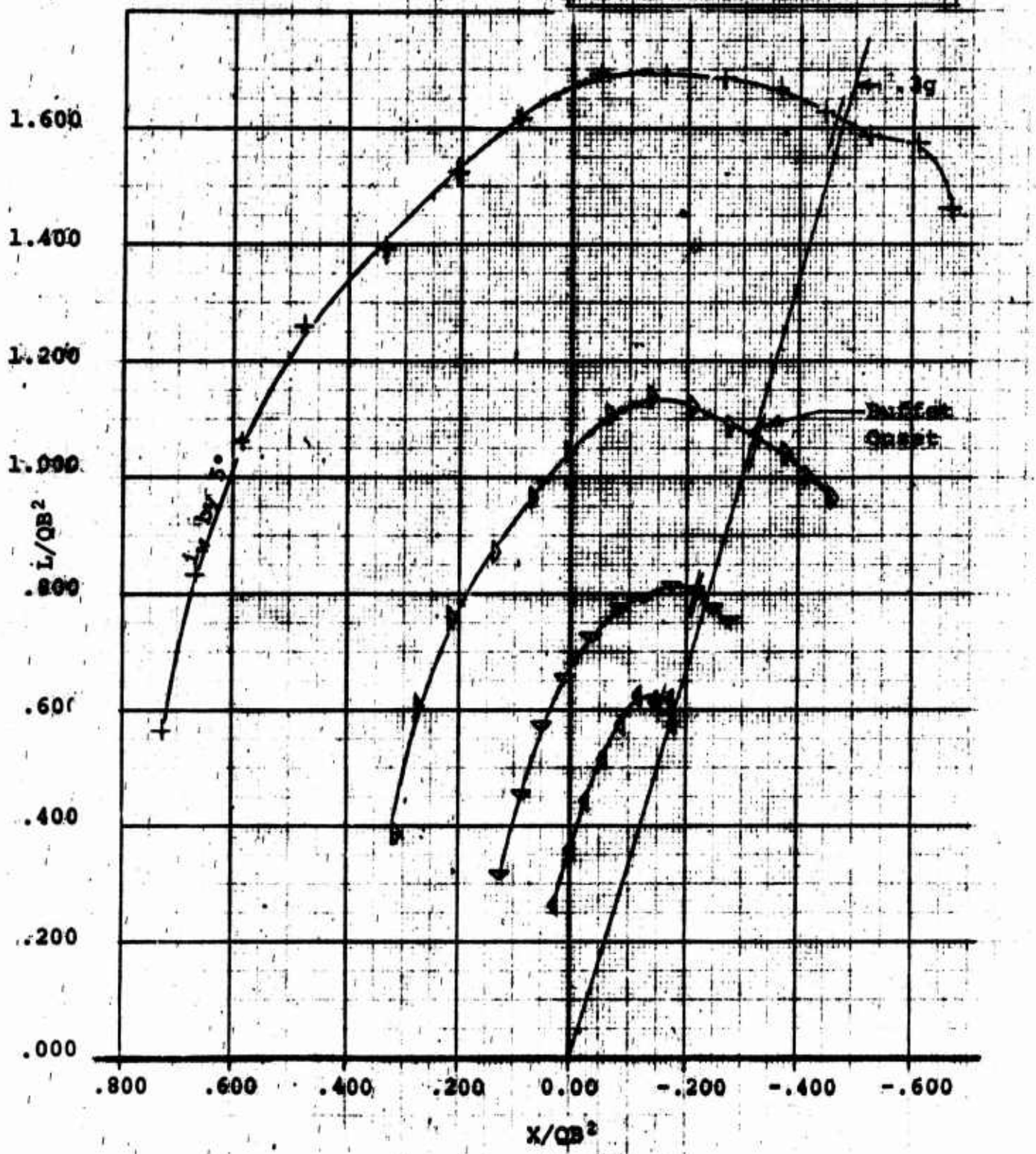

4-PROP TILT WING MODEL VRO68Q (FULL SPAN) L/QB^2 vs X/QB^2	BVWT 61 8/19/70

NOT REPRODUCIBLE

RUN	SYM	q_∞
158	+	2.36
159	▶	4.00
160	◀	[illegible]
161	◀	10.36

DOUBLE SLOTTED FLAPS 060°
[illegible] REAR SHIELDS
ZERO CYCLIC, 4750 RPM

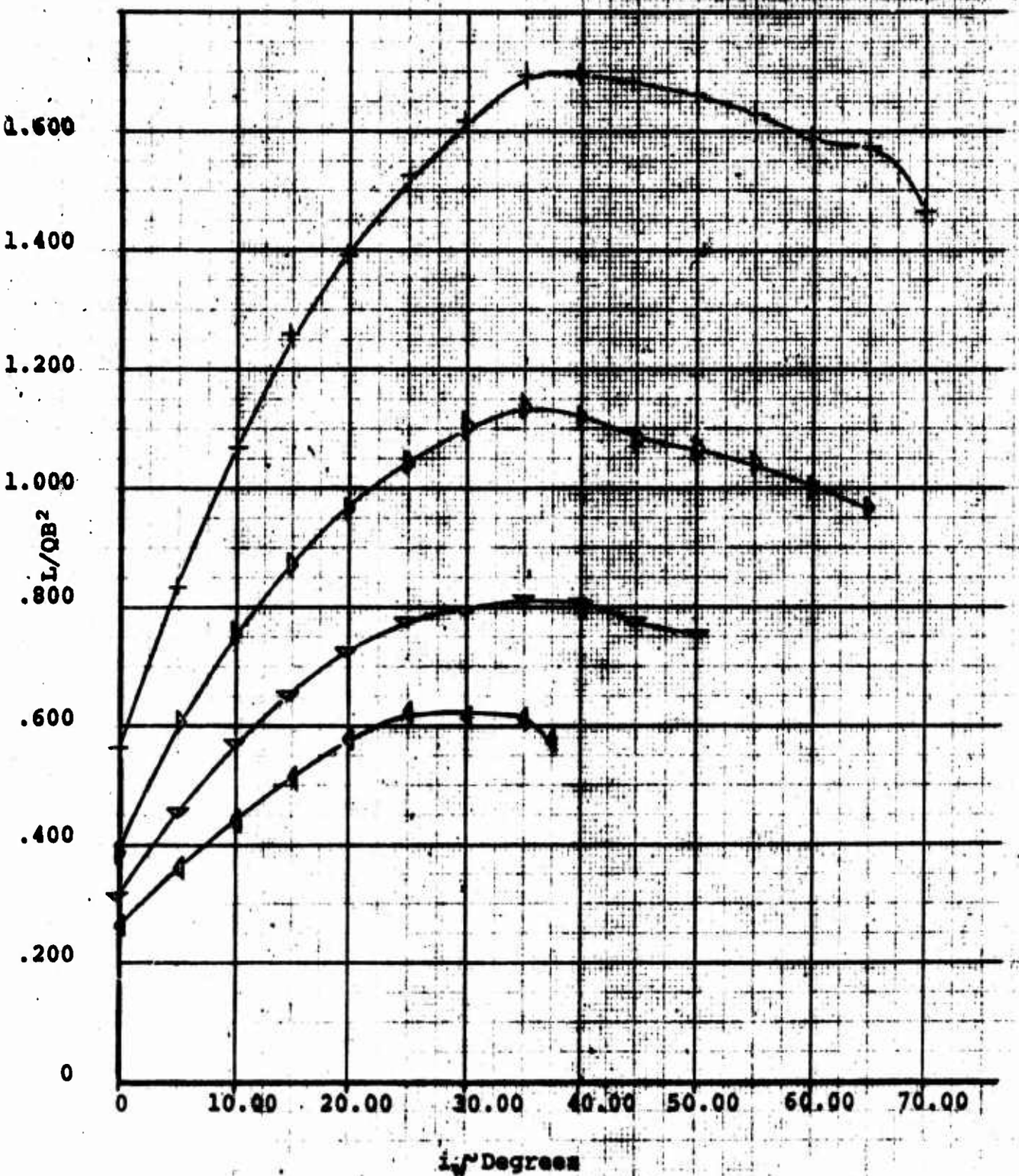

4-PROP TILT WING MODEL VRO6GQ(FULL SPAN) L/QB^2 vs i_w	BVWT 61 8/19/70

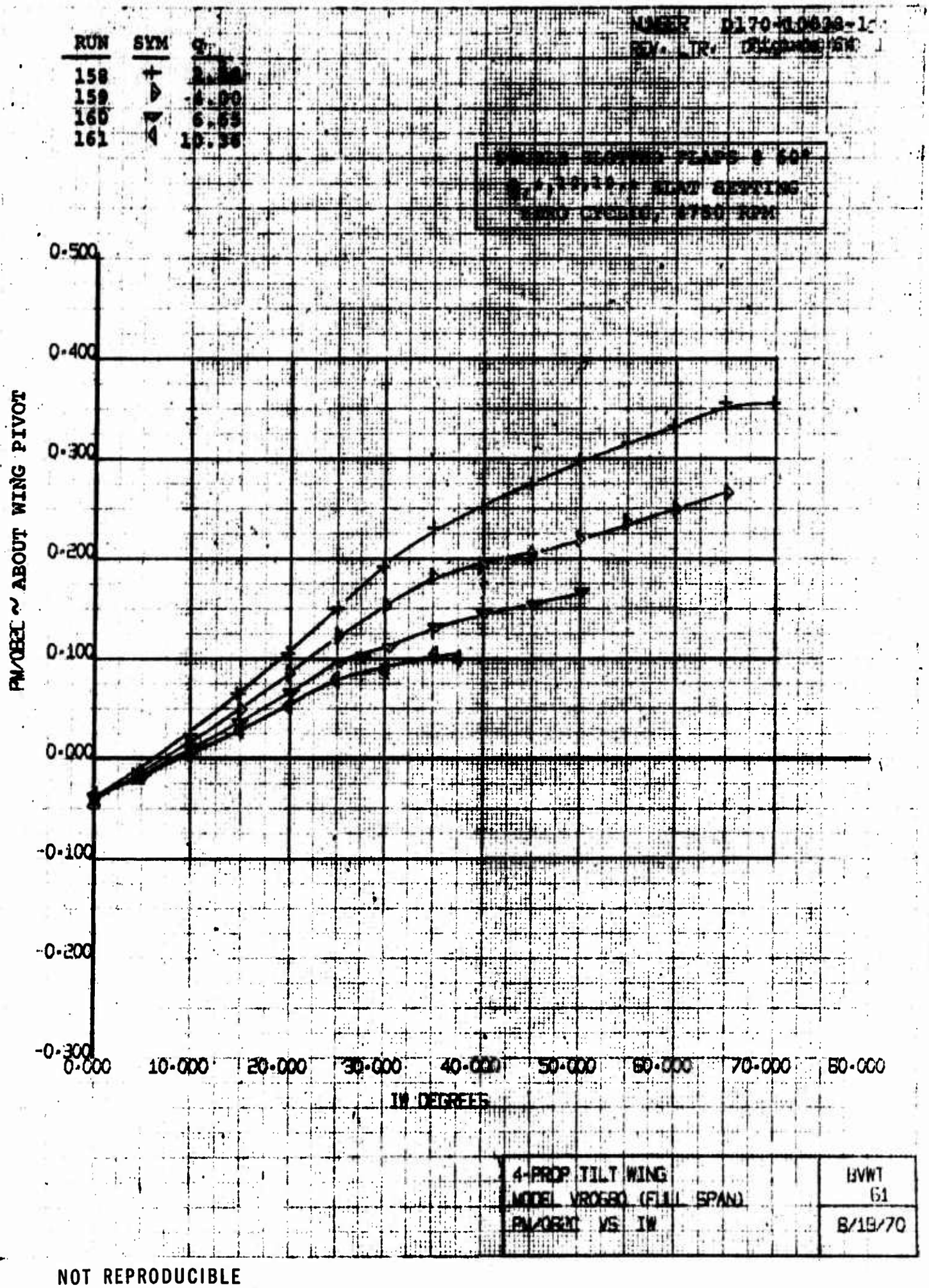

NOT REPRODUCIBLE

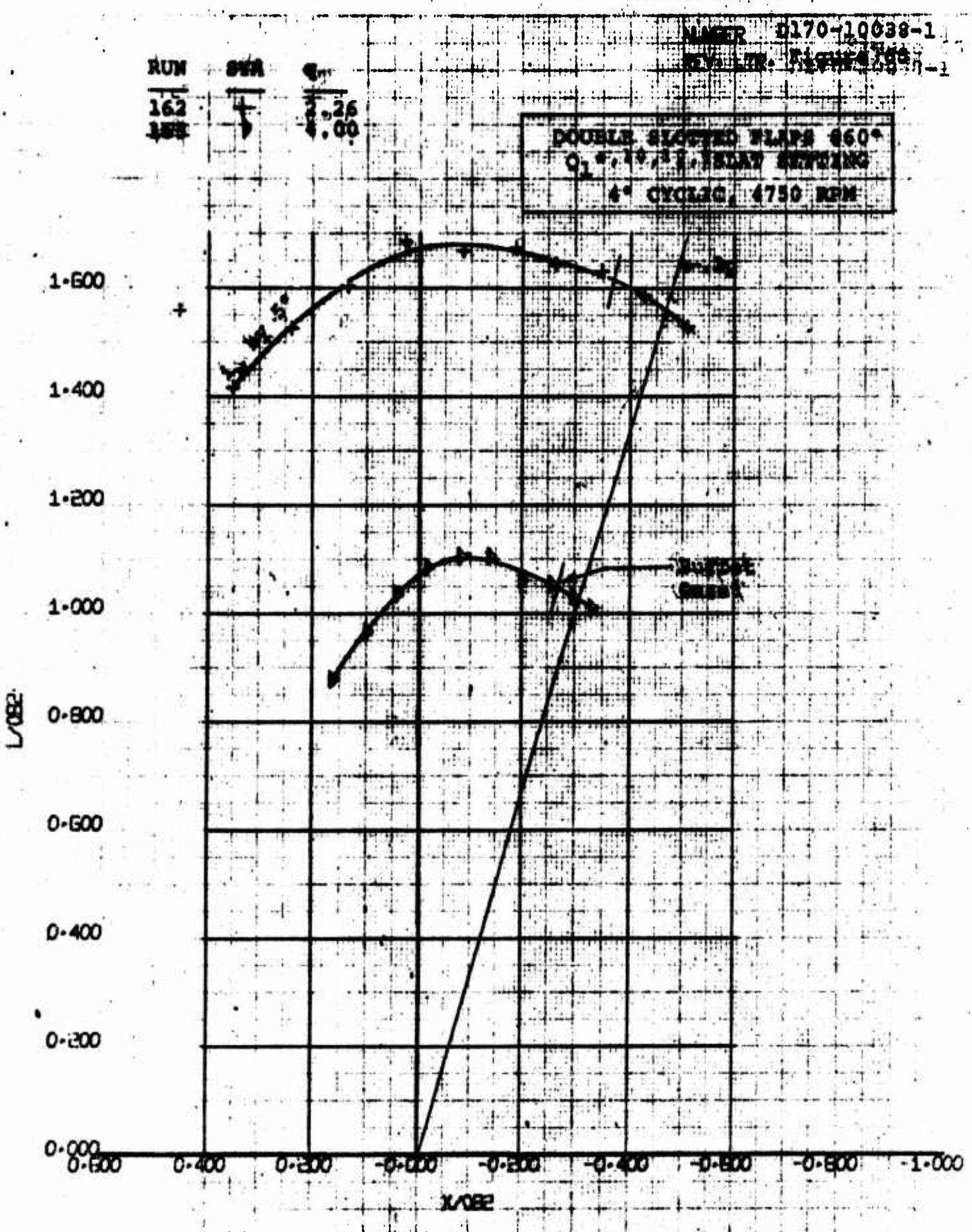

4-PROP TILT WING MODEL VROOM (FULL SPAN) L/QB2 VS X/QB2	BWT 61 8/19/70

RUN	SYM.	q
162	+	2.36
163	▷	4.80

NUMBER D210-10038-1
REF: TR. Figure 86 - 1

DOUBLE SLOTTED FLAPS 60°
0°, 11°, 28° SLAT SETTING
6° CYCLIC, 1750 RPM

L/QB2

1·600
1·400
1·200
1·000
0·800
0·600
0·400
0·200
0·000

0·000 10·000 20·000 30·000 40·000 50·000 60·000 70·000 80·000

IW DEGREES

4-PROP TILT WING MODEL VROBBO (FULL SPAN) L/QB2 VS IW	BVWT 61 8/19/70

NOT REPRODUCIBLE

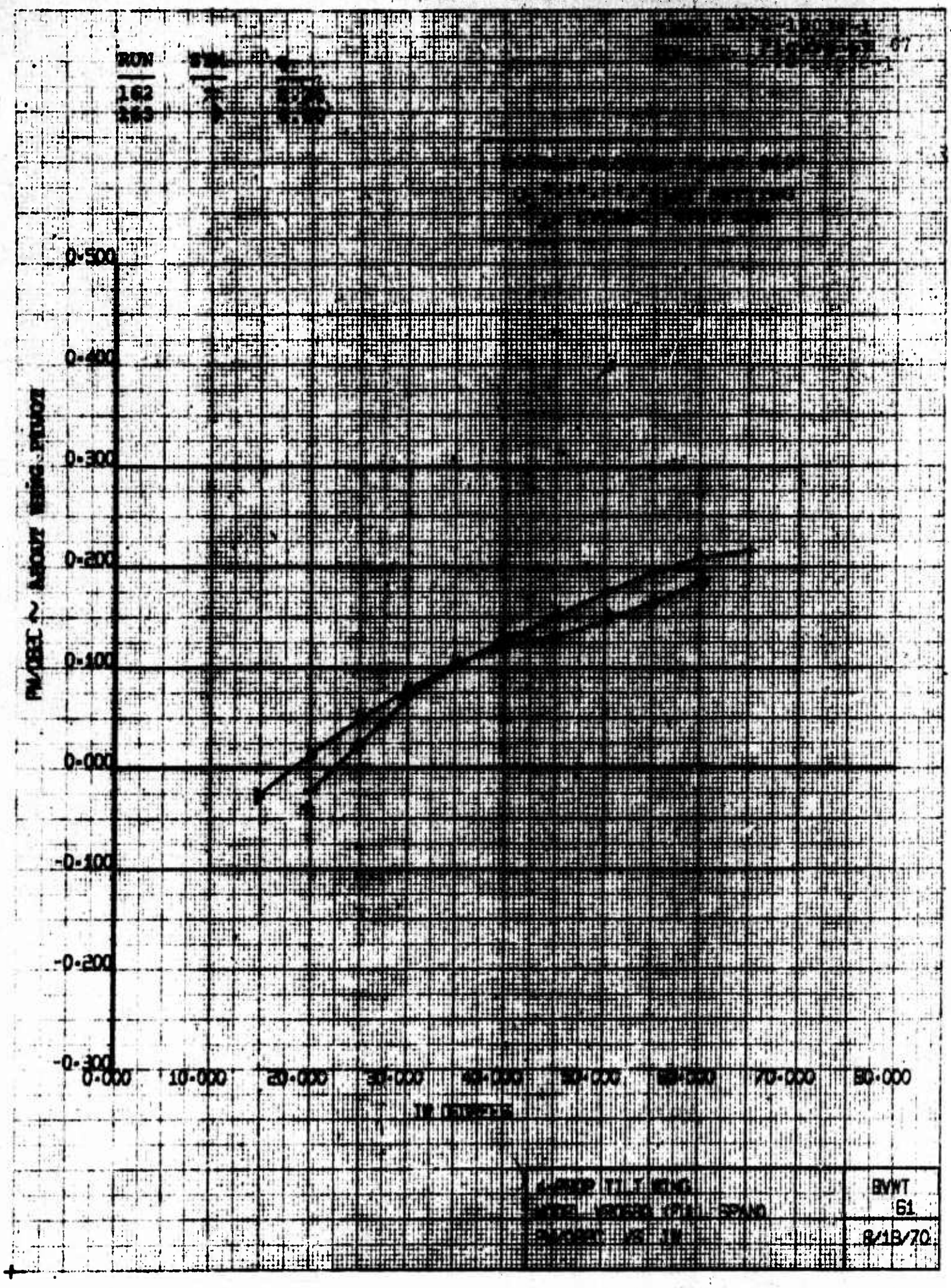

NOT REPRODUCIBLE

6.3.2 Basic Flap-Down Lift/Drag Characteristics

Tail off pitch runs were performed with 20°, 40° and 60° of flap deflection/slats extended to ascertain the basic flaps-down low speed lift/drag/pitching moment characteristics. Figure 68 presents the data along with the data from the comparative flaps up/slats retracted clean wing run.

A decision was made to perform the noted runs with the props on and operating at zero thrust instead of with the props off, so that the unpredictable increment in $C_{L_{MAX}}$ that has been found to exist between the props off case and the zero thrust/props on case would be inclusive in the data. During these runs, it was necessary to reduce the propeller RPM as the model was pitched in order to maintain zero thrust. The propeller speed for Runs 48 and 49 varied from 6800 RPM at zero angle of attack to 6175 RPM at 20°. For Runs 113 and 133 the variation was from 5950 RPM at zero angle of attack to 5350 RPM at 20°.

Figure 68 shows that the maximum lift coefficient is increased from a clean wing value of 1.4 to 3.87 by deflecting the double slotted flaps to 60° plus extending the slats. The angle of attack for $C_{L_{MAX}}$ is essentially constant at 26.5° for flap angles of 20° and 40°, but is reduced a couple of degrees when the flap is extended further to 60°.

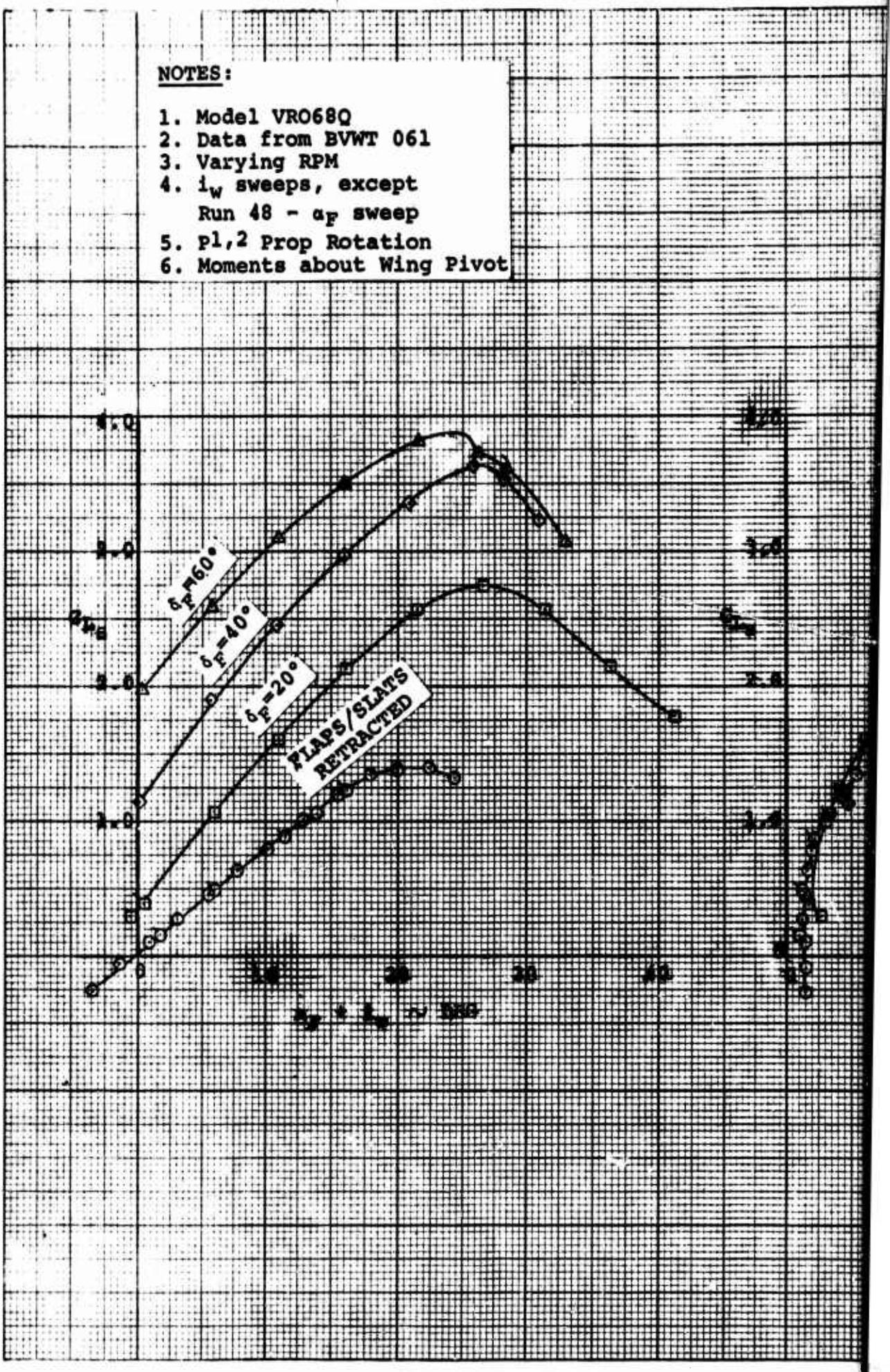

EUGENE DIETZGEN CO.
MADE IN U.S.A.
NO. 340DR-20 DIETZGEN GRAPH PAPER
20 X 20 PER INCH

NOT REPRODUCIBLE

REV LTR

Figure 46

SYM	RUN	δ_F	SLAT	q
⊙	48	0°	Q_1^*	34.5
□	49	20°	$Q_1^{*,10,10,11,*}$	✓
◇	113	40°	$Q_1^{*,10,10,*}$	29.7
△	133	60°	✓	29.5

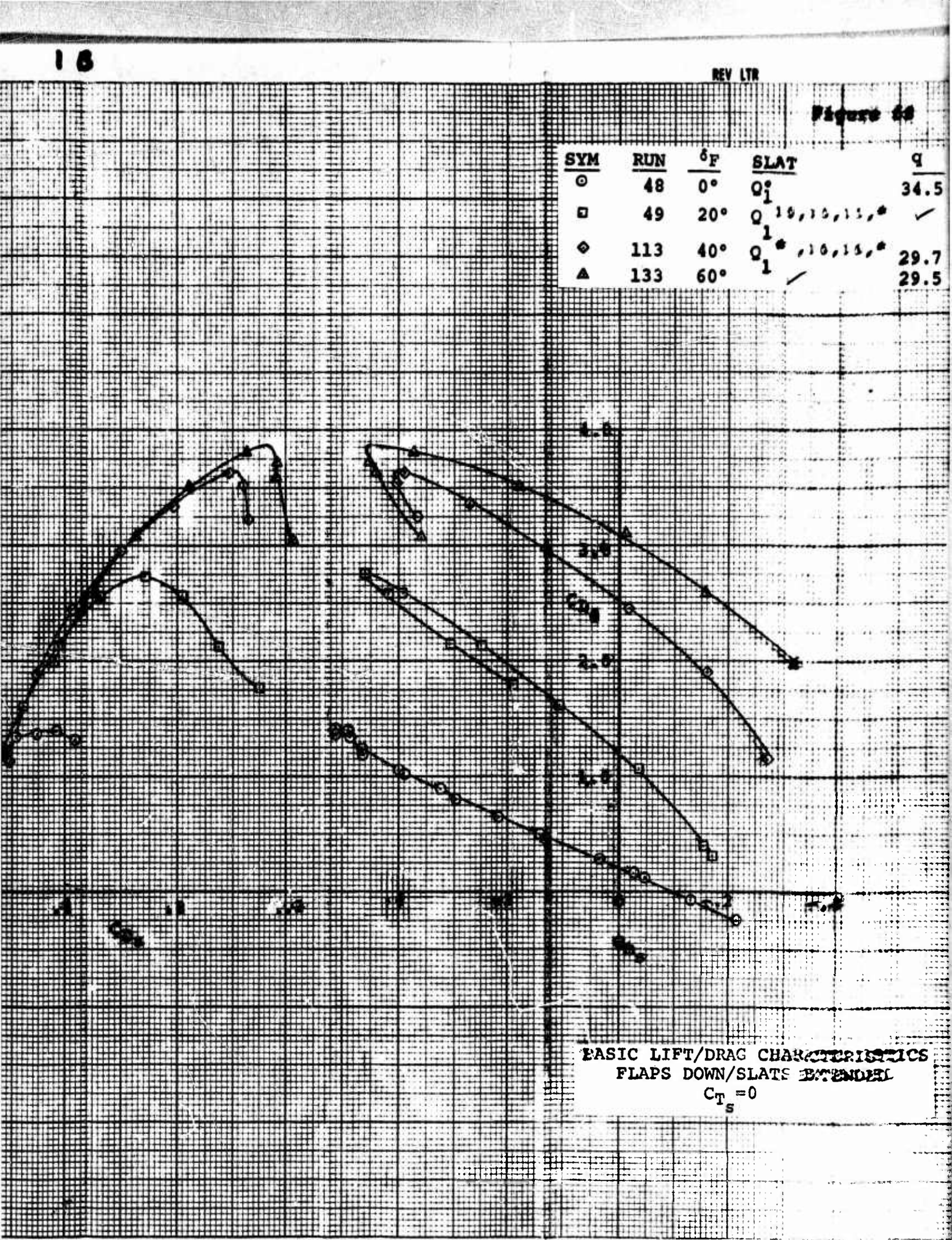

BASIC LIFT/DRAG CHARACTERISTICS
FLAPS DOWN/SLATS EXTENDED
$C_{T_S}=0$

6.4 LONGITUDINAL STABILITY AND CONTROL IN TRANSITION

Longitudinal stability/control characteristics of the four prop tilt wing model were investigated throughout the transition flight regime with and without the horizontal tail depicted in Figure 16. The high positioning of this tail on the vertical fin as illustrated in Figure 15 resulted in a horizontal tail volume coefficient of 1.33.

Fuselage pitch runs were performed at constant RPM (except the zero thrust runs) for selected combinations of wing tilt angle and flap angle that were representative of typical combinations required in transition. Data was taken at wing incidence settings ranging from zero to seventy degrees and flap angles ranging from zero to sixty degrees. The slipstream thrust coefficient (C_{T_s}) for these runs varied from zero for the zero wing tilt angle case to 0.96 for the 70° wing tilt angle case. Runs were made with a sufficient number of stabilizer angle settings at the various wing/flap combinations so that the horizontal tail effectiveness could be established over the C_{T_s} range from zero to 0.92.

As mentioned in Section 2.6 of this report, the wing angle of attack range for evaluation with a prescribed combination of wing tilt angle and thrust coefficient was adjustable per the sting "pre-bend" angle selection. These "pre-bend" angles were chosen prior to each set of runs so that the data could be acquired at or near representative flight conditions.

All moments obtained during the longitudinal stability runs were transferred to a representative mid-center of gravity. This center of gravity moves up and back as the wing tilt angle increases. Positions of the c.g. for the various wing tilt angles used, were calculated by utilizing the scaled wing-down longitudinal and vertical locations for the fixed mass c.g. and rotating mass c.g. (with respect to the wing chord line) of a representative transport-type four prop tilt wing aircraft with a V-mode gross weight of 86,930 lb. (and no dihedral), plus the wing pivot location of the model. Model scale with respect to this aircraft was 1/12.3.

Figure 69 shows the relative locations of the rotating mass c.g., fixed mass c.g., and resultant aircraft c.g. to the wing pivot for the wing down case and 70° wing tilt case. The movement of the aircraft c.g. with wing tilt angle that was used in the data reduction program is illustrated in Figure 70. As can be seen, the movement of the c.g. for a wing angle change from zero to 70° is 10.3% MAC aft and 15.5% MAC up.

Figure 69

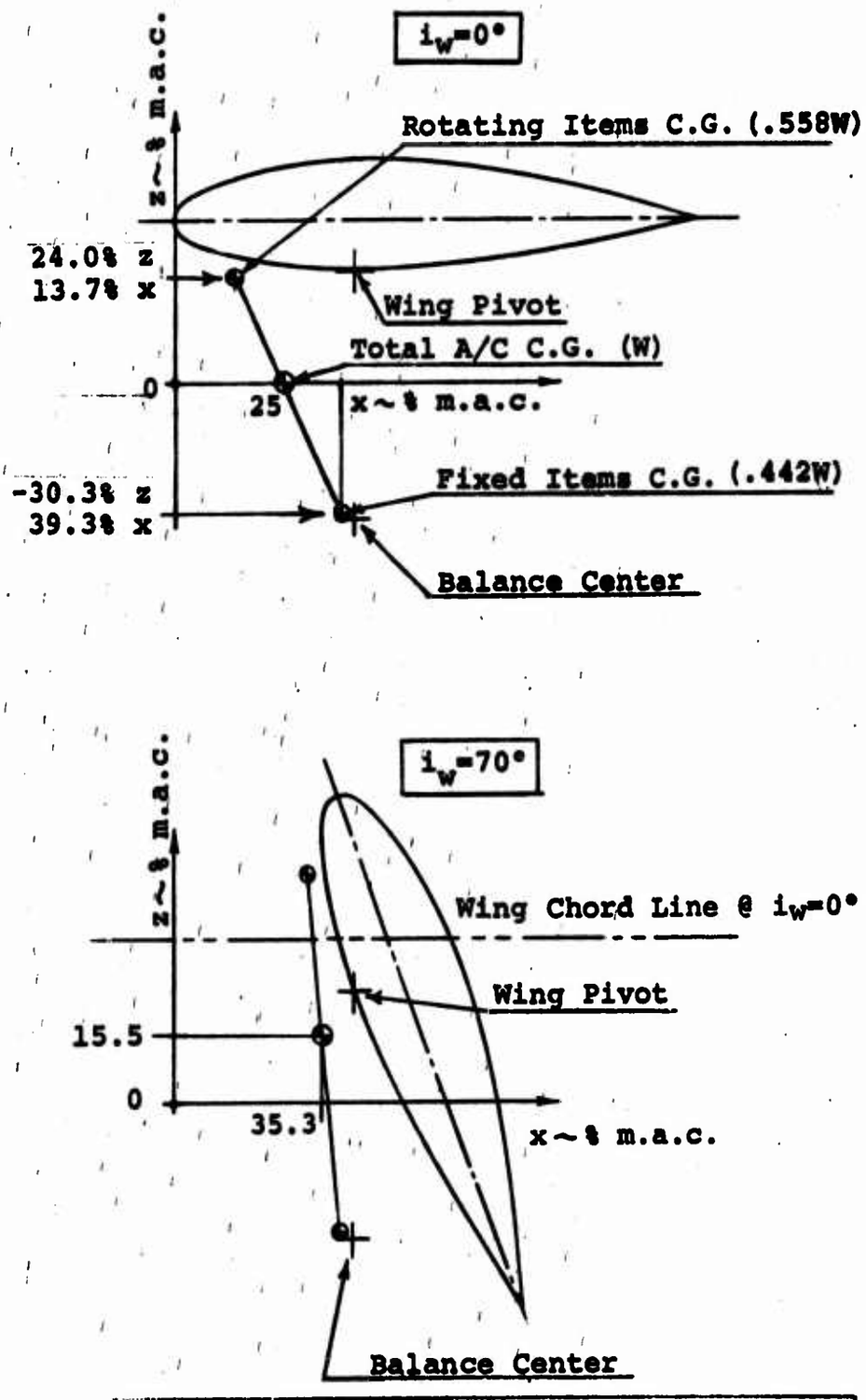

SCHEMATIC RELATIONSHP BETWEEN
FIXED AND ROTATING PORTIONS OF A/C WEIGHT

Figure 70

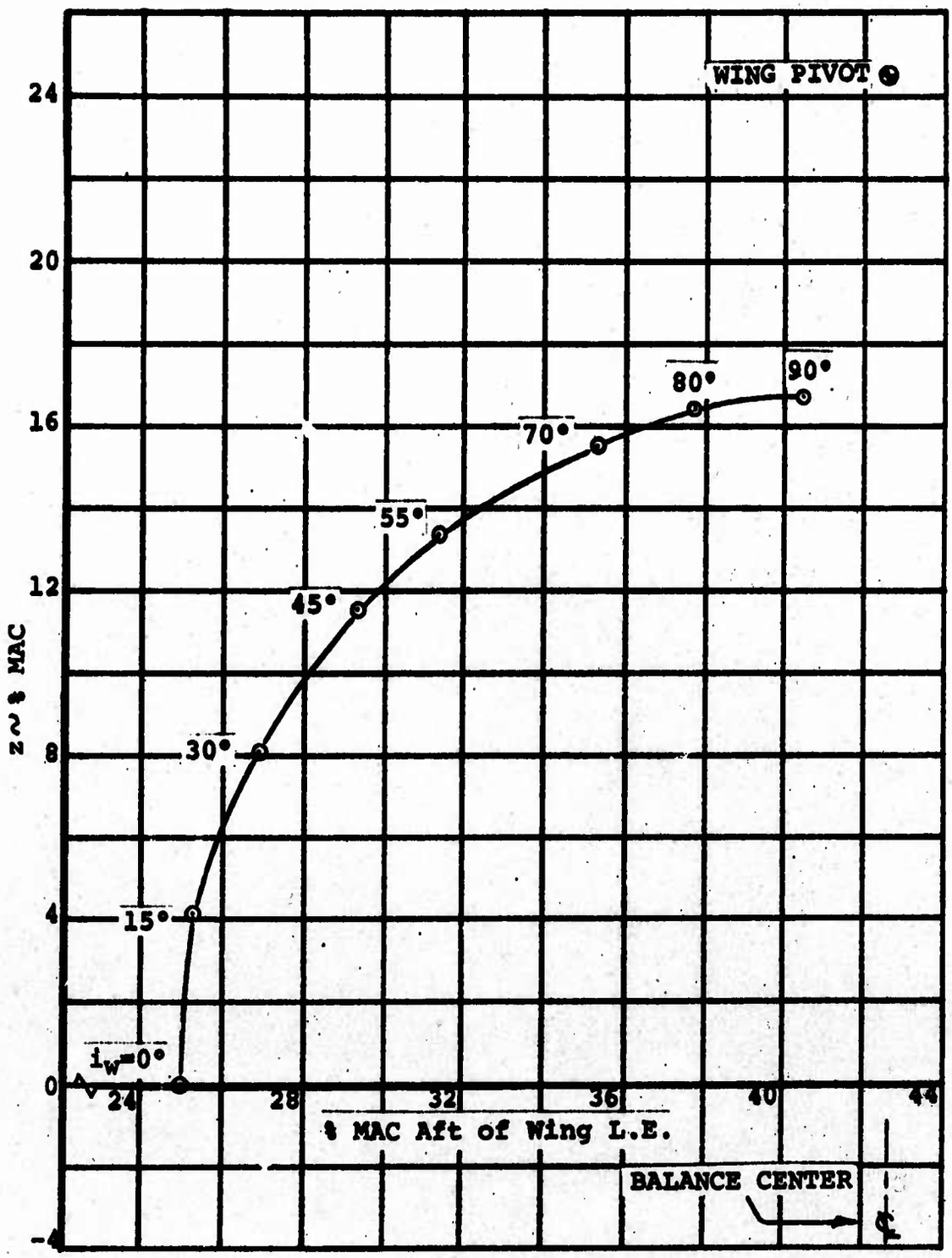

MOVEMENT OF A/C CENTER OF GRAVITY
WITH WING TILT

6.4.1 Horizontal Tail Effectiveness

The effectiveness of the horizontal tail (high position) in producing pitching moment is presented in Figure 71 in terms of $\Delta C_{m_s}/\Delta\delta$ vs C_{T_s}. Values are shown for the various combinations of wing tilt angle/flap angle/C_{T_s} evaluated.

As would be expected, the stabilizer effectiveness decreases with increasing C_{T_s} (decreasing aircraft speed). The decrease is seen to be a function of $(1-C_{T_s})$ as denoted in Figure 71. Thus it could be concluded that the horizontal tail is essentially outside the influence of the propeller slipstream and is acted upon, primarily, by freestream q.

Also noted in Figure 71 is the value of $\Delta C_{m_s}/\Delta\delta$ predicted from DATCOM for the props off (zero C_{T_s}) condition assuming a unity ratio of q at the tail to freestream or tunnel q. The maximum value of $\Delta C_{m_s}/\Delta\delta$ measured on the model is .86 of the predicted value.

Wing tilt is seen to decrease stabilizer effectineness; the reduction being a function of tilt angle magnitude.

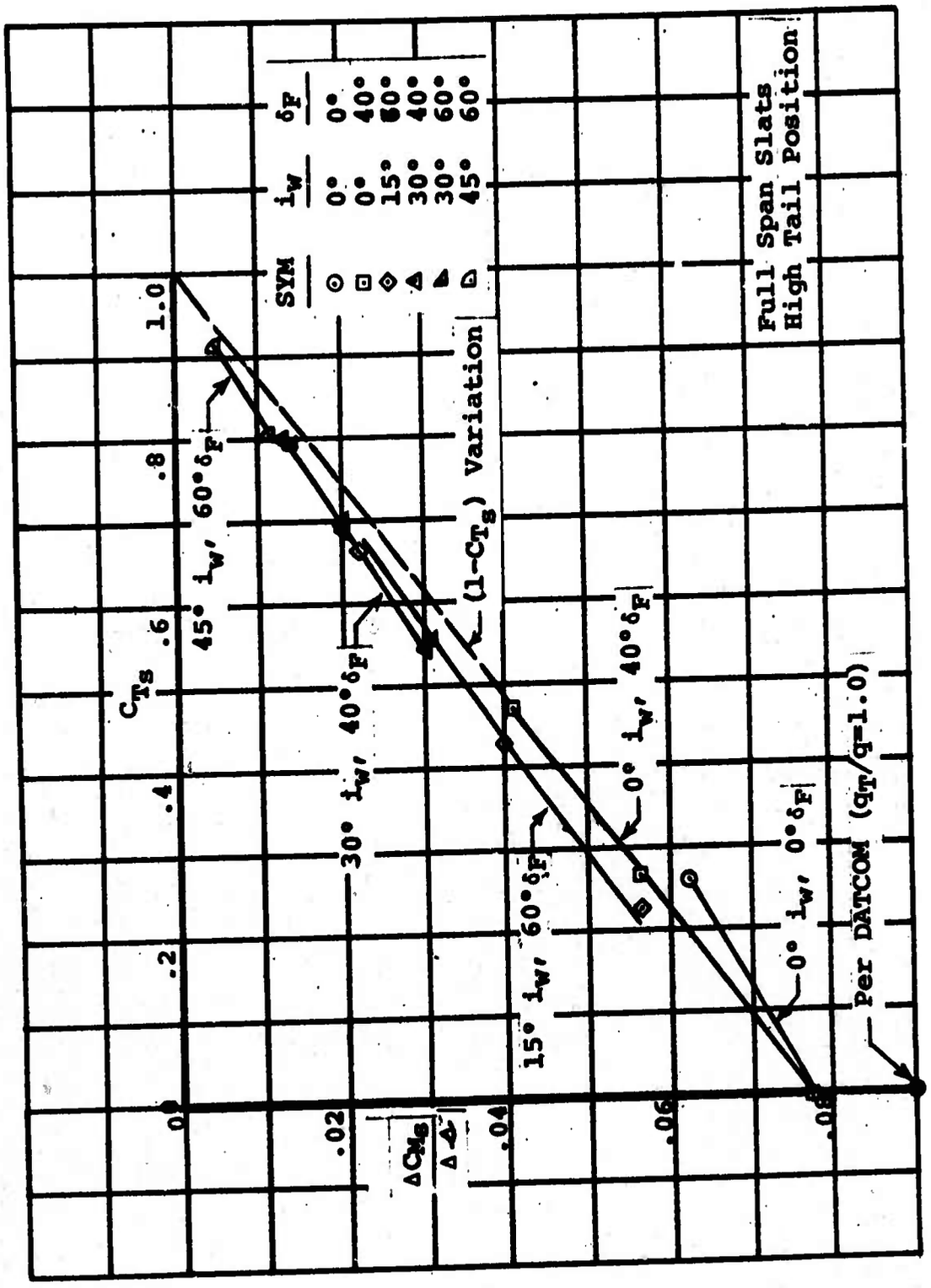

HORIZONTAL TAIL EFFECTIVENESS
HIGH TAIL POSITION

6.4.2 Downwash at the Horizontal Tail

The downwash data in terms of the variation of downwash angle (ϵ) with fuselage angle of attack (α_F) is presented in Figures 72 thru 75. Each plot shows the downwash angles measured at the various thrust coefficients (C_{T_s}) evaluated for a particular wing tilt angle. The downwash angles, defined as the angle by which the freestream flow is deflected by the lifting system, were determined from the intersection of tail off/tail on pitching moment curves presented later in Section 6.4.4. Thrust coefficients denoted in Figures 72 thru 75 are the average values over the angle of attack range for which pitching moment curve intersections were available, i.e., except for the high C_{T_s} runs, C_{T_s} varied during the sweeps at constant RPM.

Figure 72 (wing down/δ_F=0° and 40°) illustrates the change in downwash angle associated with an increase in C_{T_s} (decreasing aircraft speed) and shows the increase in downwash angle due to deflecting the flaps to the 40° position (increasing lift coefficient). An additional increase in downwash angle of approximately 1° was recorded when the flaps were deflected further from 40° to 60°. This is shown in Figure 74 (i_W=30°/ δ_F=40° and 60°).

An examination of Figures 72 thru 75 will show that for a given wing lift condition (constant α_F+i_W and C_{T_s}), the downwash angle at the high tail position is reduced when the wing is tilted beyond 15°. This is graphically depicted in Figure 76 which presents the measured downwash angle at two specific wing angles of attack (α_F+i_W) of 25° and 15°. As the wing is tilted beyond 15°, the associated change in fuselage angle geometrically raises the horizontal tail with respect to the wing/propeller slipstream wake.

In the curves presented in Figures 72 and 73, the rate of increase in downwash angle with angle of attack is seen to diminish at the higher angles of attack evaluated. A study of the pitching moment data and related tuft observations revealed that the reduction in $d\epsilon/d\alpha_F$ corresponded to the separation of the flow on top of the fuselage. The noted decrease in downwash angle occurred when the separation starting at the wing center section progressed aft to the vertical fin.

The $d\epsilon/d\alpha_F$ values measured from the linear portions of the ϵ vs α_F curves are plotted in Figure 77 as a function of C_{T_s}. This figure shows that the downwash gradient for the clean configuration is low (.2$d\epsilon/d\alpha_F$ or less) and that with the flaps down, it increases with C_{T_s} from a value of .3 at zero C_{T_s} to

a value of .5 at a C_{T_s} of approximately 0.7. Wing tilt angle can be noted to have only a small influence on $d\epsilon/d\alpha_F$. At the higher wing tilt angle (30° and 45°) and C_{T_s} (0.8 and 0.92) combinations evaluated, the rise in $d\epsilon/d\alpha_F$ with C_{T_s} is significant.

Figure 72

DOWNWASH AT HORIZONTAL TAIL
WING DOWN, i_w=0°

SYM	i_w	δ_F	C_{T_s}
⊙	0°	0°	0
⊡	0°	0°	.26
◐	0°	40°	0
■	0°	40°	.28
▲	0°	40°	.47

NOTES:
1. Model VRO68Q
2. Data from BVWT 061
3. High Tail Position
4. $P_{1,2}$ Prop Rotation
5. Full Span Slats

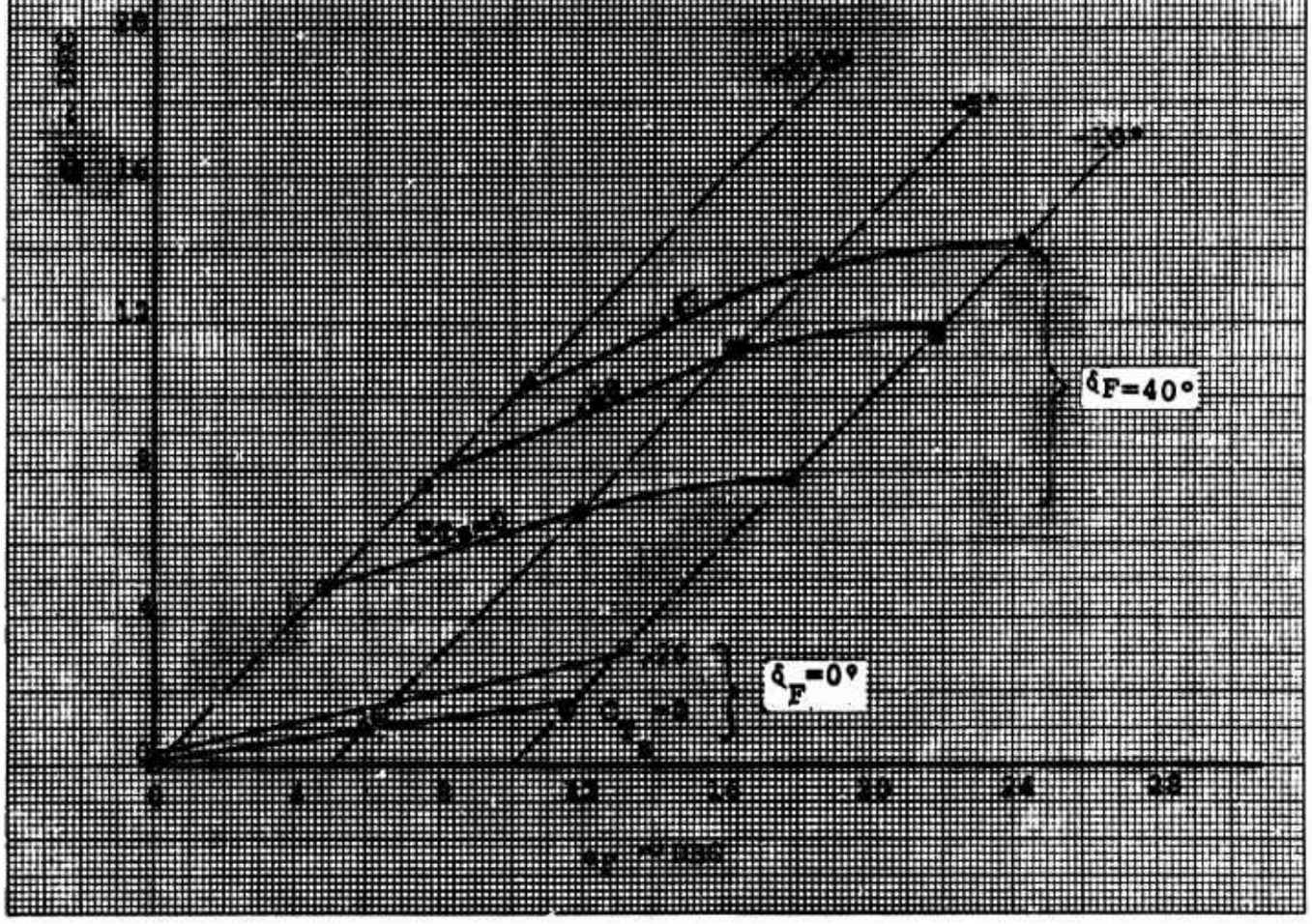

EUGENE DIETZGEN CO.
MADE IN U. S. A.
NO. 340R-MP DIETZGEN GRAPH PAPER
MILLIMETER

 NOT REPRODUCIBLE

Figure 73

DOWNWASH AT HORIZONTAL TAIL

i_w=15°/δ_F =60°

SYM	C_{T_s}
□	.23
△	.43
◇	.66

NOTES:

1. Model VRO68Q
2. Data from BVWT 061
3. High Tail Position
4. $P_1^{1,2}$ Prop Rotation
5. Full Span Slats

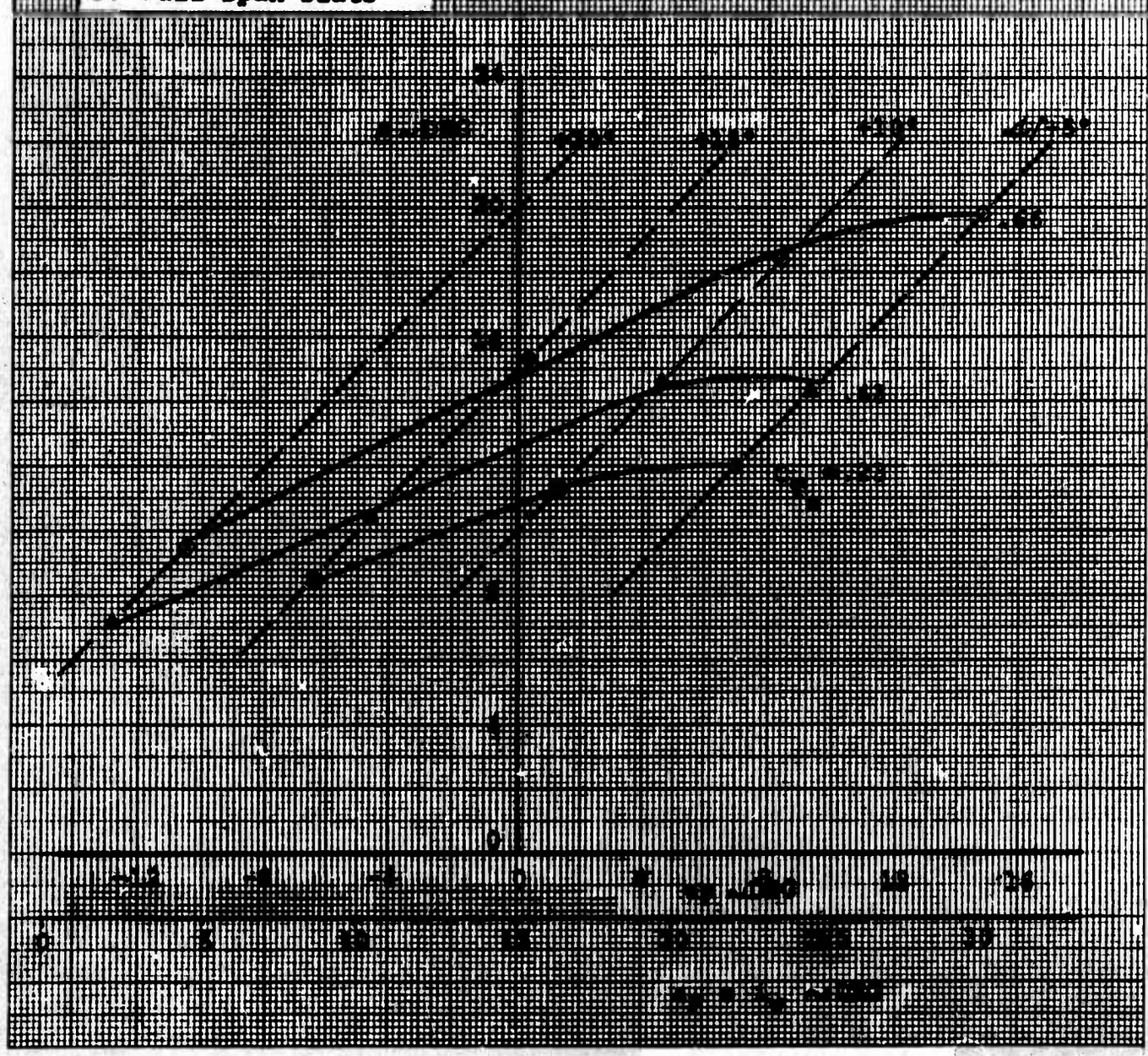

EUGENE DIETZGEN CO.
MADE IN U. S. A.

NO. 340R-MP DIETZGEN GRAPH PAPER
MILLIMETER

NOT REPRODUCIBLE

NO. 340R-MP DIETZGEN GRAPH PAPER
MILLIMETER
EUGENE DIETZGEN CO.
MADE IN U. S. A.

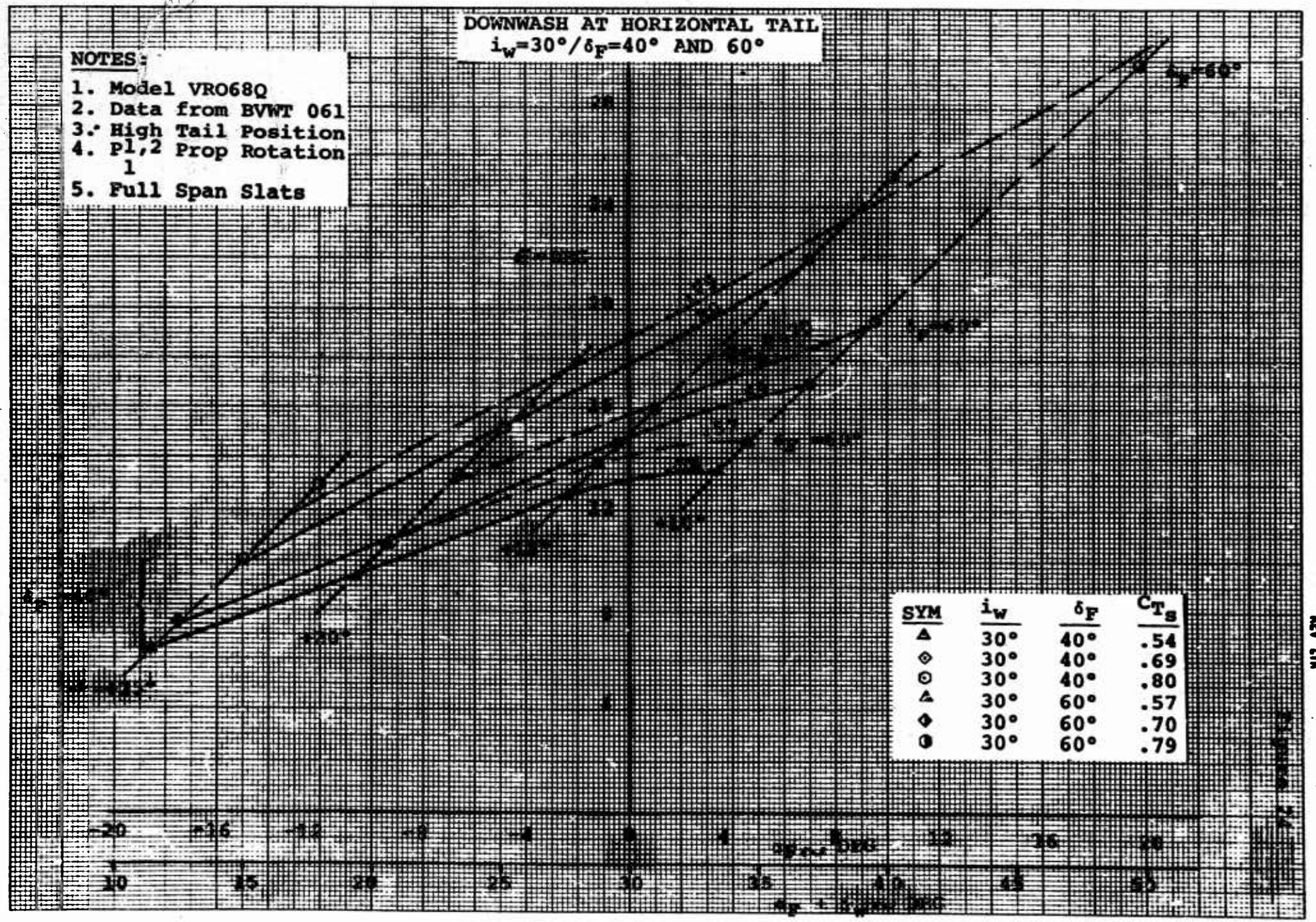

SHEET 124

NUMBER D170-10038-1
REV LTR

Figure 75.

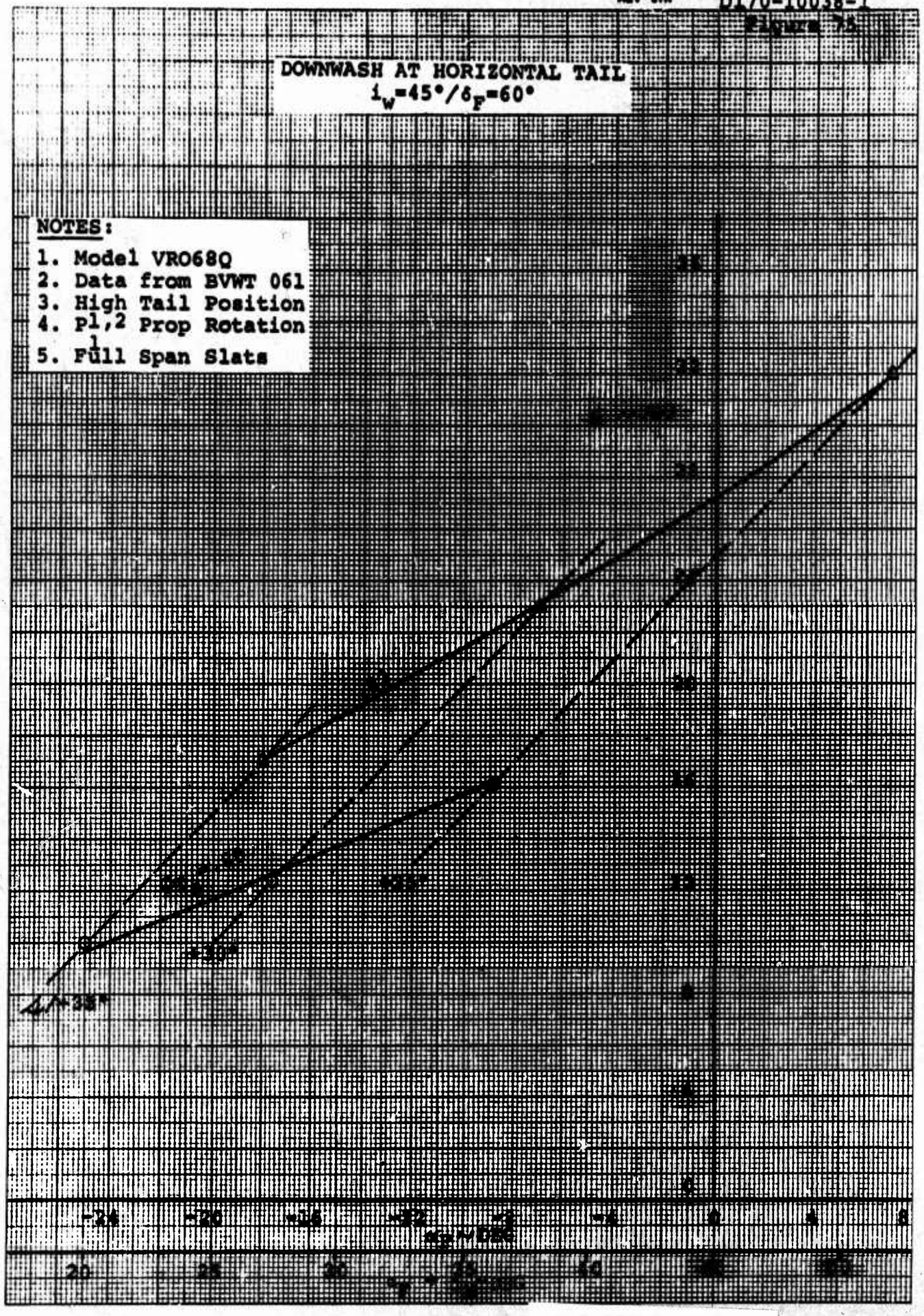

EUGENE DIETZGEN CO.
MADE IN U. S. A.
NO. 340R-MP DIETZGEN GRAPH PAPER
MILLIMETER

 NOT REPRODUCIBLE

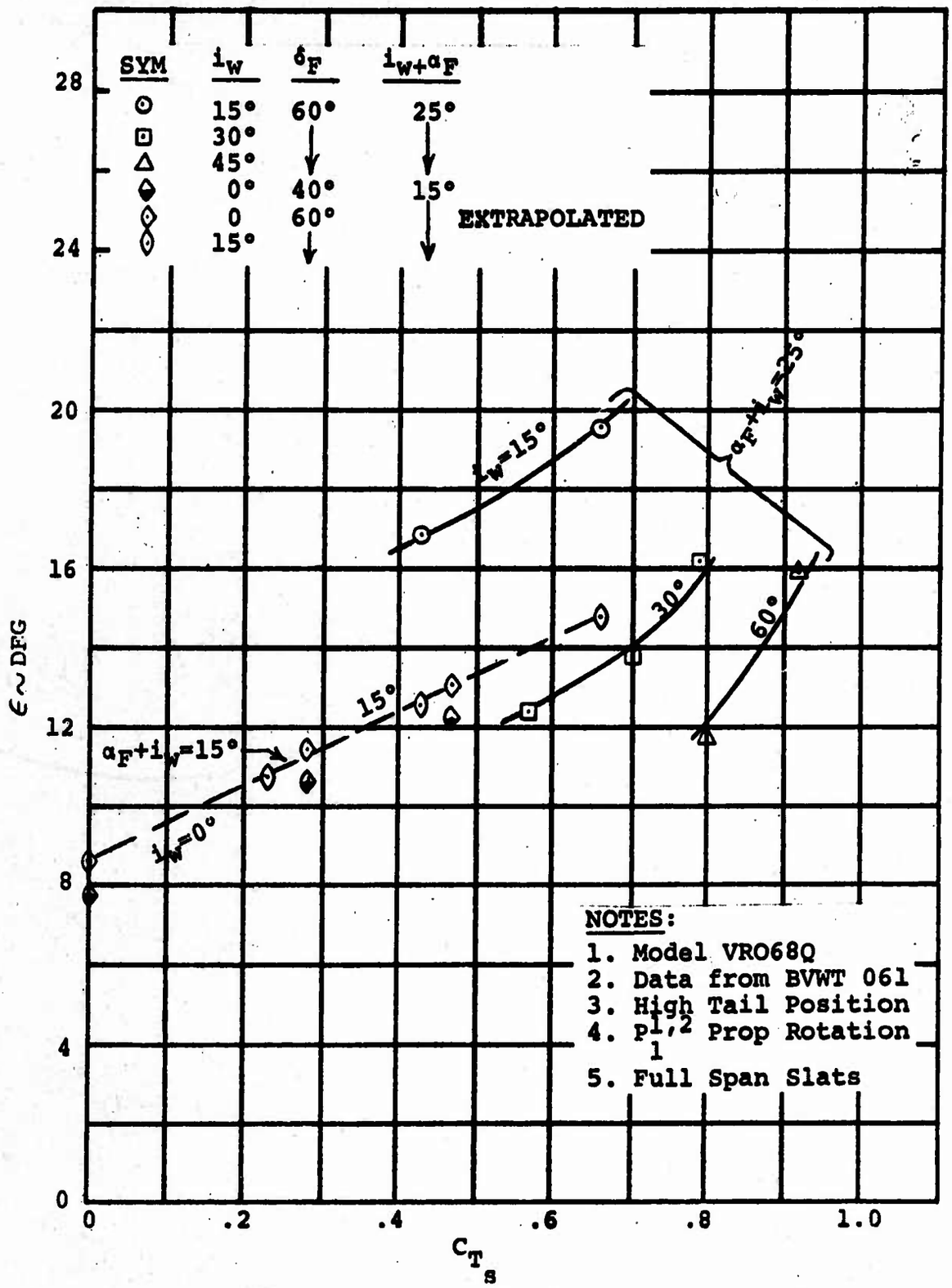

CHANGE IN DOWNWASH
AT A CONSTANT WING ANGLE OF ATTACK

Figure 77

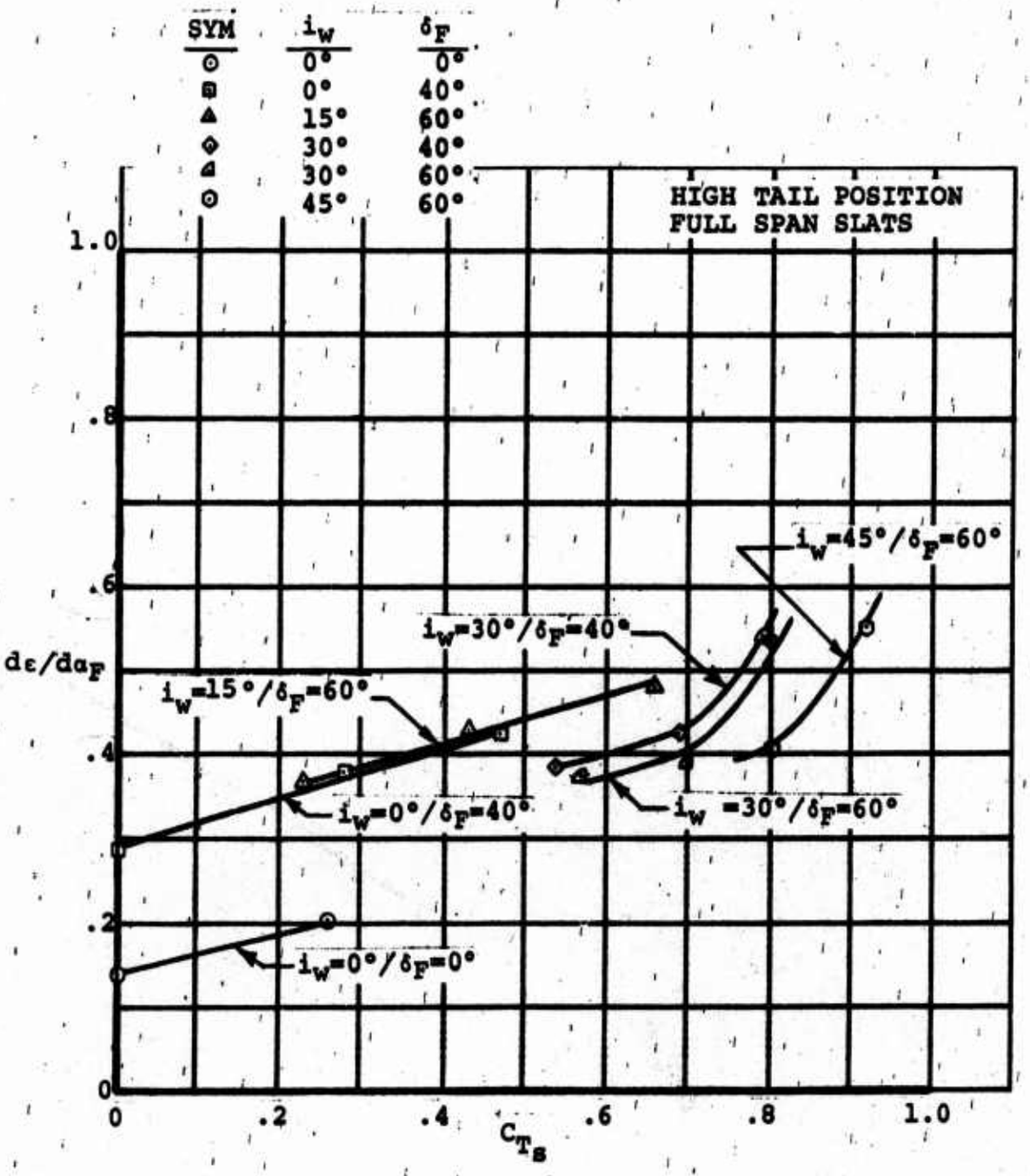

DOWNWASH GRADIENT, $d\epsilon/d\alpha_F$

6.4.3 Tail-on/Tail-off Longitudinal Stability (Mid c.g.)

Figures 78 and 79 present the measured tail-off and tail-on stability derivative $C_{M_{s_\alpha}}$ for the various wing tilt angle/flap angle combinations evaluated. This data, which encompasses a thrust coefficient (C_{T_s}) range from 0 to .96 and is presented in slipstream notation, is applicable for a mid c.g. The specific change in c.g. location with wing tilt angle was described in the introduction to Section 6.4.

Slopes shown in Figures 78 and 79 were measured from the stability plots (C_{M_s} vs α_F) presented later in Section 6.4.4 and were extracted from the linear portion of the curves. The C_{T_s} value designated for each data point is the average value for the angle of attack range considered in choosing a slope.

Tail-off data presented in Figure 78 shows a decrease in level of instability with increasing C_{T_s} that is in accord with a zero $C_{M_{s_\alpha}}$ value at a C_{T_s} of 1.0 (zero freestream q). The relatively high tail-off instability for the wing down/flaps up case is sharply reduced by deflecting the flaps to 40°. This condition reflects the aftward movement in center-of-pressure associated with the flap Fowler action. Deflecting the flaps to a higher angle (60°) did not result in a further reduction of the tail-off instability per the evaluation made with both 30° and 55° of wing tilt angle.

Tilting the wing up 15° from the wing down position produced a substantial increase in the tail-off instability. This was probably due to the adverse influence exerted by the four propeller hub moments and normal forces. An additional 15° of wing tilt (30° wing tilt angle) produced an increment in tail-off instability that was one-third of the increment recorded by the initial 15° of wing tilt. Wing tilt angles higher than 30° (45°,55°, and 70° were tested) resulted in progressive reductions in the tail-off instability. This situation reflects the aftward movement of the aerodynamic center with respect to the c.g.

The reduction in tail-on stability depicted in Figure 79 for the wing down cases with flaps up and at 40°, is indicative of the decrease in q acting upon the tail (primarily freestream q) and the increase in downwash gradient with C_{T_s} (Figure 77).

Considering the effect of flap deflection on stability, it is seen in Figure 79 that with the wing down, deflection of the flaps at 40°, has a destabilizing effect tail-on whereas the same action decreased the tail-off instability. The reason

reason for this is primarily the loss in the tail contribution to stability due to an increase in the downwash gradient (Figure 77). As in the tail-off case, additional flap extension to 60° did not change the stability.

The initial 15° of wing tilt had a substantial tail-on destabilizing effect, a direct influence of the tail-off characteristics, resulting in the aircraft being unstable at C_{T_s} values larger than .47. Increasing the wing tilt angle to 30° did not cause a further reduction in tail-on stability even though a destabilizing effect was noted tail-off, i.e., the downwash gradient decreased.

The downwash gradient effect was also evident at the higher wing tilt angles evaluated (45° and 55°). As shown in Figure 79, the net effect is an essentially constant $C_{M_{s_\alpha}}$ value of approximately +.005 from a C_{T_s} of .7 to .96 with wing tilt angles of 30° to 55° for the mid c.g. case.

Figure 78

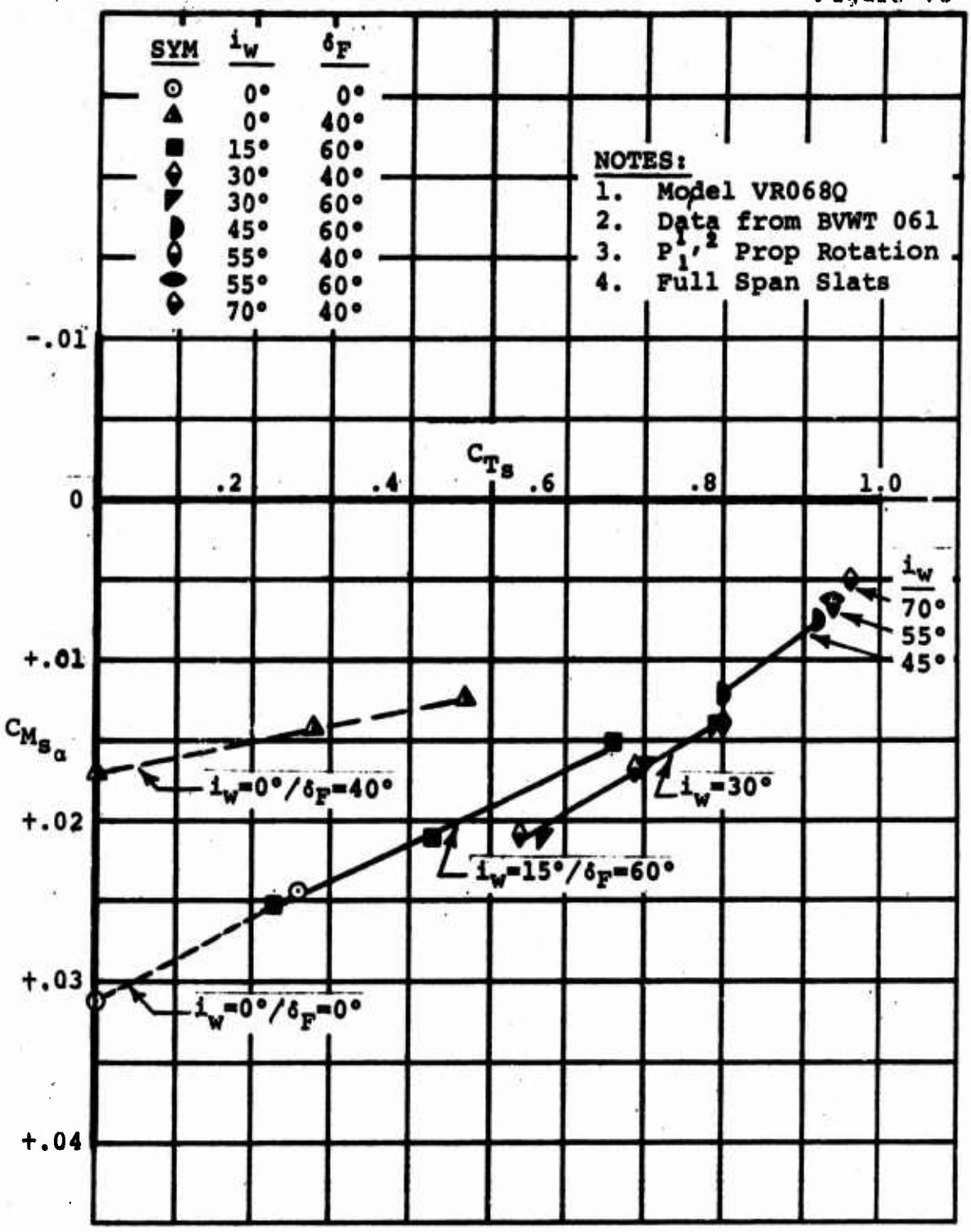

TAIL-OFF LONGITUDINAL INSTABILITY
MID c.g./ZERO CYCLIC

Figure 79

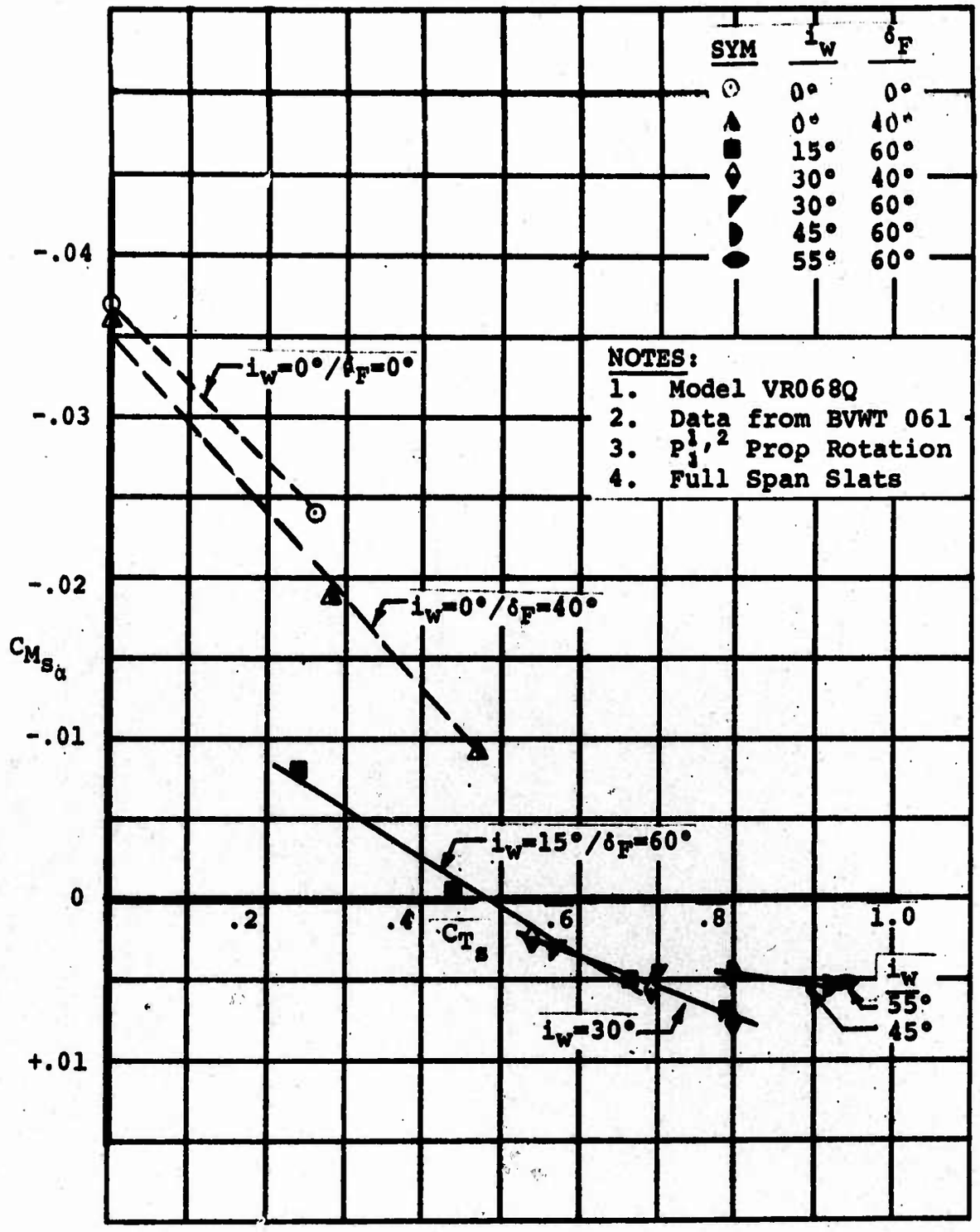

TAIL-ON LONGITUDINAL STABILITY
MID c.g./ZERO CYCLIC

6.4.4 Basic Longitudinal Stability Data

This section includes the on-line data plots (Figures 80 thru 136) obtained during the longitudinal stability investigation of the subject test. The data, in slipstream notation, is presented in sets of three plots, C_{M_s} vs α_F (pitching moment curves), C_{L_s} vs C_{X_s} (force polars), and C_{L_s} vs α_F (lift curves), in the order of increasing wing tilt angle/flap angle. In these plots, CMCS, CLCS and CXCS should be read as C_{M_s}, C_{L_s} and C_{X_s}, respectively. ALPHA signifies fuselage angle.

The following plots contain series of runs, all conducted at a constant propeller RPM or nominal C_{T_s} and a selected wing tilt/flap configuration. Each series of runs included a tail-off run, followed by three or four tail-on runs with different tail incidences relative to a fuselage waterline, so that horizontal tail effectiveness could be established. Running multiple tail incidences was not deemed necessary at the highest thrust coefficients of the test (.94 and .97 C_{T_s} with tilt angles of 55° to 70°) since the usefulness of the horizontal tail for trim at these condtions is such low percentage of that required. Noted on each force polar plot are lines corresponding to 10° descent and 10° climb conditions.

During the longitudinal stability investigation, dynamic response characteristics inside the nacelle assemblies necessitated a reduction in the test RPM from 6800 to 6000. Two tail-off check runs were made to ensure that the reduction in propeller speed had no effect on the stability data when reduced to coefficient form. The comparisons presented in Figure 89 (wing down/40° flaps/.3C_{T_s} case) and Figure 92 (wing down/40° flaps/.5C_{T_s} case) illustrate this.

An examination of the pitching moment plots, for example Figure 95 (15° wing tilt/60° flaps/.3C_{T_s}), will reveal that the pitching moment, tail-off and tail-on, varies linearly with fuselage angle of attack over the initial portion of the angle of attack range tested. At a particular angle of attack for a given test condition, the tail-off instability ($C_{M_{s_\alpha}}$) appears to decrease. A comparison of the change in pitching moment characteristics with tuft observations taken during the test, established that this condition is concurrent with flow separation on the top of the fuselage as noted on Figure 95 and accompanying figures.

Figure 95 also shows that an improvement in tail-on stability occurs at the same time that the tail-off instability decreases. This tail-on stability change reflects (in addition

to that portion due to the obvious relationship between tail-off and tail-on stability characteristics) the decrease in downwash gradient that takes place during the mentioned flow separation (discussed in Section 6.4.2).

As the fuselage was pitched, the flow separation that started at the wing center section progressed aft along the fuselage to the vertical tail. Further pitching of the model caused the separated flow region to move up the fin. At some fuselage angle of attack, the horizontal tail mounted on top of the fin entered the wake. At this point, noted on the example plot (Figure 95), the decrease in horizontal tail effectiveness is evident.

At the highest thrust coefficients evaluated (.92 to .96 C_{T_s}) with wing tilt angles from 45° to 70°, the character of the flow aft of the tilted wing changed and no separated flow was observed in the vicinity of the vertical tail. As a consequence the tail-off and tail-on pitching moment curves were linear over the angle of attack range evaluated. For example, see Figure 125 (45° wing tilt/60° flaps/.92 C_{T_s}).

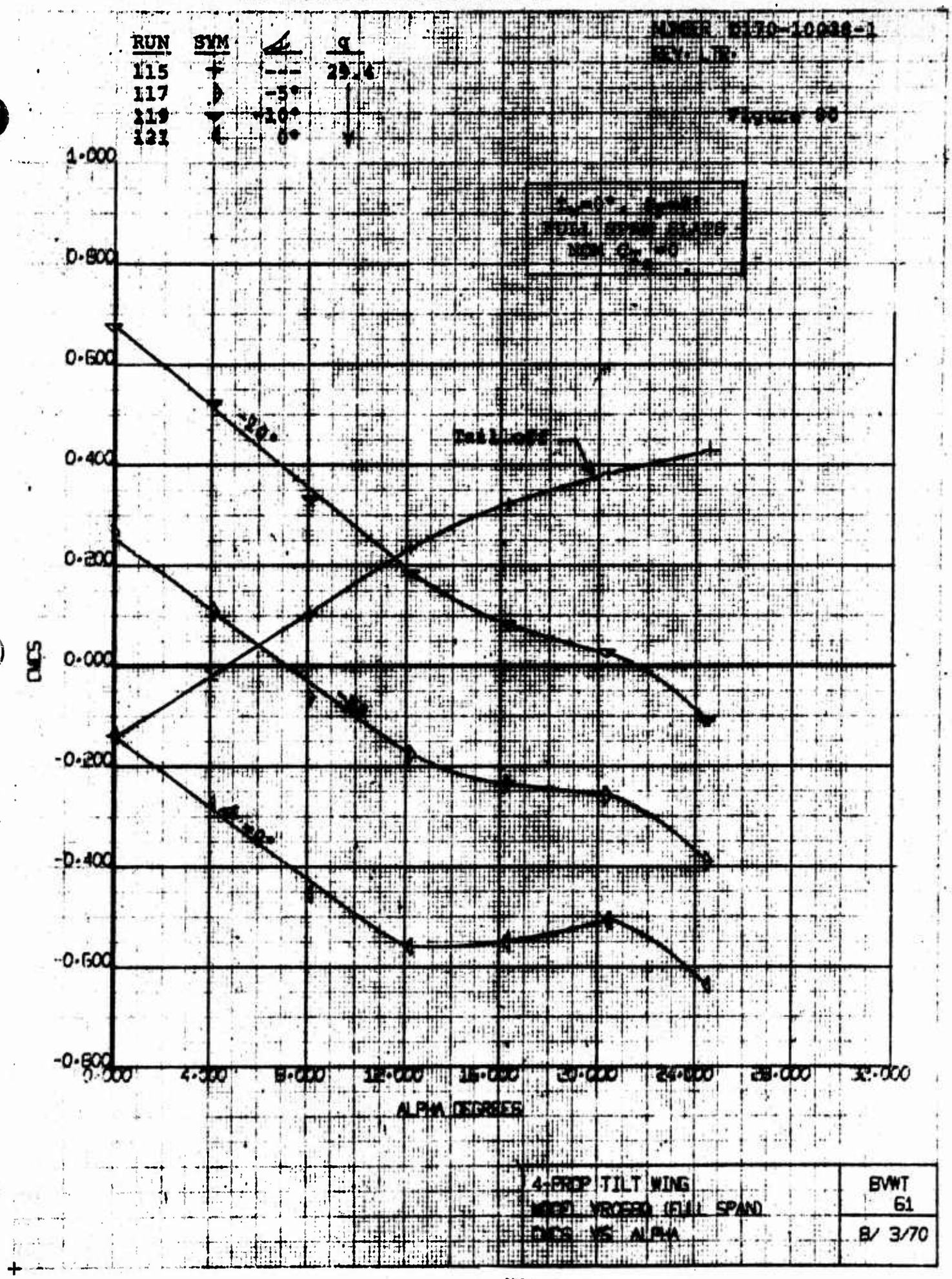

4-PROP TILT WING WING W/CROSS (FULL SPAN) CMCS VS ALPHA	BVWT 61 8/ 3/70

NOT REPRODUCIBLE

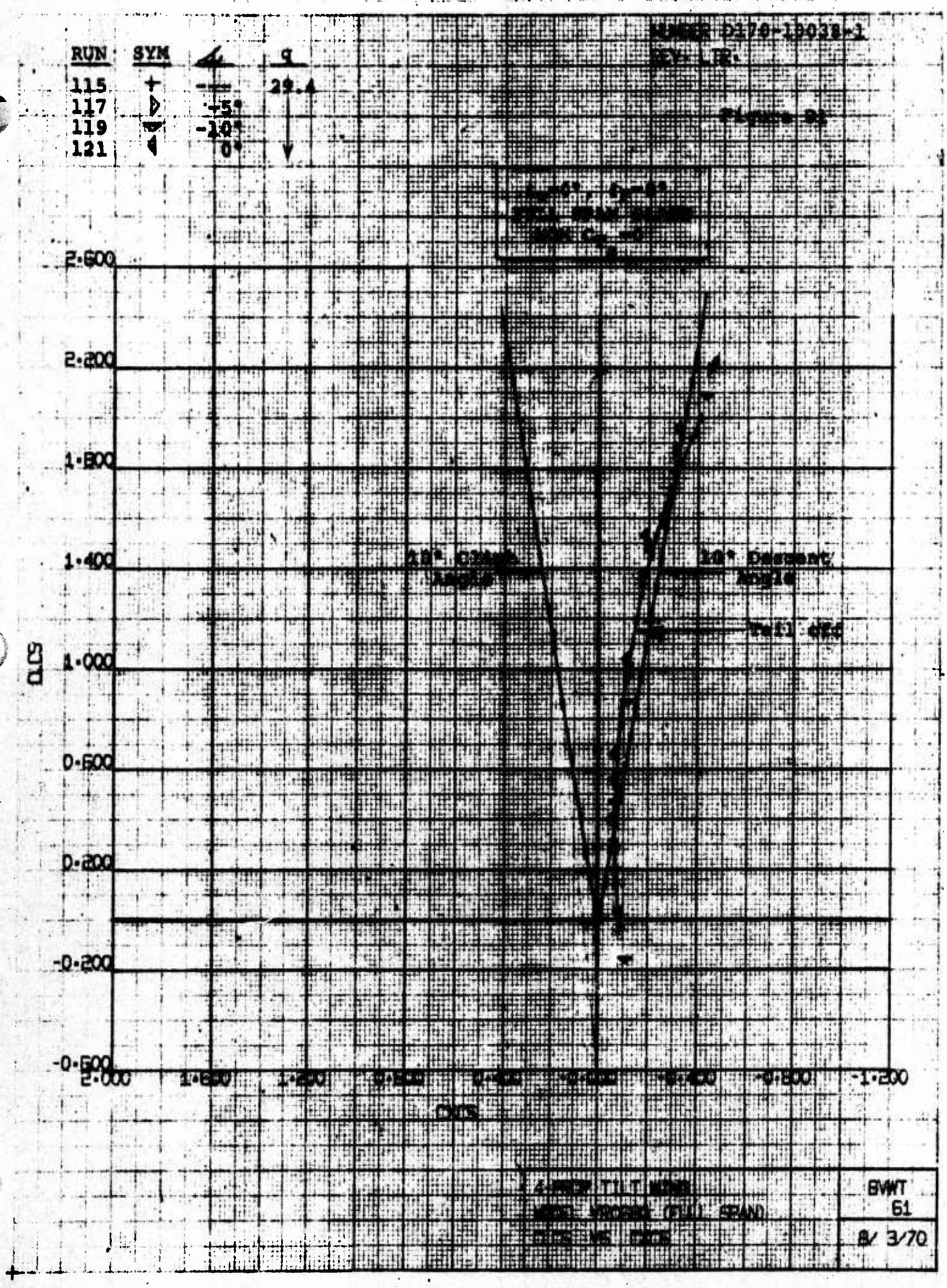
RUN SYM α q
115 + — 29.4
117 ▷ +5°
119 ▽ -10°
121 ◁ 0°
2.600
2.200
1.800
1.400
1.000
0.600
0.200
-0.200
-0.600
2.000
1.600
1.200
0.800
0.400
0.000
-0.400
-0.800
-1.200
CLS
CDS
Tail off
BWT 61
8/ 3/70

D170-10038-1

Figure 82

RUN	SYM	δ_f	q
115	+	-	29.4
117	▷	-5°	
119	◀	-10°	
121	◁	0°	▼

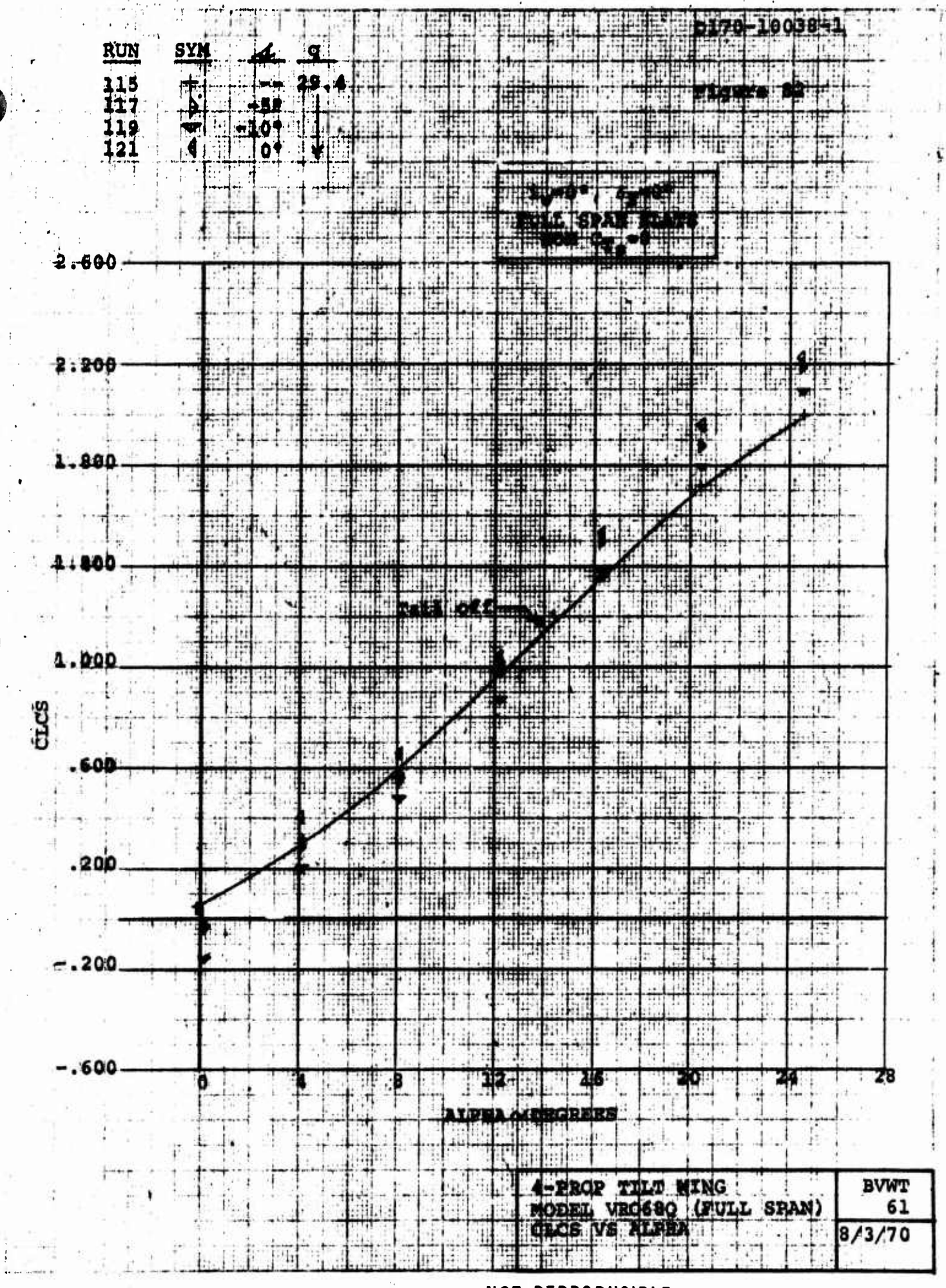

4-PROP TILT WING MODEL VRC680 (FULL SPAN) CLCS VS ALPHA	BVWT 61
	8/3/70

NOT REPRODUCIBLE

NUMBER D170-10038-1
REV. LTR.

Figure 83

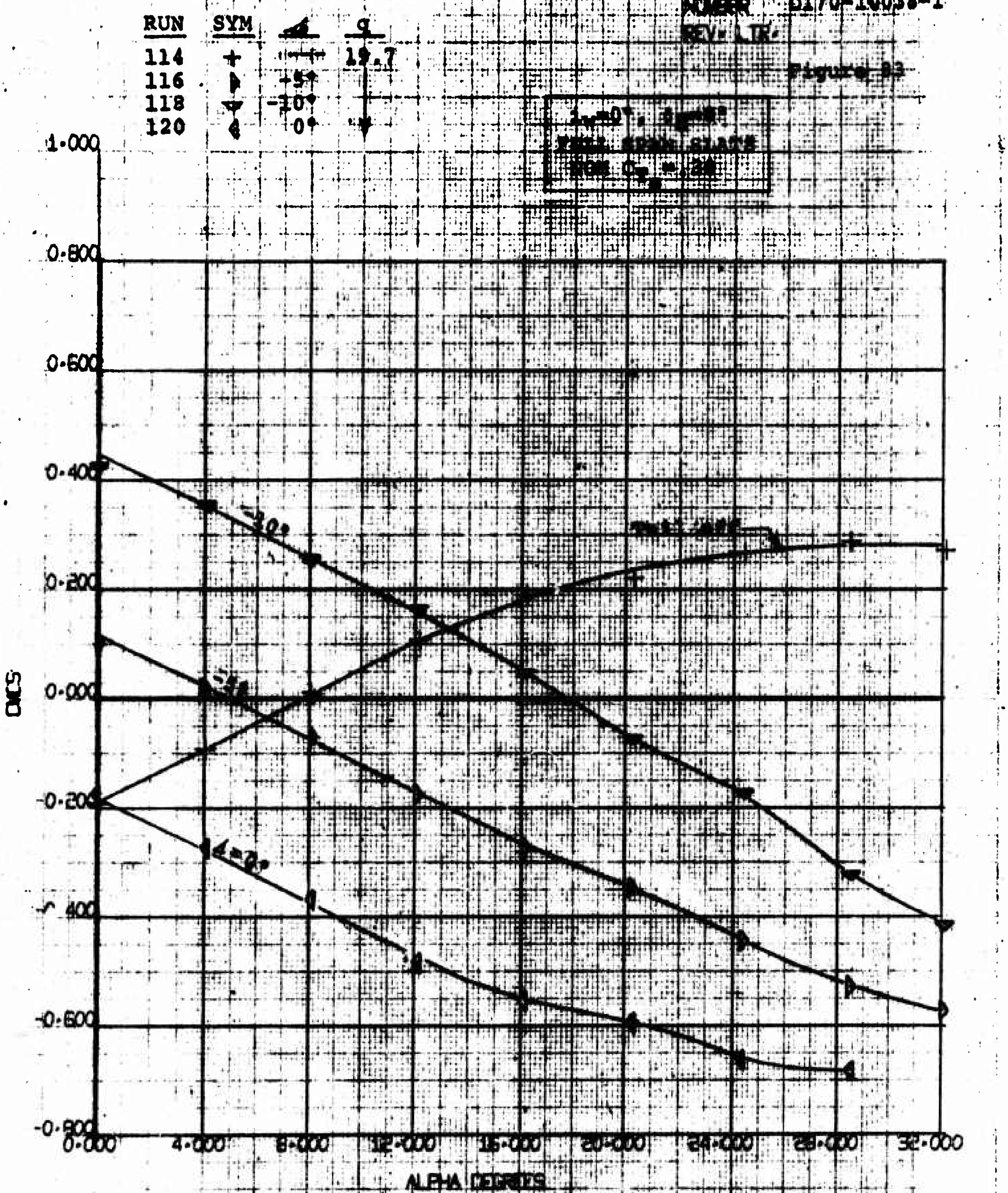

4-PROP TILT WING MODEL VR0880 (FULL SPAN) DMCS VS ALPHA	BVWT 61 8/ 3/70

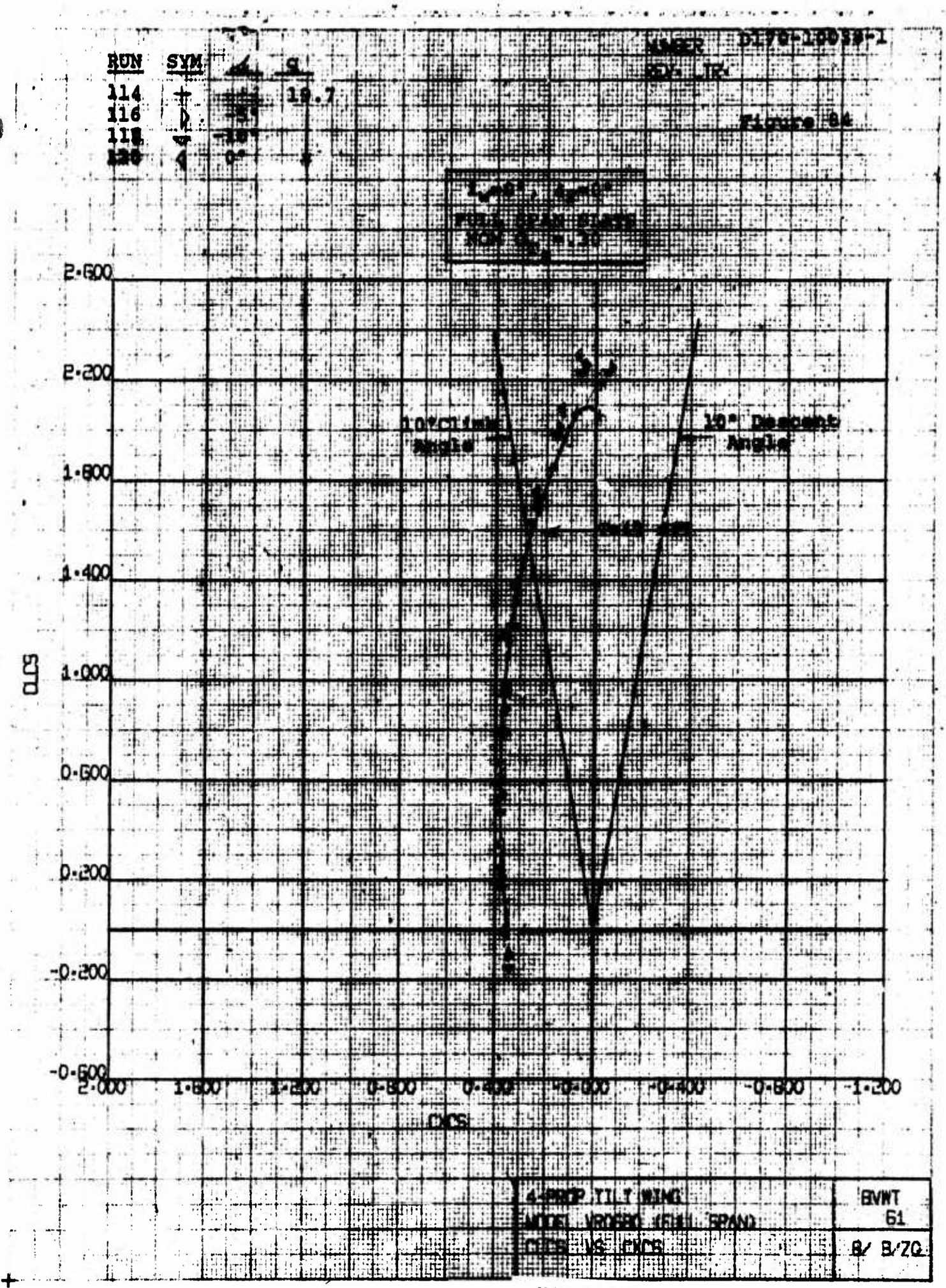

Figure 84

4-PROP TILT WING
MODEL VRORRO (FULL SPAN)
CLCS VS CXCS

BWWT 61
8/ 8/20

NOT REPRODUCIBLE

D170-10039-1

Figure 85

RUN	SYM	δ_f	q
114	+	[illegible]	19.7
116	▷	-5°	
118	◁	-10°	
120	◁	0°	

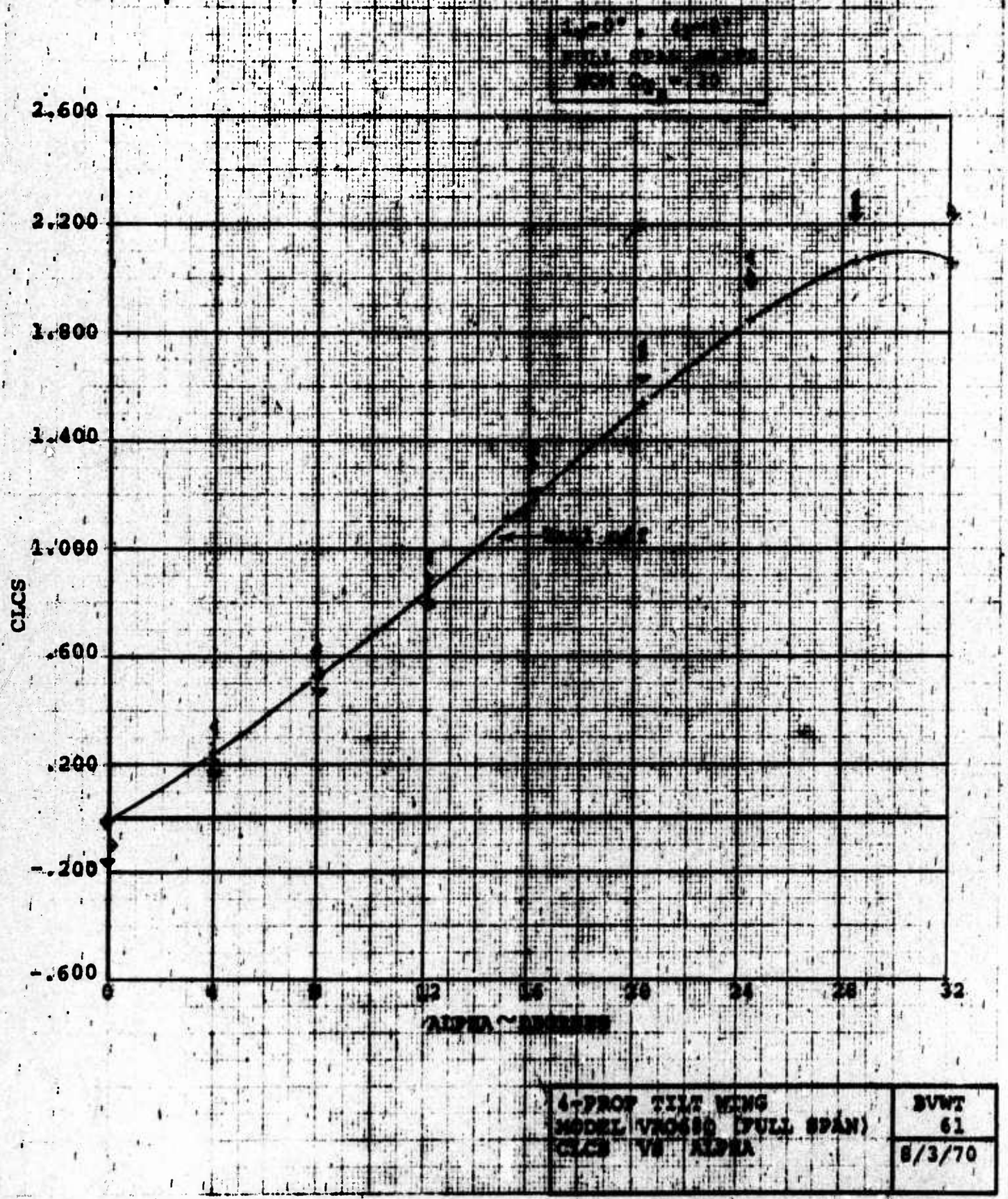

4-PROP TILT WING MODEL V/STOL (FULL SPAN) CLCS VS ALPHA	SVWT 61
	6/3/70

REV. LTR.

Figure 86

RUN	SYM	δ_f	q
105	▷	-5°	29.7
108	▽	0°	
111	◁	-10°	
112	+		

i_w=0°, δ_e=-40°

FULL SPAN SLATS

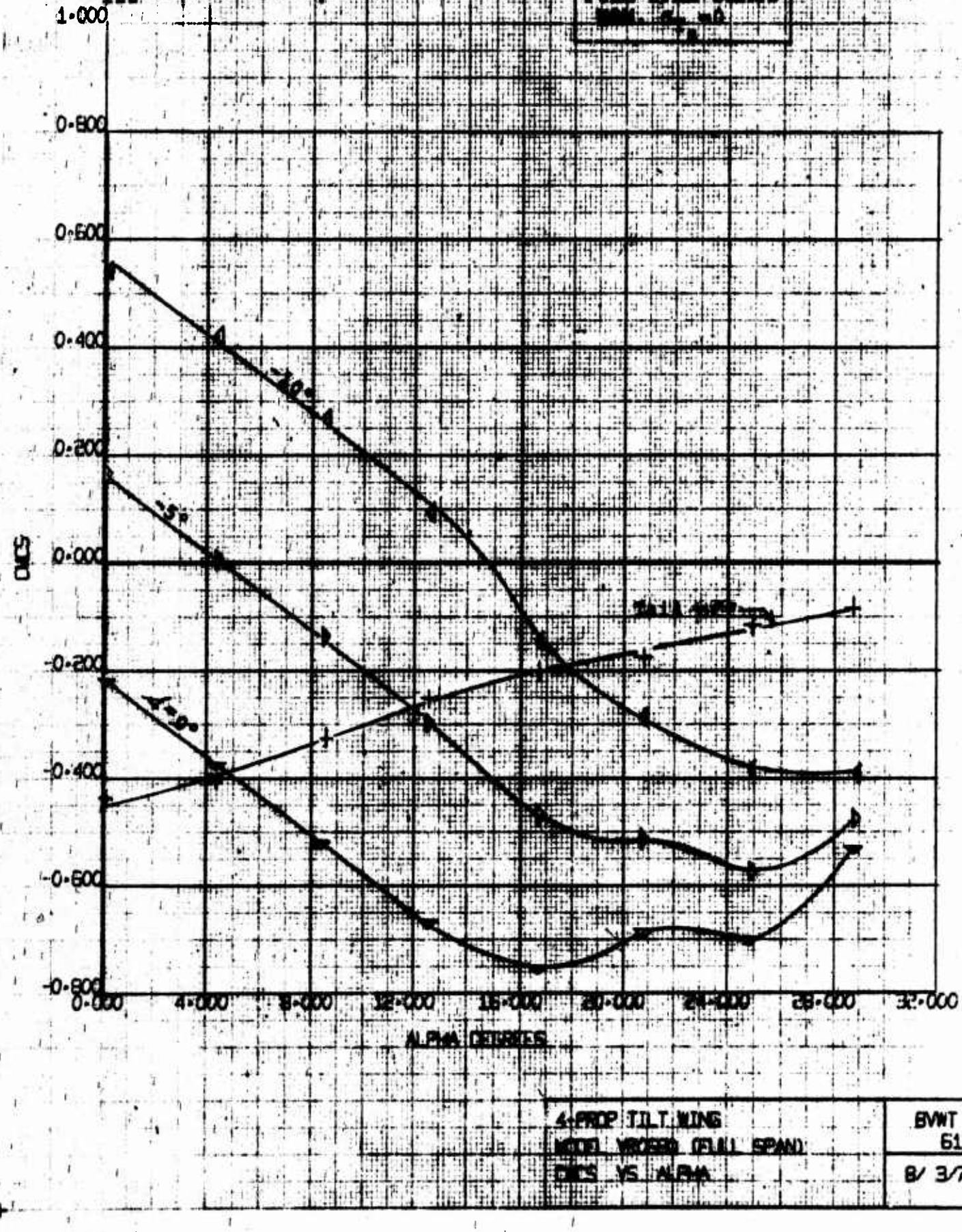

4-PROP TILT WING MODEL WROSS (FULL SPAN) CMCS VS ALPHA	BVWT 61 8/ 3/70

Figure 87

RUN	SYM	α	q
105	▷	-5°	29.7
108	⋈	0°	
111	◁	+10°	
112	+	[illegible]	

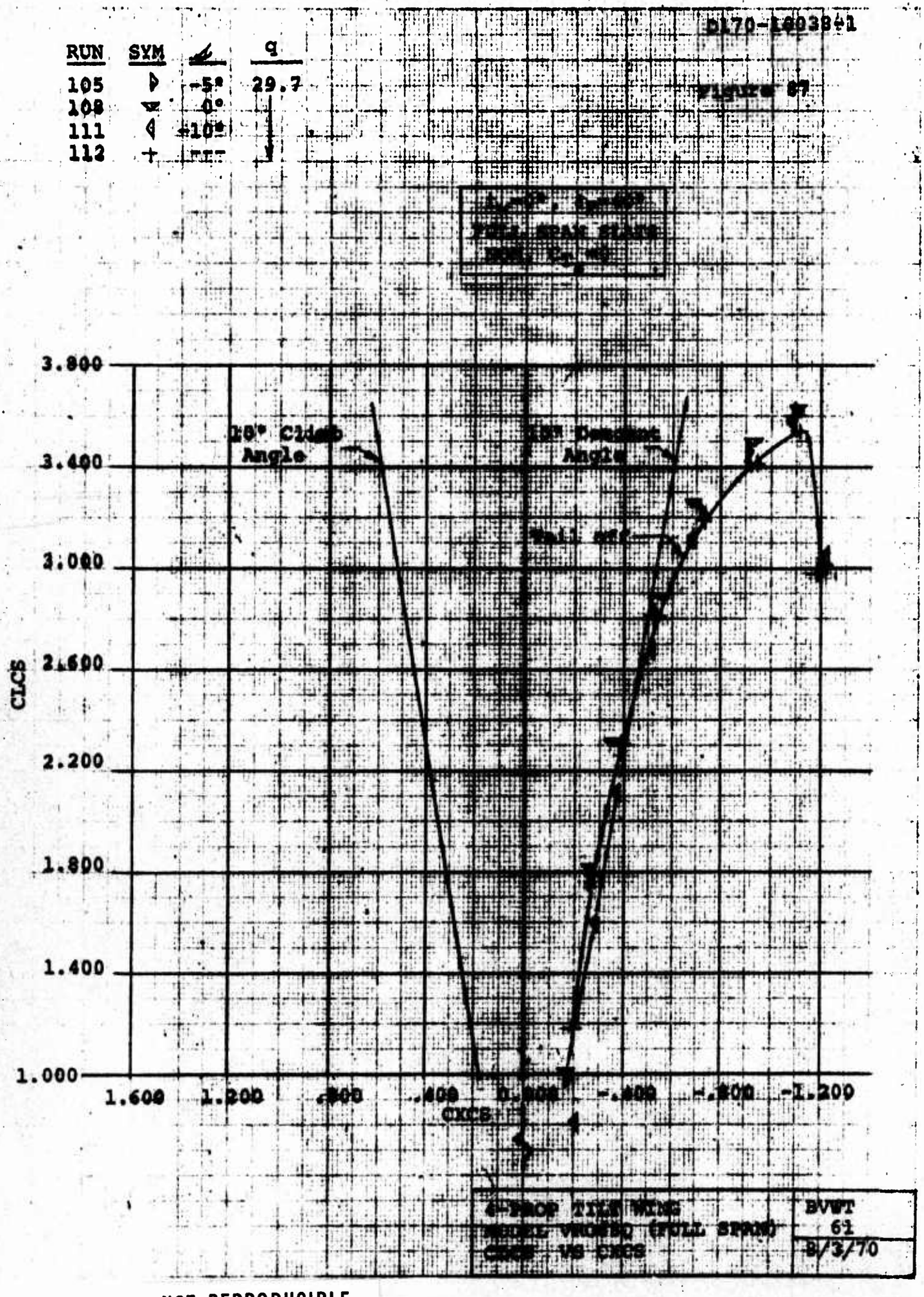

4-PROP TILT WING MODEL VEHICLE (FULL SPAN) CLCS VS CXCS

BVWT 61
8/3/70

NOT REPRODUCIBLE

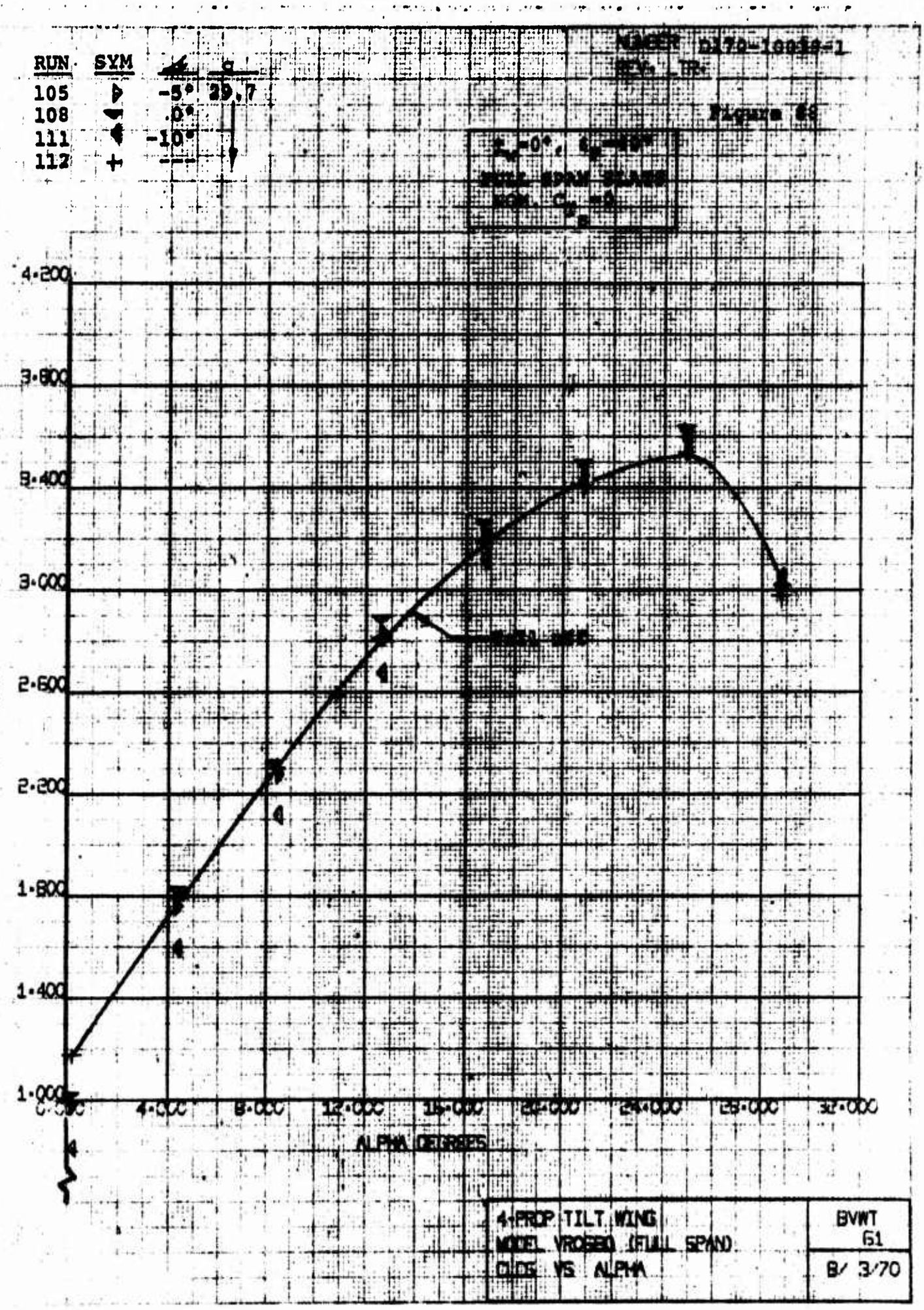

4-PROP TILT WING MODEL VROOM (FULL SPAN) CLCS VS ALPHA	BVWT 61 B/ 3/70

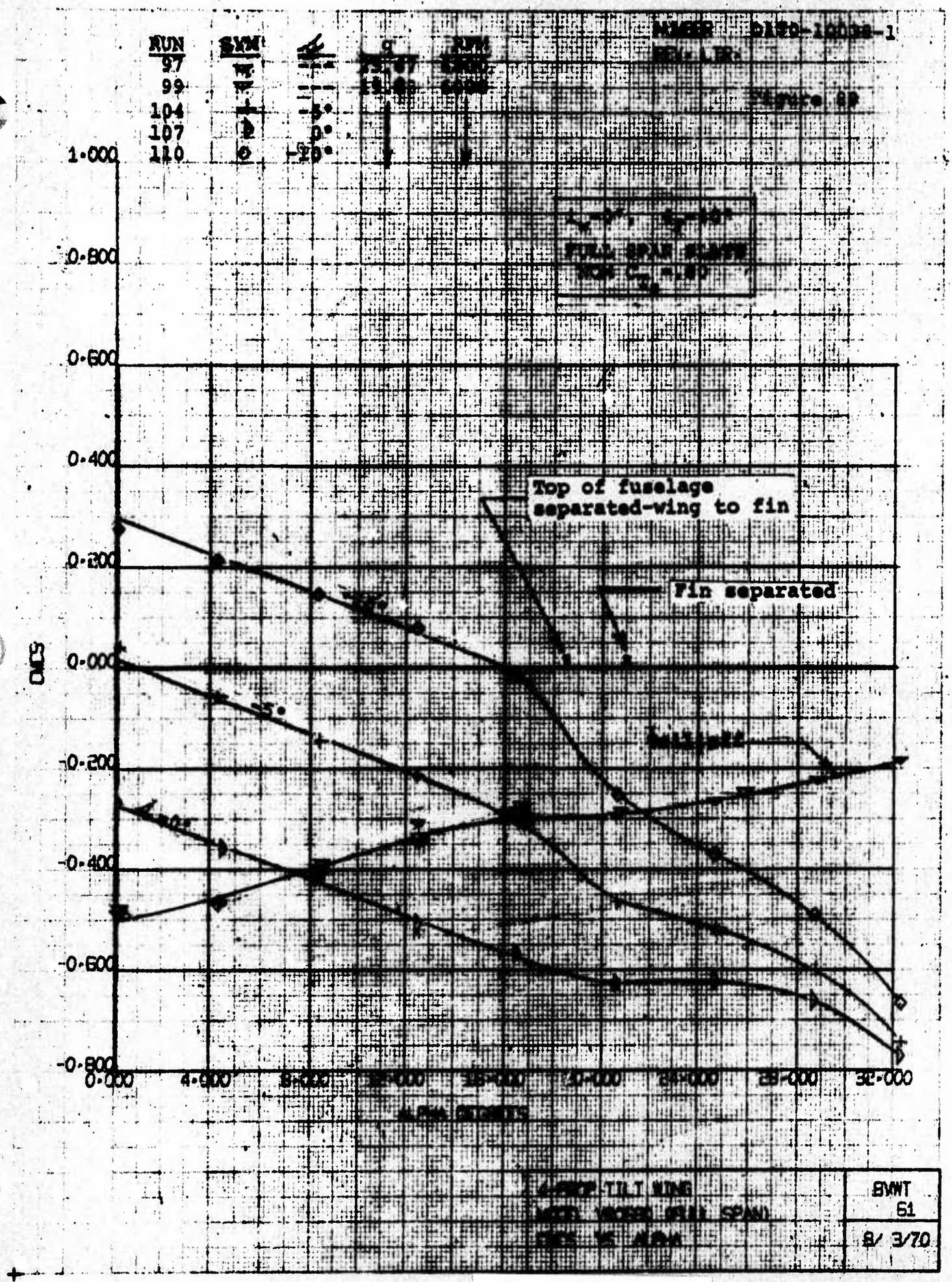

SWWT
61
8/ 3/70

NOT REPRODUCIBLE

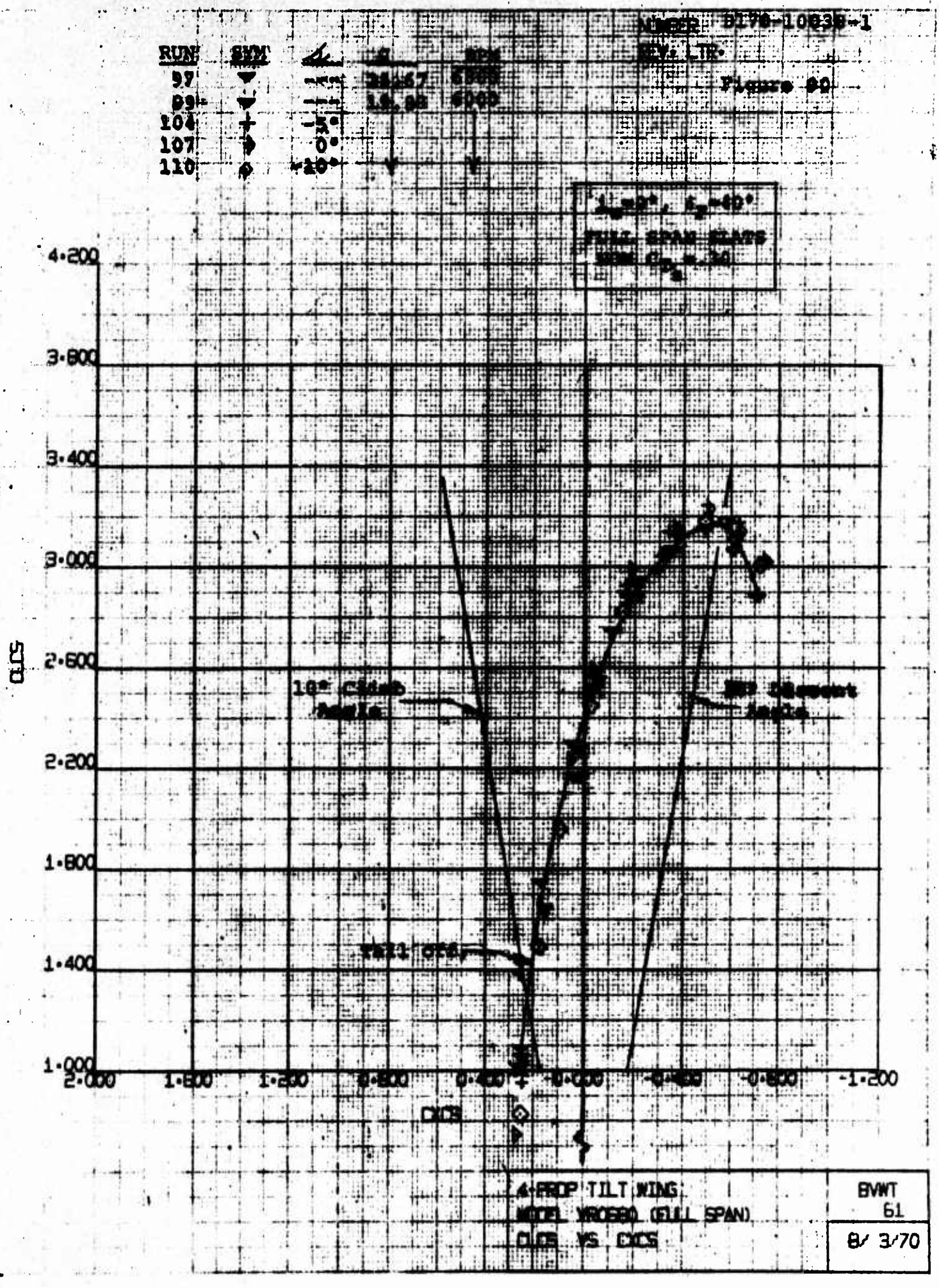
RUN
97
99
104
107
110
4.200
3.800
3.400
3.000
2.600
2.200
1.800
1.400
1.000
CLS
2.000
1.800
1.200
0.800
0.400
-0.000
-0.400
-0.800
-1.200
CXCS
10° Climb
Angle
Trail Off
4-PROP TILT WING
MODEL WROBO (FULL SPAN)
CLCS VS CXCS
BWT
61
8/ 3/70

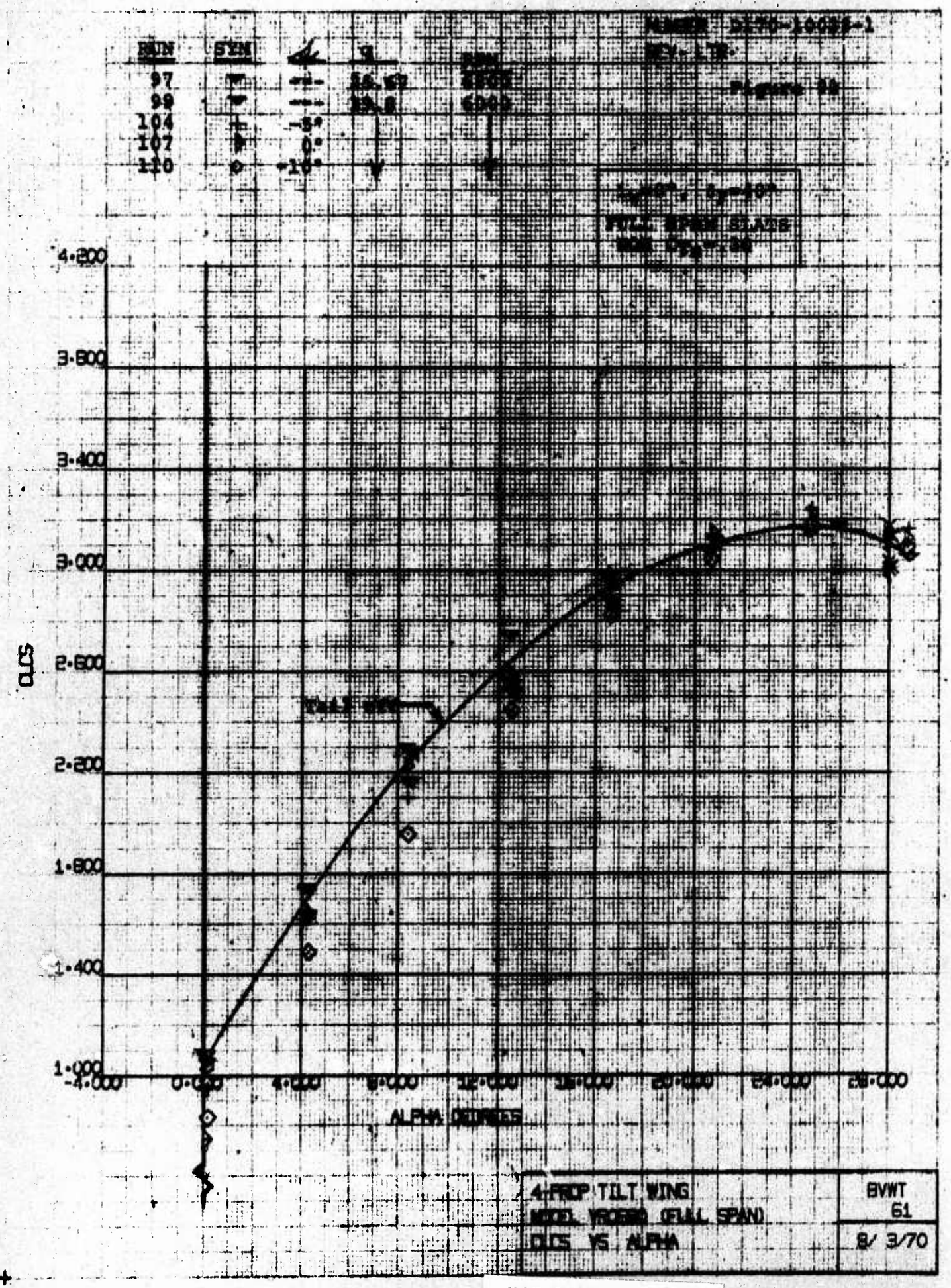

NOT REPRODUCIBLE

Figure 92.

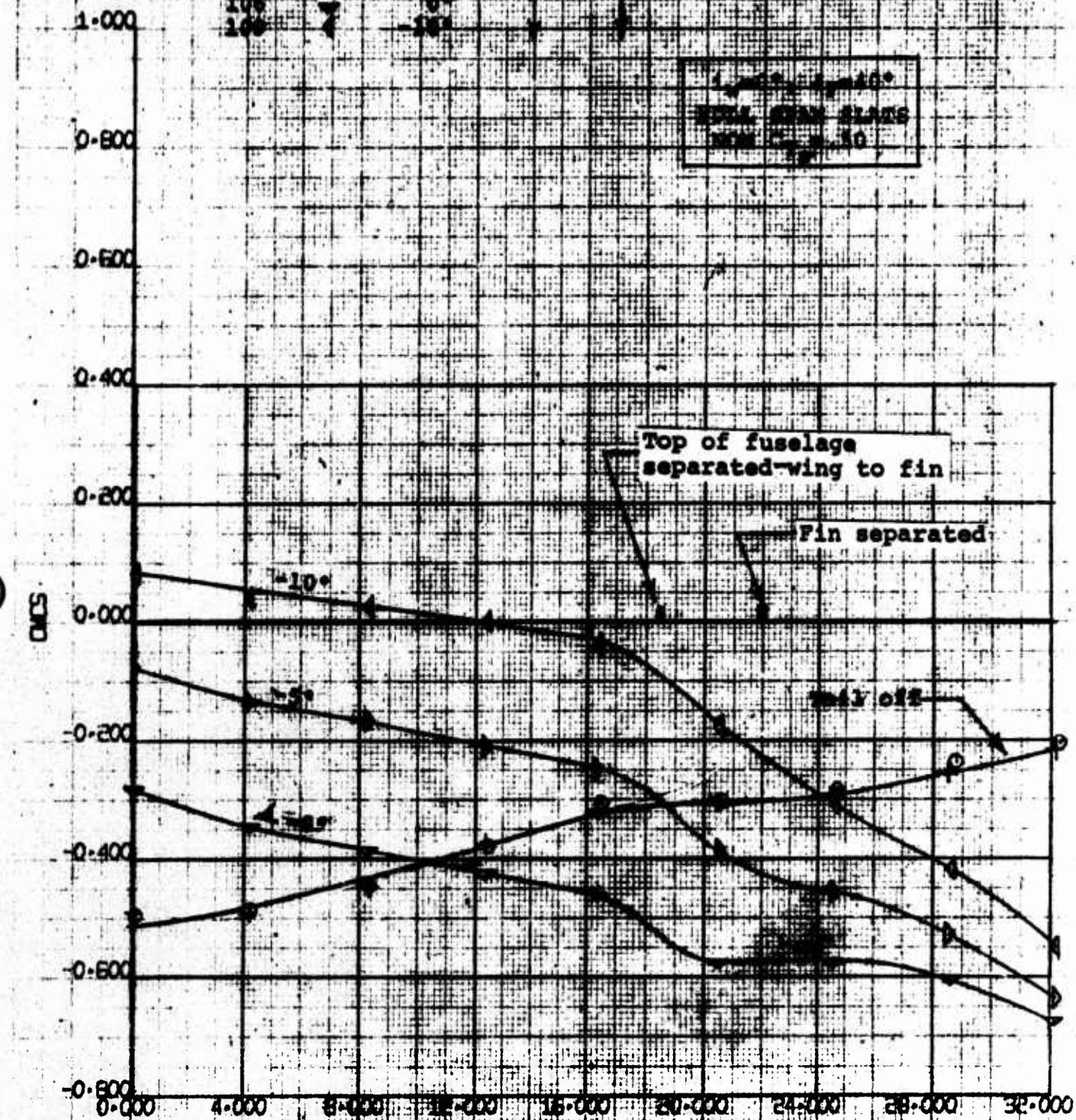

4-PROP TILT WING MODEL VRORES (FULL SPAN) CMCS VS ALPHA	BWMT 61 8/ 3/70

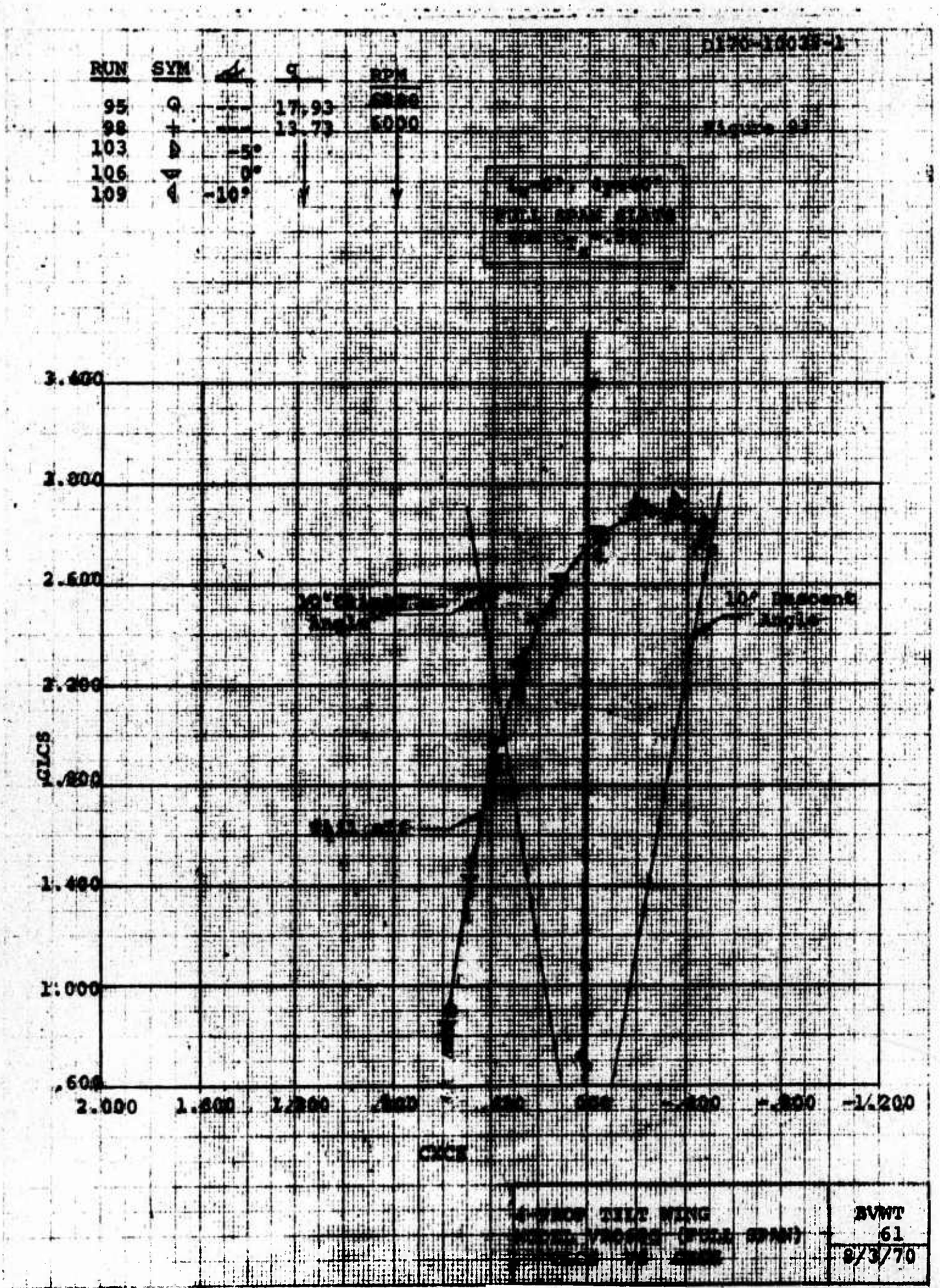

NOT REPRODUCIBLE

REF. LTR.

Figure 84

RUN	SYM	i_t	S	REM
95	○	---	17.93	6000
98	+	---	11.73	6000
103	▷	-5°		
106	▽	0°		
109	◁	-10°	"	"

i_f=0°, δ_f=40°
FULL SPAN FLAPS
WOW C_{L_0}=.70

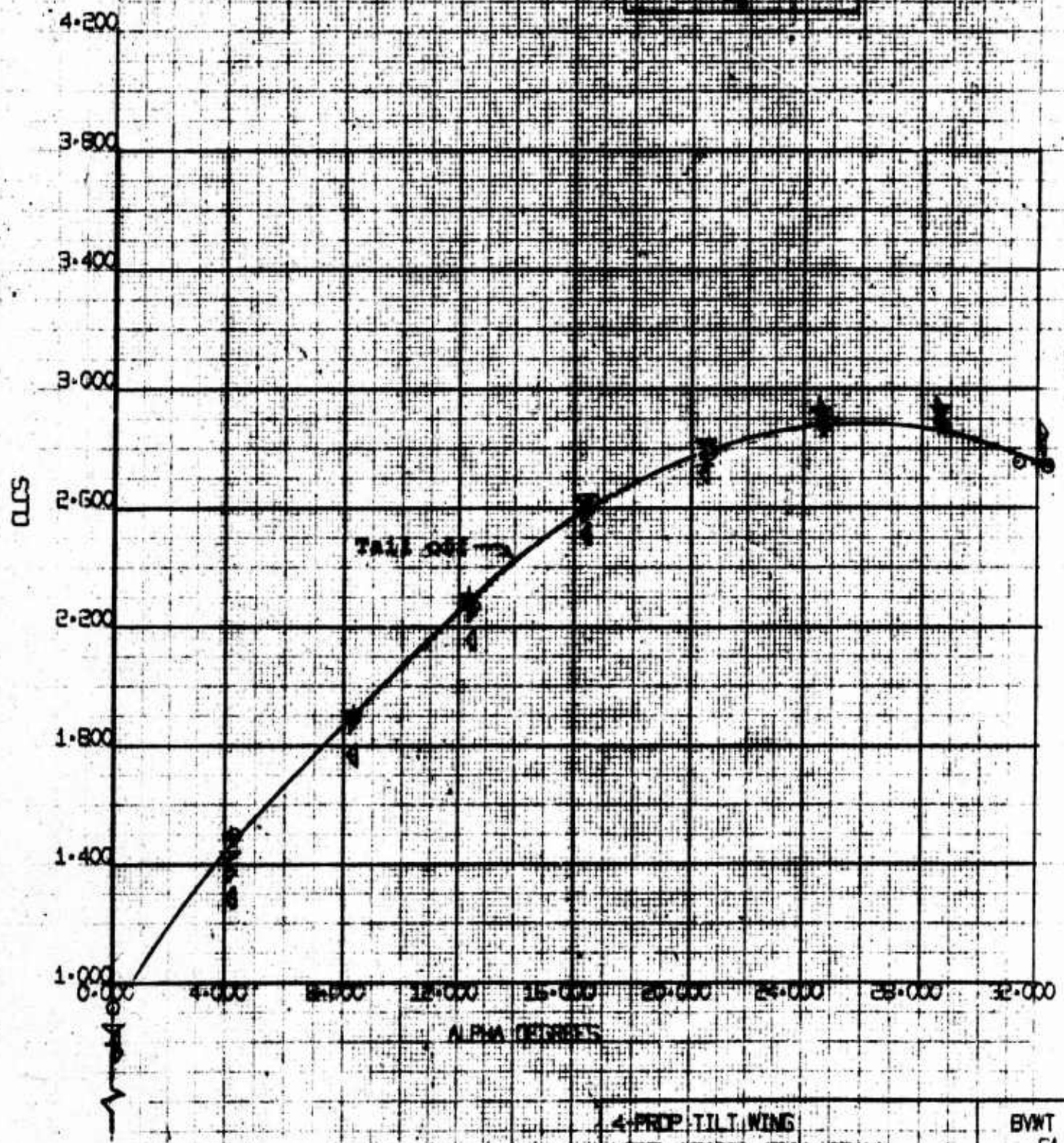

4-PROP TILT WING MODEL VRORED (FULL SPAN) CLCS VS. ALPHA	BWT 61 8/ 3/70

Figure 35

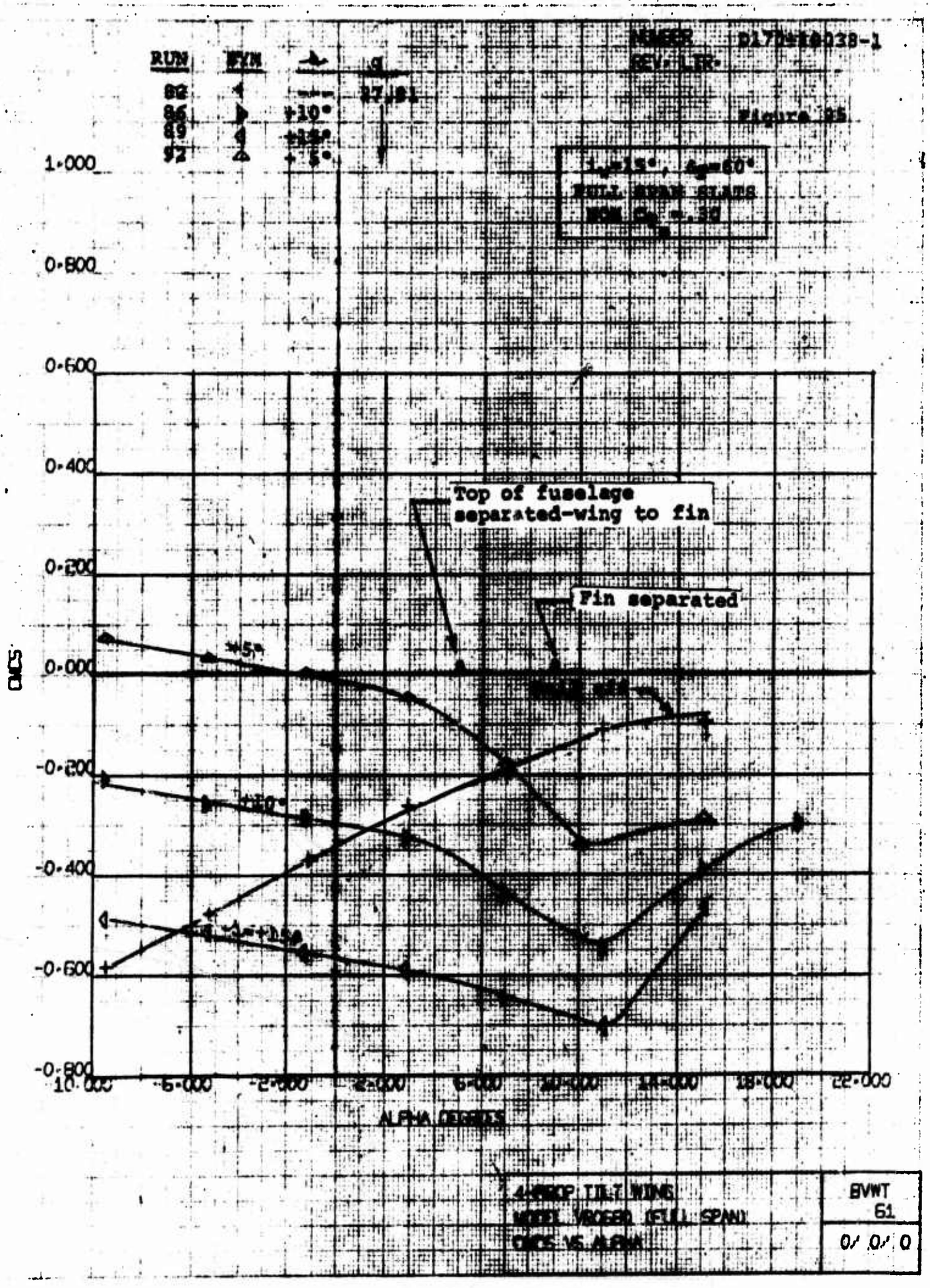

4-PROP TILT WING MODEL PROBED (FULL SPAN) CMCS VS. ALPHA	BVWT 61
	0/ 0/ 0

NOT REPRODUCIBLE

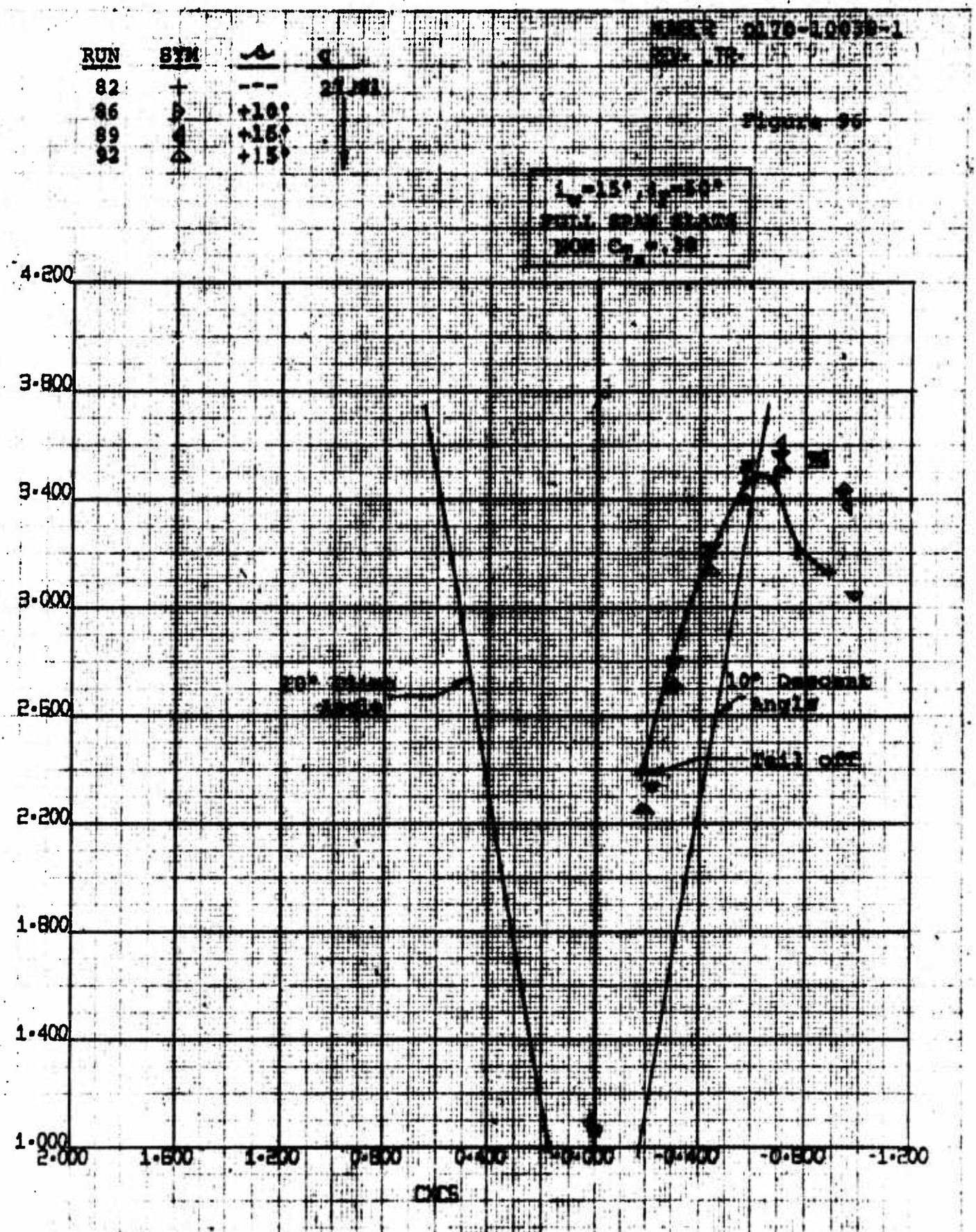

4-PROP TILT WING MODEL VROOM (FULL SPAN) CLCS VS CXCS		BVWT 61 8/ 3/70

RUN	SYM	Δ_e	ζ
82	+	---	
86	▷	+10°	
89	◁	+15°	
92	△	+ 5°	

TR.

Reynolds 97

L_e=15°, Σ_F=60°
FULL SPAN SLATS
δ_{FLAP}=30

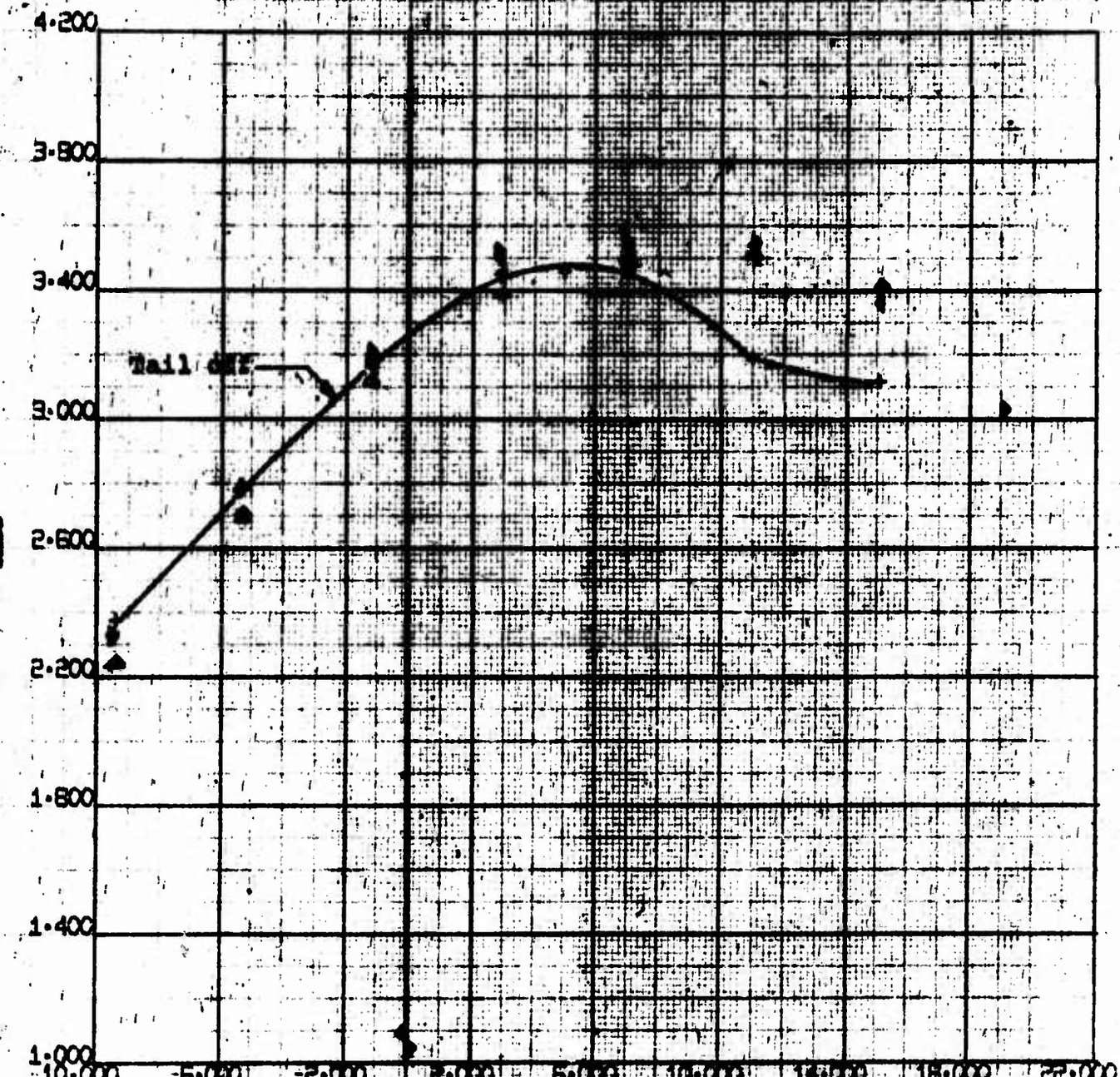

4-PROP TILT WING
MODEL VROOM (FULL SPAN)
CLO VS ALPHA

BVWT 61
B/ 3/70

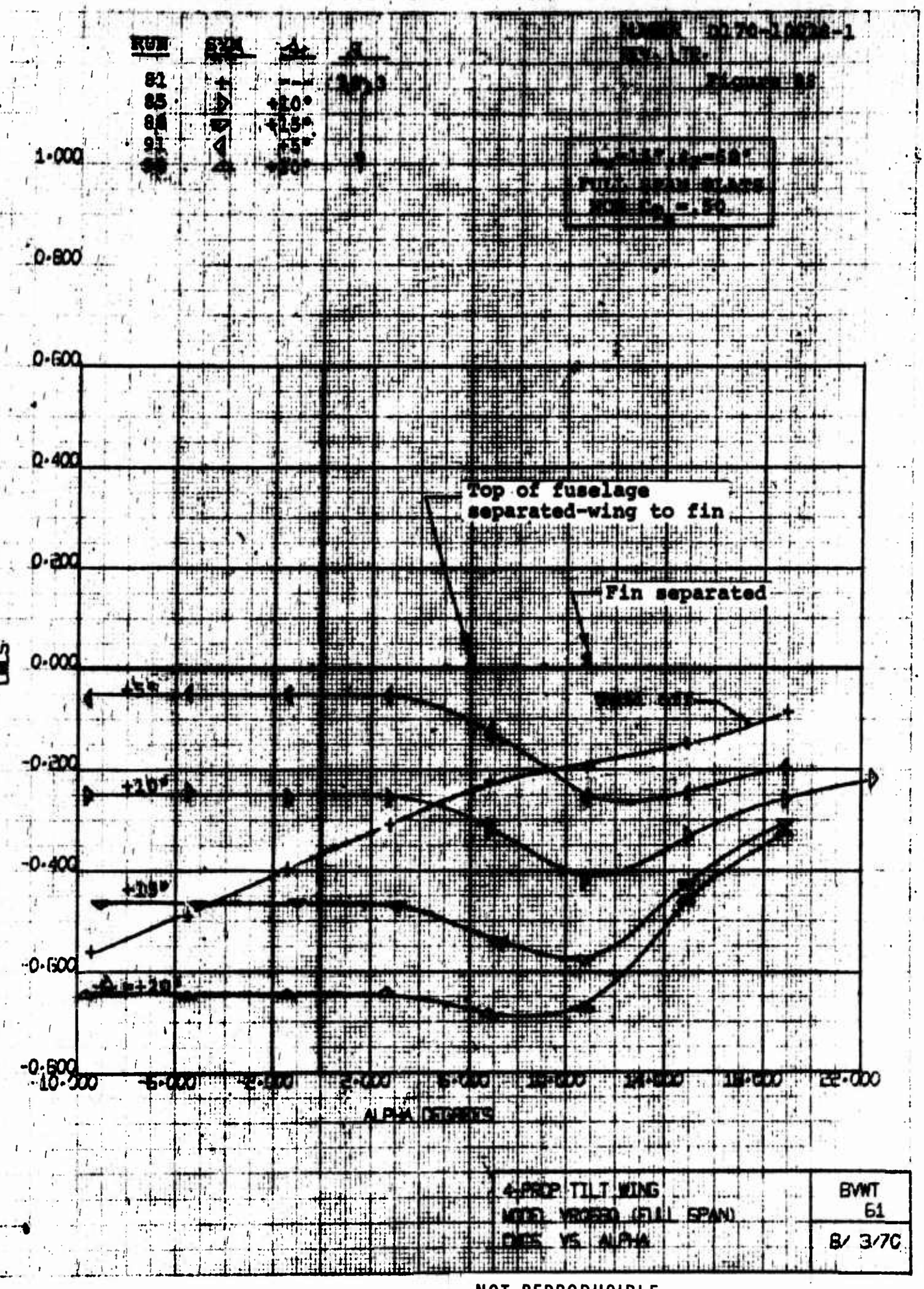

4-PROP TILT WING MODEL VRCEBO (FULL SPAN) CMS VS. ALPHA	BWT 61 8/ 3/70

NOT REPRODUCIBLE

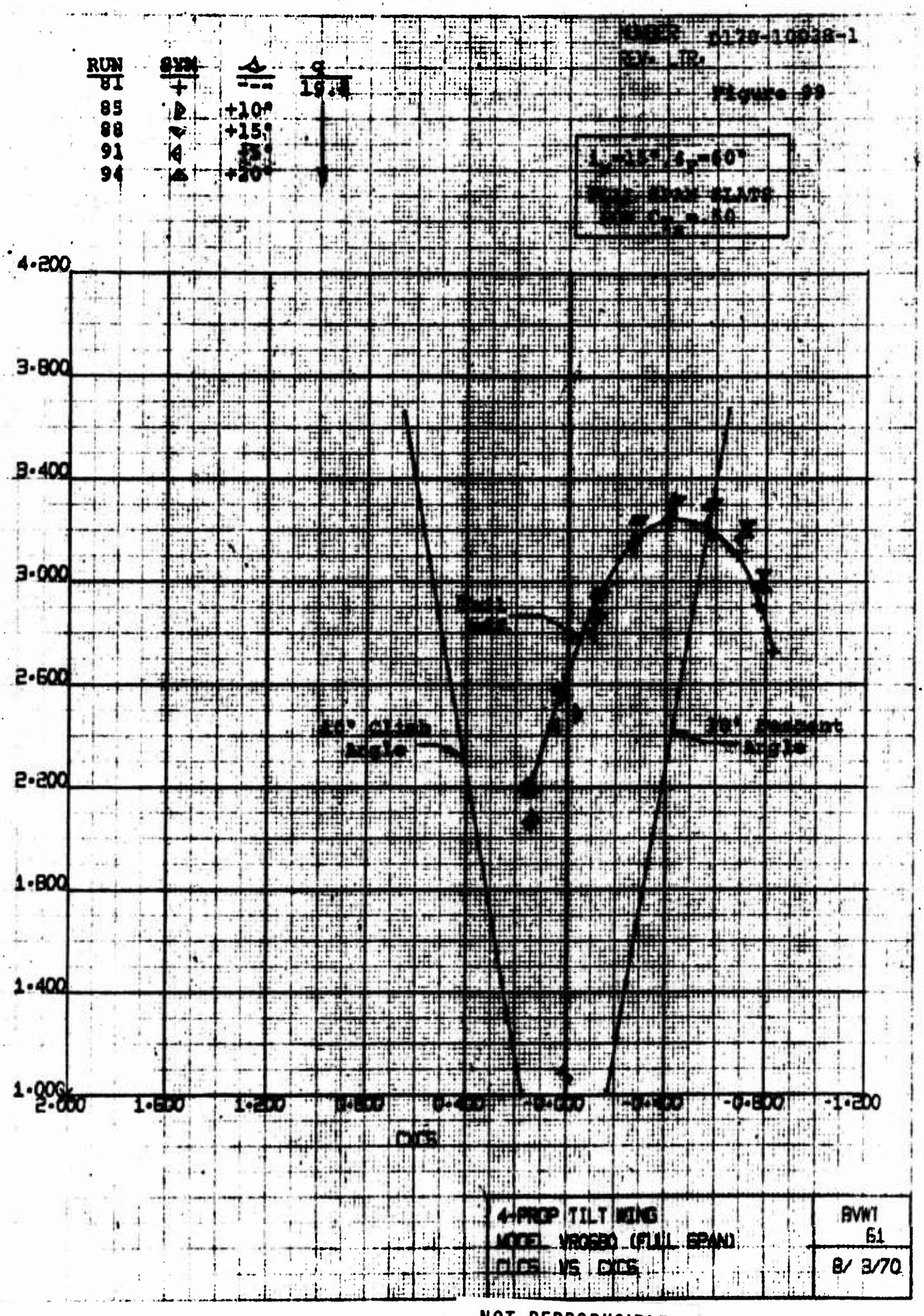

NOT REPRODUCIBLE

NUMBER D170-10038-1

REV. IR.

Figure 100

RUN	SYM	i_t	q
91	+	---	19.3
88	▶	+10°	
89	▼	+15°	
91	◀	+ 5°	
94	▲	+20°	

i_w=10° ; δ_f=60°

FULL SPAN SLATS

NOM C_{μ_j} =.50

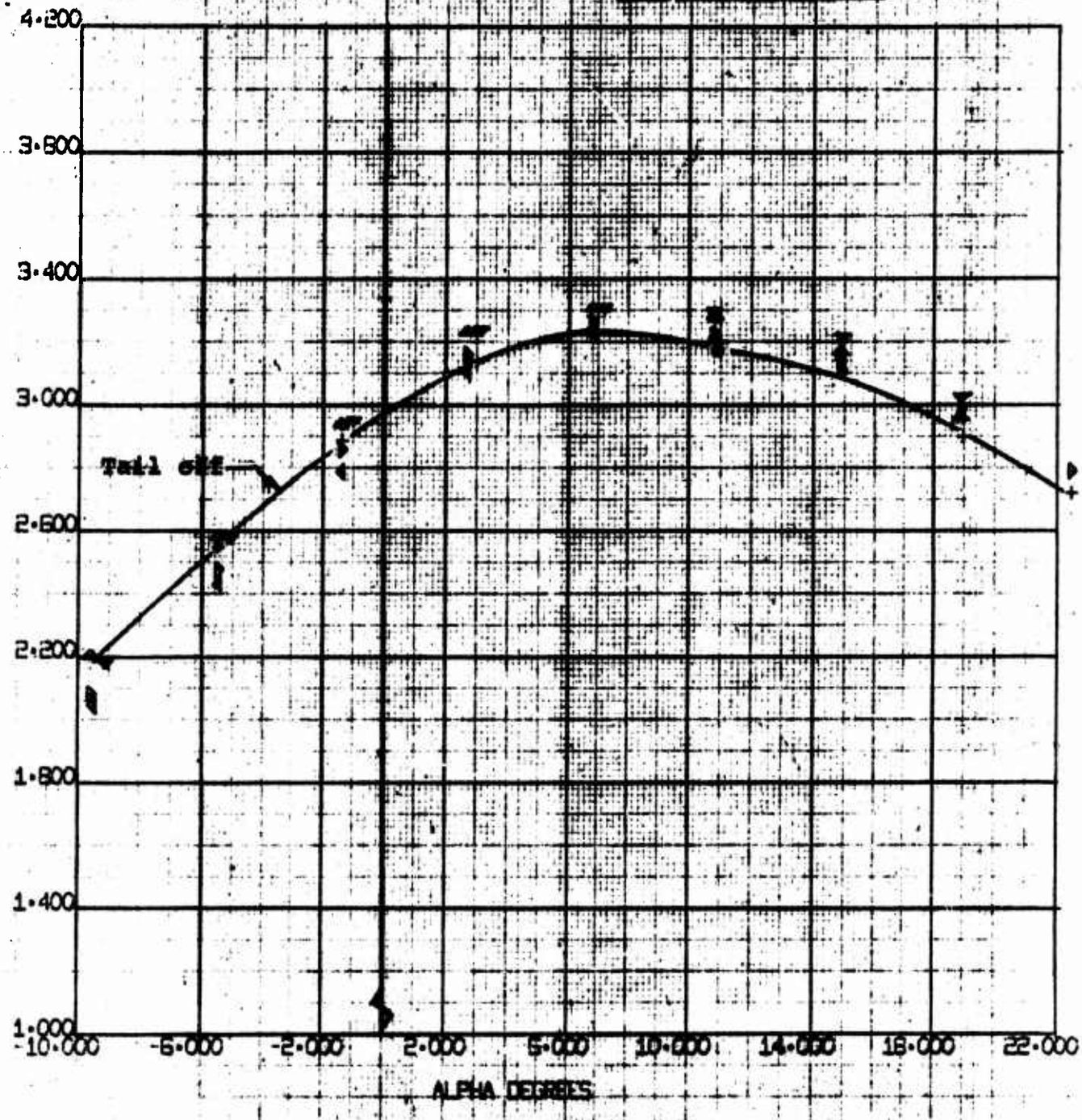

4-PROP TILT WING MODEL VROOM (FULL SPAN) CLS VS ALPHA	BWT 61 8/ 3.70

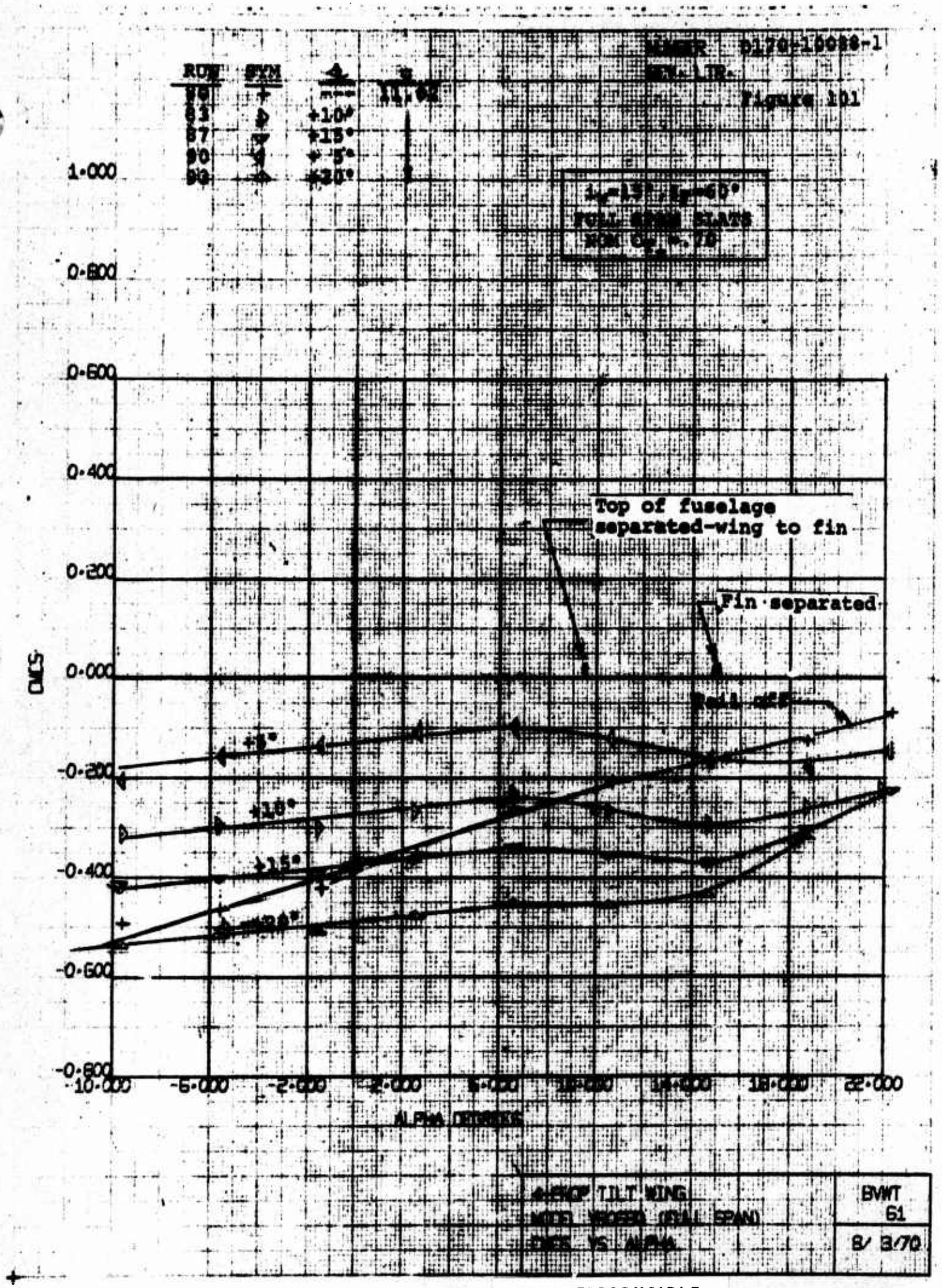

4-ENGR TILT WING	BWT 61
	8/ 3/70

NOT REPRODUCIBLE

NUMBER D170-10038-1
REV. LTR.
Figure 102

RUN	SYM	Δ_e	α
80	+	---	11.02
83	▷	+10°	
87	▽	+15°	
91	◁	+ 5°	
93	△	+20°	

i_w=15°, δ_F=60°
FULL SPAN SLATS
MOM $C_{\mu_{eff}}$ =.70

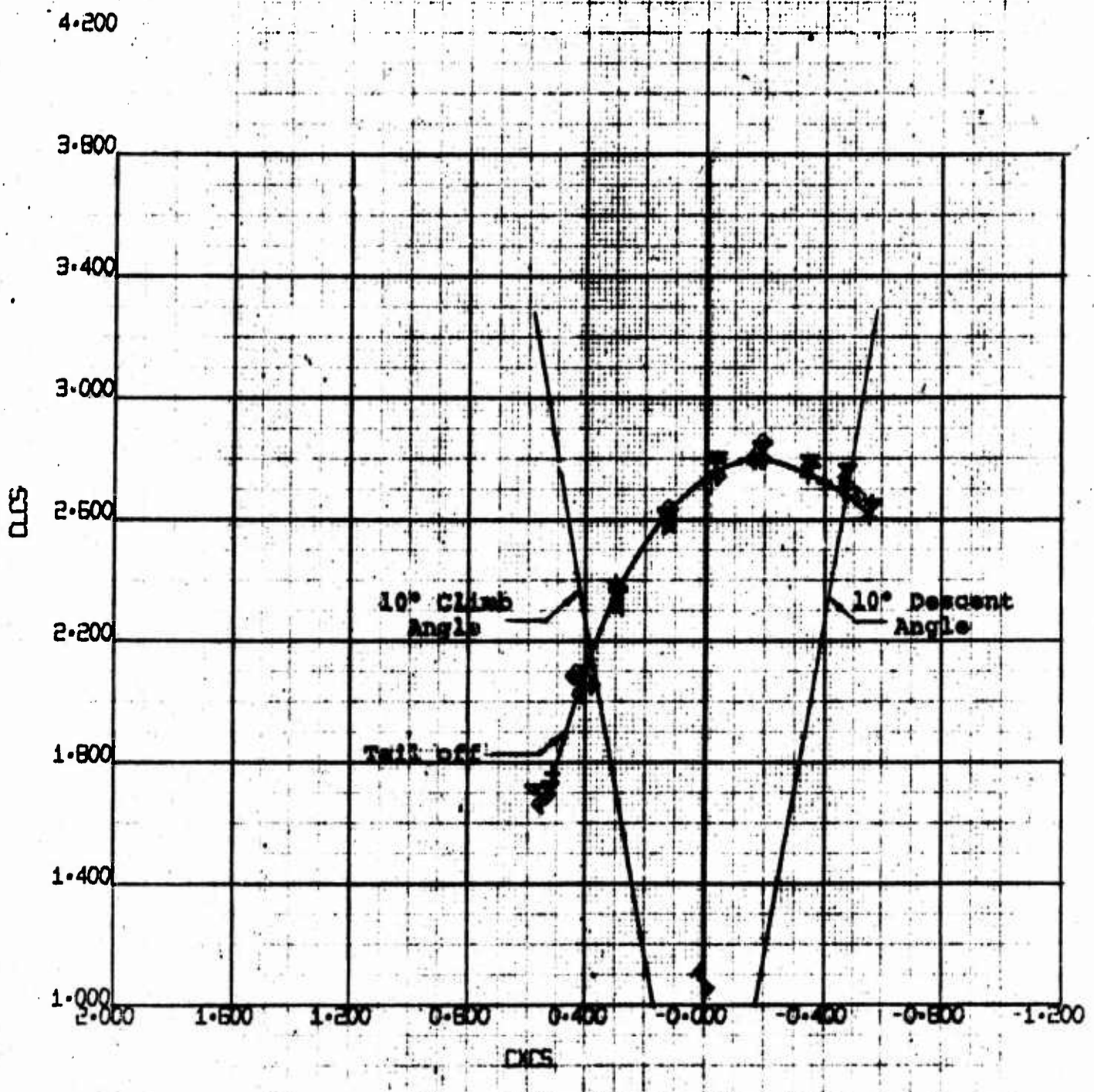

4-PROP TILT WING MODEL VROBBO (FULL SPAN) CLCS VS CXCS	BVWT 61 8/ 3/70

NOT REPRODUCIBLE

NUMBER D170-10038-1
REV. LR.

Figure 103

RUN	SYM	δ_f	q
80	+	---	11.02
83	▷	+10°	
87	▽	+15°	
90	◁	+[illegible]°	
93	△	+20°	

i_w=15°, δ_{BF}=60°
FULL SPAN SLATS
NOM C_{TC} =.70

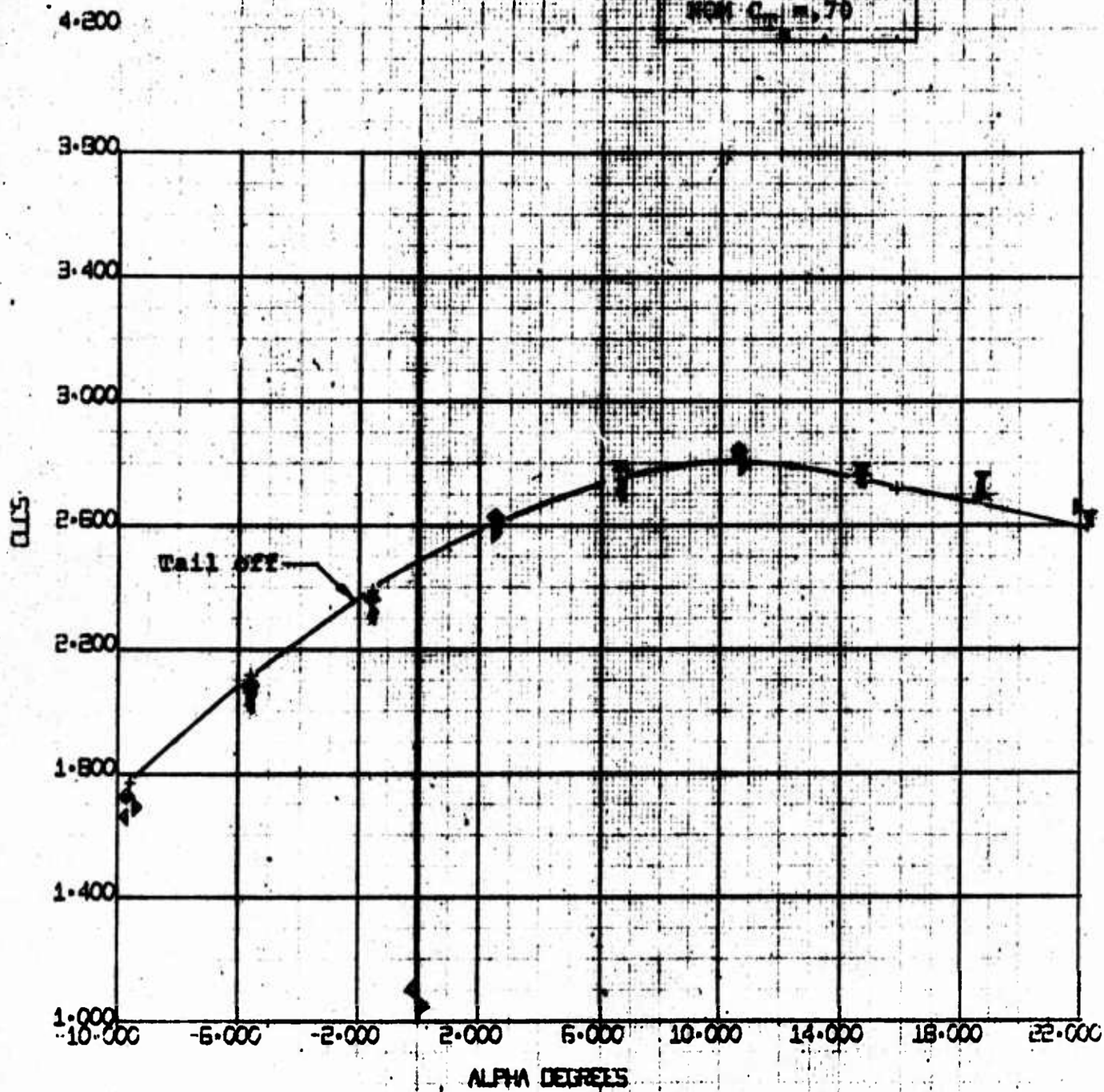

4-PROP TILT WING MODEL VROOOO (FULL SPAN) CLCS VS ALPHA	BVWT 61 8/ 3/70

NUMBER B170-10038-1
REV. LTR.

Figure 104

RUN	SYM	α	C_μ
139	+	---°	12.35
142	▶	+18°	
145	◀	+28°	
148	▲	+38°	
151	◆	+48°	

i_w=30°, δ_f=60°
FULL SPAN SLATS
NOM C_μ = .55

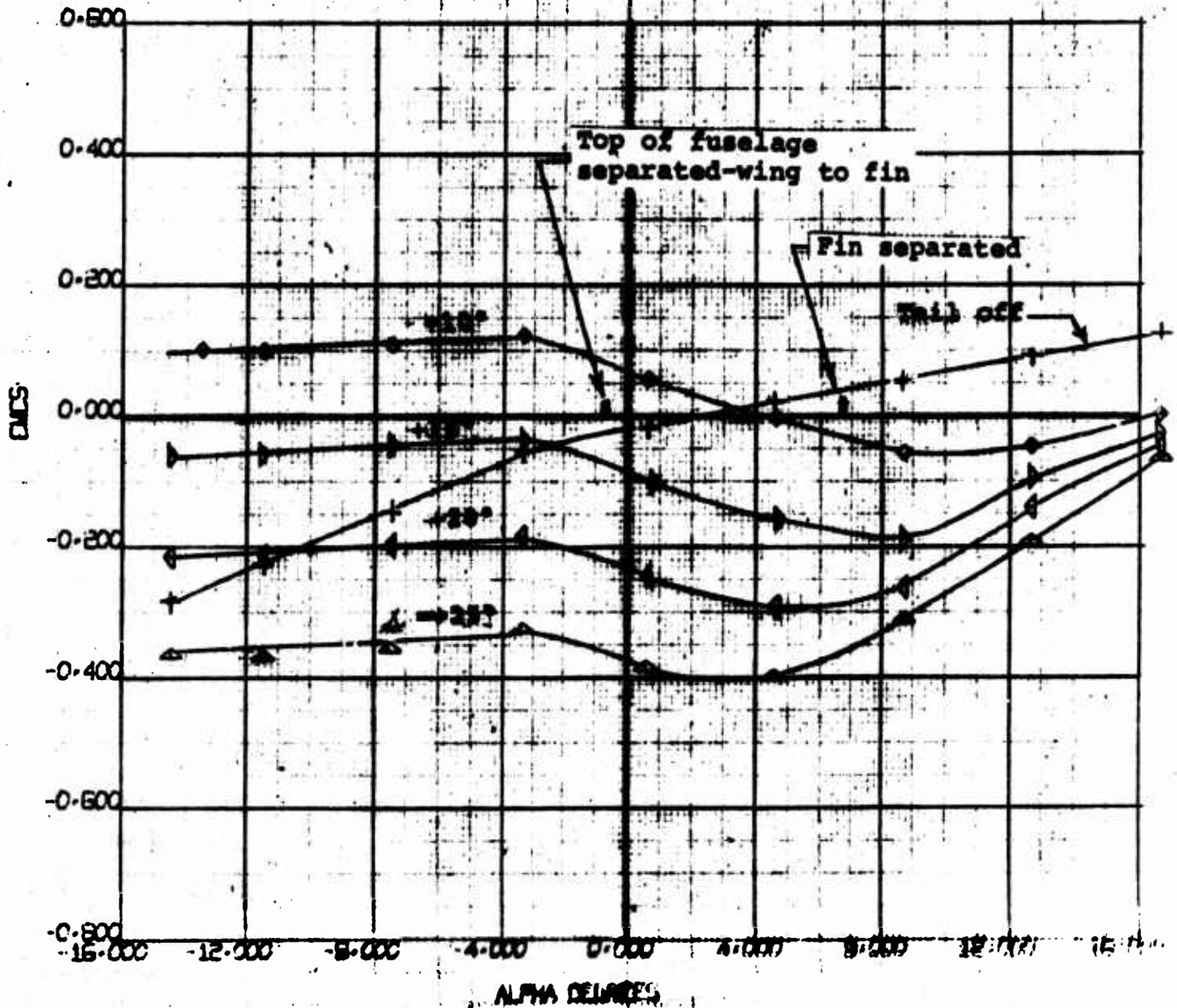

4-PROP TILT WING MODEL VRG880 (FULL SPAN) DMCS VS ALPHA	BVWT 61 9/23/70

Figure 105

RUN	SYM	i_w	α
139	+	---	10.35
142	▷	+15°	
145	◁	+20°	
149	⬭	+25°	
151	◇	+10°	

i_w=30°, δ_f=40°
FULL SPAN SLATS
NOM $C_{L_{max}}$ = 3.55

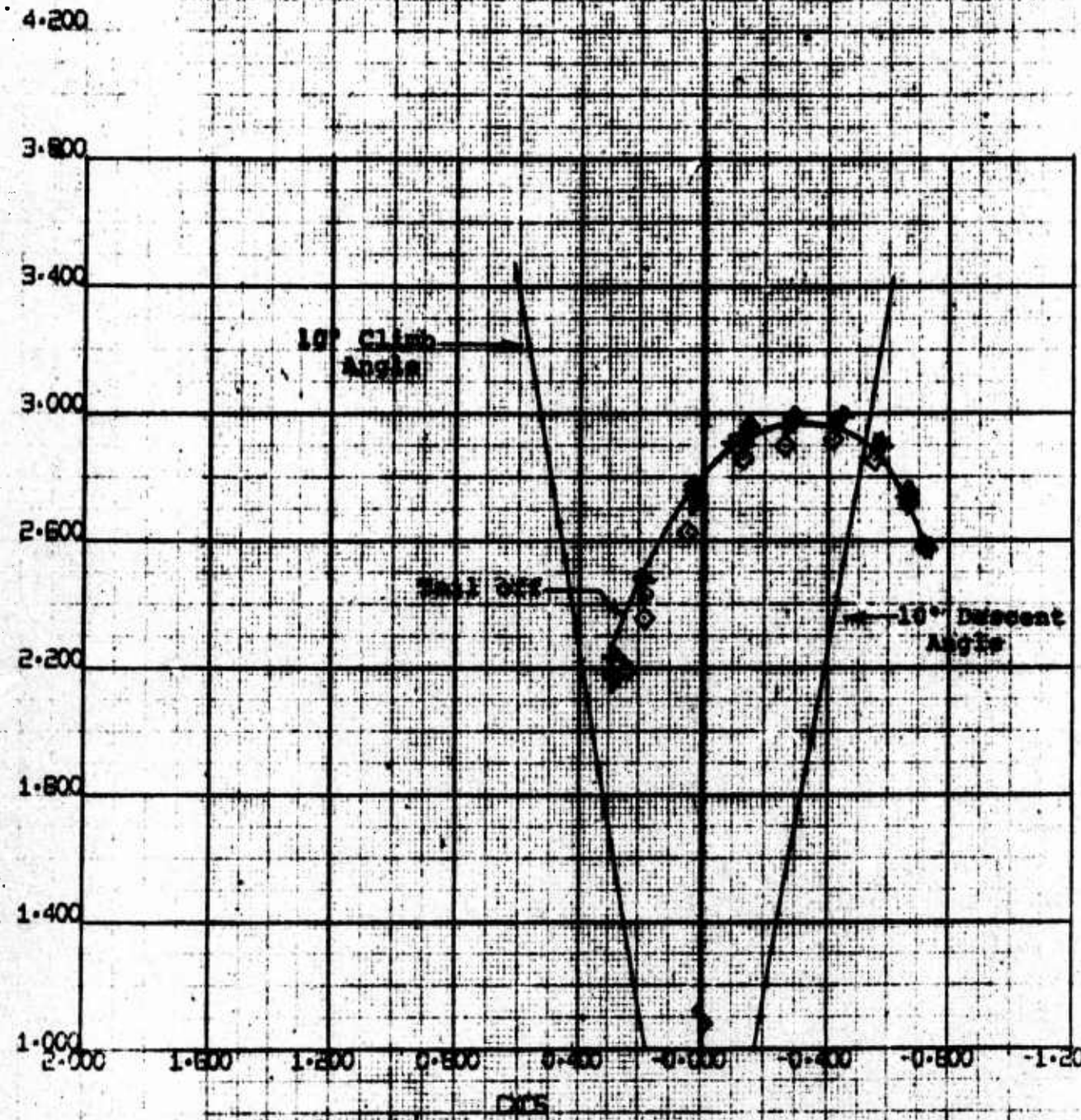

4-PROP TILT WING MODEL VR0880 (FULL SPAN) CLO VS CDO	BVWT 61 8/ 3/70

NOT REPRODUCIBLE

Figure 106

RUN	SYM	δ_f	δ_s
139	+	---	13.85
142	▷	+15°	
145	◁	+20°	
149	△	+25°	
151	◇	+10°	

i_w =30°, δ_p =40°
FULL SPAN SLATS
NOM C_{μ_j} =.35

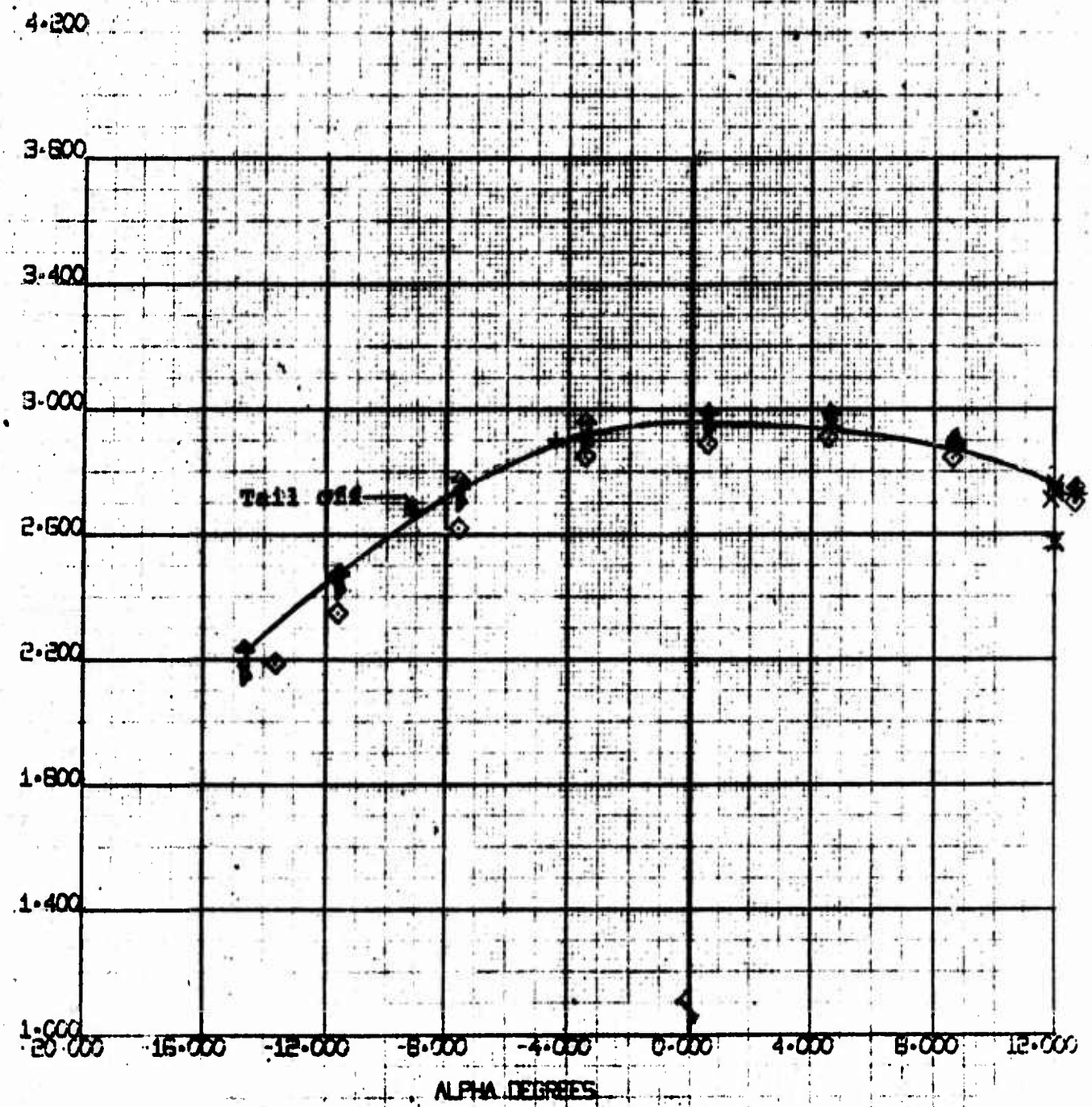

4-PROP TILT WING MODEL VR0680 (FULL SPAN) CLCS VS ALPHA	BVWT 61 8/ 3/70

Figure 107

RUN	SYM	α	$\frac{q}{q_\infty}$
138	+	---	8.06
141	▷	+15°	
144	◁	+20°	
148	△	+25°	
150	◇	+10°	

i_w=30°, δ_F=40°
FULL SPAN SLATS
NOM C_{μ_e}=.70

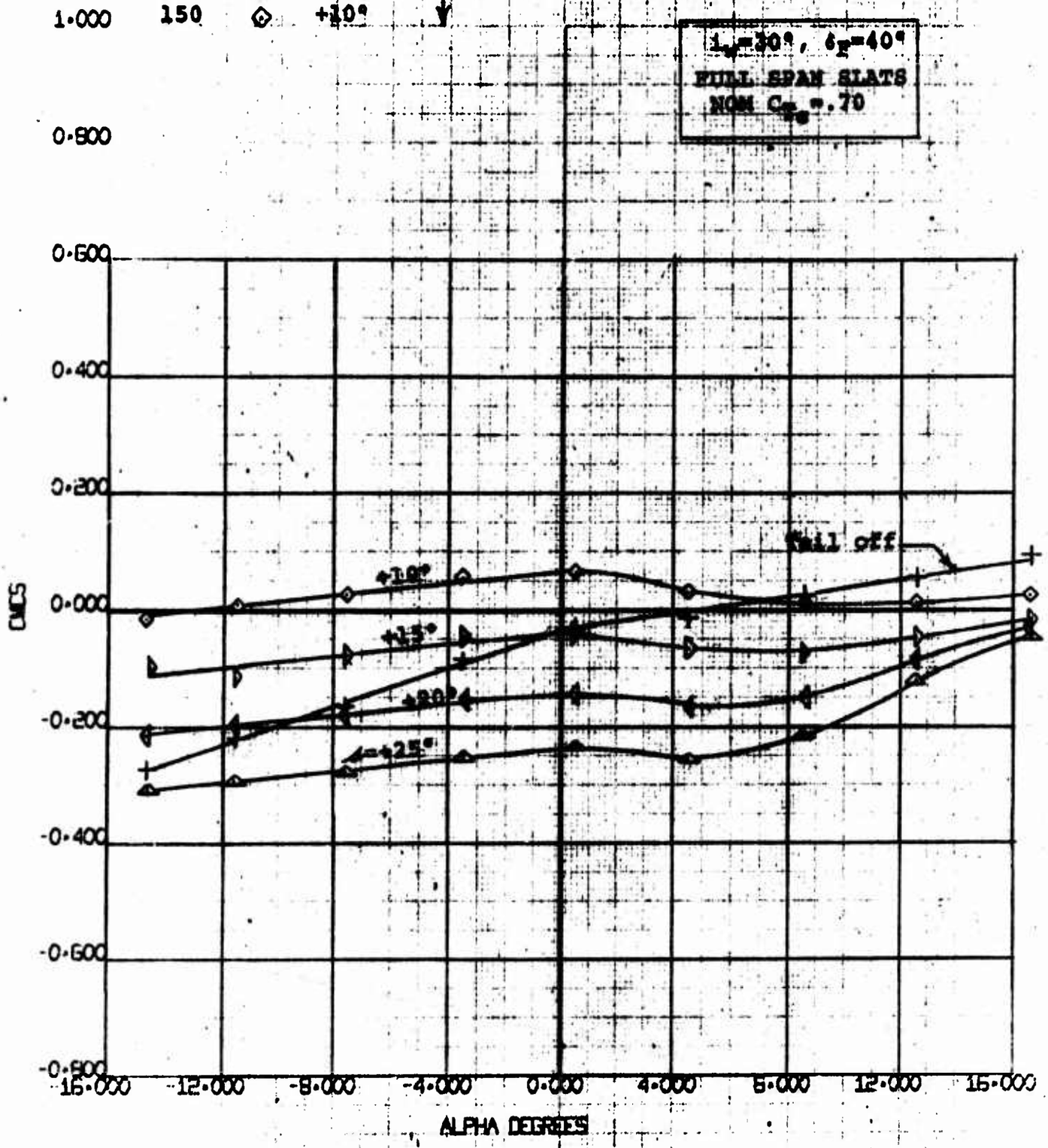

4-PROP TILT WING MODEL VROOM (FULL SPAN) CMCS VS ALPHA	DVWT 61 9/23/70

NOT REPRODUCIBLE

Figure 108

RUN	SYM.	α	q
138	+	----	8.06
141		+15°	
144		+20°	
148		+25°	
150	◇	+10°	

i_w=30°, δ_F =40°
FULL SPAN SLATS
NOM C_μ =.170

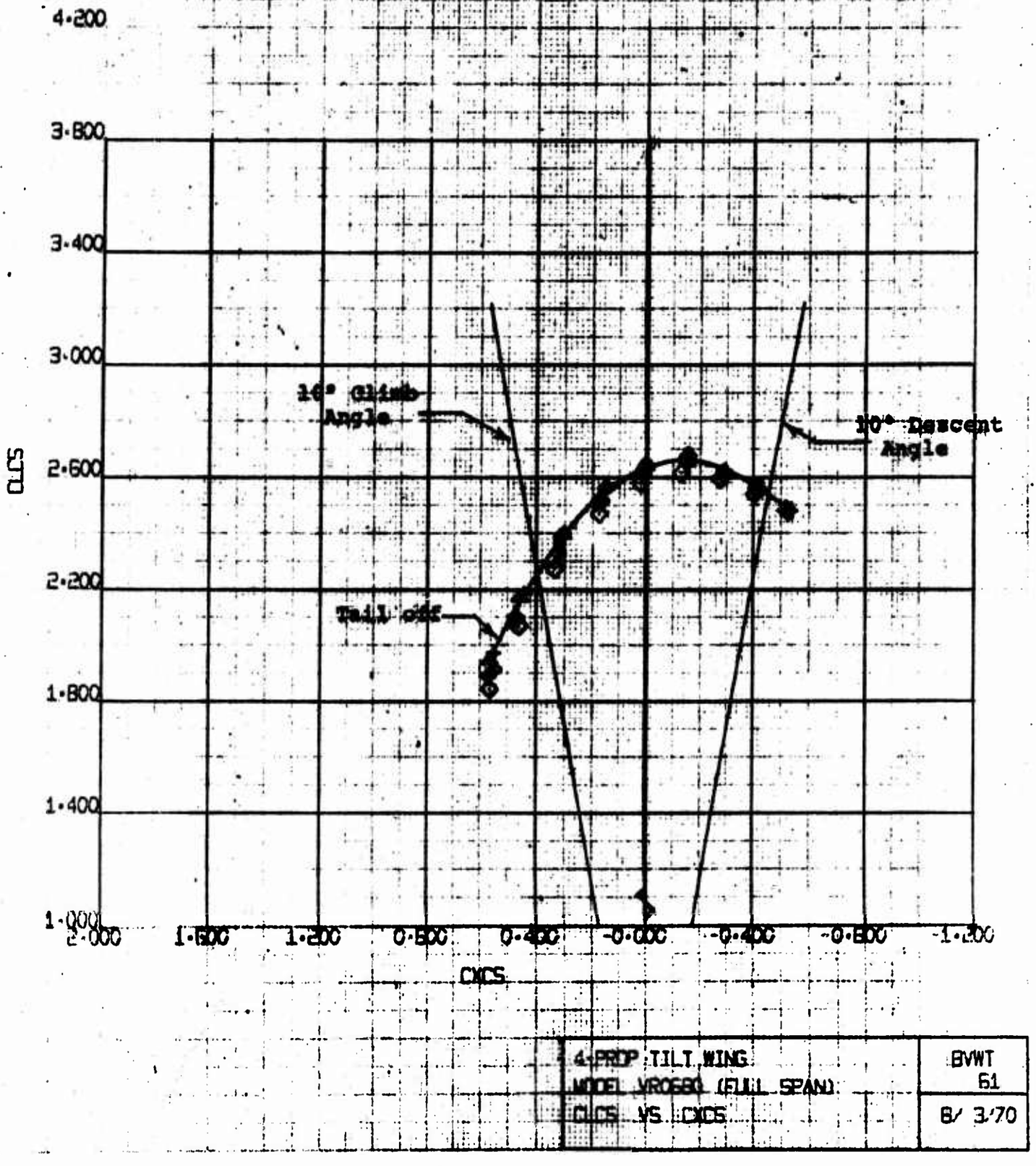

4-PROP TILT WING MODEL VROOM (FULL SPAN) CLCS VS CXCS	BVWT 61 B/ 3/70

Figure 109

RUN	SYM	α	q
138	+	---	8.0#
141	▷	+[illegible]	
144	◁	+20°	
148	△	+25°	
150	◇	+10°	

i_w=10° , Δ_F=40°
FULL SPAN SLATS
MOM. C_{μ} = .70

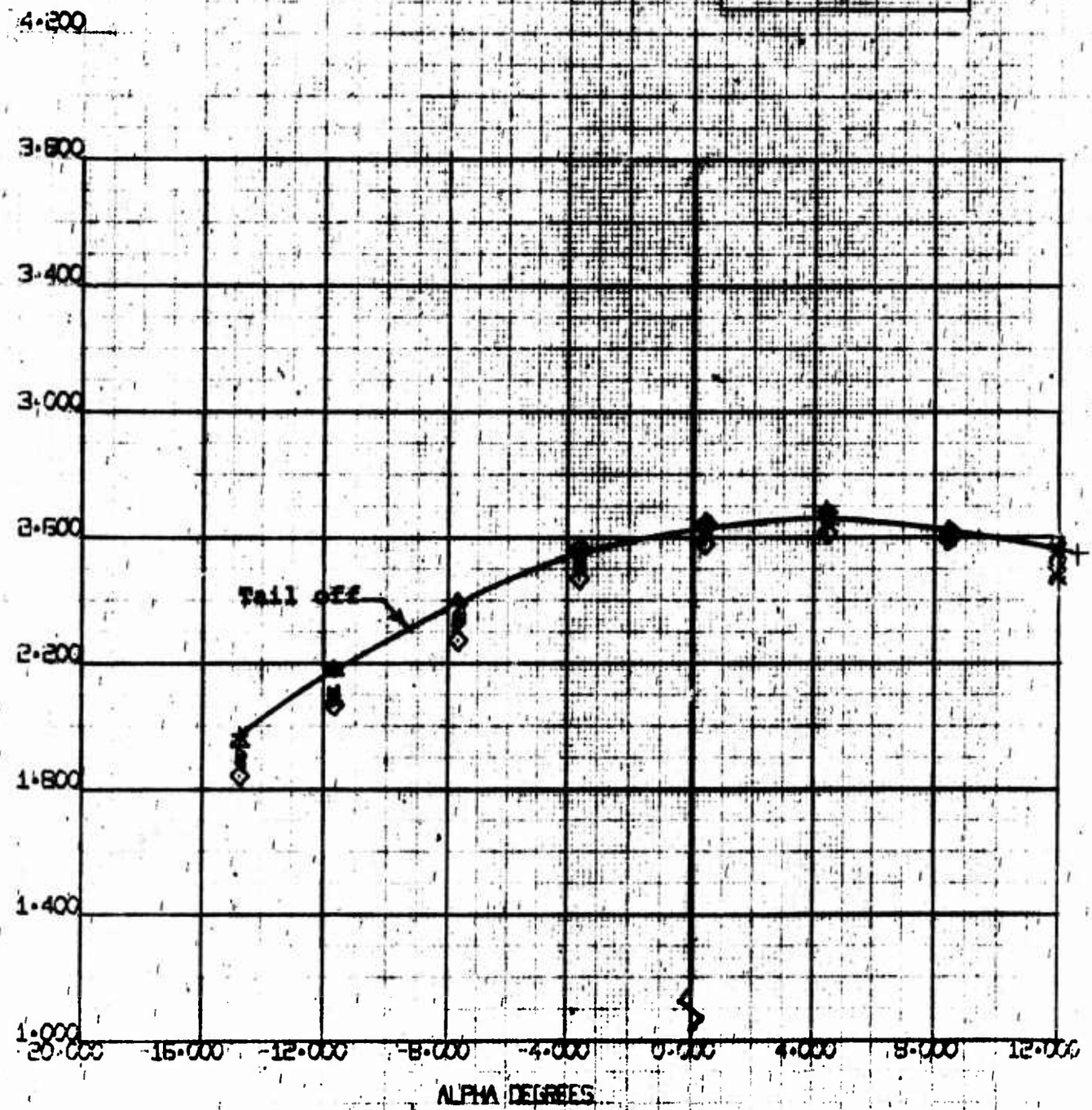

4-PROP TILT WING MODEL VROOM (FULL SPAN) CLCS VS ALPHA	NWT (L) 8/ 3/70

NOT REPRODUCIBLE

NUMBER D170-10038-1
REV. LTR.

Figure 110

RUN	SYM	α	q
137	+	---	5.08
140		+15°	
143		+20°	
147		+25°	

i_w = 30°, δ_F=40°
FULL SPAN SLATS
NOM C_{T_s} = .80

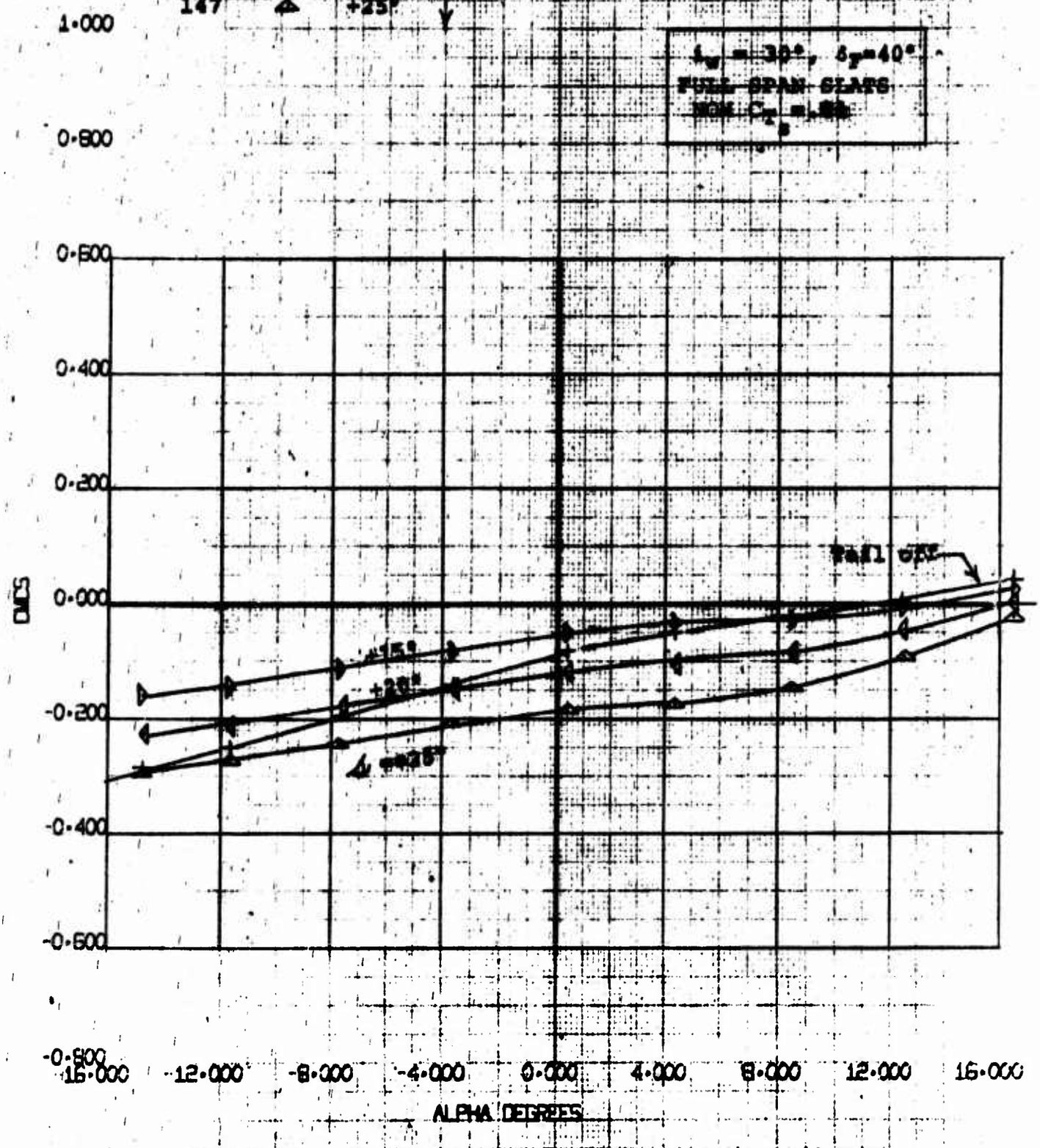

4-PROP TILT WING MODEL VROBBO (FULL SPAN) DMCS VS ALPHA	BVWT 61 9/23/70

Figure 111

RUN	SYM	α_s	q
139	▼	---	5.98
140	◆	+15°	
143	◀	+20°	
147	▲	+25°	

i_w=30°, i_T=40°
FULL SPAN FLAPS
WITH $C_{L_{max}}$=4.61

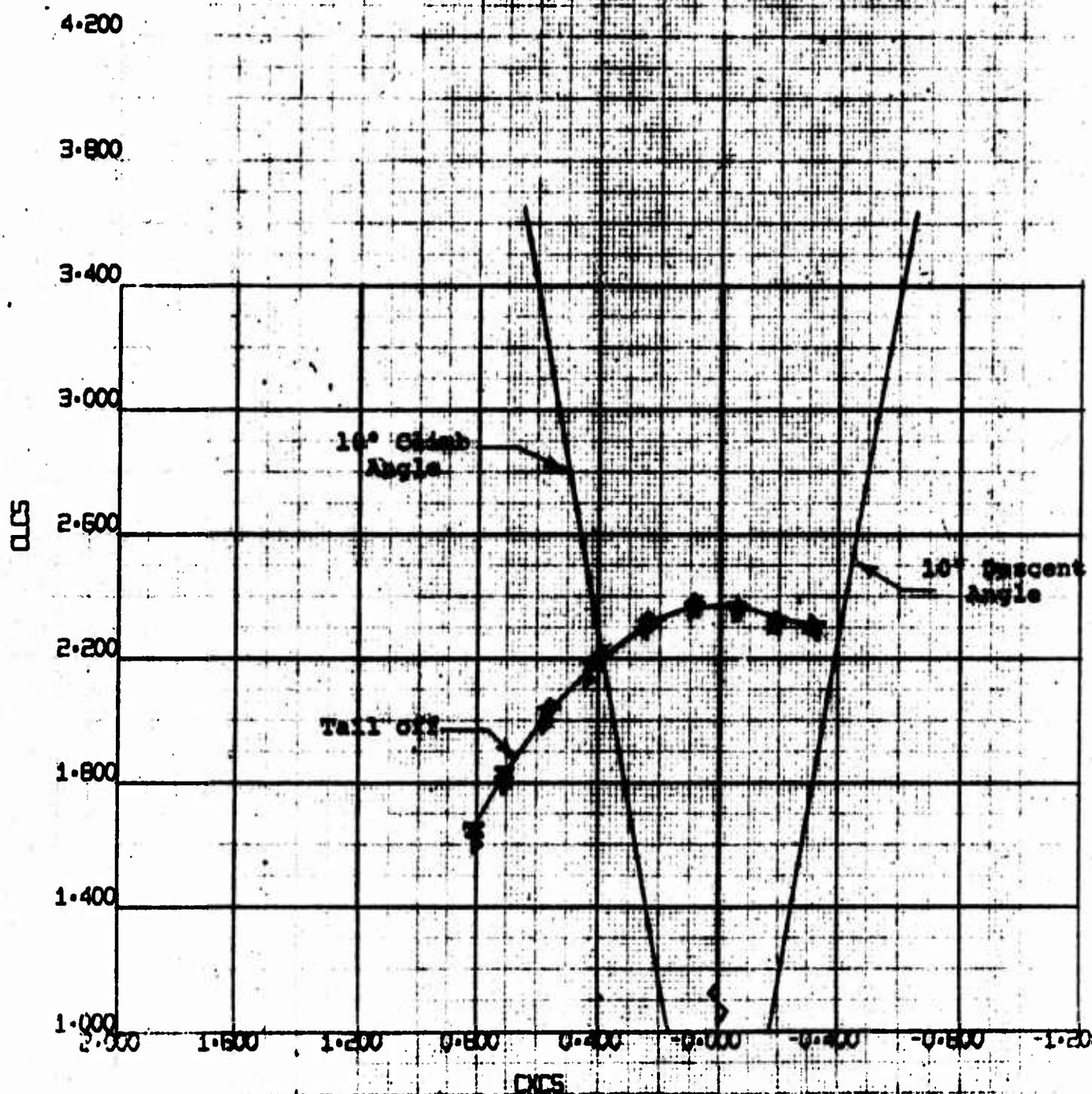

4-PROP TILT WING MODEL VROSBO (FULL SPAN) CLCS VS CXCS	BVWT 61 8/ 3/70

NOT REPRODUCIBLE

NUMBER D170-10038-1
REV. LTR

Figure 112

RUN	SYM	δ_f
137	▽	0
140	▷	+15°
143	◁	+20°
147	△	+25°

i_w=3.0° δ_F=40°
FULL SPAN SLATS
WOW C_T=.81

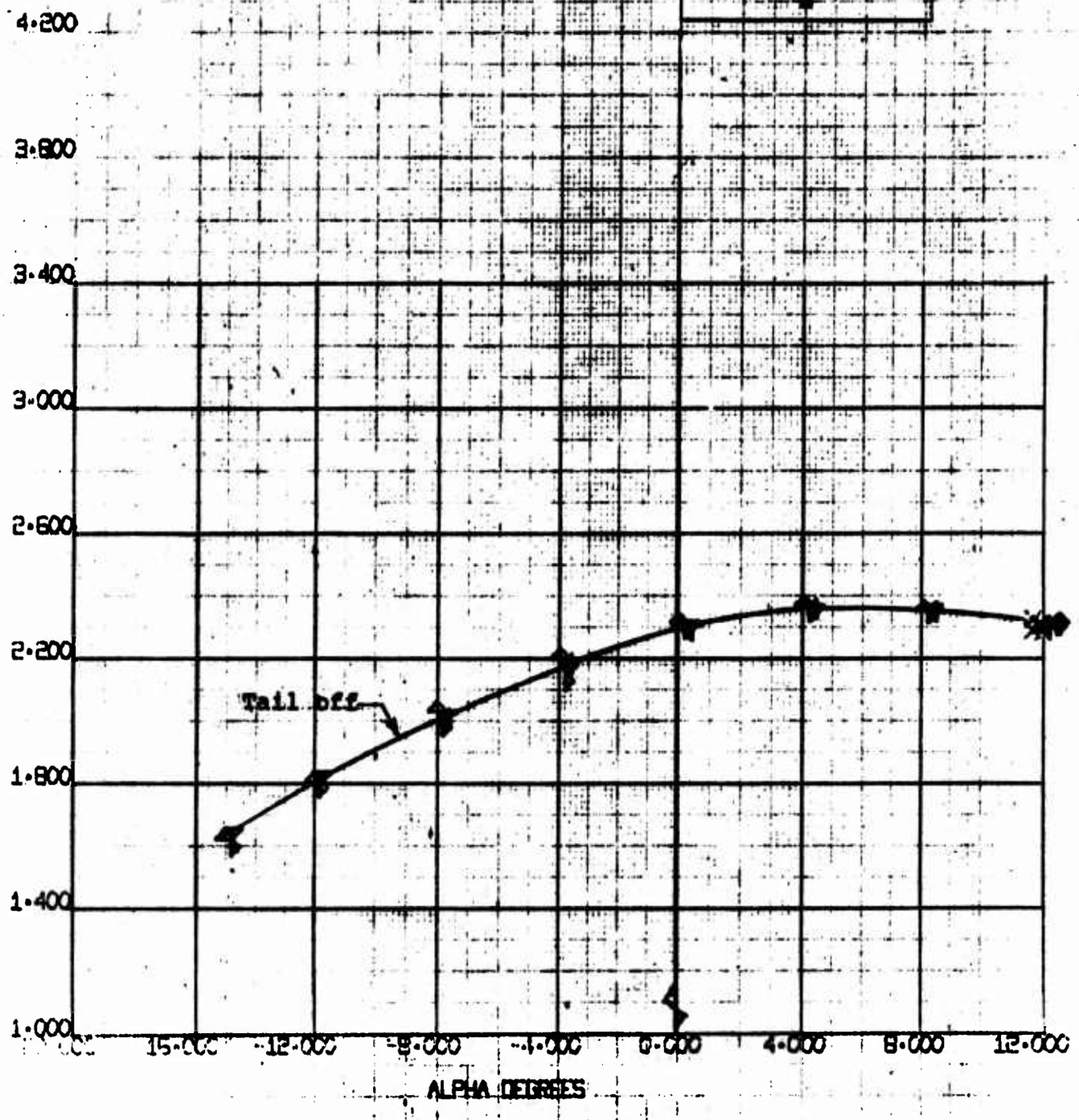

4-PROP TILT WING MODEL VROBBO (FULL SPAN) CLCS VS ALPHA	BVWT 61 8/ 3/70

Figure 113

RUN	SYM	δ_f	q
63	+	---	16.34
68	▷	+20°	
71	▽	+15°	
74	◁	+10°	

i_w=30°, i_T=60°
FULL SPAN SLATS
ROK $C_{L_{max}}$ = .56

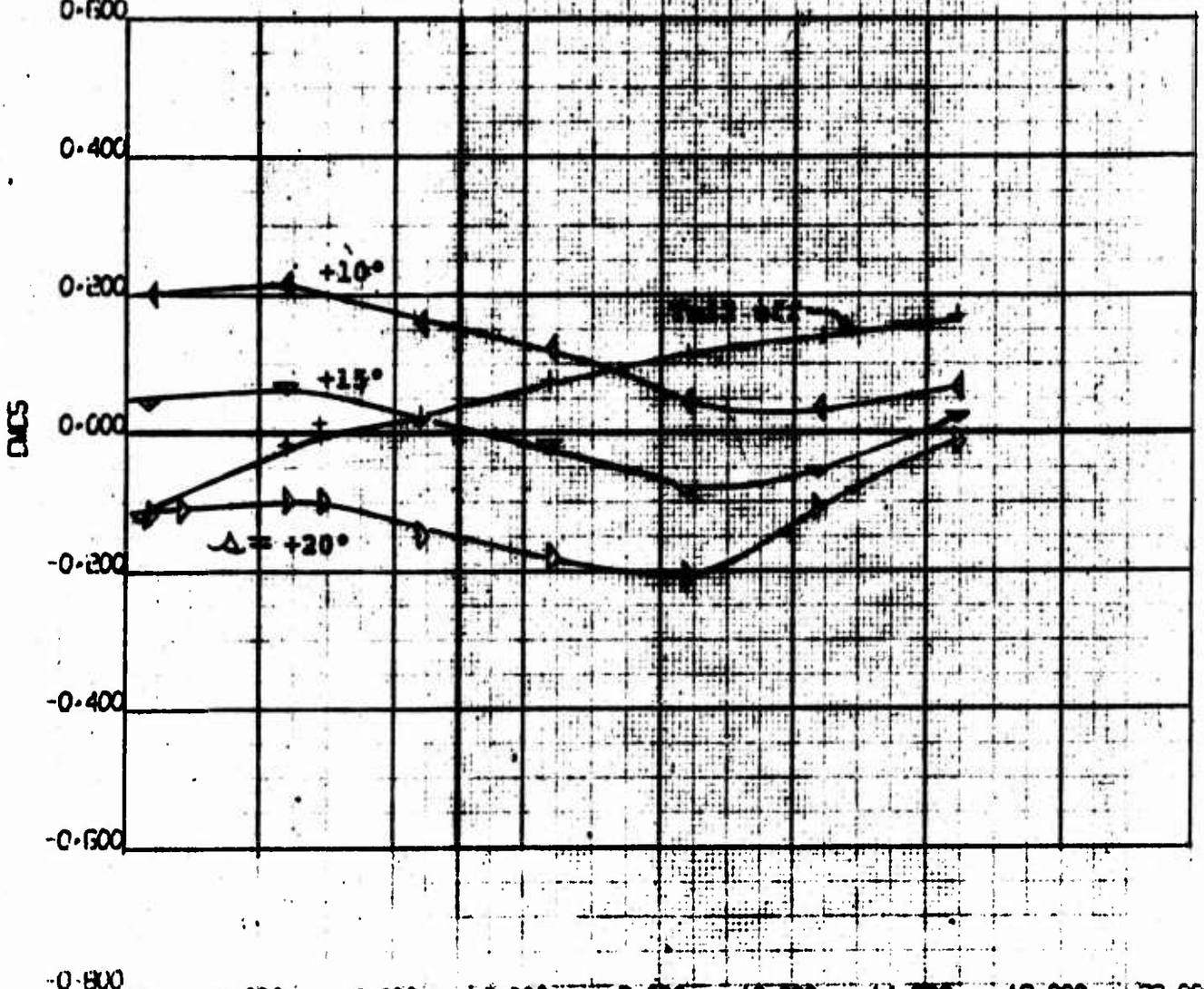

4-PROP TILT WING MODEL VROOM (FULL SPAN) DCS VS ALPHA	BVWT 61 8/ 3/70

NOT REPRODUCIBLE

Figure 114

RUN	SYM	δ_f	q
63	+	---	16.30
68	▷	+20°	
71	▽	+15°	
74	◁	+10°	

i_w=30° δ_f=60°
FULL SPAN SLATS
NOM C_μ =.55

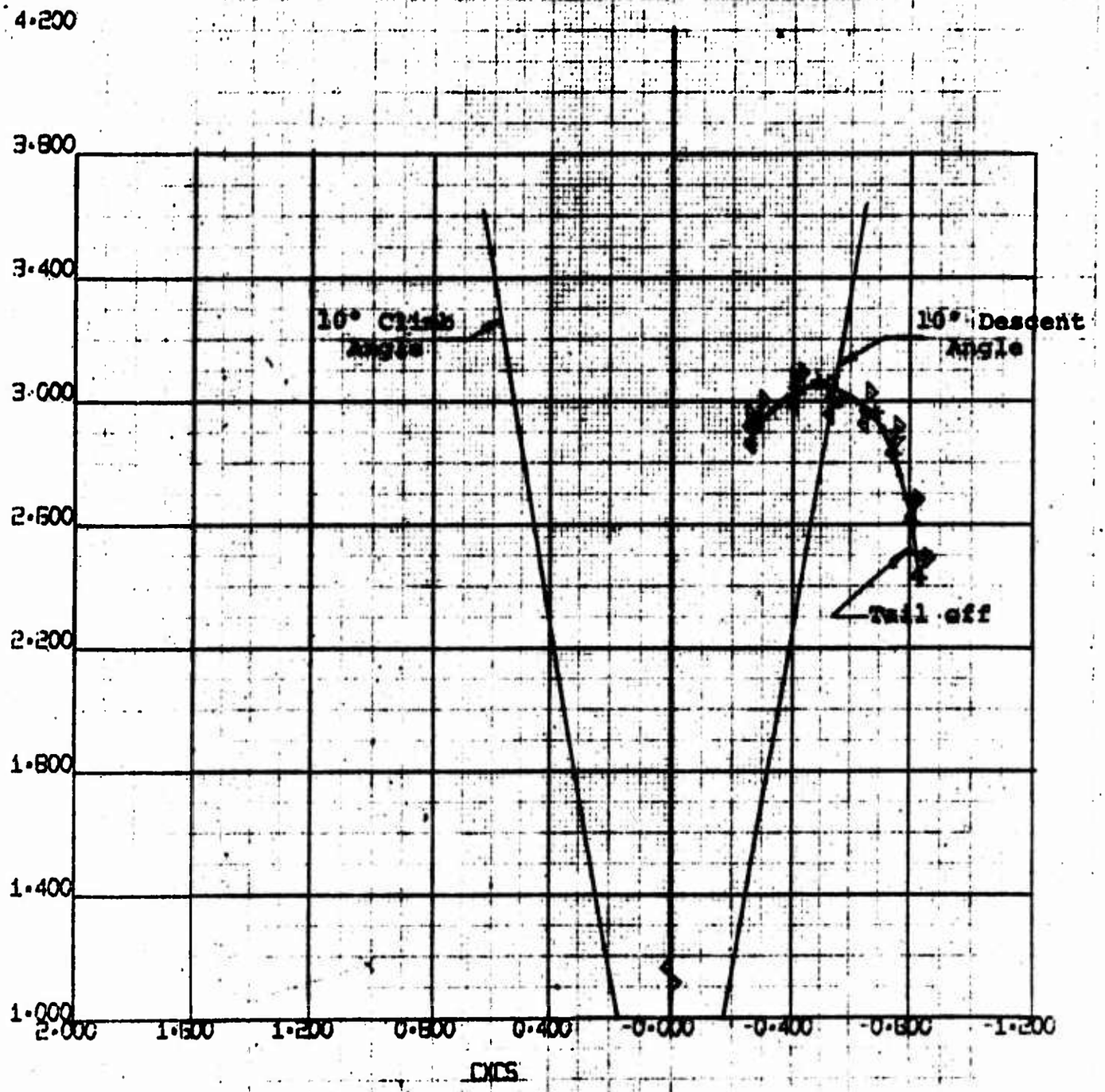

4-PROP TILT WING MODEL VROOM (FULL SPAN) CLCS VS CXCS	BVWT 61 8/ 3/70

Figure 115

RUN	SYM	δ_e	R
63	+	---	16.30
68	▶	+20°	
71	▼	+15°	
74	◀	+10°	

i_w=20°, i_T=60°

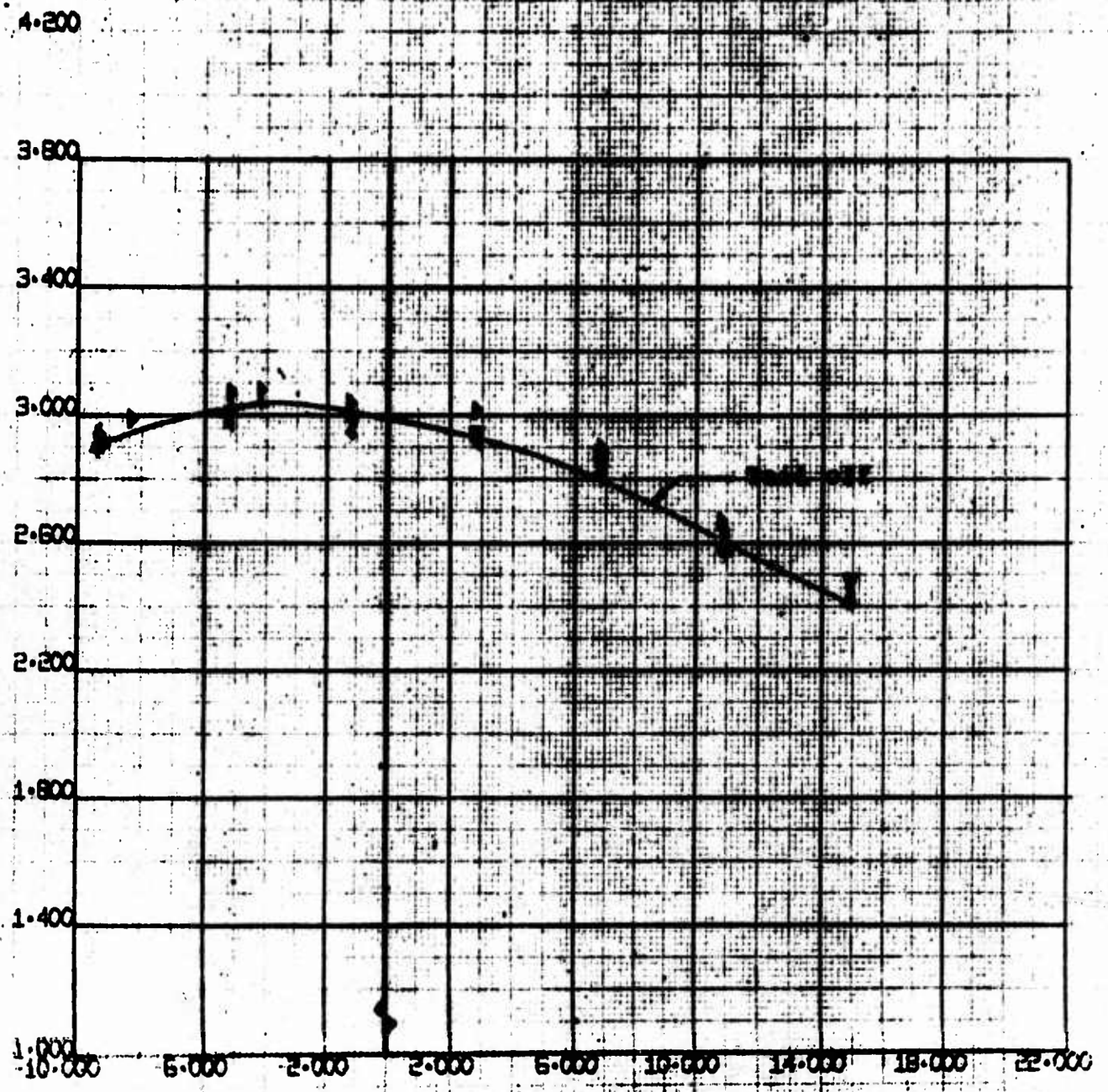

4-PROP TILT WING MODEL VROOM (FULL SPAN)	BVWT 61
CLCS VS ALPHA	8/ 3/70

NOT REPRODUCIBLE

Figure 116

RUN	SYM	α_T	q
64	+	---	10.51
67	▷	+20°	
70	▽	+15°	
73	◁	+10°	

i_w=30°, δ_F=60°
FULL SPAN SLATS
NOM C_{T_B}=.70

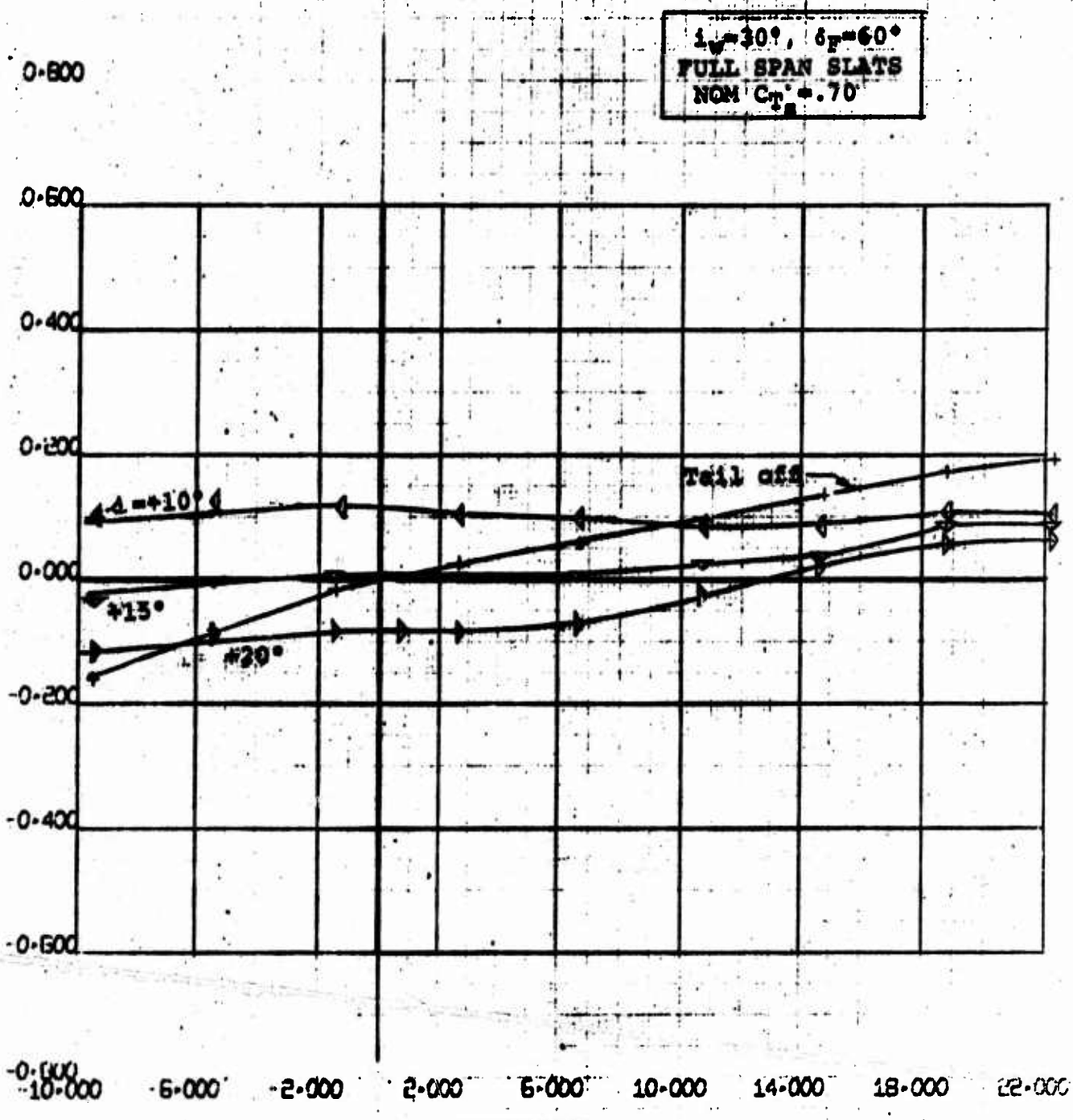

4-PROP TILT WING MODEL VRGBO (FULL SPAN) DMCS VS ALPHA	BVWT 61 8/ 3/70

Figure 117

RUN	SYM	δ_f	q
64	+	---	10.51
67	▶	+20°	
70	▼	+15°	
73	◀	+10°	

i_w=30°, δ_f=60°
FULL SPAN SLATS
NOM C_{μ_j} = .30

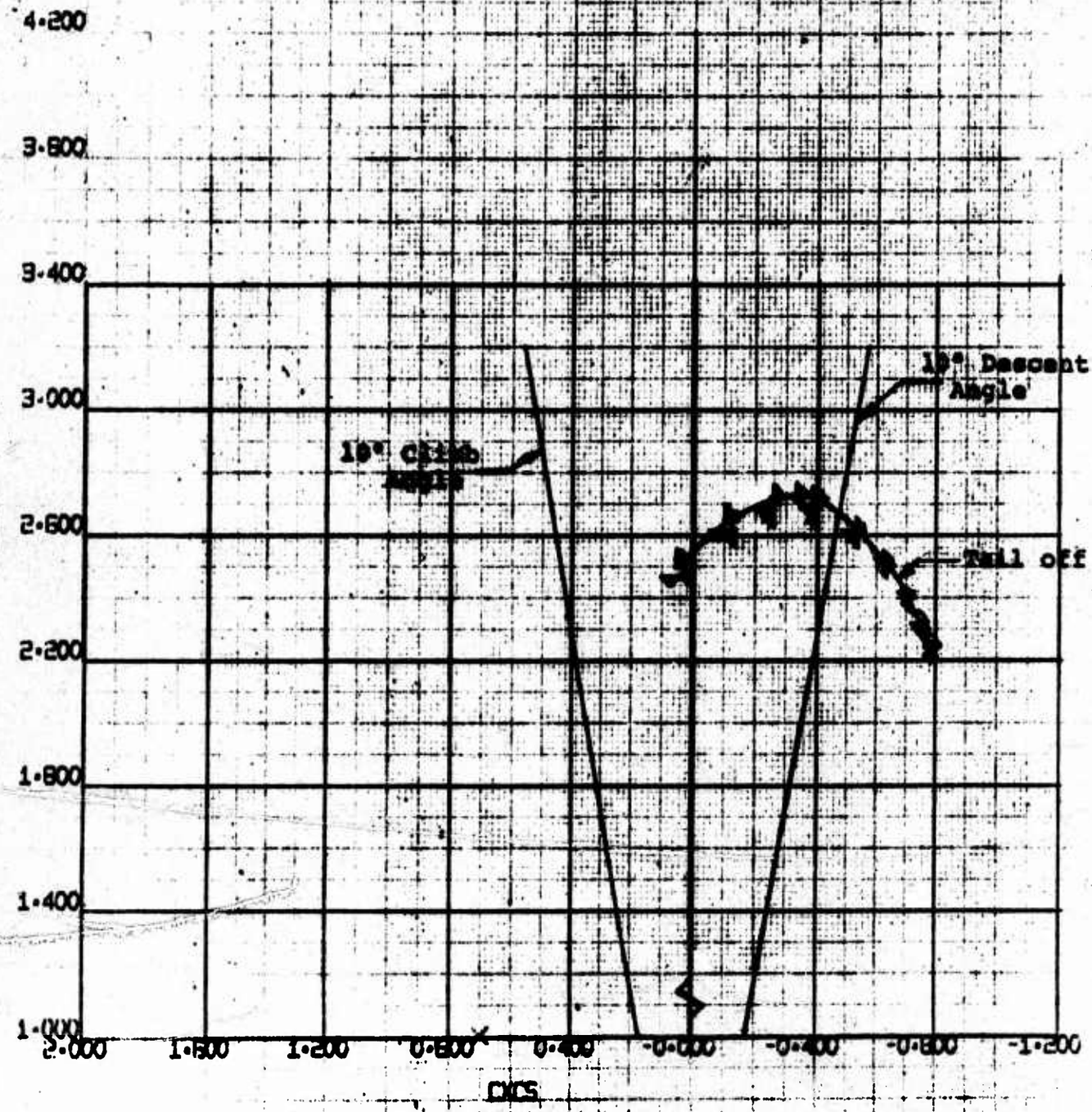

4-PROP TILT WING MODEL VROOM (FULL SPAN) CLCS VS CXCS	BVWT 61 8/ 3/70

NOT REPRODUCIBLE

NUMBER D170-10038-1
REV. LTR.

Figure 118

RUN	SYM	$\Lambda_{c/4}$
64	+	---
67	▷	+20°
70	▽	+15°
73	◁	+10°

δ_e 10.51

i_w=50°, i_T=0°
FULL SPAN SLATS
MOM C_{T_R} =.70

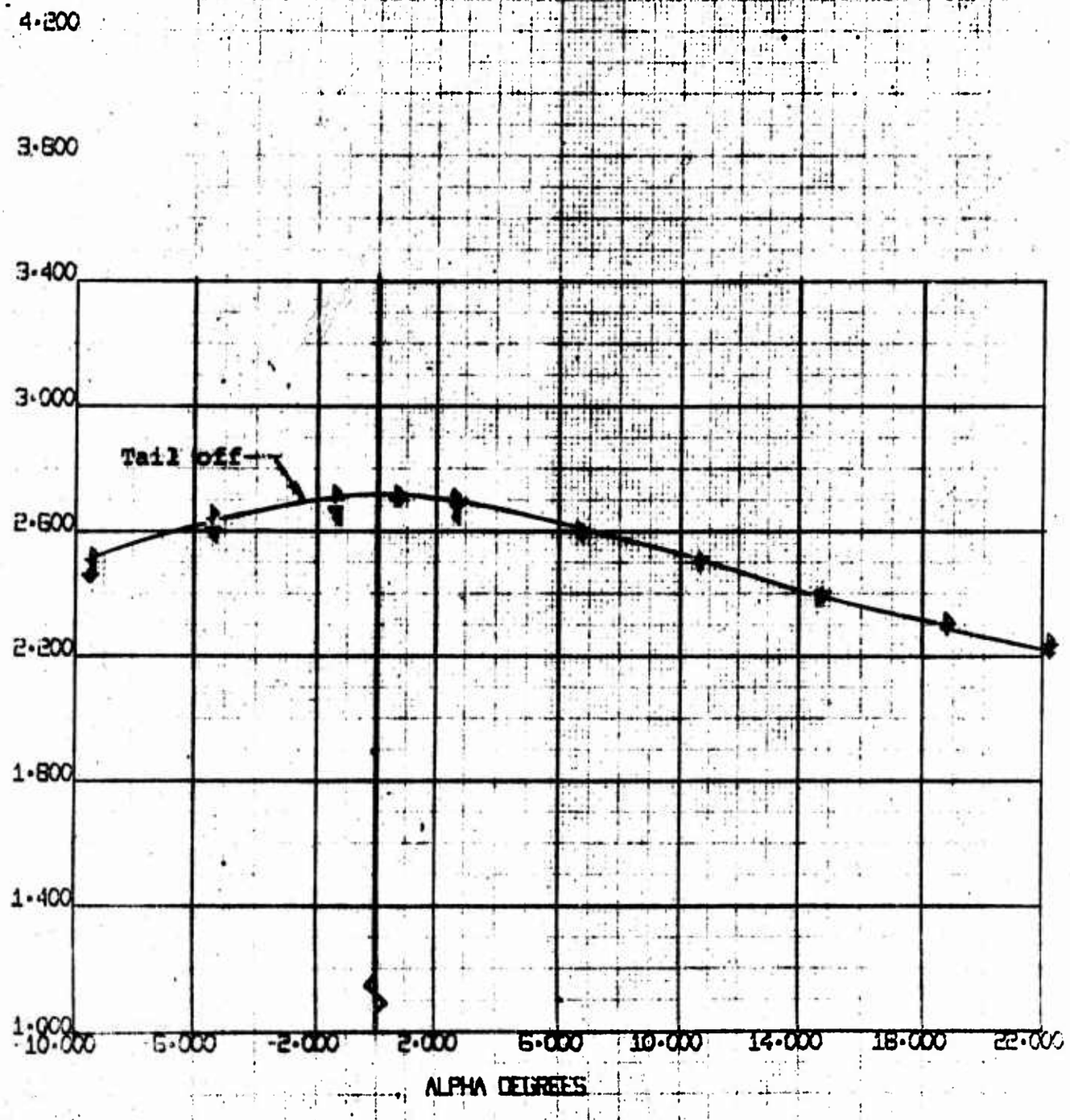

4-PROP TILT WING MODEL VROBBC (FULL SPAN) CLCS VS ALPHA	BVWT 61 6/ 3.70

NUMBER D170-10038-1
REV- LTR.

Figure 119

RUN	SYM	δ_f	q
65	+	---	6.80
66	▷	+20°	6.95
69	▼	+15°	
72	◁	+10°	
75	◁	+25°	

i_w=30°, δ_f=60°
FULL SPAN SLATS
MOM C_{T_c}=0.82

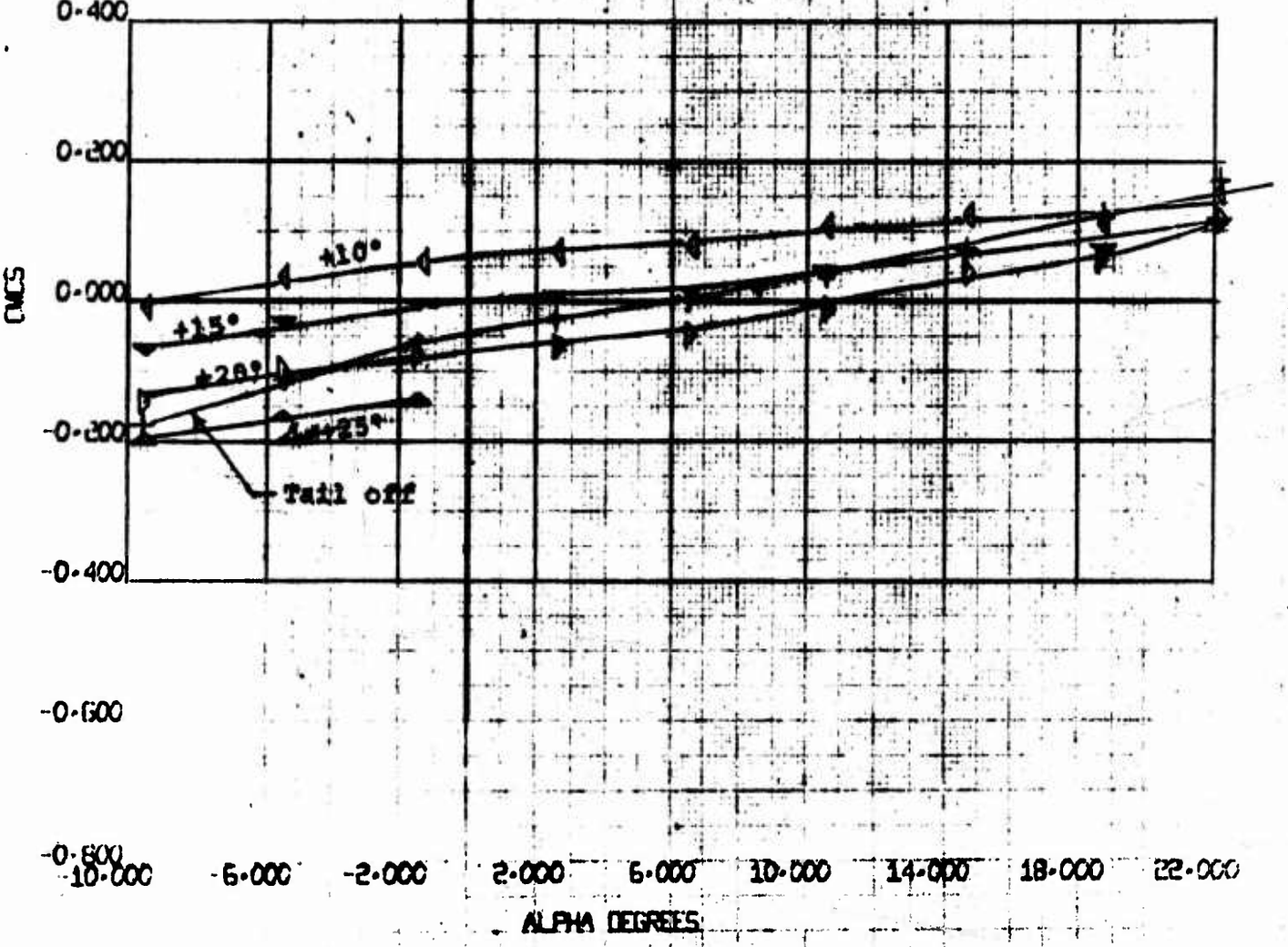

4-PROP TILT WING MODEL VROBBO (FULL SPAN) CMCS VS ALPHA	BVWT 61 8/ 3/70

NOT REPRODUCIBLE

NUMBER D170-10038-1
REV. LTR.

Figure 120

RUN	SYM	α	q
65	+	---	6.80
66	▷	+20°	6.95
69	◁	+15°	
72	◁	+10°	
75	△	+25°	

i_w=30°, i_p=60°
FULL SPAN SLATS
NOM C_{T_p}=0.81

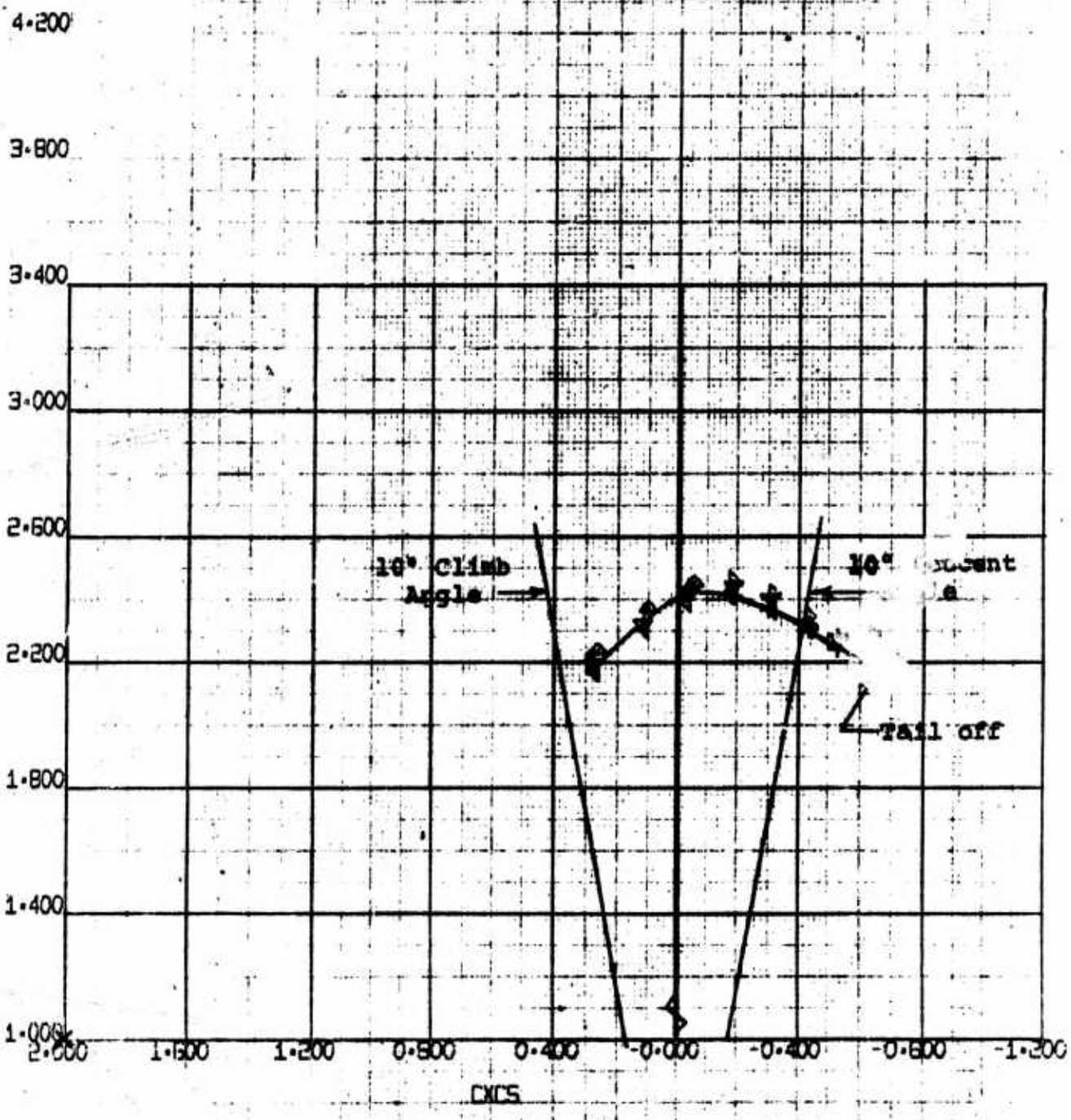

4-PROP TILT WING MODEL VRO880 (FULL SPAN) CLCS VS CXCS	BVWT 61 8/ 3/70

Figure 121

RUN	SYM	δ_f	q
65	+	---	6.80
66	▶	+20°	6.95
69	▼	+15°	↓
72	◀	+10°	
75	▲	+25°	

i_w=30°, δ_F=60°
FULL SPAN SLATS
NOM C_{μ_B}=0.81

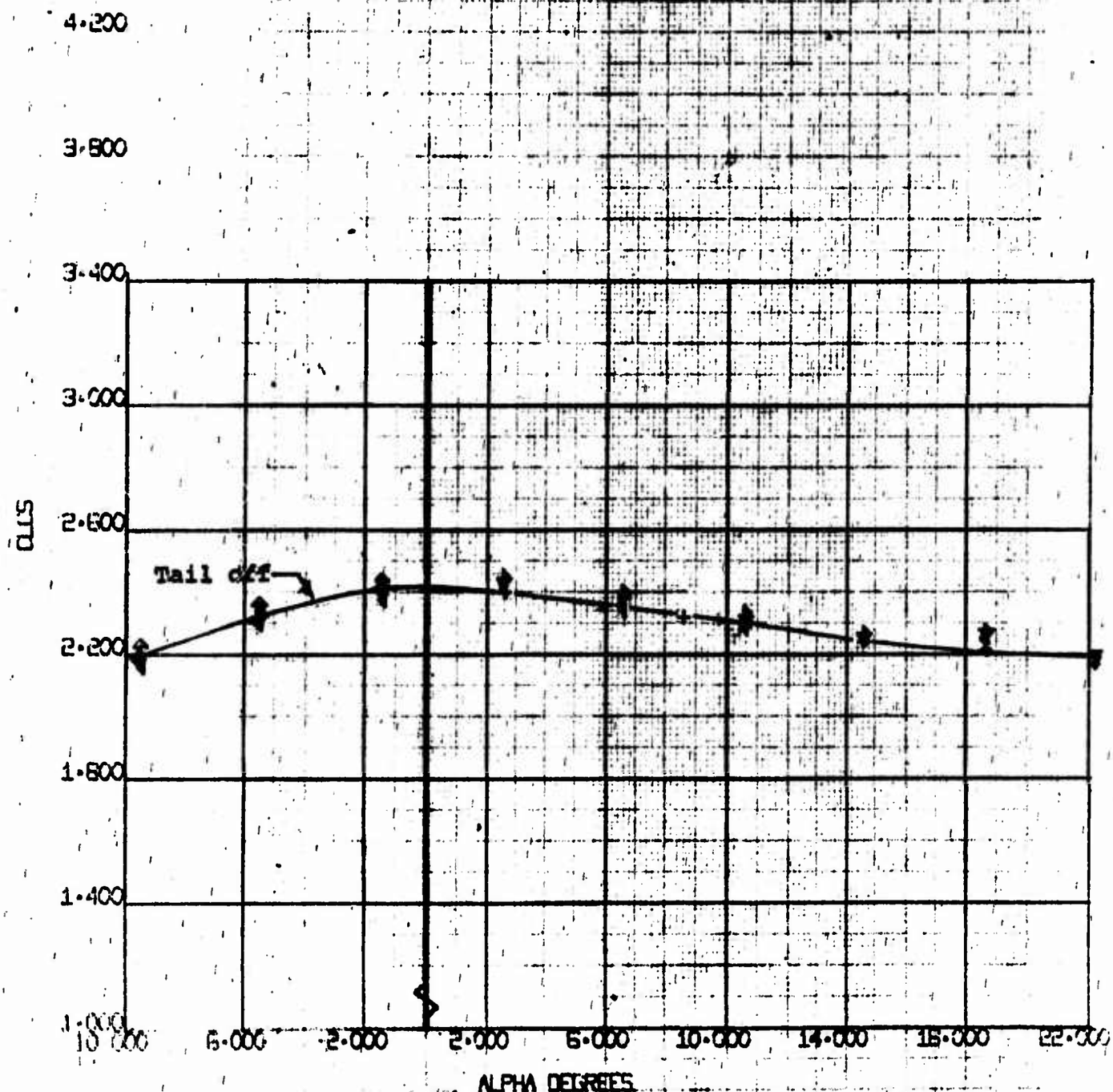

4-PROP TILT WING MODEL VROSBO (FULL SPAN) CLCS VS ALPHA	BVWT 61 8/ 3/70

NOT REPRODUCIBLE

NUMBER D170-10038-1

Figure 122

RUN	SYM	$\Lambda_{c/4}$	C_μ
123	+	---	5.20
125	◇	+35°	
127	▽	+30°	
129	◁	+25°	
130	△	+20°	
131	○	+25°	

i_w=45°, δ_F=60°
FULL SPAN SLATS
NOM C_μ = .81

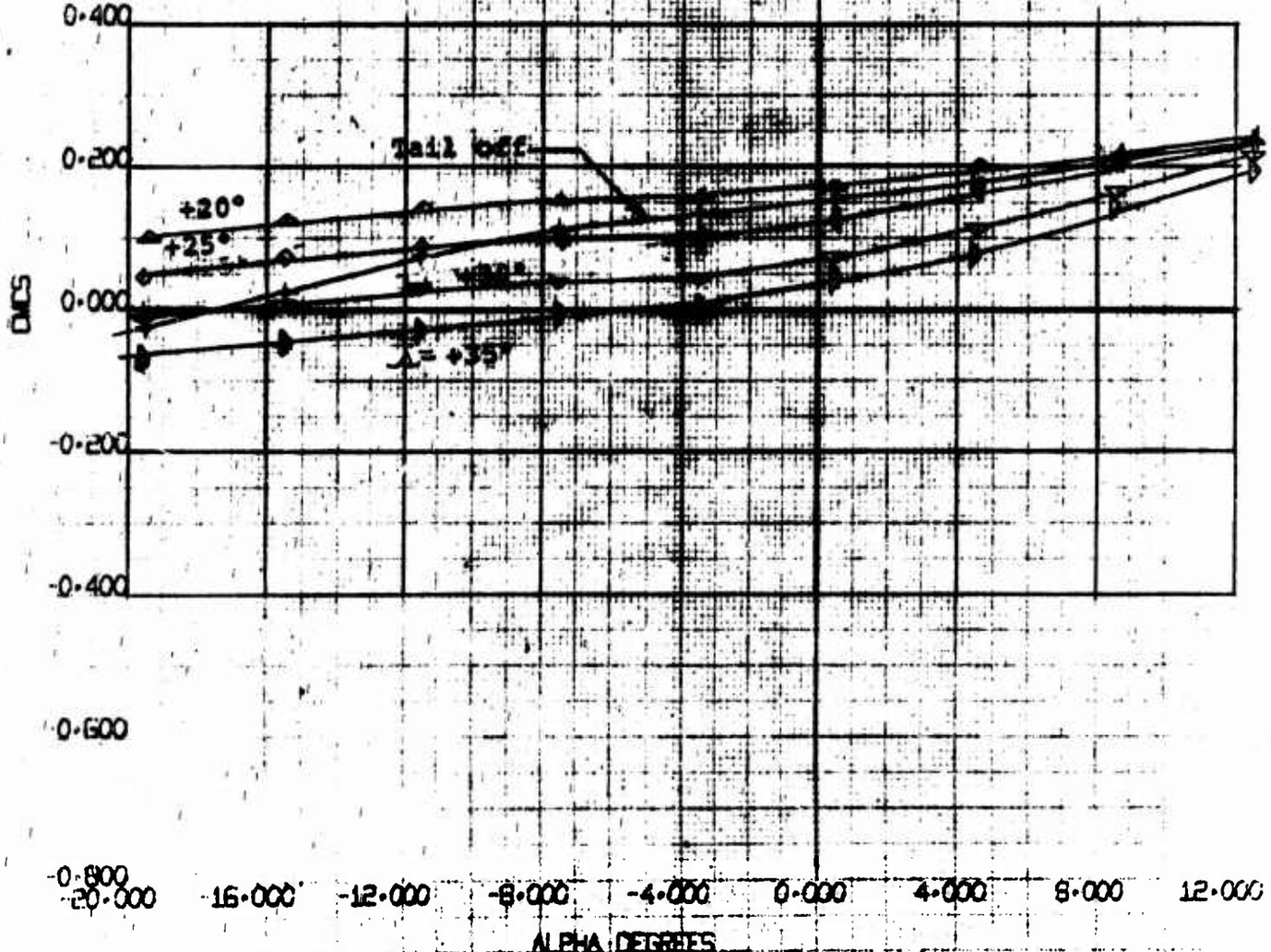

4-PROP TILT WING MODEL VROBBO (FULL SPAN) DCS VS ALPHA	BVWT 61 9/23/70

NUMBER D170-10038-1

REV. LTR.

Figure 123

RUN	SYM	δ_f	q
123	+	-+-	5.20
125	▶	+35°	
127	▼	+30°	
129	◀	+25°	
130	▲	+20°	
131	◇	+25°	

i_w=45°, δ_f=60°

FULL SPAN FLAPS

MOM $C_{m_{cg}}$=-.91

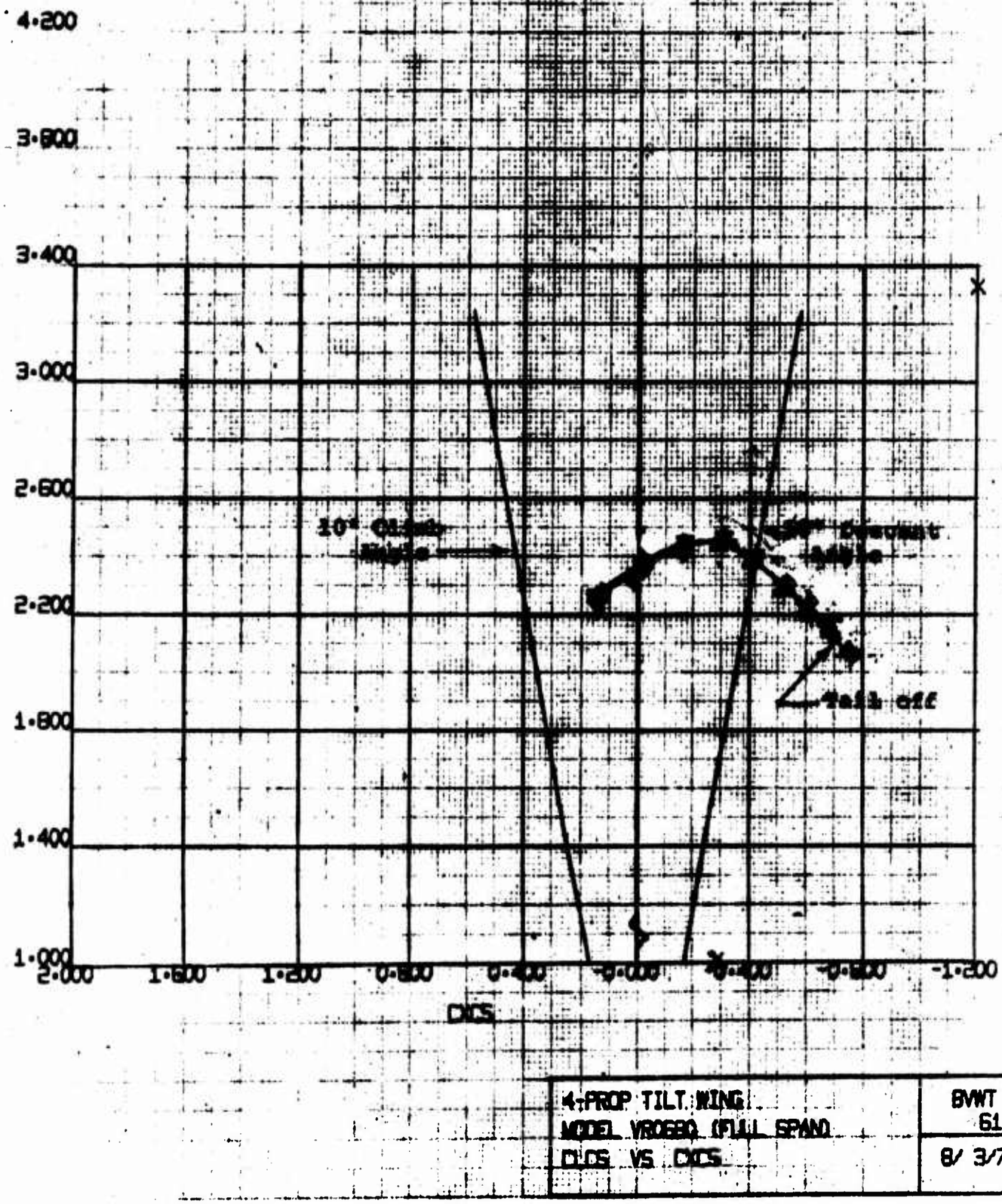

4-PROP TILT WING MODEL VROBBO (FULL SPAN) CLOS VS CDCS	BWT 61 8/ 3/70

NOT REPRODUCIBLE

Figure 124

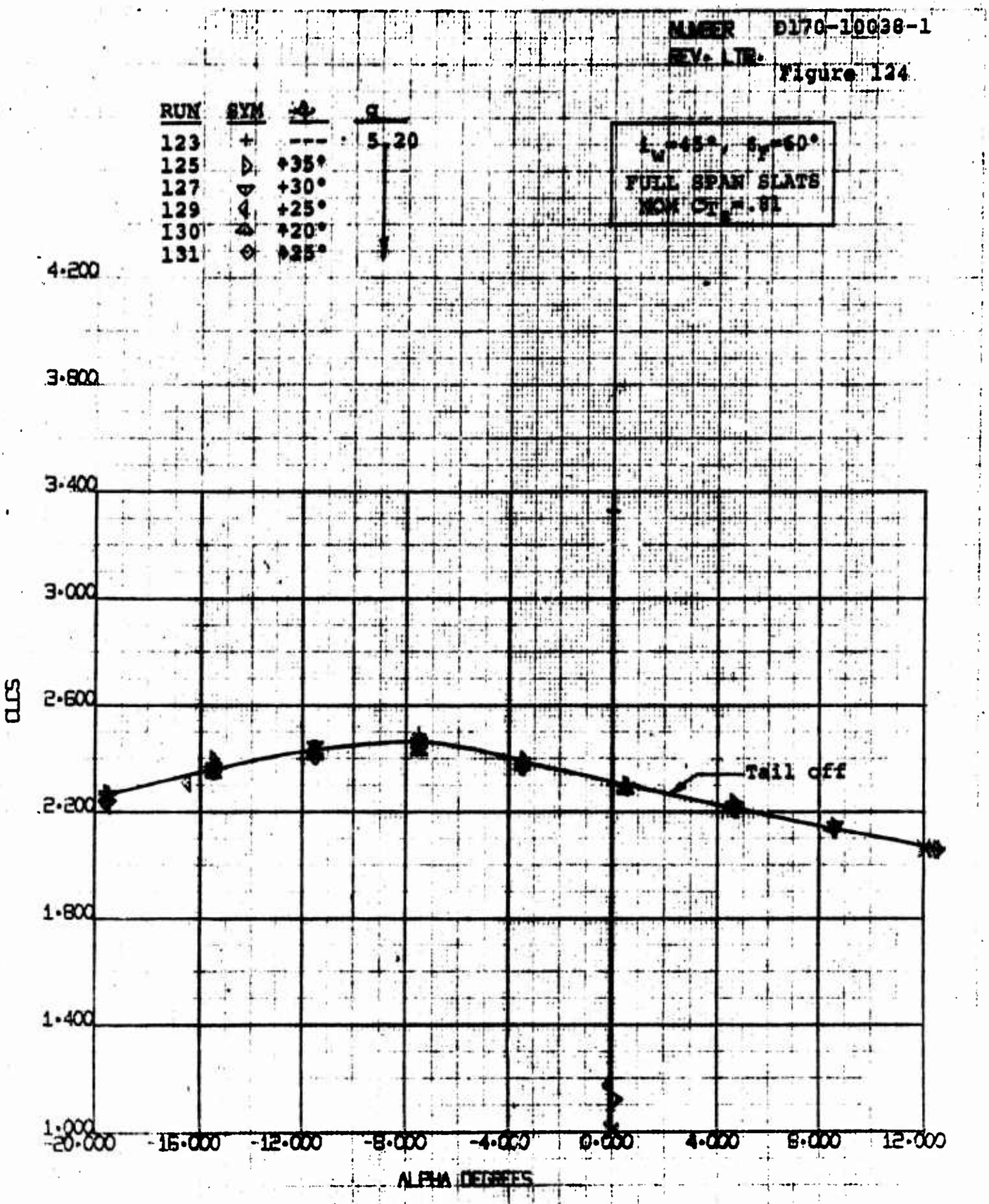

4-PROP TILT WING MODEL VROBBO (FULL SPAN) CLCS VS ALPHA	BVWT 61 8/ 3/70

NUMBER D170-10038-1
REV. LTR.

Figure 125

RUN	SYM	δ_f	q
122	+	---	2.20
124	▶	+35°	
126	▬	+30°	
128	◀	+25°	
131	◀	+25°	

i_w=45°, ϕ_p=60°
FULL SPAN SLATS
NOM C_{T_s}=.92

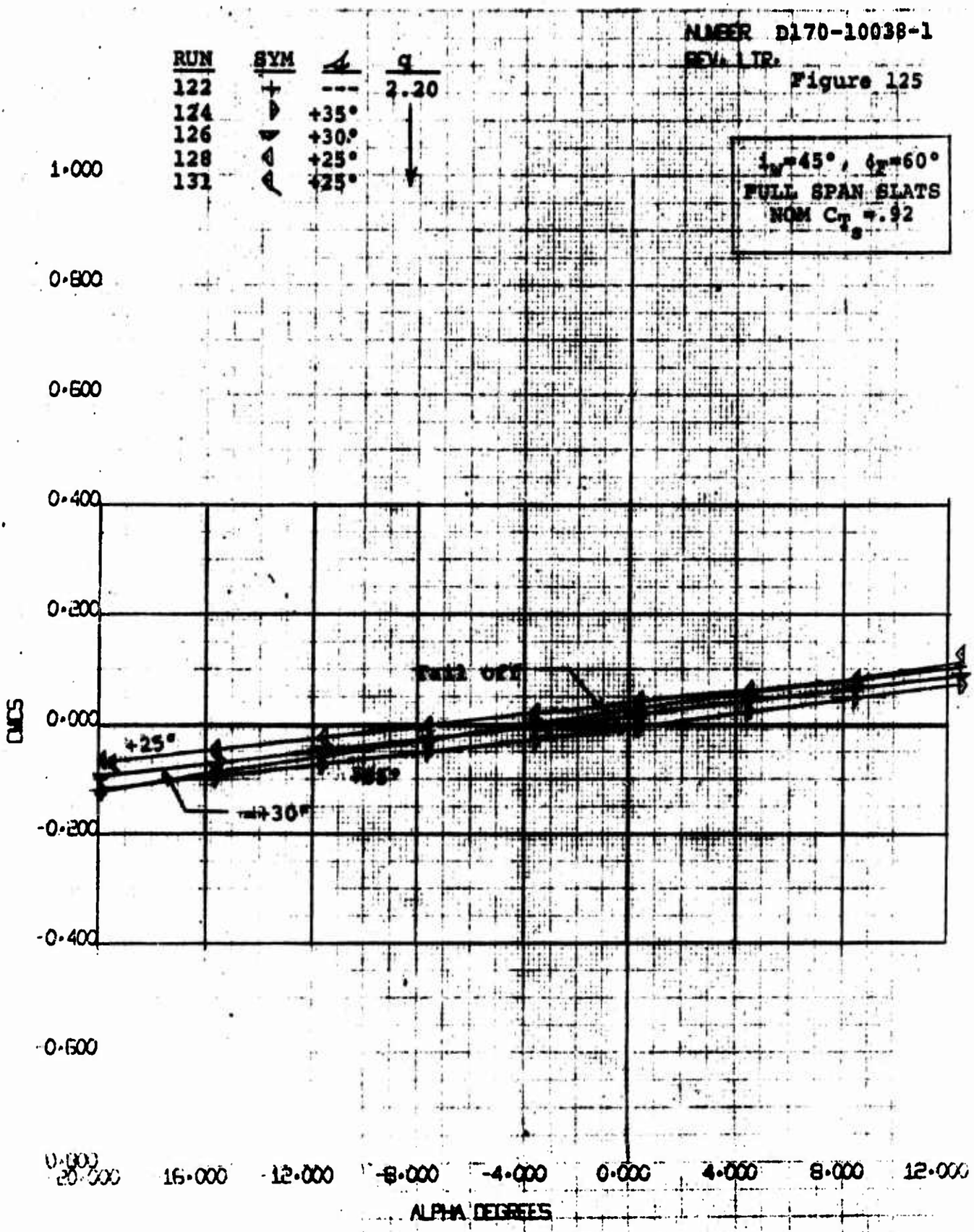

4-PROP TILT WING MODEL VRO880 (FULL SPAN) CMCS VS ALPHA	BVWT 61 9/23/70

NUMBER D170-10038-1
REV. LTR.

Figure 126

RUN	SYM	α	q
122	+	---	2120
124	▶	+35°	
126	▼	+30°	
128	◀	+25°	

i_w=45°, δ_F=60°
FULL SPAN SLATS
NOM C_{T_s} =.92

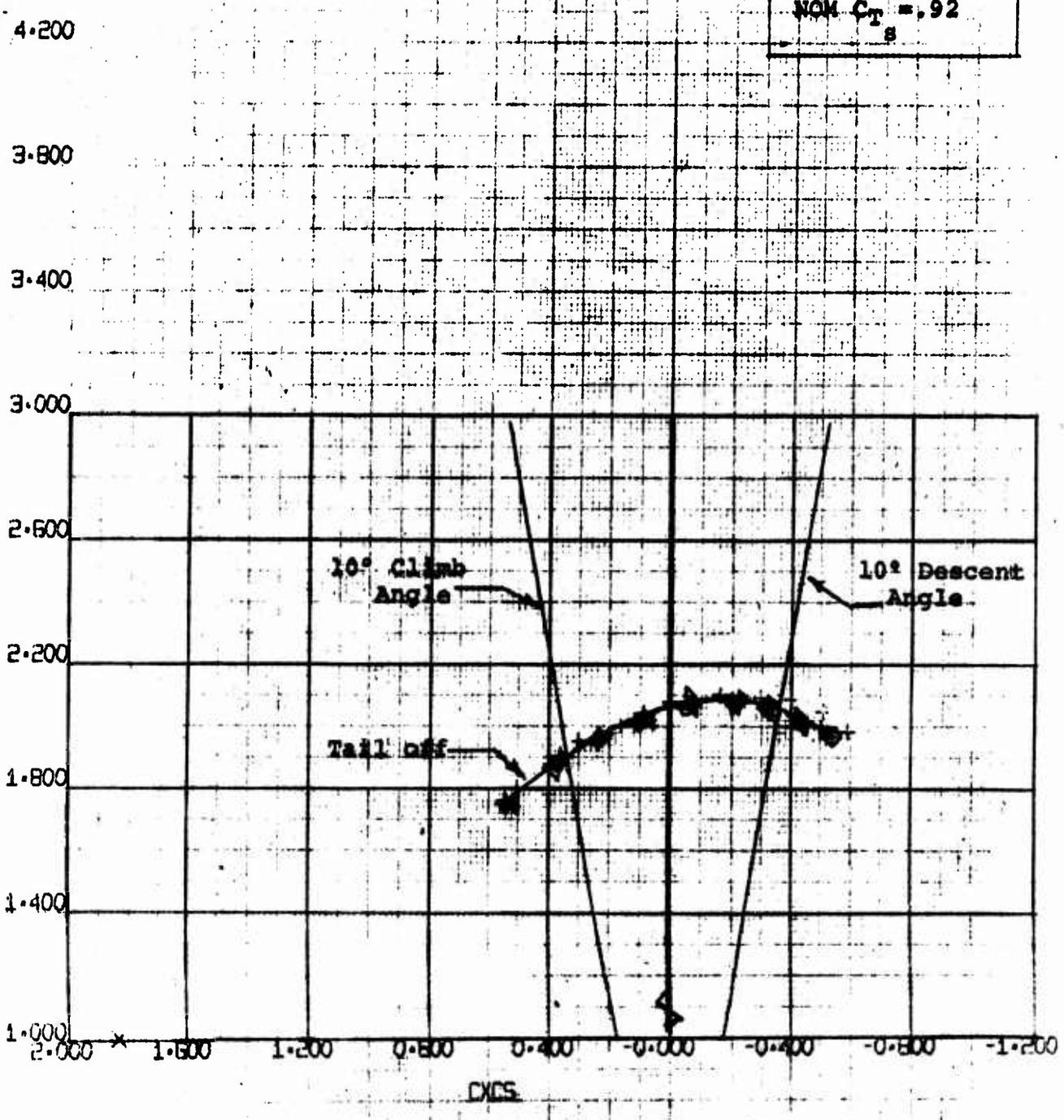

4-PROP TILT WING MODEL VROBBO (FULL SPAN) CLCS VS CXCS	BVWT 61 8/ 3/70

NOT REPRODUCIBLE

NUMBER D170-10038-1
REV. LTR

Figure 127

RUN	SYM	δ_f	q
122	+	---	2.20
124	▶	+35°	
126	▼	+30°	
128	◀	+25°	

i_w=65°, ϕ_p=60°
FULL SPAN SLATS
NOM C_T = .82
s

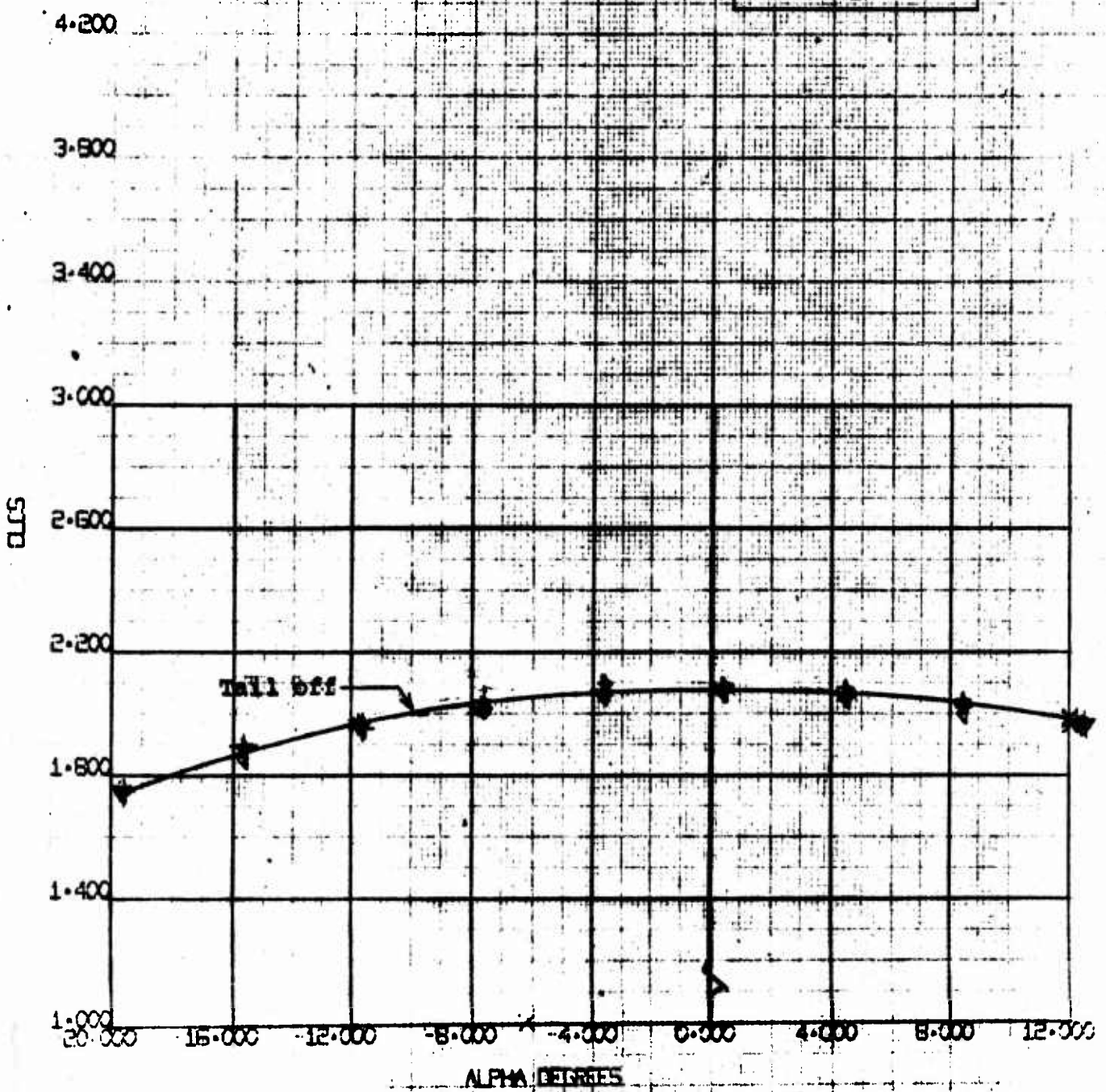

4-PROP TILT WING MODEL VROBBO (FULL SPAN) CLCS VS ALPHA	BVWT 61 8/ 3/70

D170-10038-1

Figure 128

RUN	SYM	i_w	q	δ_f
132	+	--->	1.57	40°
135	▷	---	↓	60°

i_w=55°, δ_f=40° and 60°
FULL SPAN SLATS
NOM C_{μ_s} = .24

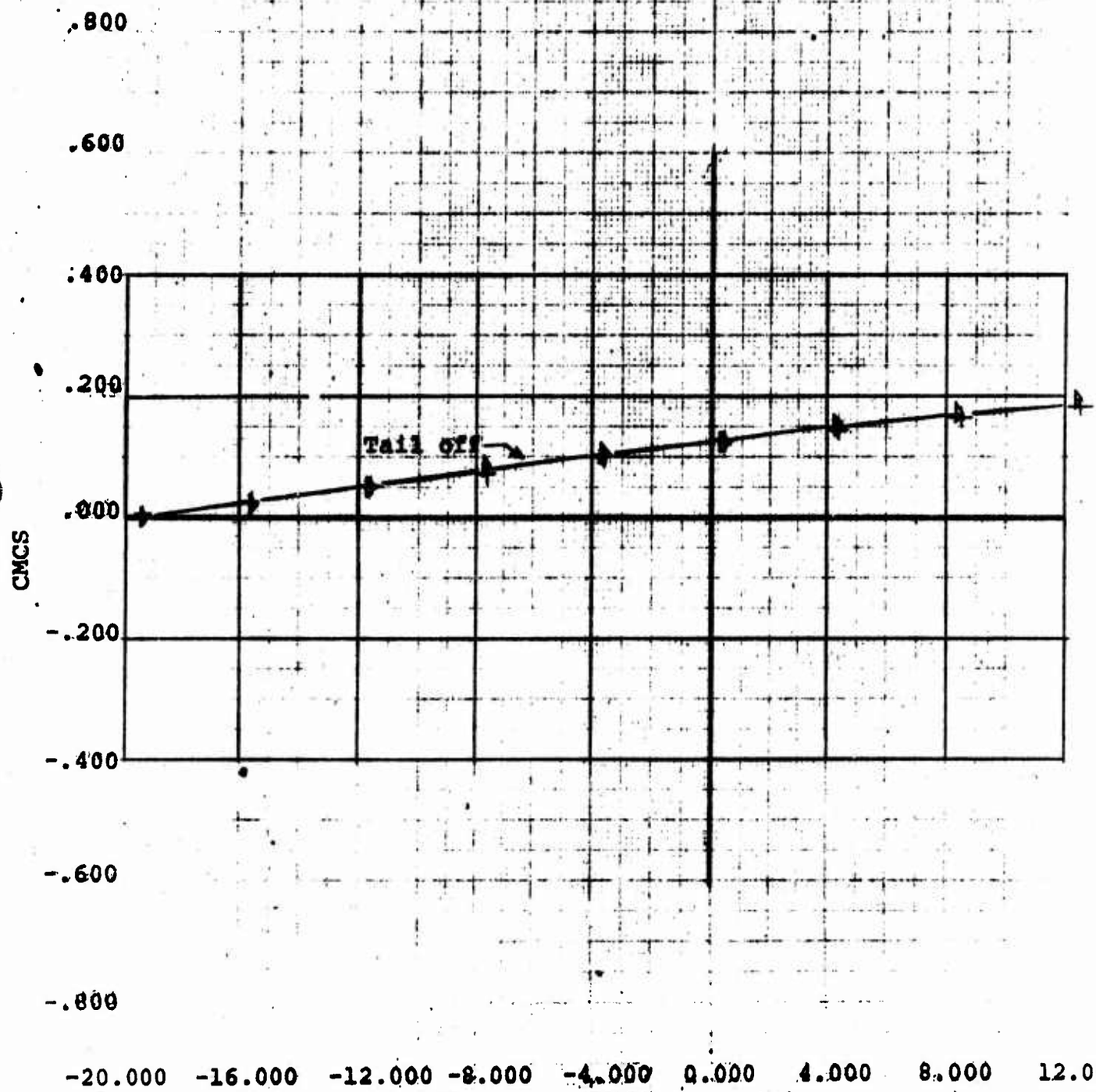

-20.000 -16.000 -12.000 -8.000 -4.000 0.000 4.000 8.000 12.000

ALPHA~DEGREES

4-PROP TILT WING MODEL VRC68Q (FULL SPAN) CMCS VS ALPHA	BVWT 61 8/3/70

NOT REPRODUCIBLE

D170-10038-1

Figure 129

RUN	SYM	α	q	δ_F
132	+	---	1.57	60°
135	▷	---	↓	40°

i_w=52°, δ_F=40° and 60°
FULL SPAN SLATS
NOM C_{T_s}=.94

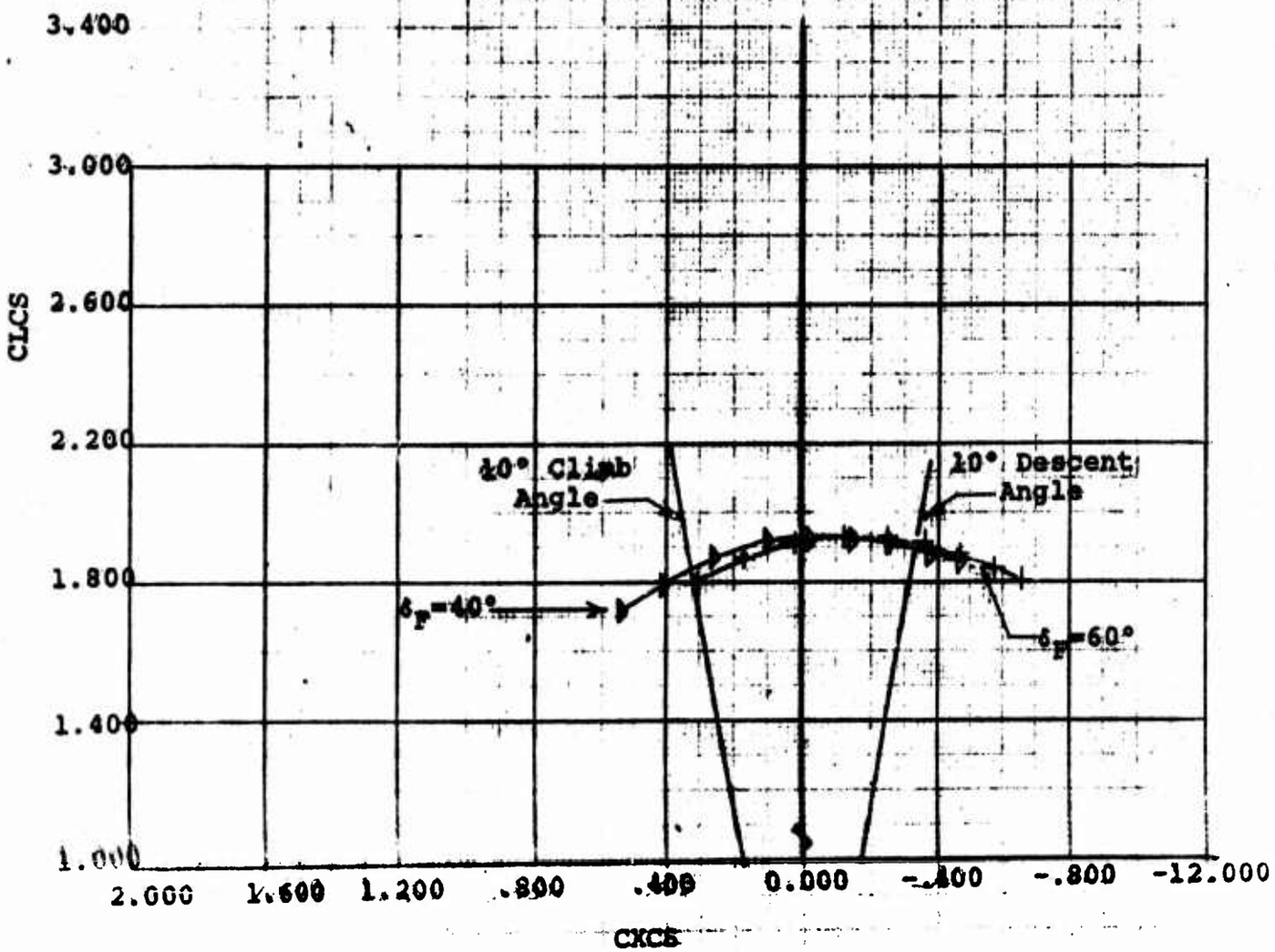

4-PROP TILT WING MODEL VRO68Q (FULL SPAN) CLCS VS CXCS	BVWT 61 8/3/70

Figure 130

RUN	SYM	α	q	δ_F
132	+	---	1.57	60°
135	▷	---	↓	40°

i_w=55°, δ_F=40° and 60°
FULL SPAN SLATS
NOM C_{T_s} =.94

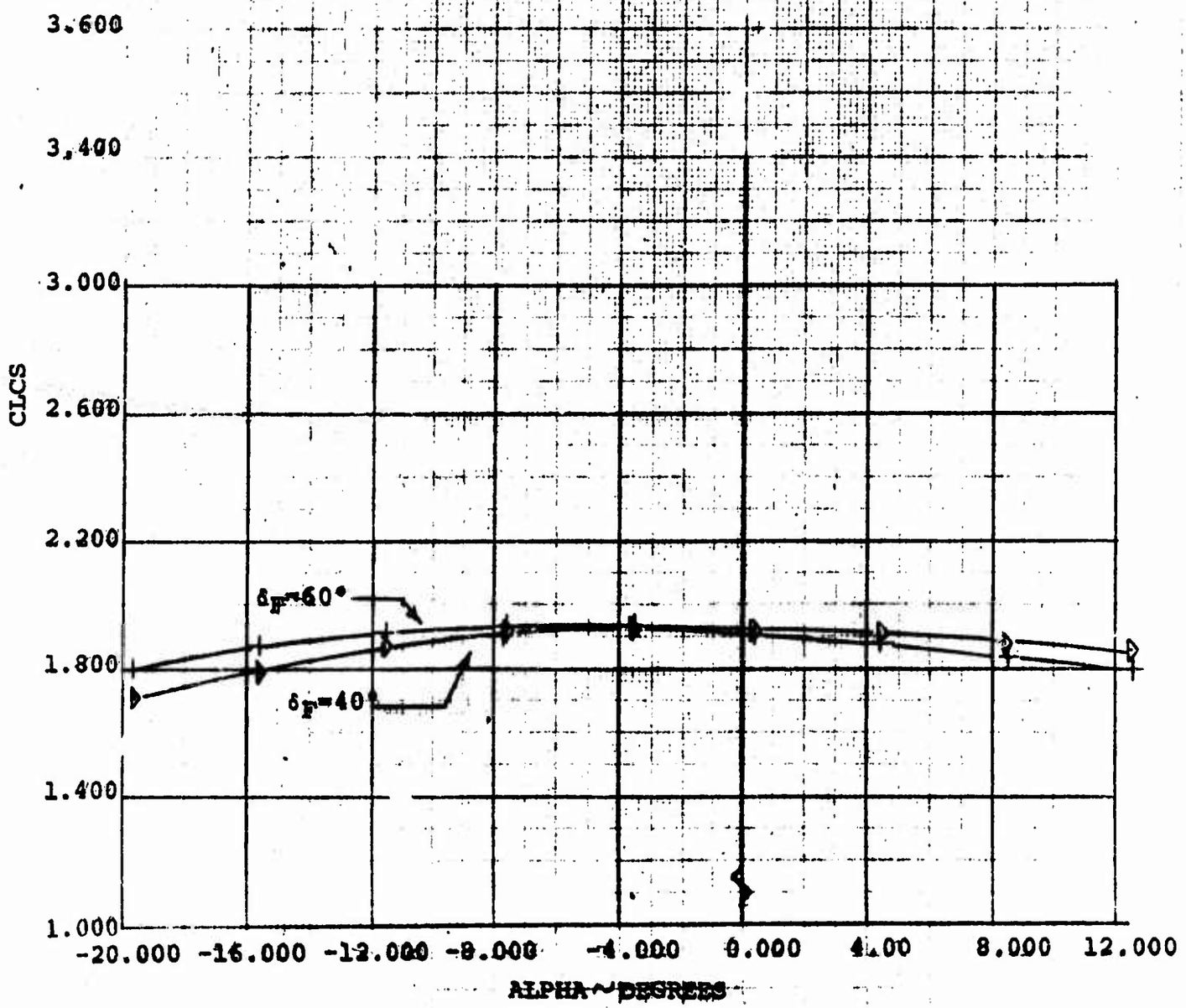

4-PROP TILT WING MODEL VRO68Q (FULL SPAN) CLCS VS ALPHA	BVWT 61 8/3/70

NOT REPRODUCIBLE

Figure 131

RUN	SYM	α	q
132 134	▷	45°	1.57

i_w=55°, δ_F=60°
FULL SPAN SLATS
NOM C_T = .94

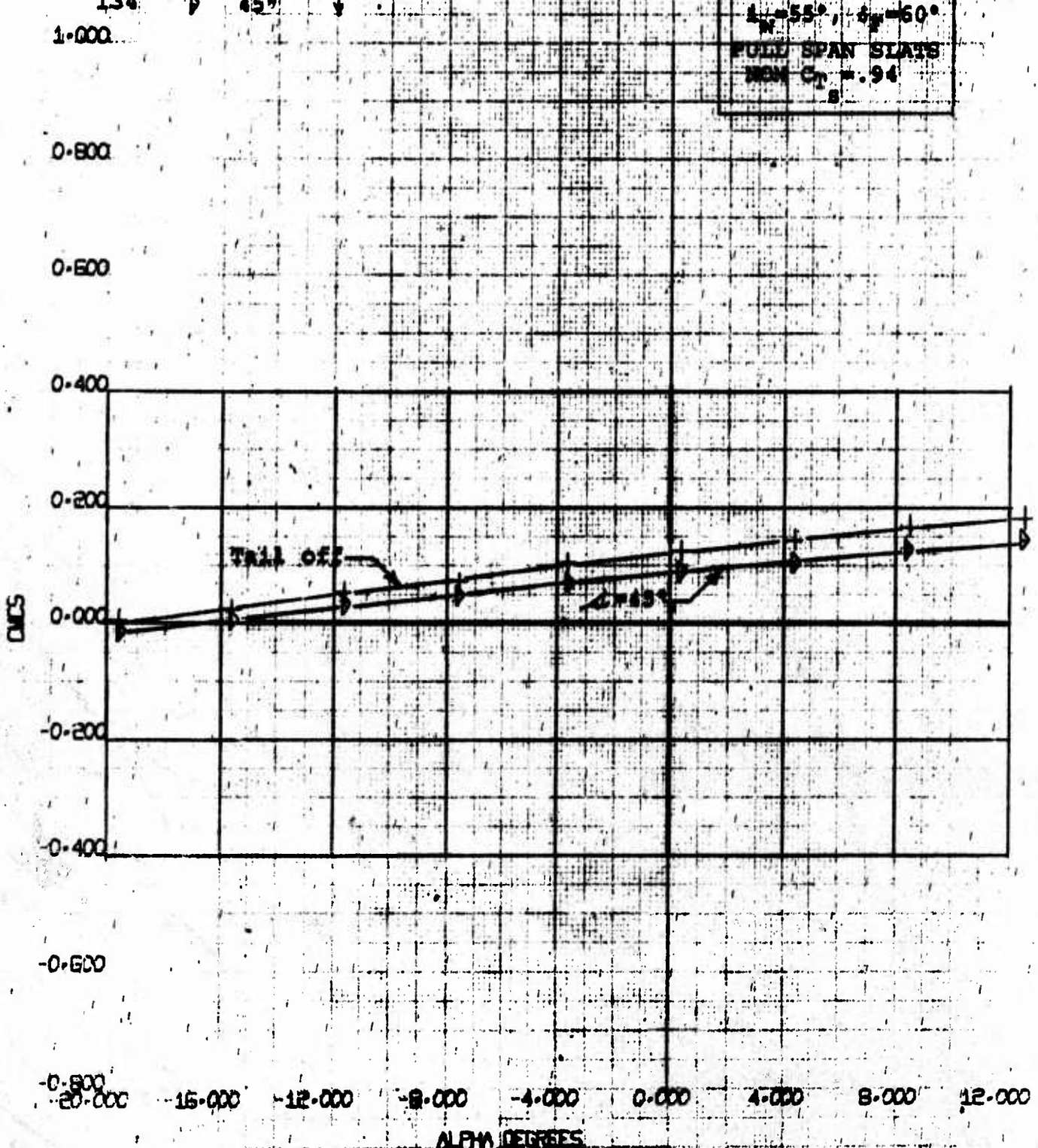

4-PROP TILT WING MODEL VROOM (FULL SPAN) CMCS VS ALPHA	BVWT 61' 9/23/70

Figure 132

RUN	SYM	α	q
132	+	---	1.57
134	▷	45°	↓

i_w=55°, δ_F=60°
FULL SPAN SLATS
NOM C_{T_S}=.94

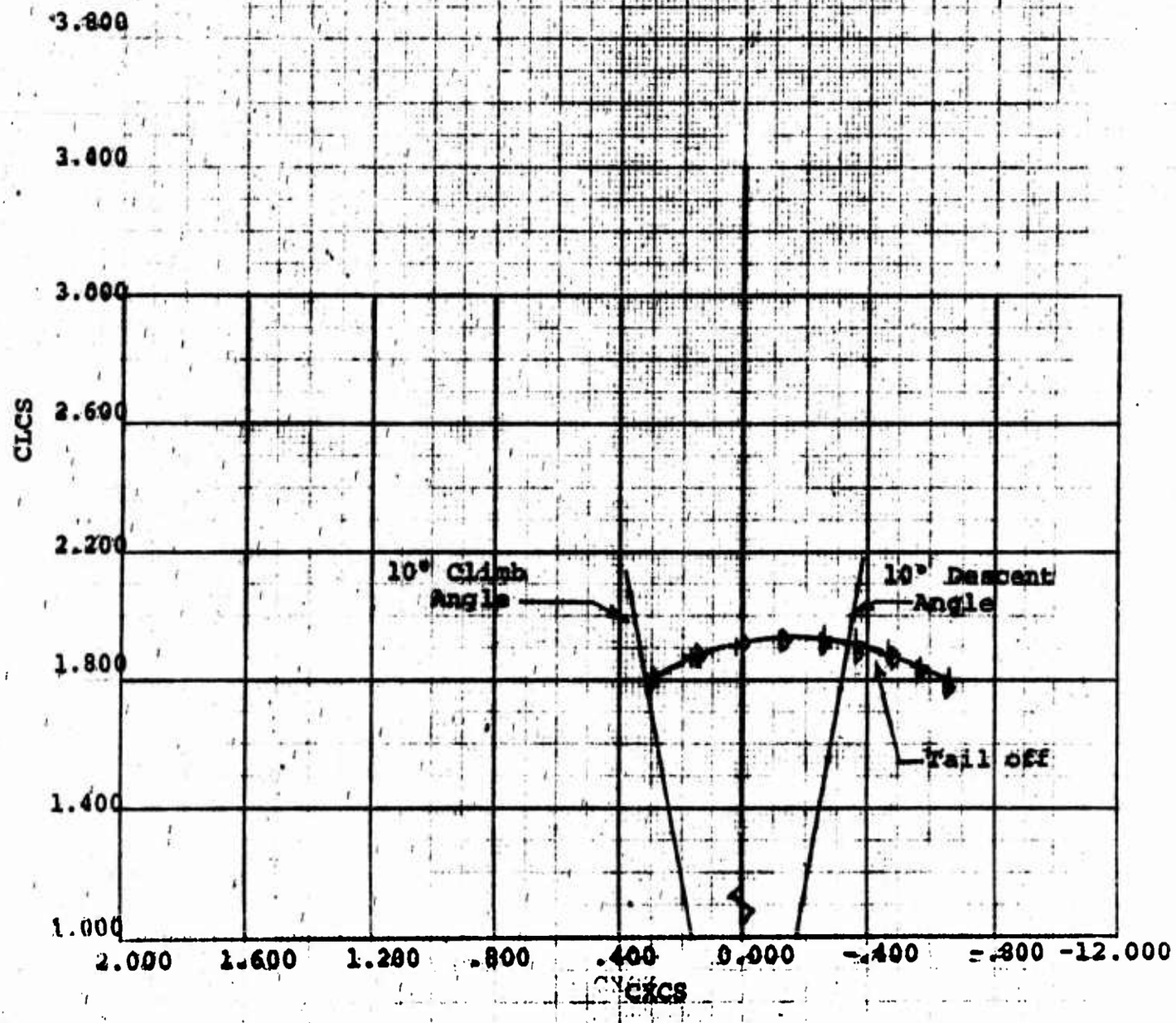

4-PROP TILT WING MODEL VRO68Q (FULL SPAN) CLCS VS CXCS	BVWT 61 9/23/70

NOT REPRODUCIBLE

Figure 133

RUN	SYM	δ_f	q
132	+	---	1.57
134	▷	45°	↓

i_w=55°, δ_F=60°
FULL SPAN SLATS
NOM C_{T_R} = .9

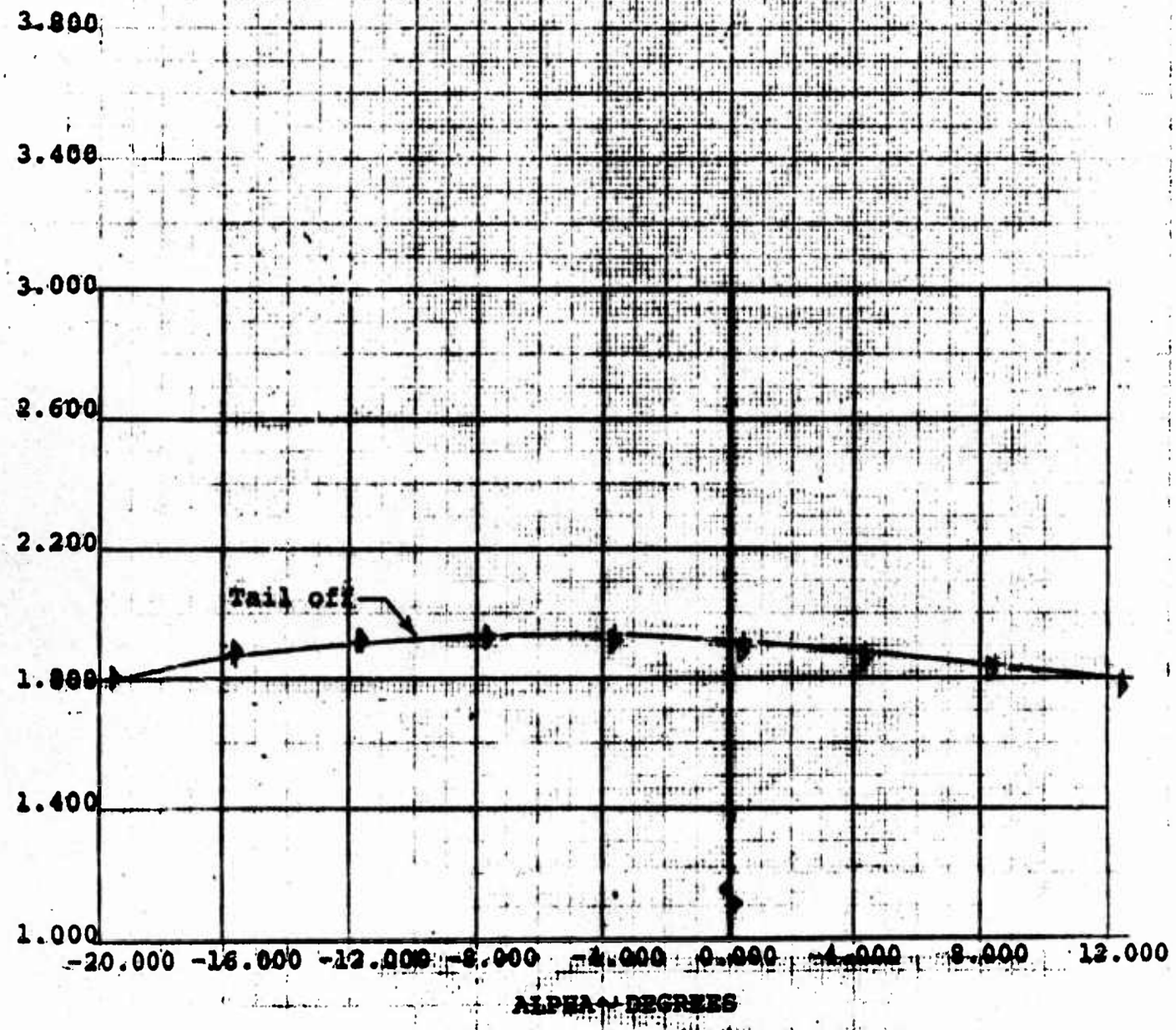

4-PROP TILT WING MODEL VRO68Q (FULL SPAN) CLCS VS ALPHA	BVWT 61 9/23/70

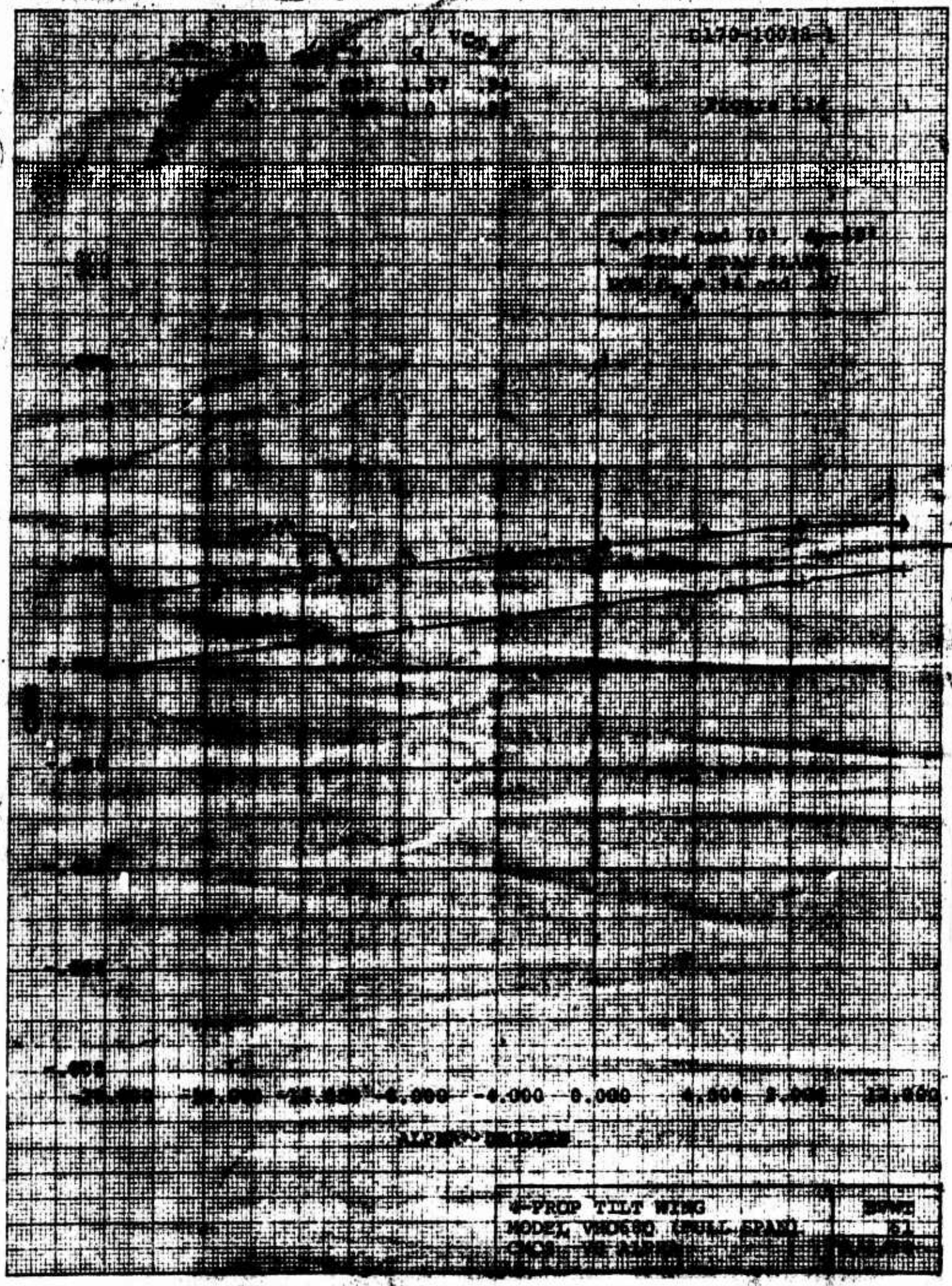

NOT REPRODUCIBLE

RUN	SYM	α	i_{w_1}	Q	C_{T_S}
135		---	55°	1.57	.84
136		---	70°	1.8	.87

Figure 135

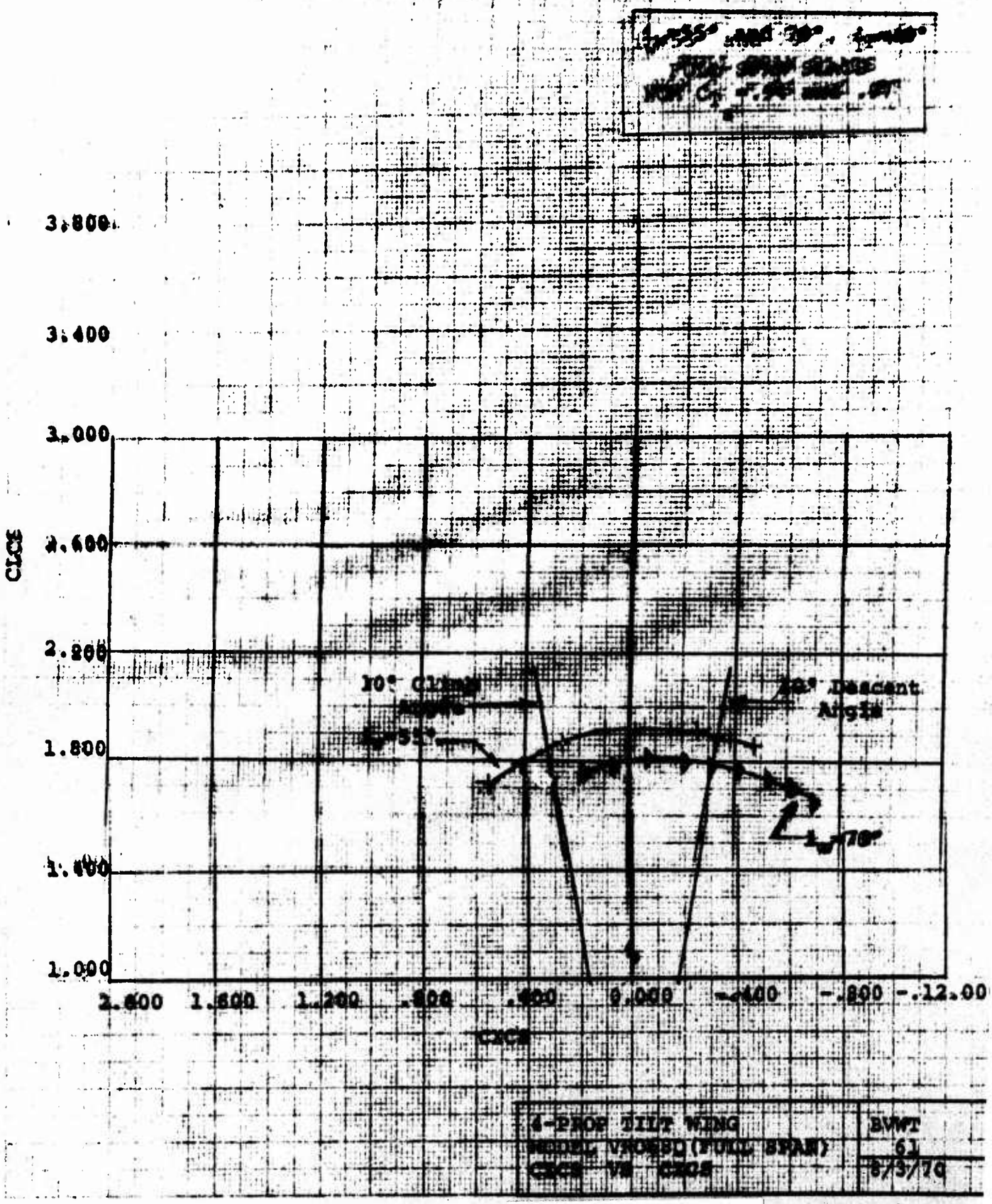

4-PROP TILT WING
MODEL VSTOL (FULL SPAN)
CLCE VS CDCE

BWT 61
8/3/70

NOT REPRODUCIBLE

RUN	SYM	α_w	i_w	q	C_T
135	+	---	55°	1.57	.24
136		---	70°	1.57	.24

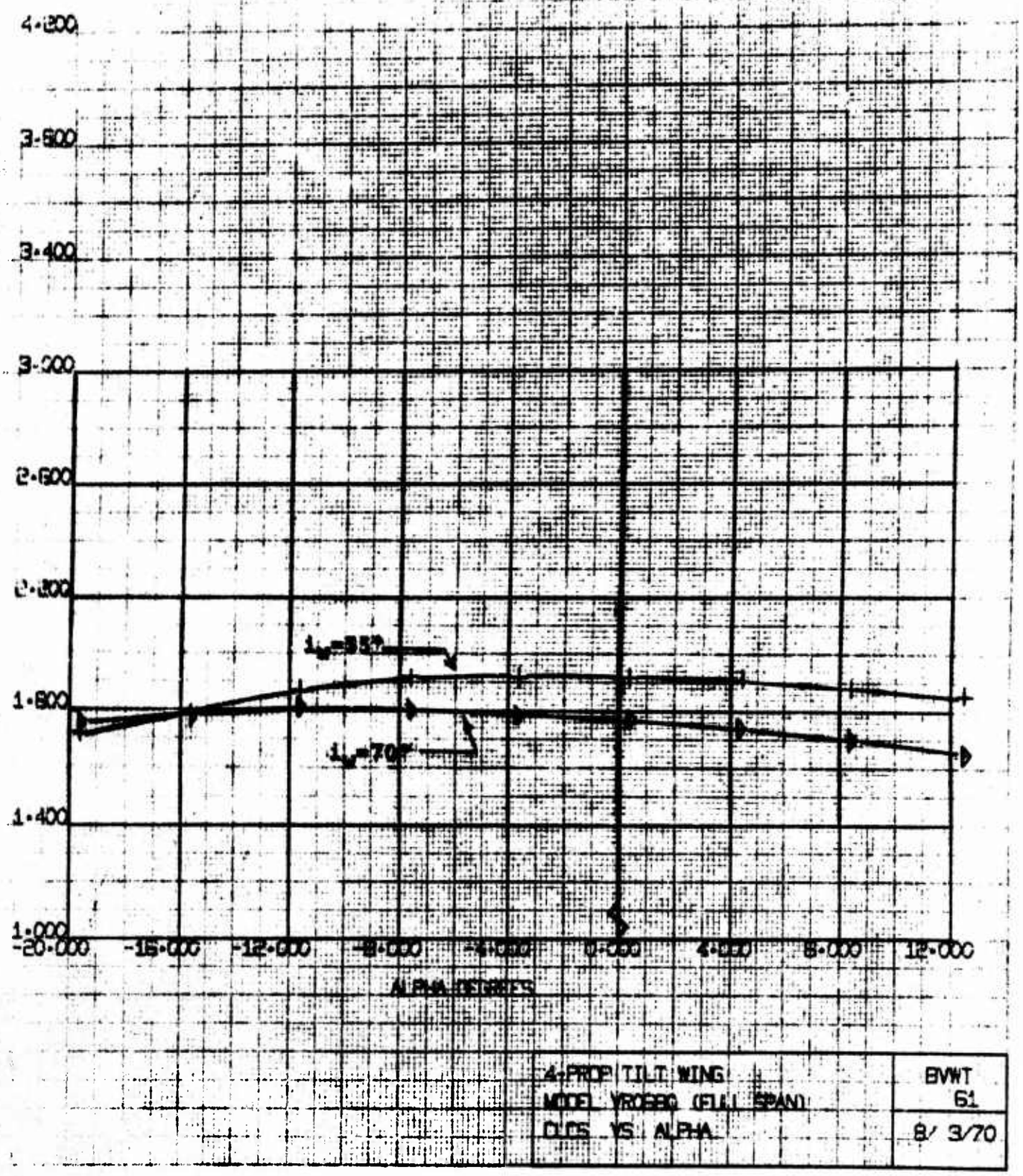

4-PROP TILT WING MODEL VROBIG (FULL SPAN)	BVWT 61
CLCS VS ALPHA	8/ 3/70

NOT REPRODUCIBLE

6.4.5 Horizontal Tail Buffet

During the longitudinal stability testing, the fuselage, side of the fin, and top and bottom surfaces of the stabilizer were tufted. Tuft observations were continuously recorded throughout the runs.

Section 6.4.4 discussed the formation of the separated flow emanating from the wing center section and its subsequent progression up the fin as the fuselage angle of attack was increased. The first visual indication of the horizontal tail encountering the wake was a slight buffeting or "flicking" of the tufts, usually at the root section of the tail. Further pitching of the model lowered the tail with respect to the disturbed flow and increased the buffeting or tuft activity. Complete immersion of the tail in the wake was evidenced by total flow separation (stall) on both the top and bottom surfaces of the tail.

The results of the stabilizer tuft observations for the majority of the wing tilt angle/flap angle/C_{T_s} combinations tested are presented in Figure 137 as a function of C_{T_s}. For each wing tilt/flap angle combination, a band of fuselage angles over which tail buffeting was observed, are shown. The bottom of the band corresponds to initial buffeting or "tuft flicking" and the top of the band corresponds to heavy buffeting or essentially total flow separation.

From this plot, it can be seen that the fuselage angle at which tail buffeting is encountered, increases with increasing C_{T_s} and decreases with wing tilt as would be expected. No tail tuft activity or buffeting was recorded at the 45° wing tilt/ .92 C_{T_s} test condition or at combinations of higher thrust coefficients (.94 and .97 C_{T_s}) and wing tilt angles (55° and 70°). This was noted previously in Section 6.4.4 in the discussion of the moment curves.

There is a strong possibility of increasing the fuselage angle of attack at which tail buffeting occurs by application of leading edge BLC (boundary layer control) to the wing center section region. The effect of leading edge BLC on wing center section stall was investigated and reported in Reference 3.

The effect of removing the center section slat on the aft fuselage wake and its intersection with the horizontal tail was investigated with the 30°/60° wing tilt/flap angle combination at C_{T_s} values of .55 and .70. Data from these two runs are compared in Figures 138 thru 143 with corresponding full span slat runs.

Noted on the pitching moment plots are the fuselage angles at which it was observed that the separated flow has progressed to the vertical fin. These tuft observations correlate well with the change in slope of the pitching moment curves. It is apparent that the removal of the center section slat had an adverse effect on the formation of the center section wake, in that the separated flow reached the fin at fuselage angles of attack from 5° to 6°lower. From horizontal tail tuft observations it was also apparent that initial tuft buffeting occurred at lower fuselage angles (approximately 4° less) when the center slat was removed.

The loss of lift due to the removal of the slat segment is evident by referring to the lift curve and force polar comparisons.

Figure 137

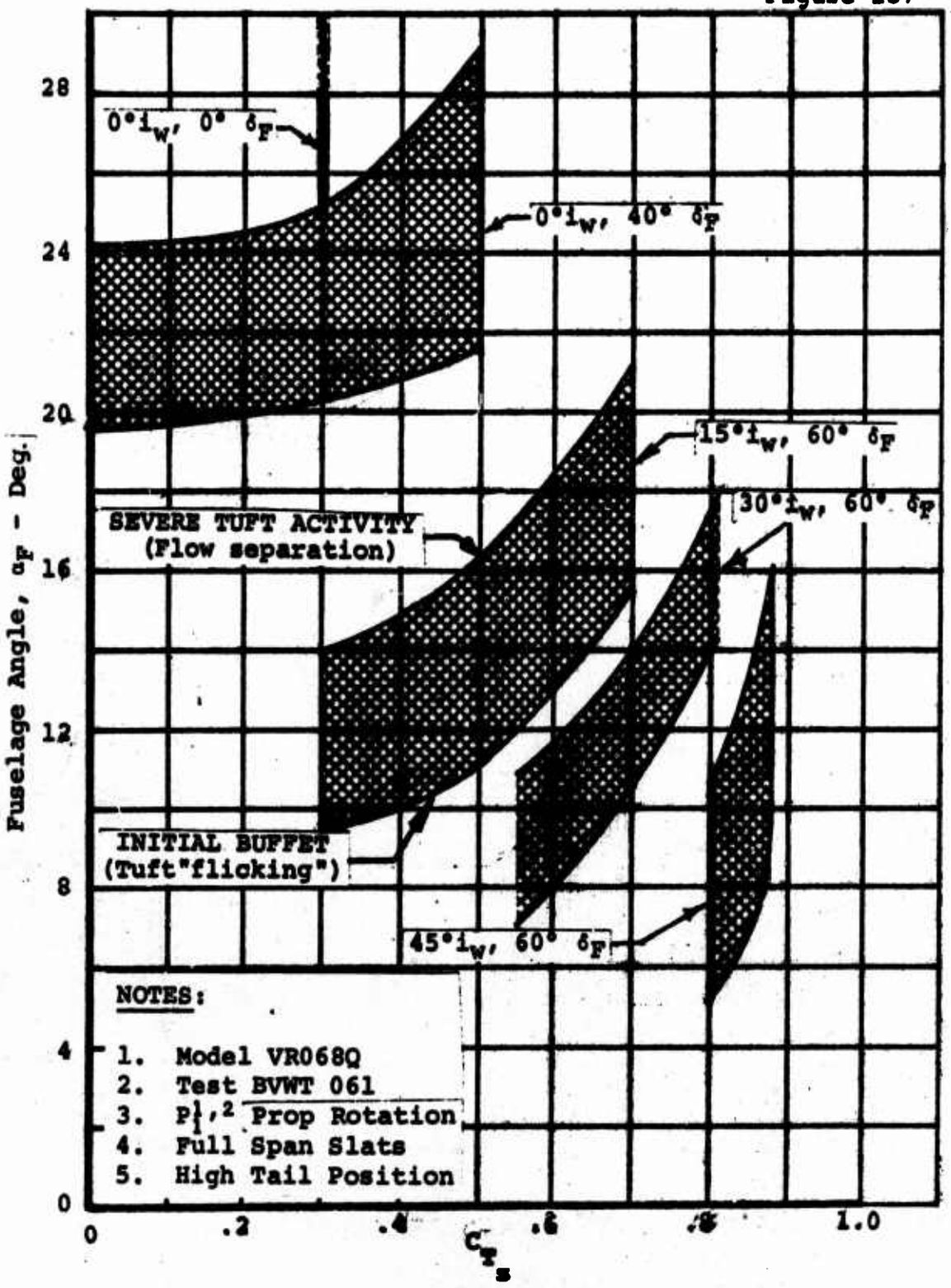

HORIZONTAL TAIL BUFFET
TUFT OBSERVATIONS

Figure 118

RUN	SYM	α_T	q
153	+	+20°	12.68
155	▷	〃	〃

Center Section Flap Removed

EFFECT OF REMOVING CENTER SECTION SLAT

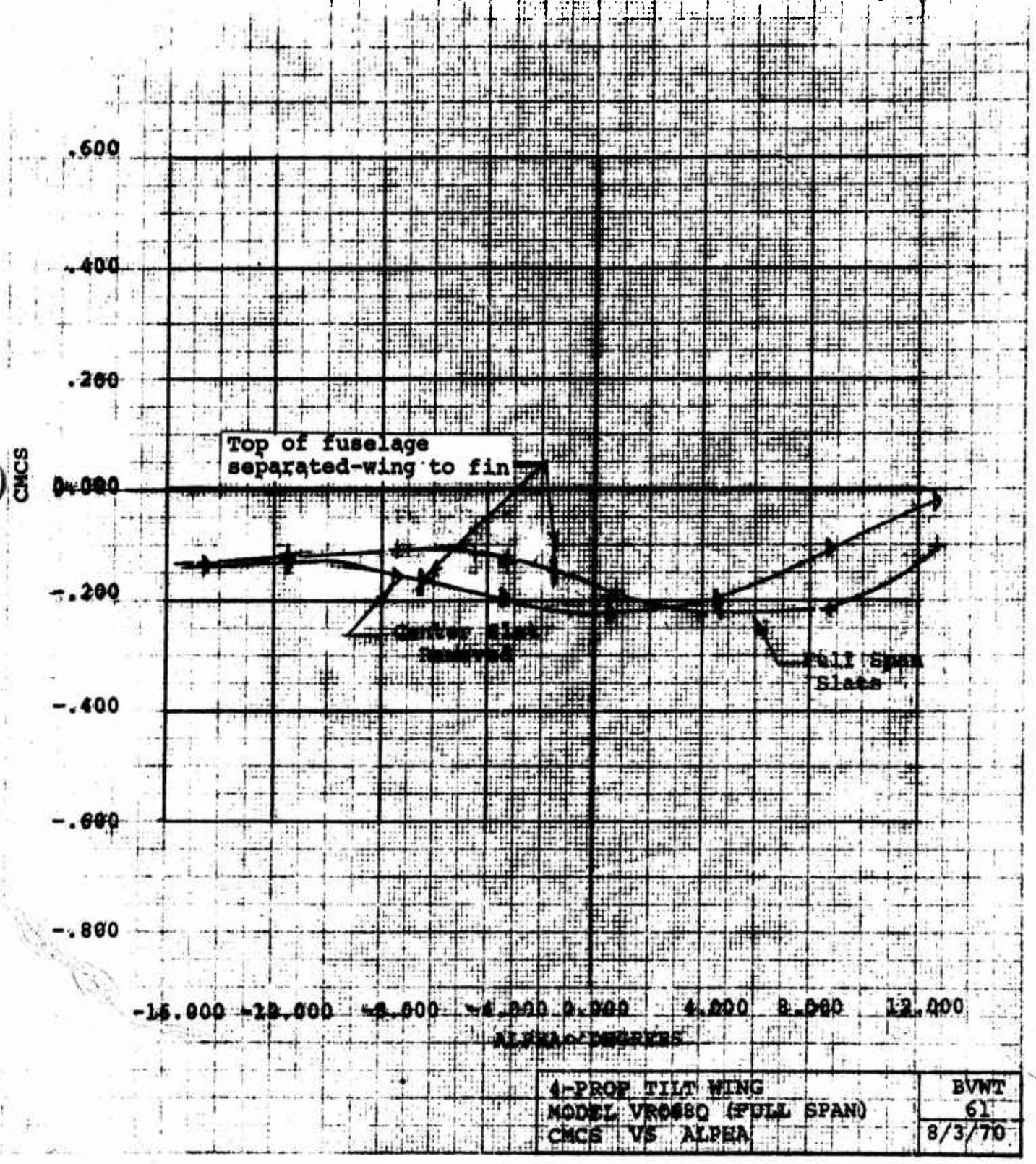

4-PROP TILT WING MODEL VR0880 (FULL SPAN) CMCS VS ALPHA	BVWT 61 8/3/70

NOT REPRODUCIBLE

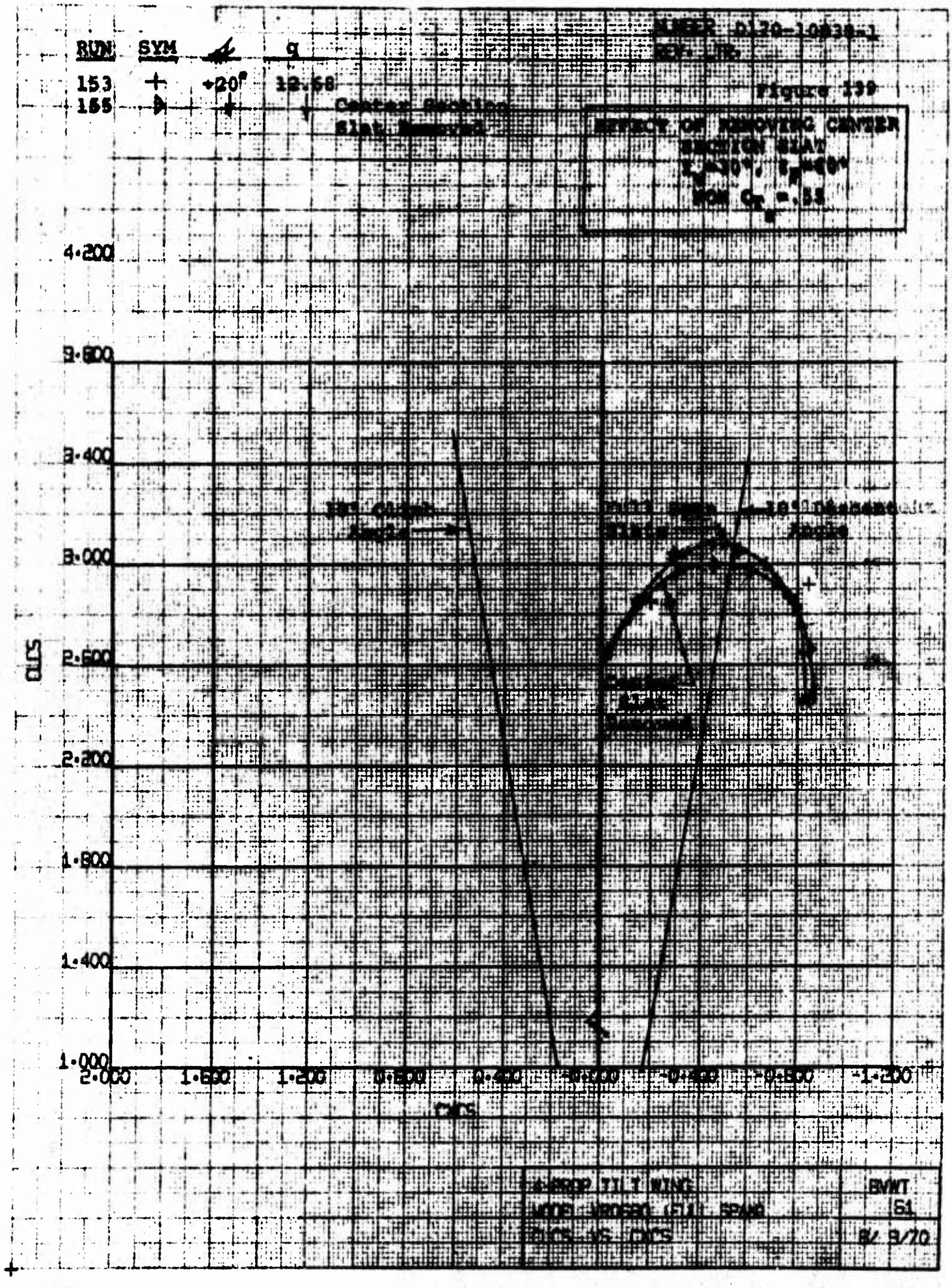
RUN SYM
153
155
Center Section Slat Removed
Figure 139
EFFECT OF REMOVING CENTER SECTION SLAT
4.200
3.800
3.400
3.000
2.600
2.200
1.800
1.400
1.000
CLCS
2.000
1.600
1.200
0.800
0.400
-0.400
-0.800
-1.200
CDCS
4-PROP TILT WING
WING AIRFOIL (T/C) SPAN
CLCS vs CDCS
BWT 61
8/ 9/70

Figure 140

RUN	SYM	α	q
153	+	+20°	12.68
155	↑	↓	↓

Center Section Slat Removed

EFFECT OF REMOVING CENTER SECTION SLAT
i_w=90°, δ_F=60°
NON C_{T_δ}=.55

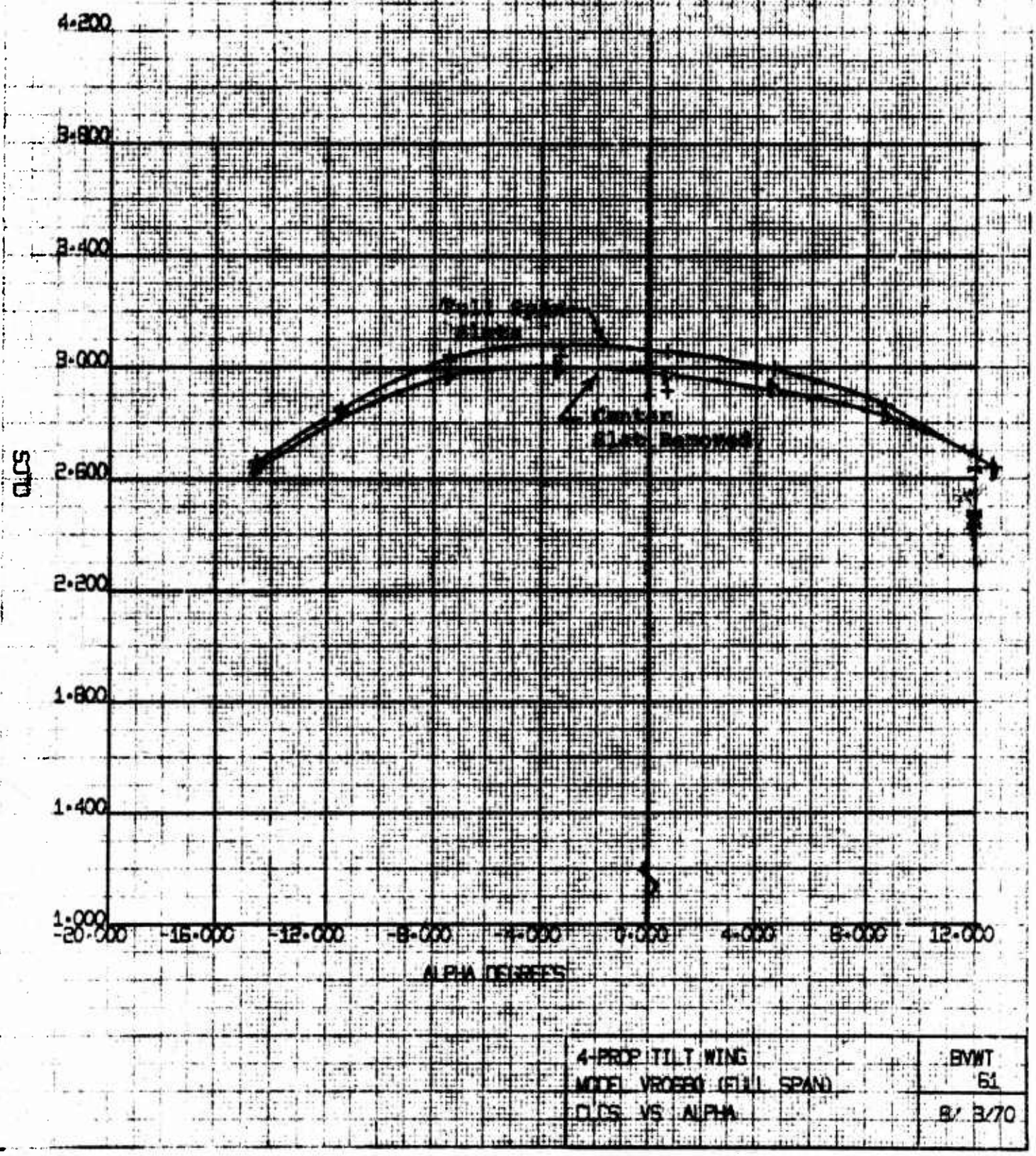

4-PROP TILT WING MODEL VROBBO (FULL SPAN) CLCS VS ALPHA	BWT 61 B/ 3/70

NOT REPRODUCIBLE

Figure 161

RUN	SYM	α	q
152	+	+26°	8.24
154	▷	↓	↓

Center Section Slat Removed

EFFECT OF REMOVING CENTER SECTION SLAT

δ_f=30° δ_s=60°

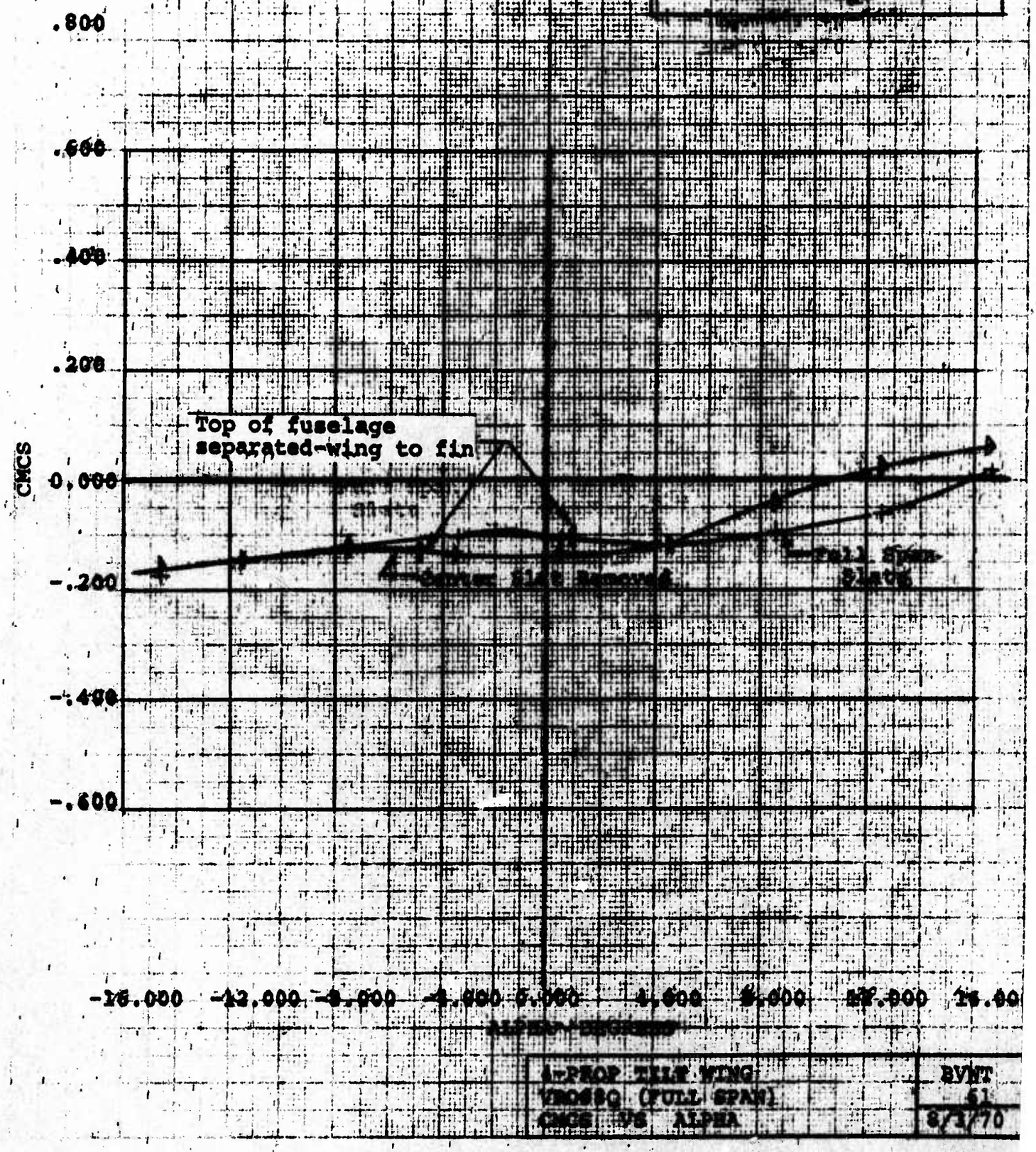

4-PROP TILT WING	BVHT
VRO88Q (FULL SPAN)	51
CMCS VS ALPHA	8/1/70

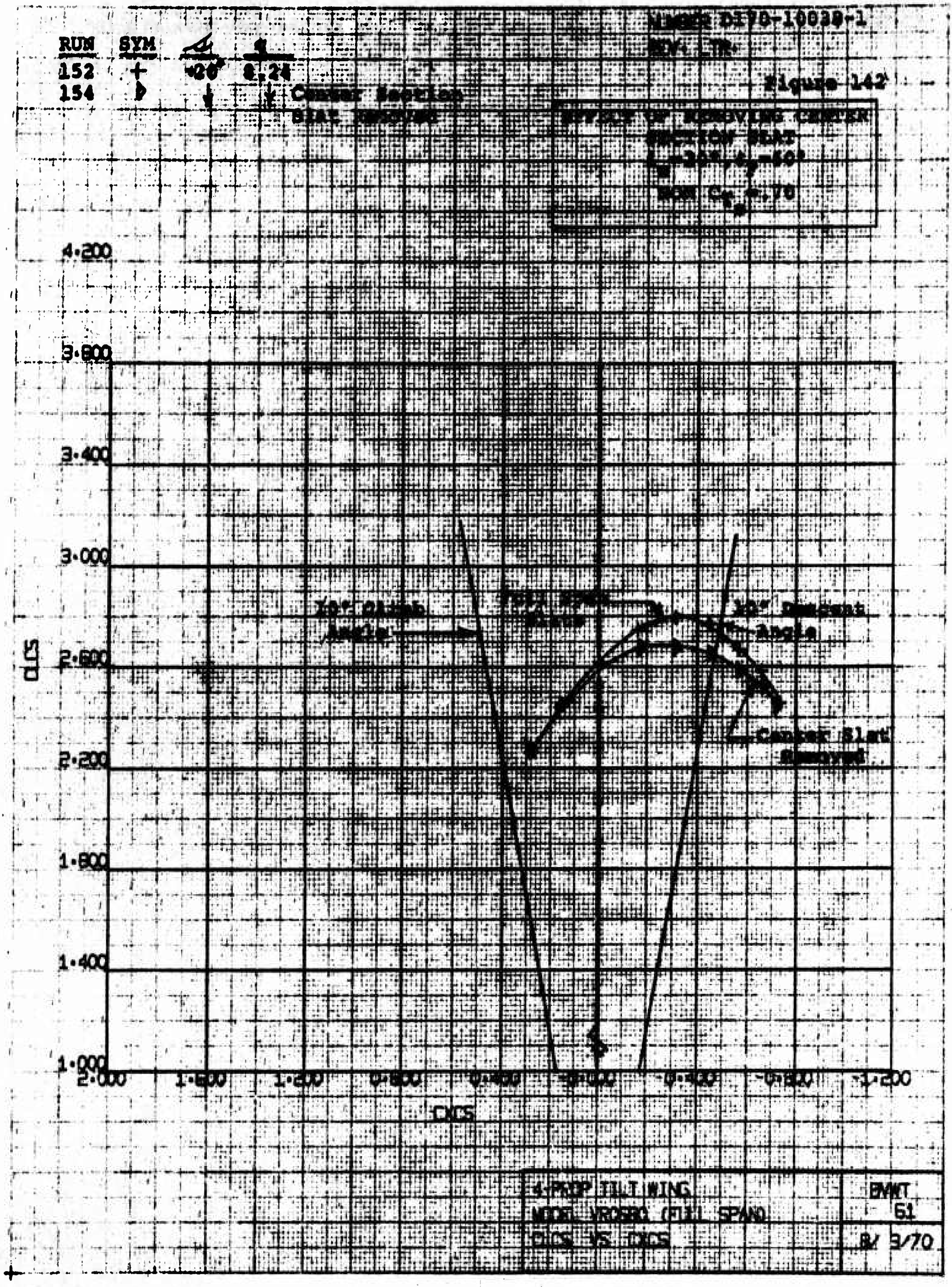

NOT REPRODUCIBLE

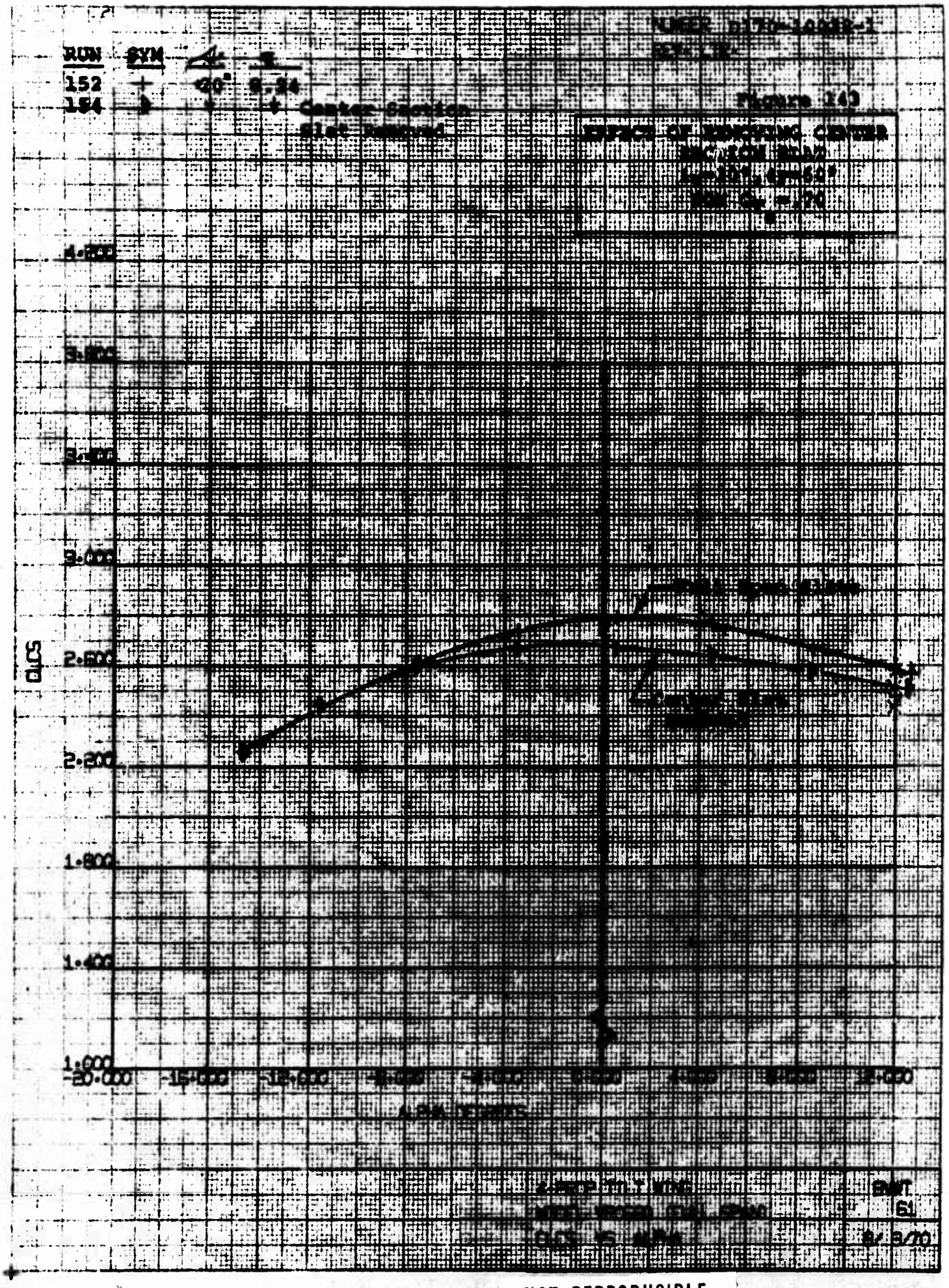

NOT REPRODUCIBLE

6.5 WING/FLAP/FUSELAGE EFFECTS ON PROPELLER FORCES AND MOMENTS

The nacelle hub/balance/motor assemblies used in this test were identical with the one used in the isolated propeller test BVWT 057 (Reference 1). It was pointed out in the Reference 1 report that the propeller used in BVWT 057 was a left hand rotation prop, that is, the rotation was counterclockwise when viewed from behind. Left hand rotation propellers were installed on Model VR068Q at the left wing inboard nacelle and at the right wing outboard nacelle.

Since the left hand and right hand propellers were constructed (fiberglass lay-ups) using different molds, some dissimilarity in performance was expected. During the thrust balancing process in forward flight with collective hubs (Runs 51 thru 53/6800 RPM) a difference in collective settings at .75 radius of +0.75° to 1.0° was required between the right hand and left hand propellers to achieve a thrust balance. The collective setting fixture was not involved in this difference, since the same fixture was used for both left hand and right hand propellers.

Thrust balancing in forward flight with the cyclic hubs (Runs 156 and 157/4750 RPM) required an average difference in collective setting of +1.25° to 1.50° between the right hand and left hand propellers. Influencing this difference was the two separate blade angle setting fixtures (one for a left hand prop and another one for a right hand prop) used to set both collective pitch and cyclic pitch on the cyclic hubs.

6.5.1 Wing/Flap/Fuselage Effects on Propeller Normal Force

Figure 144 compares the average normal force (propeller notation) measured on the inboard propellers and on the outboard propellers with the isolated propeller data. This data was collected in wing sweep Runs 54 thru 58 with the large double slotted flaps deflected 60°, full span slats extended, and a constant propeller speed of 6800 RPM. Propeller advance ratios, J, prevalent during the runs are denoted in the figure. A decision was made to present the normal force data as an average of the inboard propellers and an average of the outboard propellers via an examination of the individual propeller normal forces which deemed that any differences that could be noted could not be ascribed to propeller rotation differences (left hand vs right hand propellers).

As shown by the comparison presented in Figure 144, the installed propeller normal force is of a magnitude approximately 2.5 times larger than measured on the isolated propeller for the same geometric propeller angle of attack. This increase of normal force is undoubtedly due to the change in propeller inflow conditions produced by the highly flapped wing. Except for wing incidence angles above 40°, Figure 144 indicates that the inboard propellers generally developed higher normal forces than the outboard propellers. Two items could have produced this increment: the larger wing/flap chord behind the inboard propeller and the proximity of the fuselage.

Figure 145 is similar to Figure 144, differing primarily in that the propeller normal forces were measured during wing sweep Runs 158 thru 161 with cyclic prop/hubs operating at 4750 RPM. In addition, the average collective setting was 12.4° instead 14.0°. Data obtained during the isolated prop test indicated that this difference in collective setting would have only a small effect on prop normal force, with the lower setting generating somewhat lower forces. The increase in data scatter that occurred during the testing at 4750 RPM is understandable when it is realized that the magnitude of the prop normal forces was reduced by a factor of 2 over those measured during 6800 RPM testing (RPM squared effect) and that the largest value of prop normal force during the 4750 RPM runs was 12 lbs.

A check was made to verify the non-dimensional characteristic of the prop normal force coefficient, that is, if prop normal force is entirely an aerodynamic effect, it should non-dimensionalize with RPM^2. This was essentially the case as shown in Figure 146, wherein C_{NF_p} did not vary to any extent with RPM. The effect of RPM is also evaluated later in the report in Section 6.6 which discusses the proportionality of model forces (prop normal force is a component) with RPM.

Figure 144

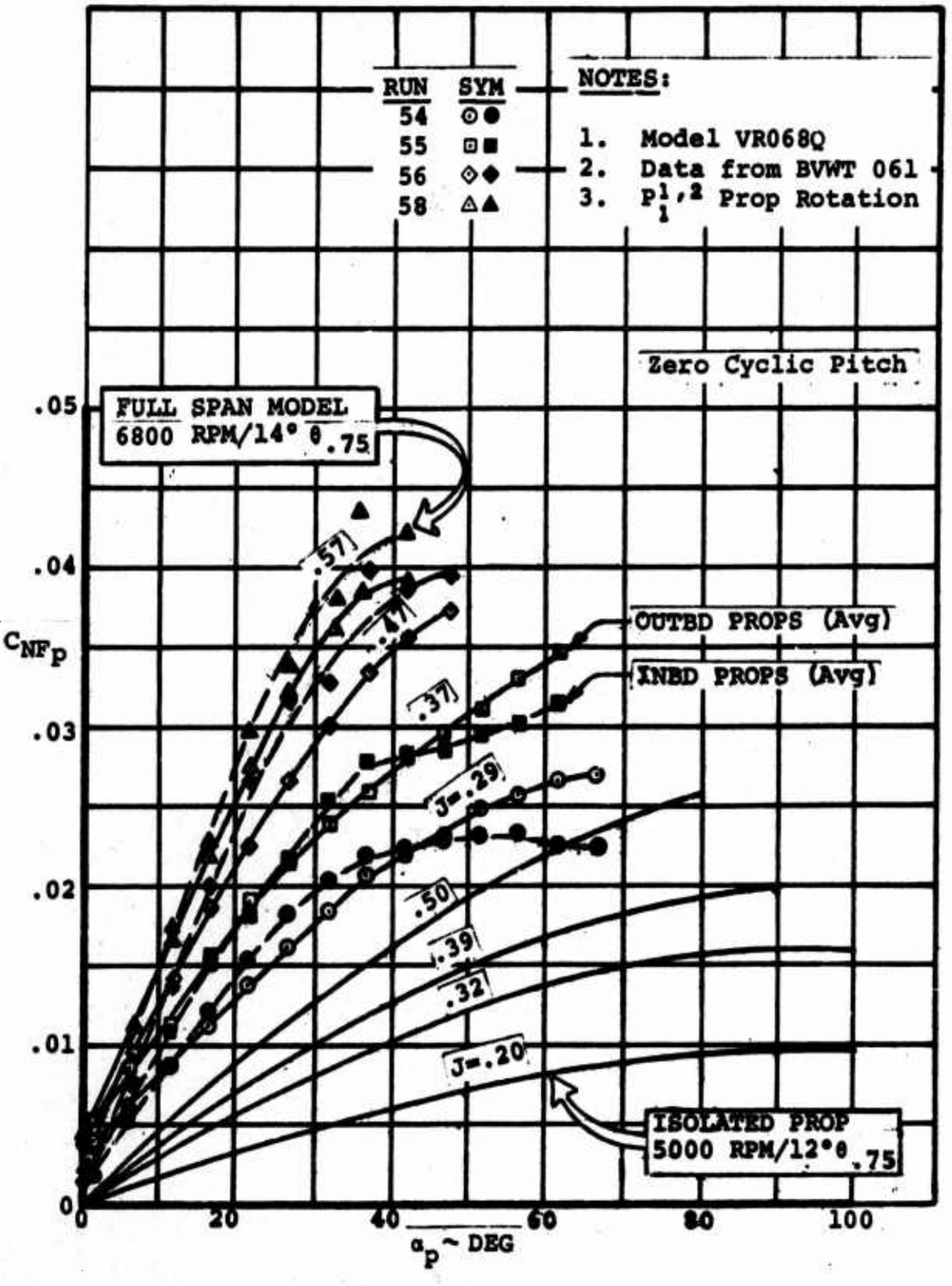

PROPELLER NORMAL FORCE
60° FLAPS/FULL SPAN SLATS
6800 RPM/14° θ.75

Figure 145

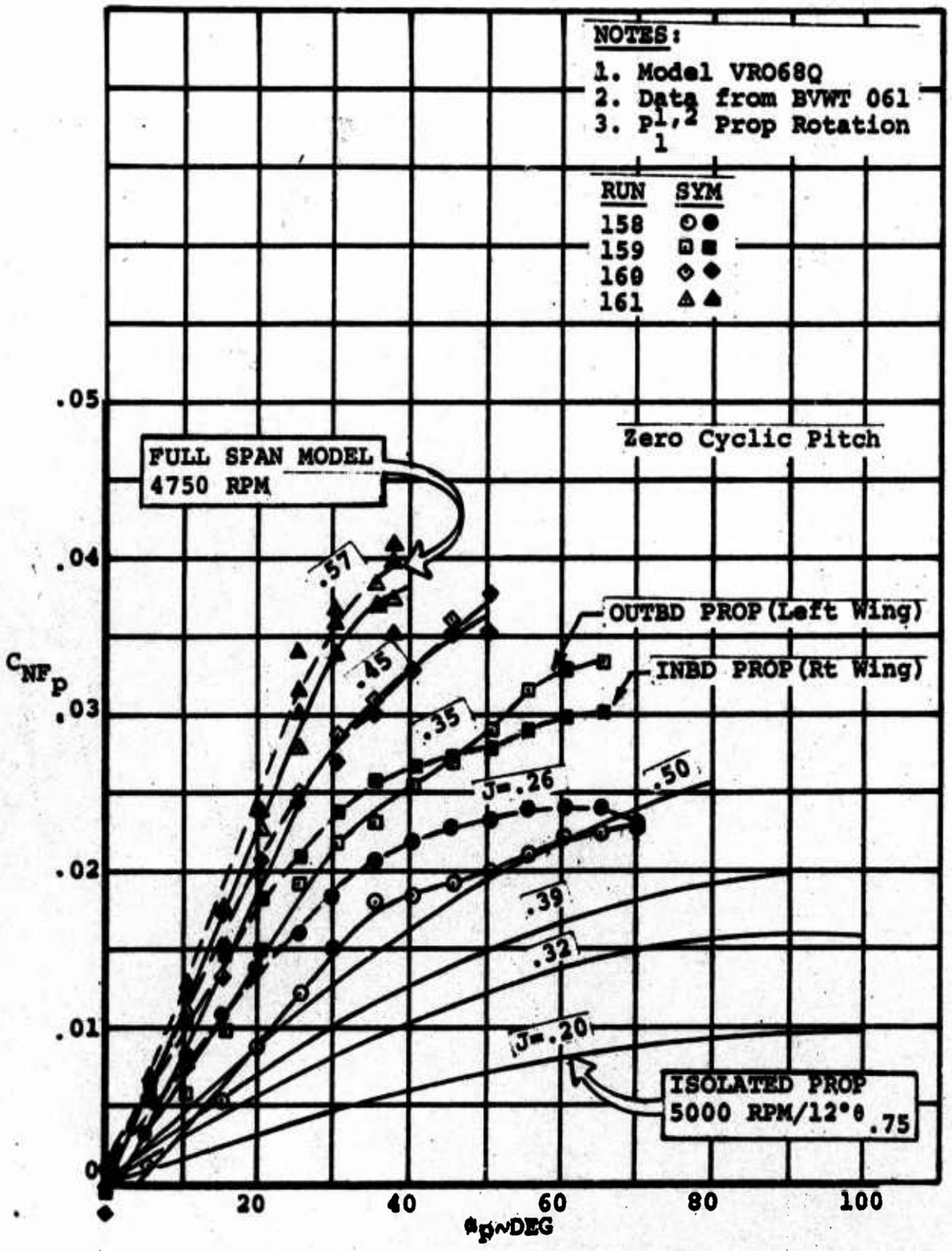

PROPELLER NORMAL FORCE
60° FLAPS/FULL SPAN SLATS
4750 RPM/12.4°@.75

Figure 146

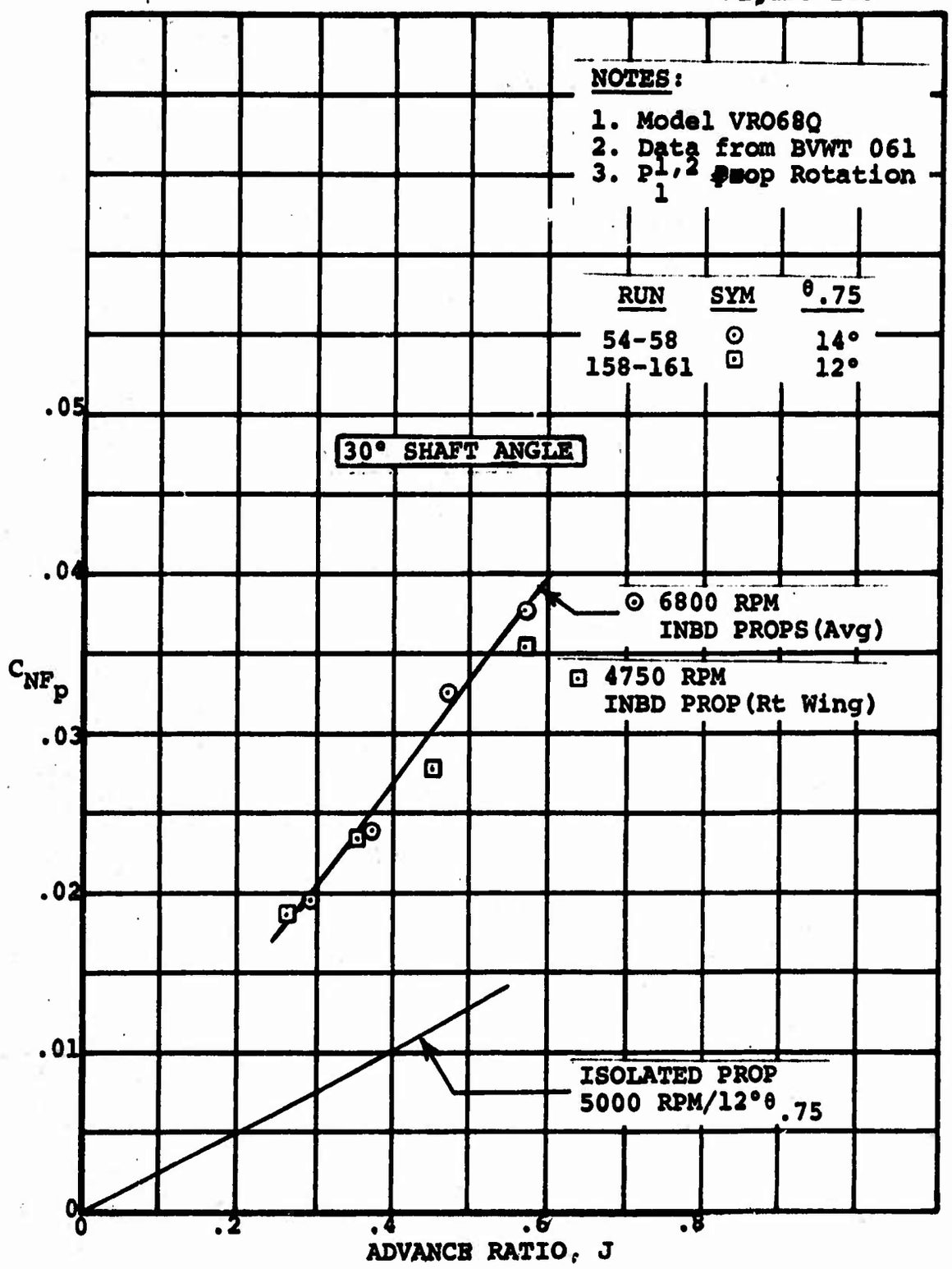

VARIATION OF PROP NORMAL FORCE
WITH J AND RPM
60° FLAPS/FULL SPAN SLATS

6.5.2 Wing/Flap/Fuselage Effects on Hub Pitching Moment

A comparison of the measured hub pitching moment coefficients for the installed propellers with that for the similar isolated propeller is presented in Figure 147. As in the prop normal force comparison, wing sweep Runs 54 thru 58 (6800 RPM) were used, inboard prop and outboard prop data were averaged and the data is plotted as a function of propeller shaft angle (α_p) which is equivalent to $\alpha_F + i_W$ (accounts for the fuselage deflecting upward on the sting). In averaging the inboard prop data and outboard prop data for presentation in Figure 147, the observed differences were judged to be within test data accuracy. Any differences due to blade angle differences were deemed negligible per Reference 1.

Figure 147 shows that the initial rate of build up of hub pitching moment on the installed propeller is about three times that of the isolated prop. However, the curves, especially for the outboard props appear to be bending over (decrease in $\Delta C_{M_p}/\Delta\alpha_p$) at much lower angles of attack than the isolated prop. Peak values of C_{M_p} were not reached on this test, and should be investigated during Phase II for the critical conditions.

As in the case of prop normal force (Section 6.5.1), the difference is undoubtedly due primarily to the change in inflow from the wing-induced upwash and circulation. It should be noted that the highly flapped wing is itself producing a large nose down pitching moment on the aircraft, opposing the nose up moment from the propeller, so that as discussed in Section 6.4.3, the total aircraft still has static angle of attack stability at speeds above about 60 kts (C_{T_s}=.47) and is only slightly unstable at lower speeds.

Figure 148 is a similar presentation illustrating the results of the 4750 RPM wing sweep Runs 158 thru 161. In this graph, the averaged inboard prop moments are compared to the measurements on the right wing outboard prop. The outboard prop data shows a similar trend to the inboard prop data with respect to the increase in hub pitching moment with shaft angle. The incremental difference between the inboard and outboard prop moments would largely be accounted for by the zero shift noted in the outboard prop data.

A crossplot of the data from Figures 147 and 148 in terms of ΔC_{M_p} for 25° of shaft angle (linear range of data) was made to determine whether the measured coefficients were essentially independent of the test RPM. Figure 149 presents the crossplot. No definite trend other than that C_{M_p} was not a function of RPM, can be established within the normal data scatter. As

mentioned in the discussion of prop normal force, the effect of RPM on model forces (hub pitching moment is a component) is discussed later in Sectior 6.6.

Blade stiffness is an issue in the subject of hub pitching moment. An analysis of the fiberglass propeller blades used on Model VRO68Q predicted a 1ST blade flap bending frequency of 11,000 cycles/minute for 4750 RPM, which corresponds to an essentially rigid blade. The blade retention system in the collective hubs used during Runs 54 thru 58 (6800 RPM) did not detract from the rigidity, however, the blade retention system used in the cyclic hubs (Lamiflex bearings both thrust and radial) during Runs 158 thru 161 (4750 RPM) undoubtedly had a marked effect on the overall stiffness. The net effect per estimate would be to reduce the frequency ratio (ratio of 1ST flap bending frequency to the rotational frequency) for the 4750 RPM runs below that for the 6800 RPM runs. Current prop/rotor theory predicts a slight increase in hub pitching moment with a decrease in the frequency ratio for the prop/hub configuration used on Model VRO68Q. The data presented in Figure 149 is not in disagreement with this theory.

Figure 147

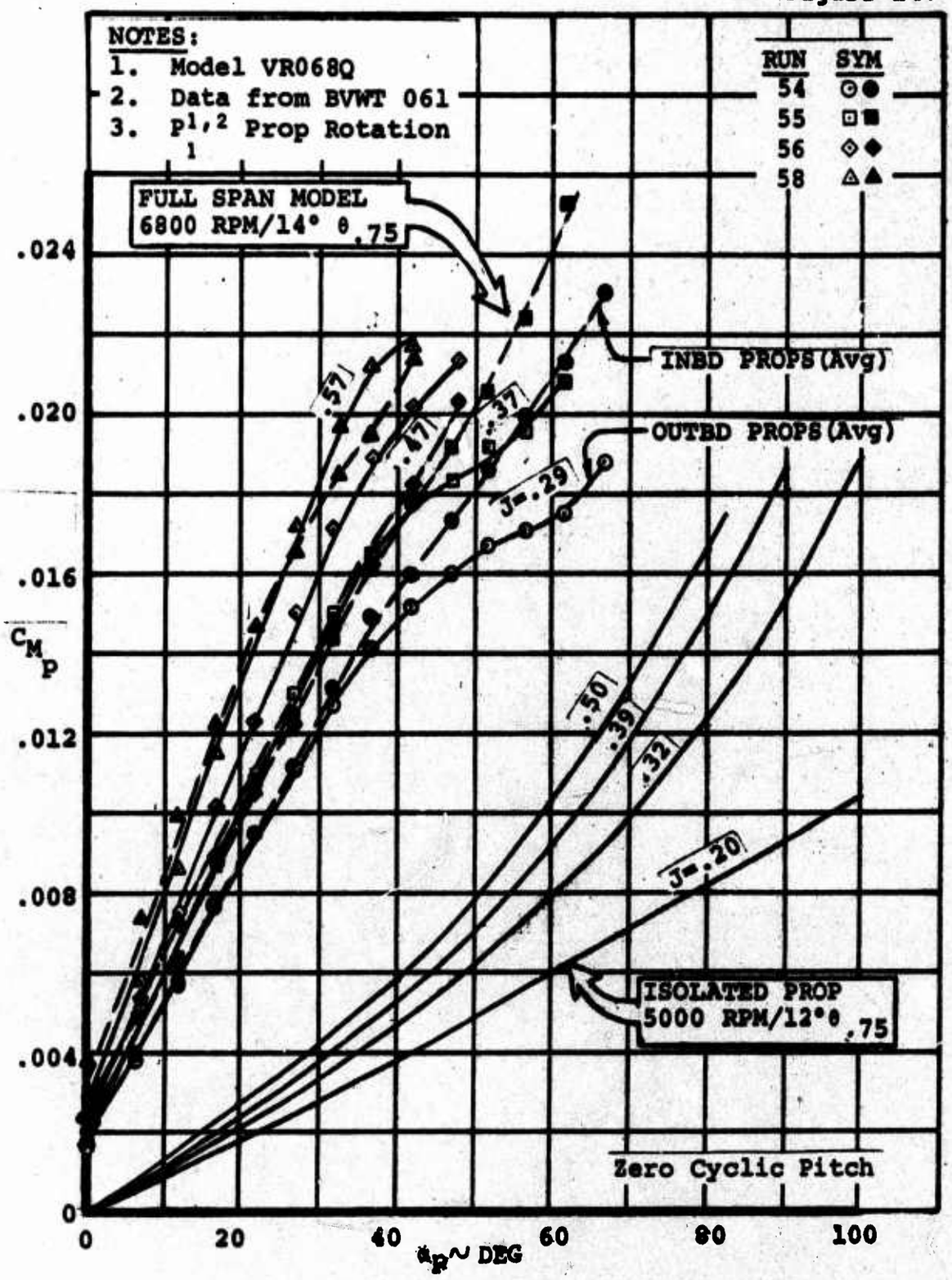

HUB PITCHING MOMENT
60° FLAPS/FULL SPAN SLATS
6800 RPM/14° θ.75

Figure 148

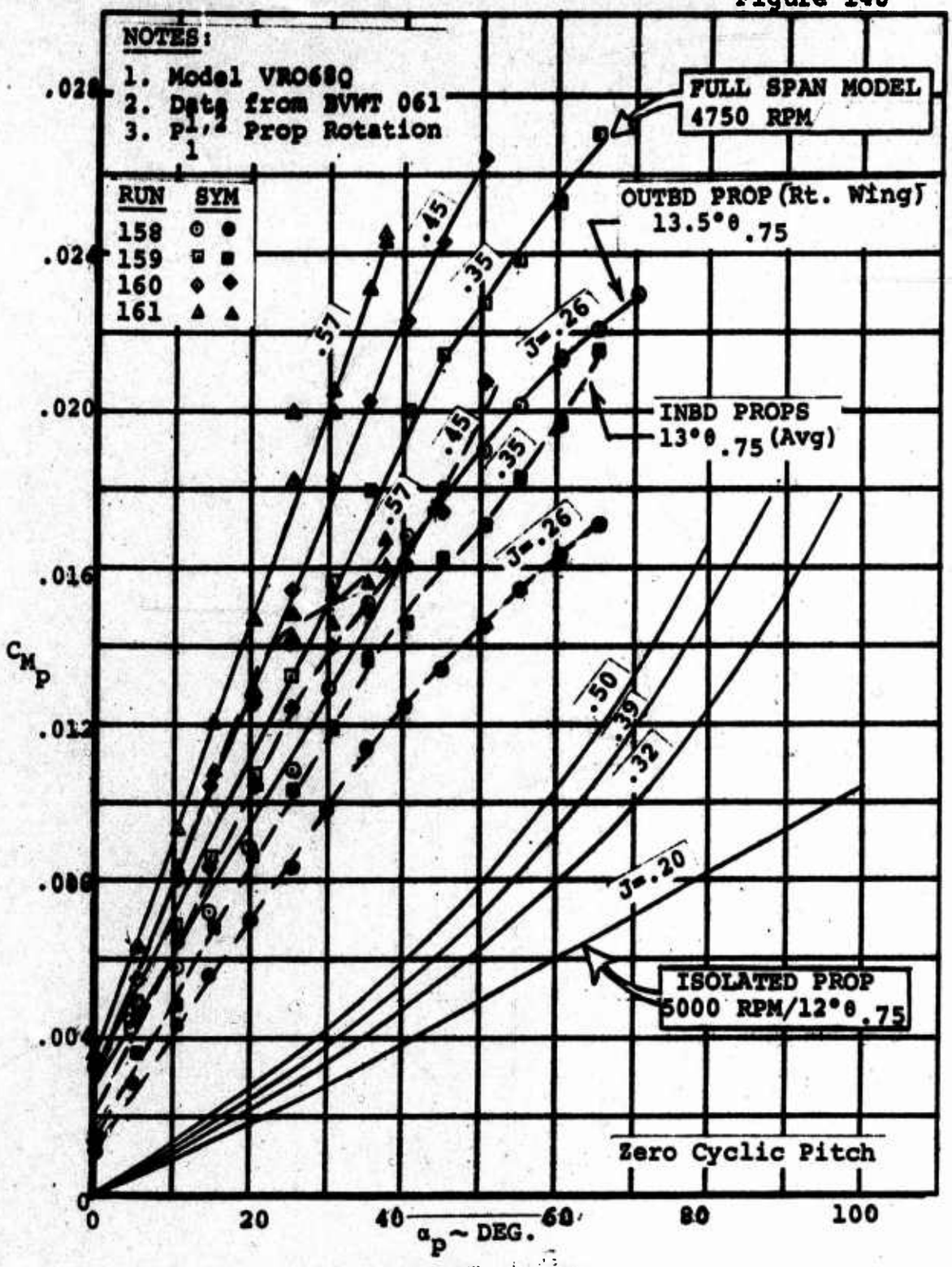

HUB PITCHING MOMENT
60° FLAPS/FULL SPAN SLATS
4750 RPM θ.75

Figure 149

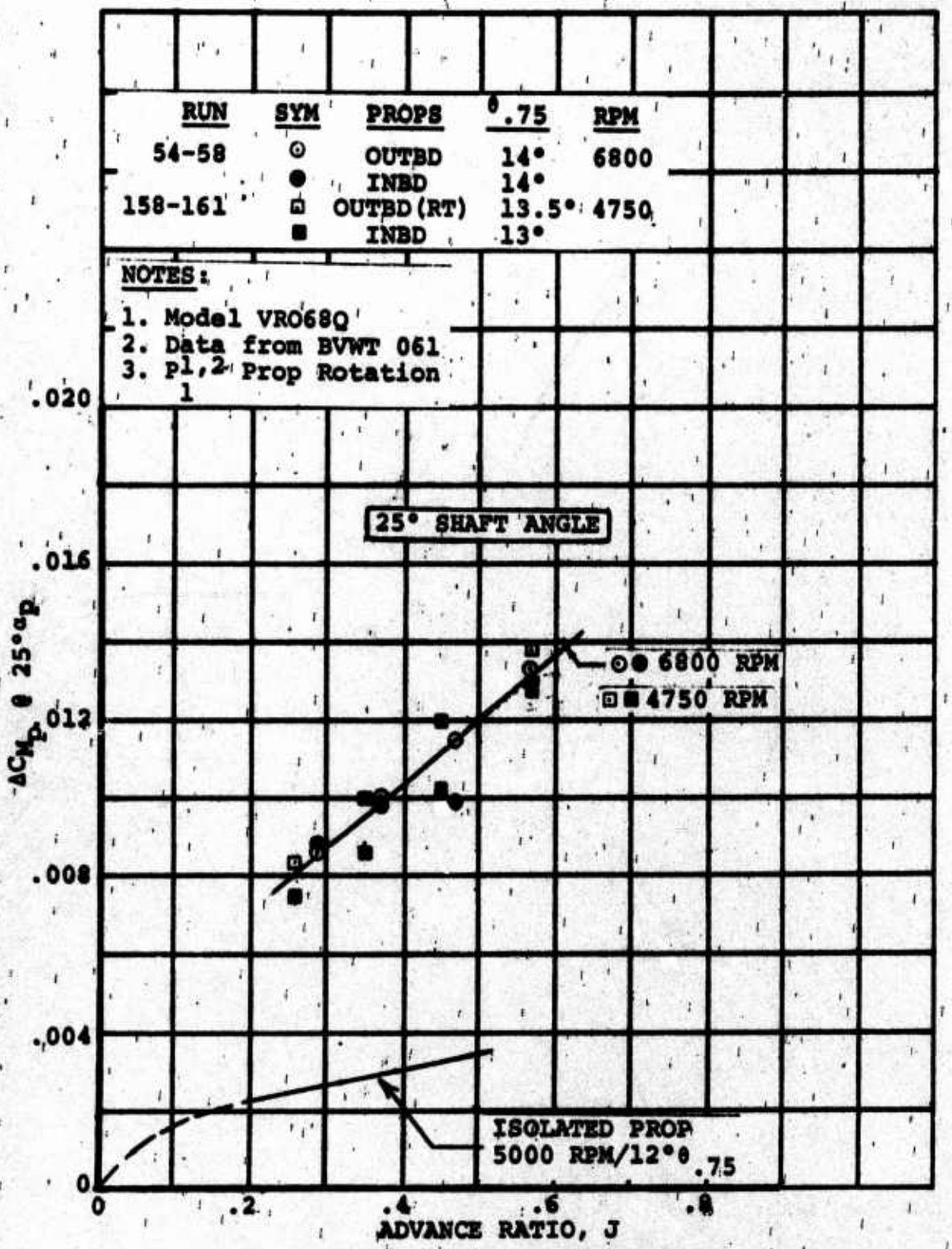

VARIATION OF HUB PITCHING MOMENT
WITH J AND RPM
60°FLAPS/FULL SPAN SLATS

6.5.3 Wing/Flap/Fuselage Effects on Propeller Thrust

Since propeller thrust coefficient (C_T in propeller notation) is a function of blade characteristics such as blade angle and twist, the left hand rotation propellers on the model (left wing inboard and right wing outboard) have been used to compare the thrust characteristics of the installed propeller with those of the left hand rotation isolated propeller. Figure 150 presents the data for the wing sweep Runs 54 thru 58 performed with a propeller speed of 6800 RPM.

Note that the isolated propeller utilized a collective setting of 12° whereas the average collective setting of the installed propellers was 14.4°. As will be shown in a later plot, this blade angle difference accounts for a large percentage of the difference in thrust coefficient noted at zero shaft angle. Additional analysis is required at other shaft angles. Even so, the increase in thrust with shaft angle for the installed propeller is obviously larger than that for the isolated propeller not operating in the influence of a highly flapped wing. Except for shaft angles beyond 40°, the inboard and outboard props exhibited similar thrust/shaft angle characteristics.

Figure 151 shows the same trends as Figure 150 for the 4750 RPM data acquired during wing sweep Runs 158 thru 161. In Figure 151, the lower thrust coefficient for the outboard prop is partially accounted for by its lower blade angle (13.5°) with respect to the inboard prop (14.0°).

The effect of wing/60° flaps on thrust at zero shaft angle is presented in Figure 152. Data from Figures 150 and 151 was averaged for this presentation. When the different collective settings are taken into consideration, it is found that the lifting system increases the propeller thrust up to an increment in C_T of .015 over the advance ratio range evaluated. The thrust coefficient generated at 4750 RPM (cyclic hubs) should be slightly lower than that generated at 6800 RPM (collective hubs) due to the lower net blade area, i.e., in installing the blades in the cyclic hubs, the "deeper" blade retention system necessitated moving the blades outward and trimming the tips (less than .125") to maintain the same prop diameters.

The companion power data at zero shaft angle is shown in Figure 153. Differences in power between the inboard and outboard props were such that the division of the power plot into separate presentations for the inboard prop and outboard prop was not warranted.

Figure 154 presents the calculated propeller efficiency (η_p) corresponding to the thrust and power data shown in Figures 152 and 153. The conclusion that can be arrived at from examining this figure, is that the wing/flaps/slats did not have an adverse influence on the propeller efficiency.

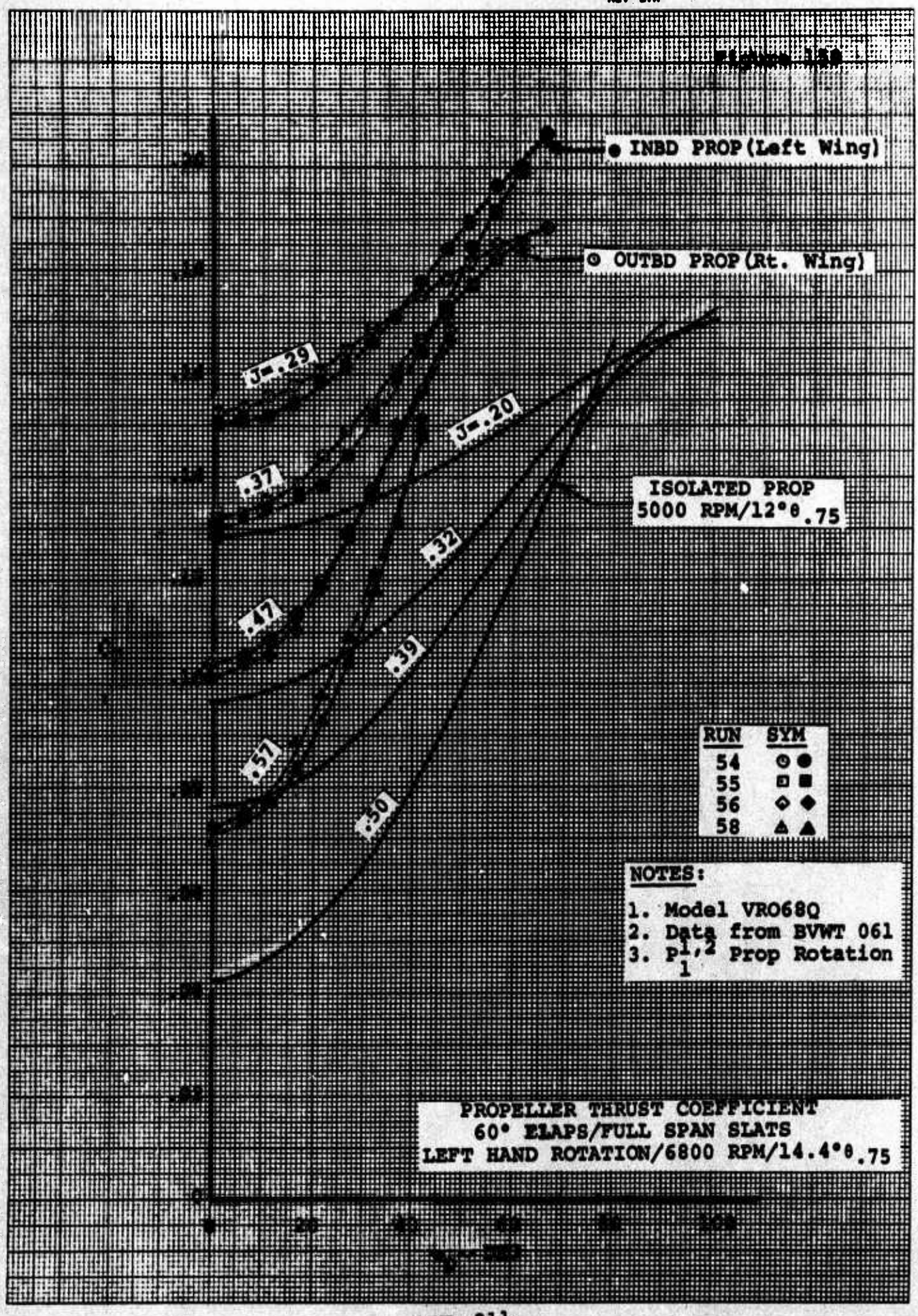

EUGENE DIETZGEN CO.
MADE IN U. S. A.
NO. 340R-MP DIETZGEN GRAPH PAPER
MILLIMETER

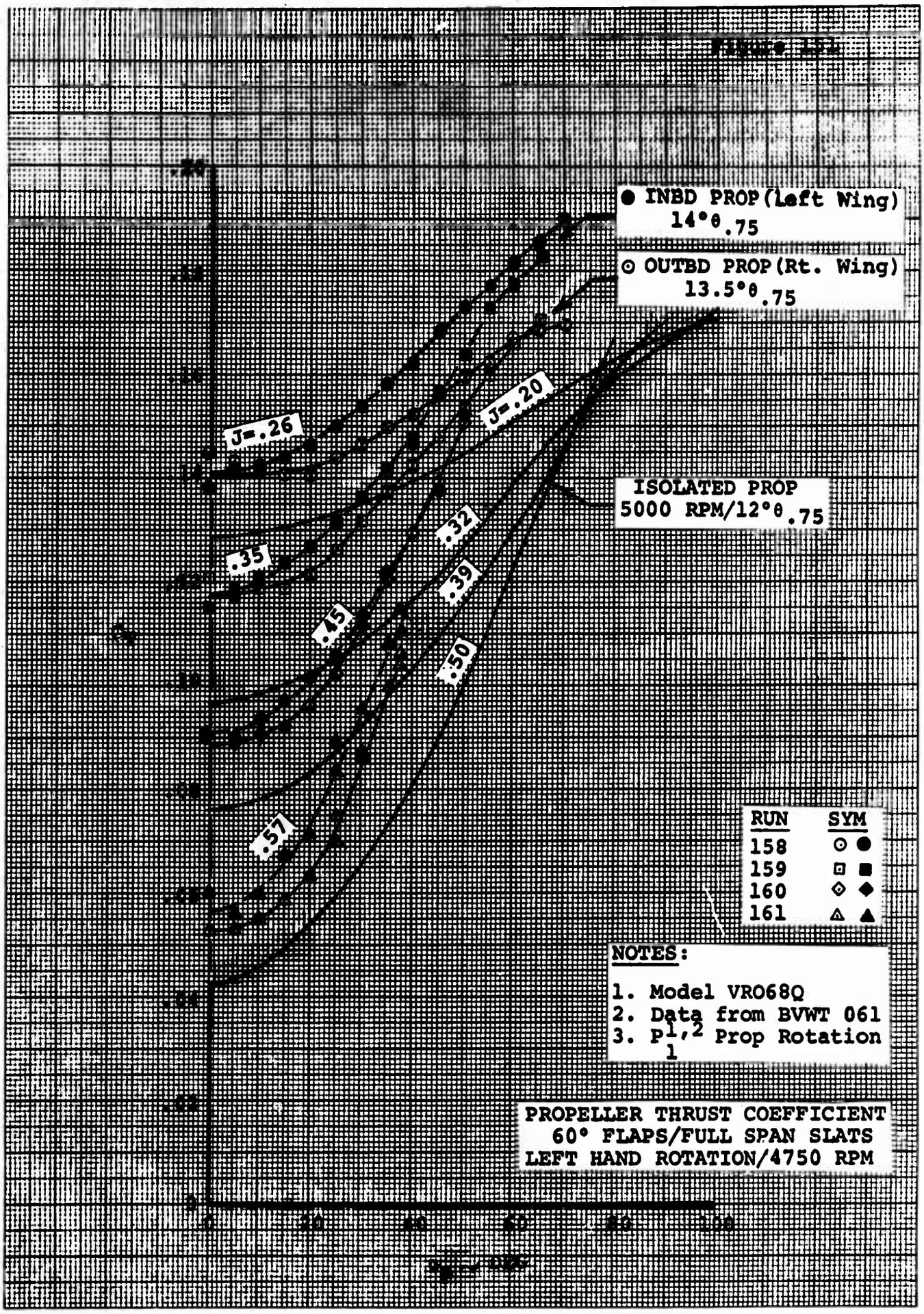

EUGENE DIETZGEN CO.
MADE IN U. S. A.
NO. 340R-MP DIETZGEN GRAPH PAPER
MILLIMETER

Figure 152

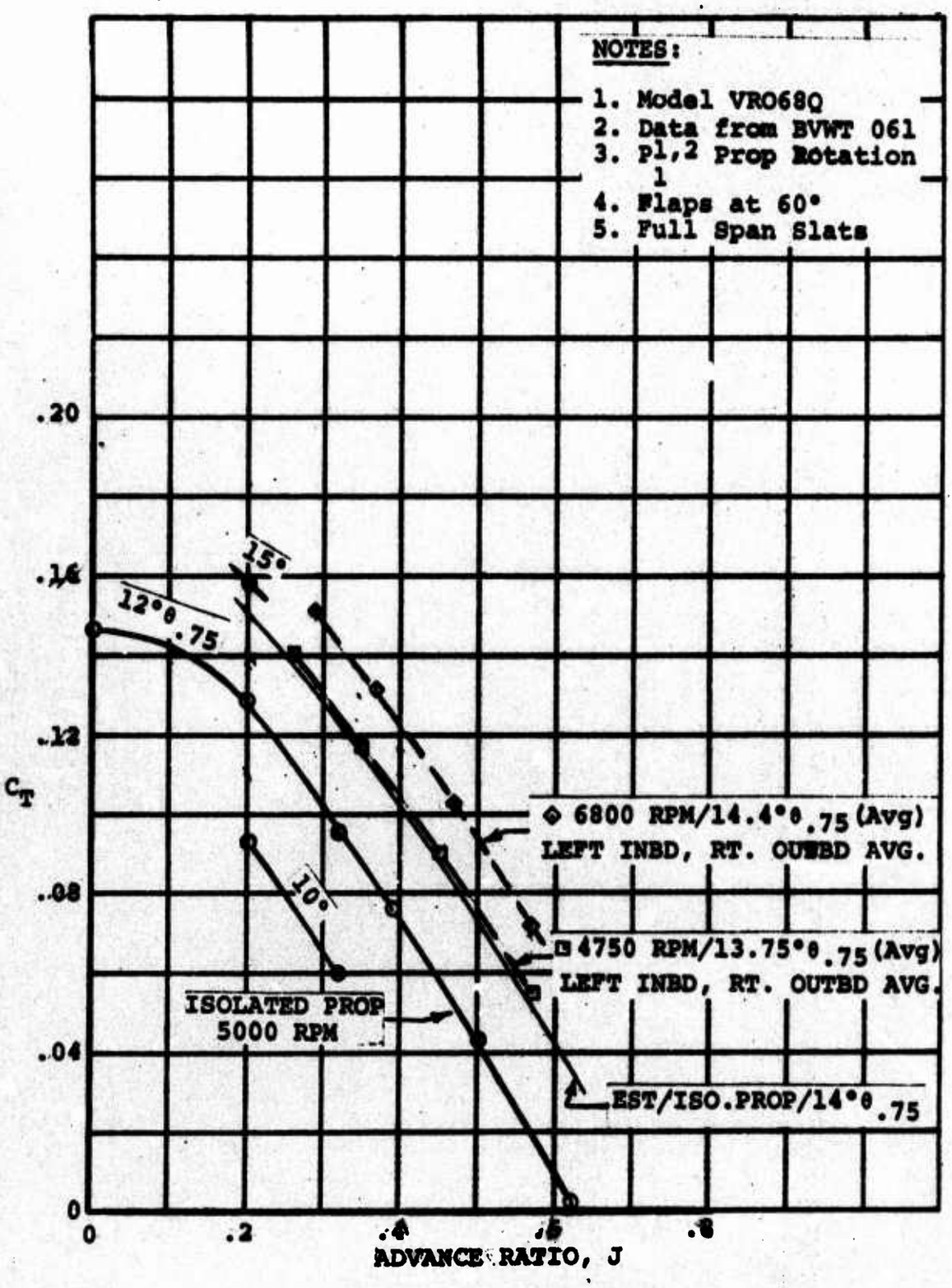

EFFECT OF WING/FLAPS ON THRUST
LEFT HAND PROPS/ZERO SHAFT ANGLE

Figure 153

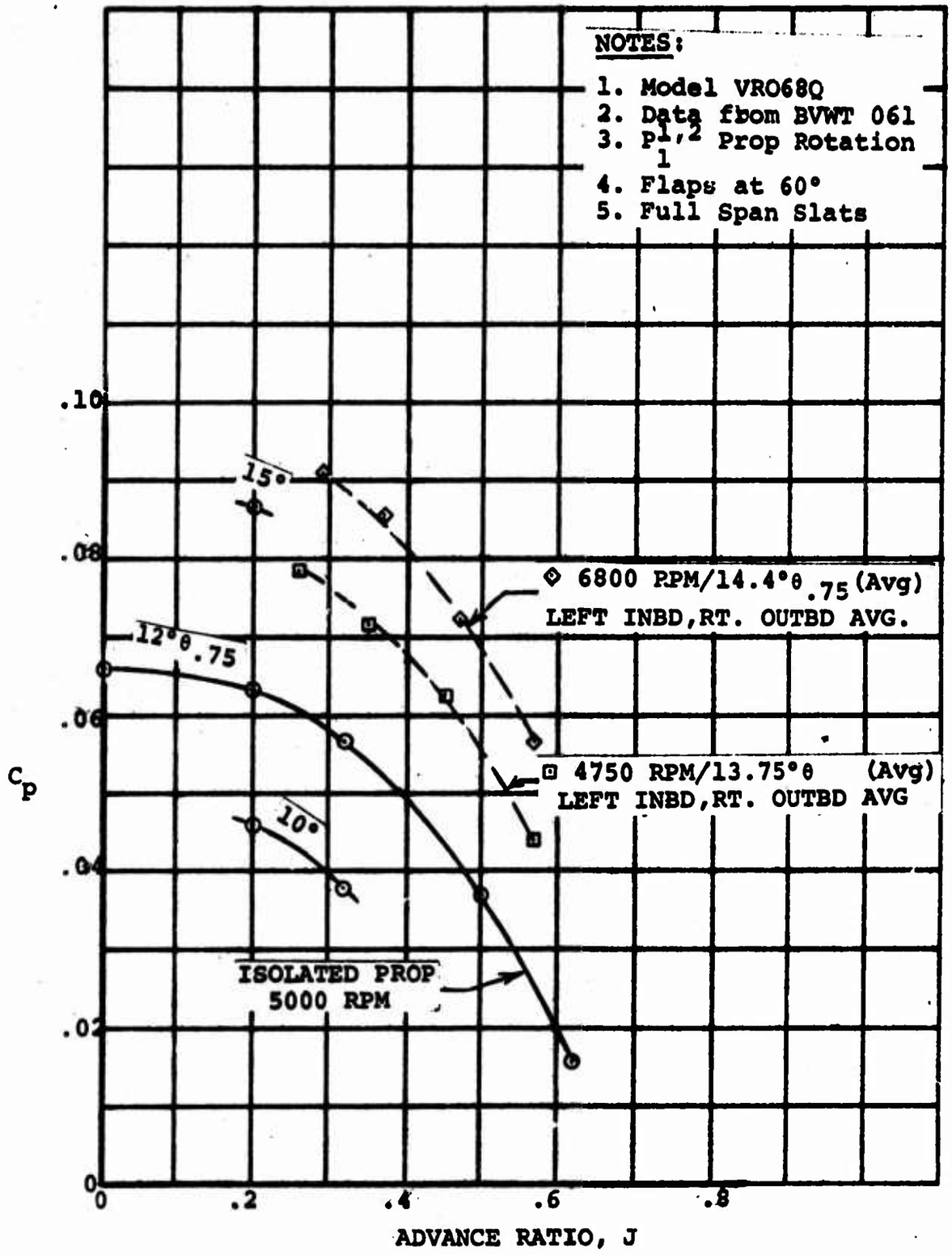

EFFECT OF WING/FLAPS ON POWER
LEFT HAND PROPS/ZERO SHAFT ANGLE

Figure 154

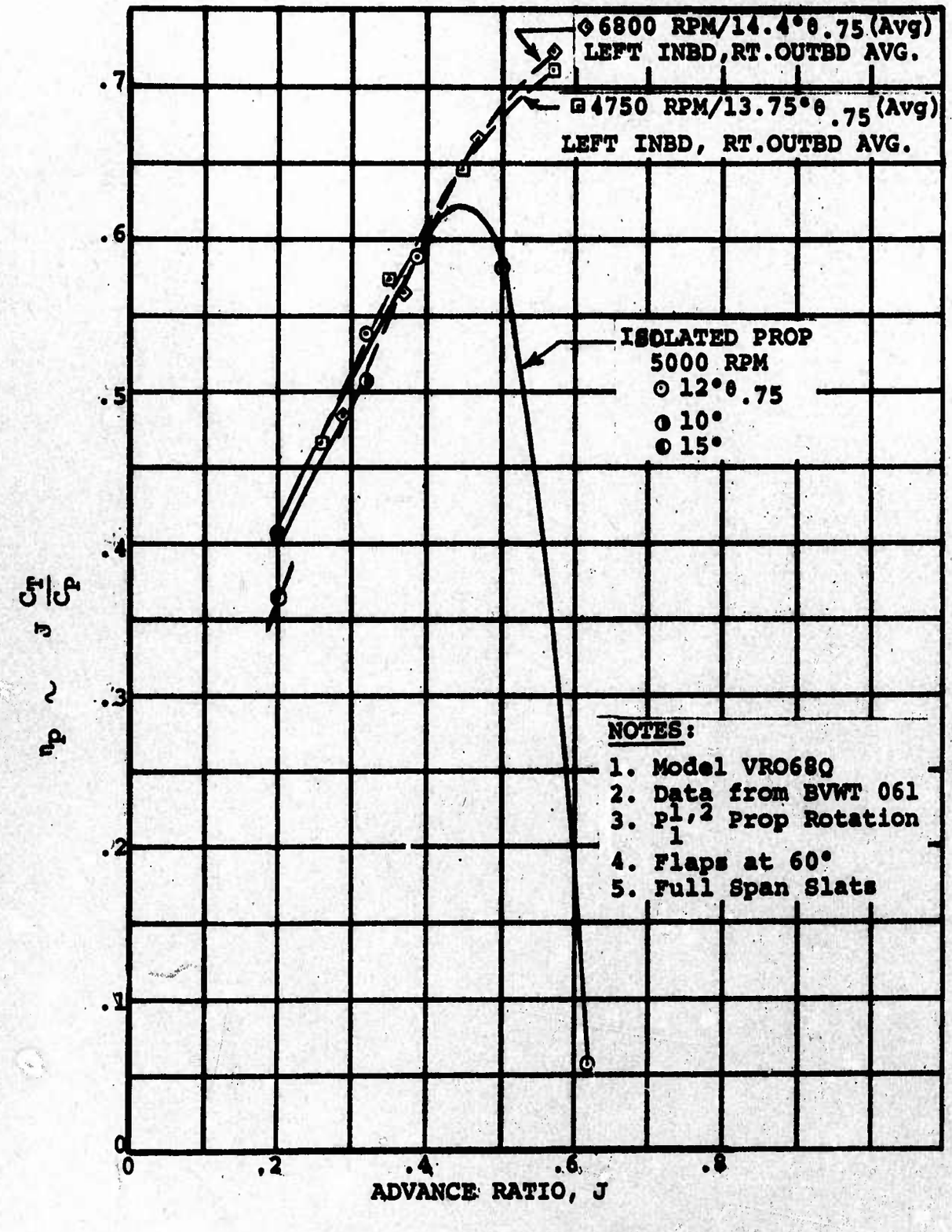

EFFECT ON WING/FLAPS ON PROPELLER EFFICIENCY
LEFT HAND PROPS/ZERO SHAFT ANGLE

6.6 EFFECT OF DISC LOADING (RPM) ON MODEL FORCES

Since the propeller RPM used during test BVWT 061 varied from 6800 to 4750 RPM, a check was made of the proportionality of the model forces with disc loading. Run 101 (with check points in Run 102) was performed statically (zero tunnel q) with a model configuration consisting of flaps deflected to 40°, full span slats extended, wing down, and zero fuselage angle. The induced flow in the test section probably did not exceed 0.4q.

The results presented in Figure 155 depict a linear variation of model normal force, axial force, and pitching moment with RPM^2. Figure 156 illustrates a similar type curve for normal force when it is plotted as a function of disc loading.

For Run 102 (same model configuration) the model was pitched up to an average fuselage angle of attack of 20.4°, and an RPM sweep was made at a constant Advance Ratio (J) of 0.61 by adjusting the tunnel q. Figure 157 shows the degree of linearity of model normal force, axial force, and pitching moment with RPM^2. Both normal force and axial force are essentially linear from zero RPM to the maximum RPM evaluated. The low nose down pitching moments measured at the smaller RPM's (4000 RPM and less) probably reflects some localized flow separation on the flaps due to the low Reynolds number. Figures 158 and 159 show the linearity of model normal force with disc loading and tunnel q, respectively.

Figure 155

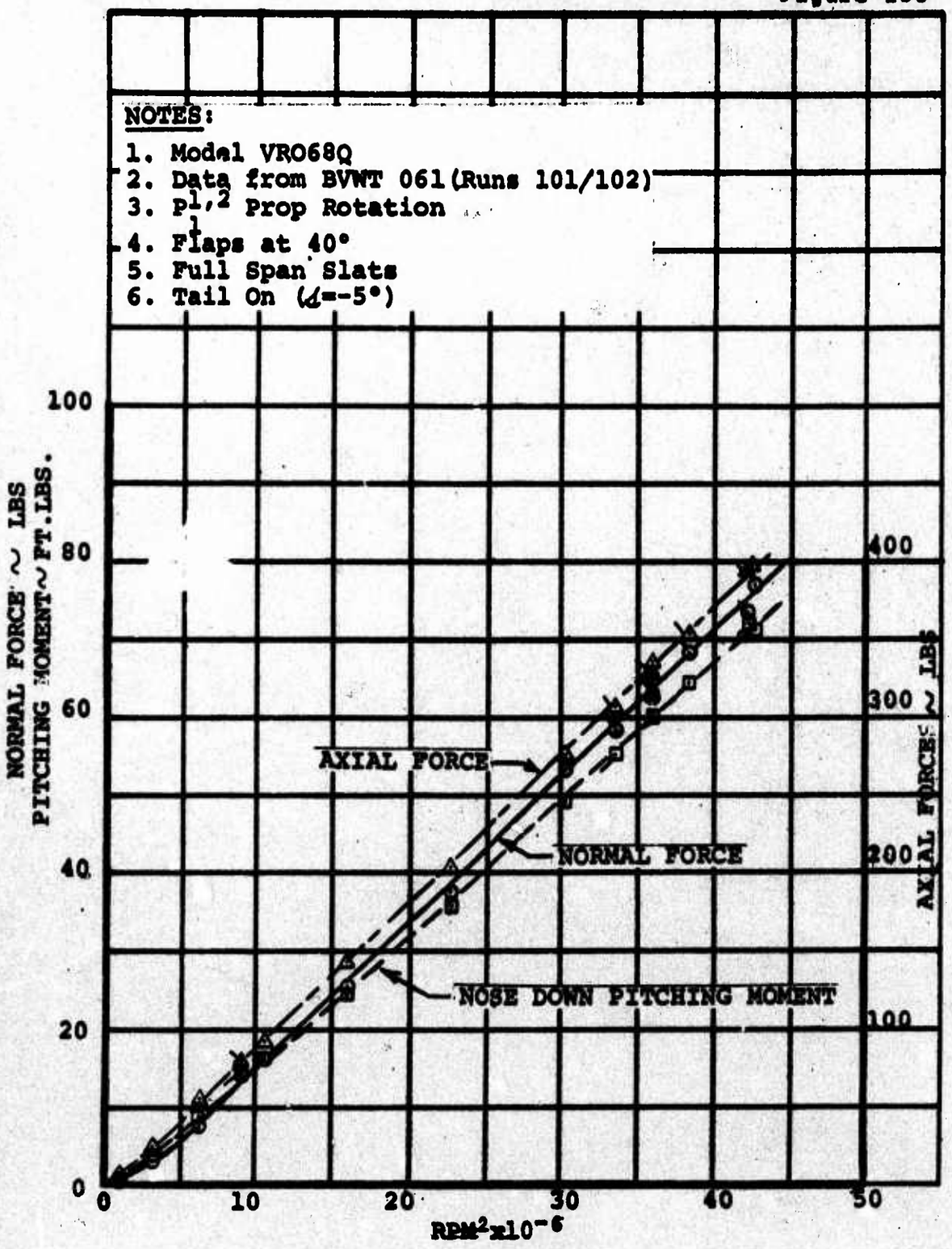

VARIATION OF MODEL FORCES
WITH RPM^2/ZERO q

Figure 156

VARIATION OF MODEL NORMAL FORCE
WITH DISC LOADING/ZERO q
NOTES:
1. Model VRO68Q
2. Data from BVWT 061 (Runs 101/102)
3. P1,2 Prop Rotation
4. Flaps at 40°
5. Full Span Slats
6. Tail On (i=-5°)
NORMAL FORCE ~ LBS
DISC LOADING T/A ~ PSF
0
20
40
60
80
0
4
8
12
16
20
24
28

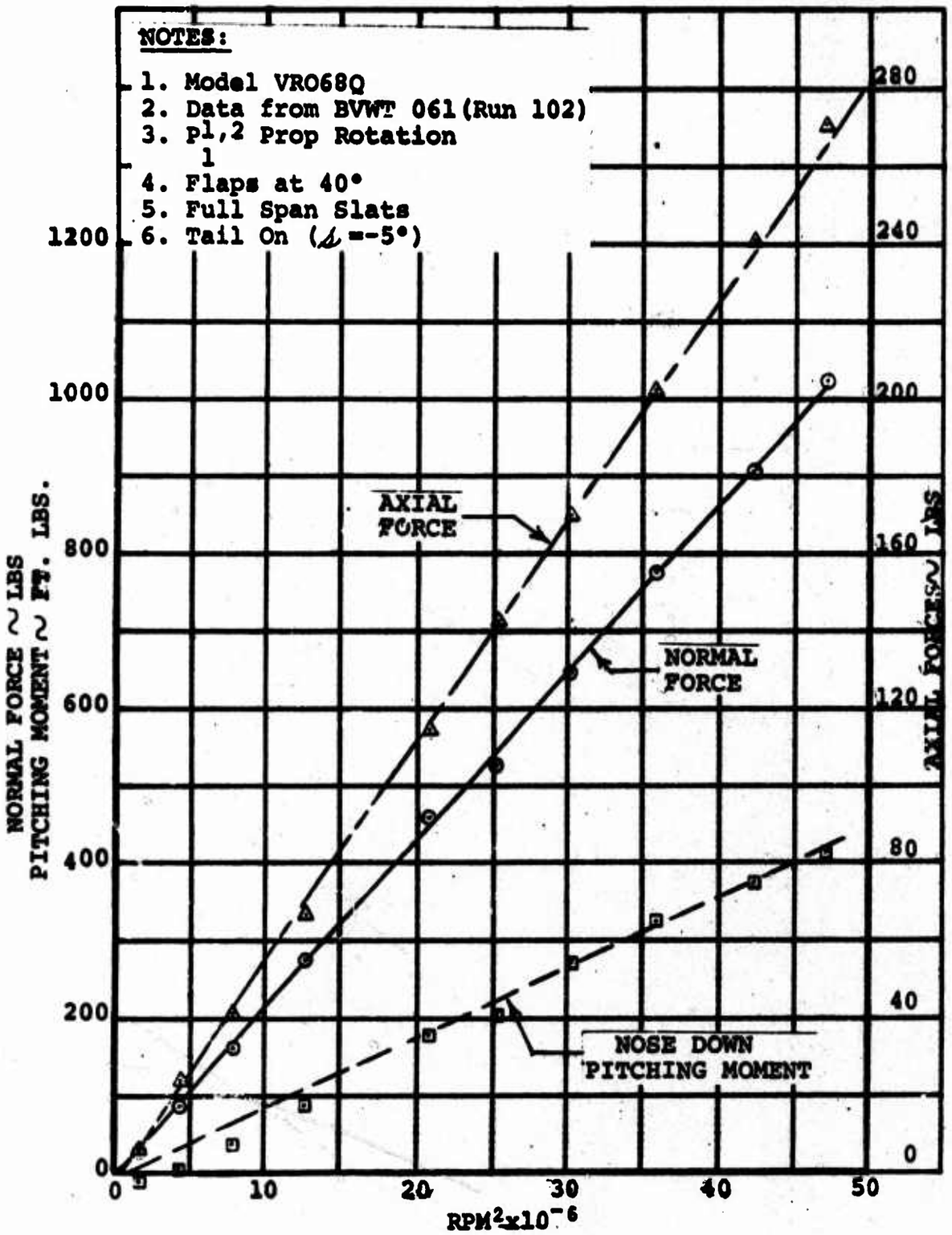

VARIATION OF MODEL FORCES
WITH RPM²
20.4°ϕ_F 0.61J

Figure 158

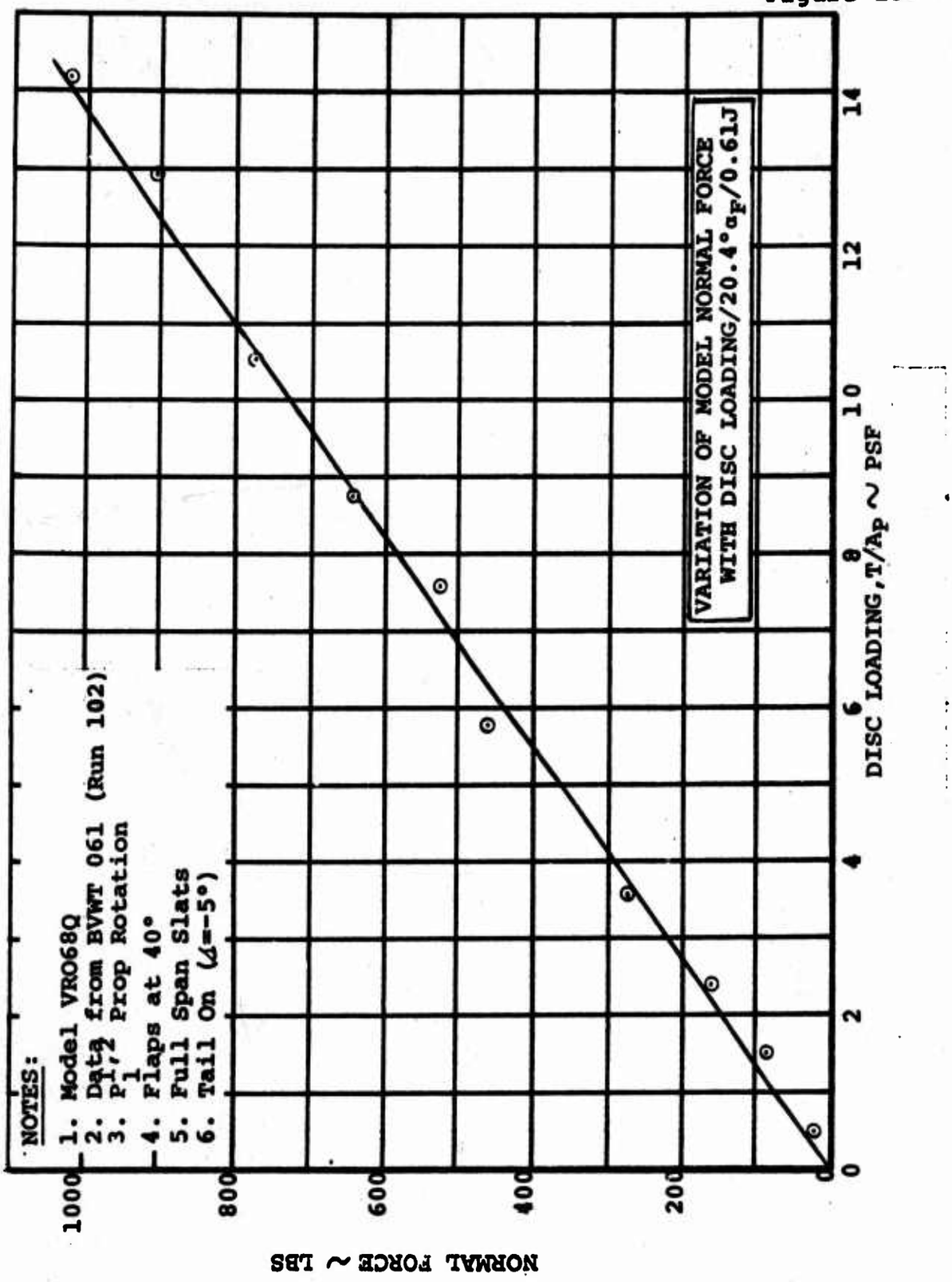
VARIATION OF MODEL NORMAL FORCE
WITH DISC LOADING/20.4°α_F/0.61J
NOTES:
1. Model VRO68Q
2. Data from BVWT 061 (Run 102)
3. P1, 2 Prop Rotation
4. Flaps at 40°
5. Full Span Slats
6. Tail On (i=-5°)
NORMAL FORCE ~ LBS
DISC LOADING, T/Ap ~ PSF
0
200
400
600
800
1000
2
4
6
8
10
12
14

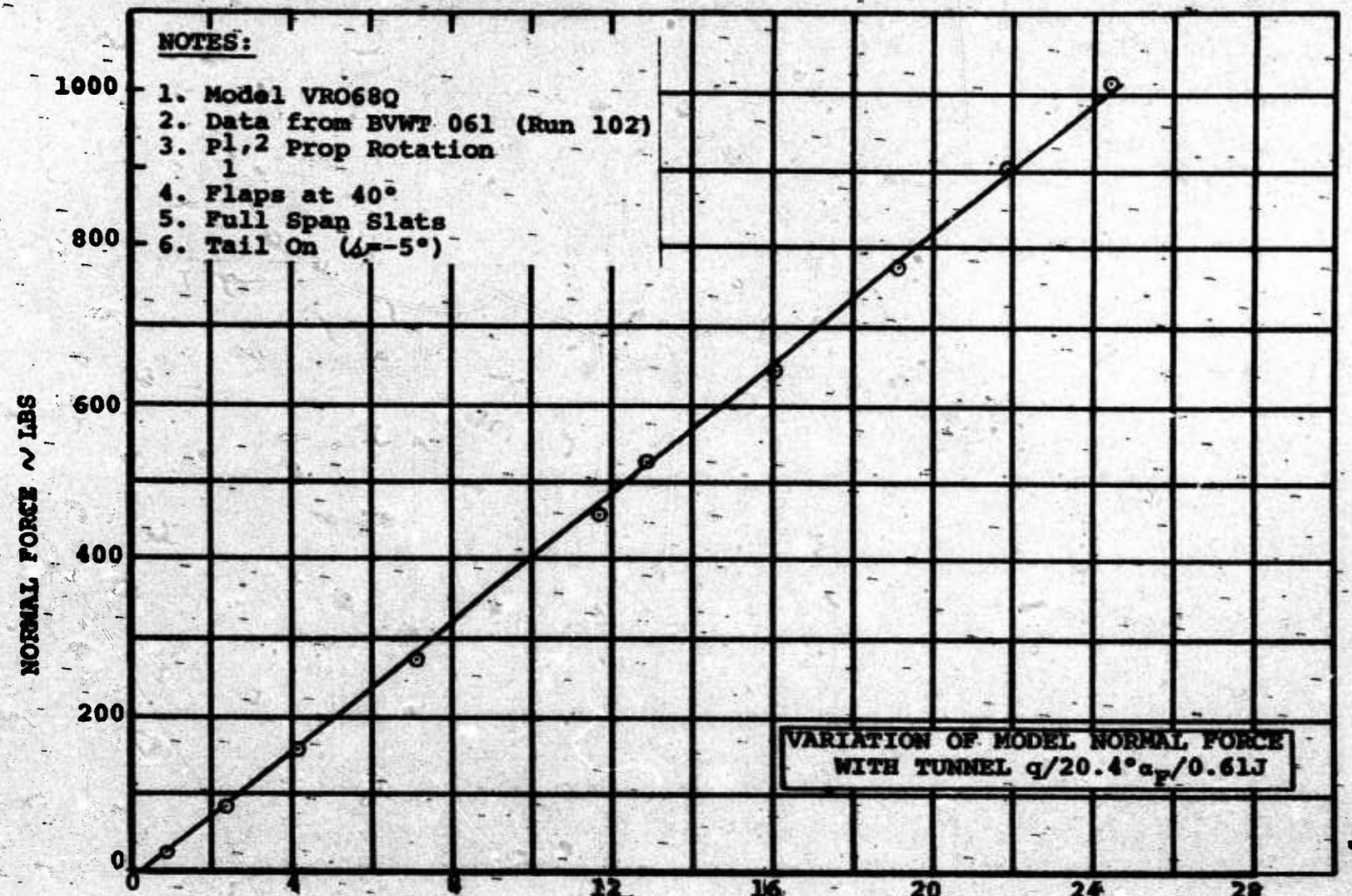

D170-10038-1

Figure 159

7.0 CONCLUSIONS

The primary conclusions derived from this test are listed below:

a. Aircraft pitching moment due to cyclic pitch in the hover mode varies linearly with cyclic angle over the range of cyclic pitch angles evaluated (-8° to +8°) and is essentially invariant with ground height. This aircraft pitching moment was 27% greater than that contributed by the measured hub moments, the difference probably being due to the contribution of propeller normal force.

b. The average value of hub pitching moment coefficient per degree of cyclic pitch obtained in the hover evaluation, agreed well with the corresponding value measured during the isolated propeller test (Reference 1), that is $-.0021\ \Delta C_{M_p}/\Delta\gamma$.

c. The propeller normal force generated by cyclic pitch action in hover was not present in the measured aircraft longitudinal force.

d. The power increase in hover (after subtracting model friction power) due to the application of 8° of cyclic pitch averaged 14.5%. This was the same value measured during the isolated propeller test.

e. The required value of non-dimensional hover yawing moment (.29Y.M./ℓT) for a representative transport-type tilt wing aircraft, to match a requirement for yaw angular acceleration in hover of 0.5 radian/sec^2 was essentially achieved out-of-ground effect with a yaw control configuration consisting of 60° downward deflection of double slotted flaps on one wing and 40° upward flap deflection on the opposite wing. Combined flap/spoiler controls will be evaluated in Phase II.

f. The available hover yaw control with differential flaps decreases to 55% of the out-of-ground effect value when the ground height is reduced to an I.G.E. (in ground effect) condition of hovering with the wheels 2 ft. from the ground.

g. The hover download associated with the noted differential flap deflections was 11.7% of the total thrust.

h. With 60° of double slotted flap deflection and full span slats extended, the data indicated the availability of a low speed descent angle of 17° (corresponds to a descent rate of 1350 fpm at a flight speed of 45 kts).

i. Use of positive cyclic pitch (nose down pitching moments) has been found to have a detrimental effect on the low speed rate of descent capability. A loss in descent rate

of 50 fpm per degree of cyclic pitch was measured in this test. This compares to a value of 100 fpm/deg measured in previous tests such as Reference 3.

j. The noted descent capability was achieved with a high lift system which provided a maximum lift coefficient of 3.87 with 60° of flap deflection, full span slats extended and a zero thrust or zero C_{T_s} condition.

k. The effectiveness of the high horizontal tail for trim ($\Delta C_{M_s}/\Delta i_t$) was found to vary linearly with C_{T_s} and the maximum measured value of $\Delta C_{M_s}/\Delta i_t$ (zero C_{T_s}) was 87% of that predicted by DATCOM. Thus it can be concluded that the high tail was acted upon, primarily, by free-stream q.

l. For the wing tilt/flap angle combinations evaluated throughout the transition regime, the downwash gradient ($d\epsilon/d\alpha_F$) varied from a value of .3 at zero C_{T_s} to a value above 0.5 at .8 C_{T_s}.

m. The initial 15° of wing tilt plus 60° of flap deflection had a substantial destabilizing effect, resulting in the aircraft being unstable (tail on/mid c.g.) at C_{T_s} values larger than .47. At higher wing tilt angles, up to 70°, the level of instability was essentially constant at a value of +.005 $C_{M_{s_\alpha}}$ over the C_{T_s} range from .7 to .96.

n. Flow separation emanating from the wing center section encountered the horizontal tail when the model was pitched resulting in tail buffeting per tuft observation. The fuselage angle of attack at which buffeting occurred decreased with wing tilt angle and increased with C_{T_s} per Figure 137.

o. Removal of the wing center section slat reduced the fuselage angle of attack at which tail buffet occurred by approximately 4°.

p. The propeller normal force produced in the influence of the wing/60° flaps/fuselage was 2.5 times the value measured during the test of an isolated propeller.

q. The propeller hub pitching moment measured at the same time was approximately 3 times the isolated propeller value.

8.0 REFERENCES

1. D170-10037-1, ISOLATED CYCLIC PITCH PROPELLER: RESULTS OF WIND TUNNEL TEST, The Boeing Company, Vertol Division, Philadelphia, Pa.

2. USAF STABILITY AND CONTROL DATCOM, Section 9.2.1., AFFDL, Wright-Patterson Air Force Base, Ohio.

3. D170-10036-1, FOUR PROP TILT WING WITH LEADING EDGE BLC: RESULTS OF SEMI-SPAN WIND TUNNEL TEST, The Boeing Company, Vertol Division, Philadelphia, Pa.

APPENDIX A - TEST CONDITIONS FOR LONGITUDINAL STABILITY AND CONTROL RUNS

The supplementary information presented in Appendix A complements the basic three-component longitudinal stability/control data included in Section 6.4.4 of this report and consists of the following items:

a. The variation of thrust coefficient (C_{T_S}) with fuselage angle of attack (α_F) for the different wing tilt angle/flap angle/nominal C_{T_S} combinations tested. In this test (BVWT 061), the thrust coefficient (C_{T_S}) varied with fuselage angle as a result of the runs (except for the zero thrust runs) being conducted with a constant propeller speed (RPM).

b. The calculated full scale aircraft velocity (along the flight path) as a function of C_{T_S} for the various wing tilt angle/flap angle combinations tested. Speeds for three steady flight cases are shown: 10° climb angle, level flight, and 10° descent angle.

c. The tunnel q used for the various sets of longitudinal stability/control runs as a function of C_{T_S}. Values are shown for both RPM's utilized: 6800 and 6000 RPM. In addition, the tunnel q's used for the 4750 RPM runs with cyclic hubs are shown.

Figures 160 thru 166 present the C_{T_S} variation with fuselage angle of attack (α_F). Each plot is applicable for runs conducted with a particular wing tilt angle/flap angle combination. Each curve in a particular figure is identified as to the nominal C_{T_S} ascribed to that particular run. During the test, tunnel q was chosen so that the noted nominal C_{T_S} was achieved in approximately the middle of the α_F range to be evaluated. The variation of C_{T_S} with α_F is seen to decrease with increasing values of nominal C_{T_S}, however, at high values of nominal C_{T_S} (above .81), the C_{T_S} is virtually invariant with α_F.

The full scale flight speed increases with decreasing C_{T_S} as shown in Figure 167. These speeds along the flight path were calculated for a representative transport-type four prop tilt wing aircraft with a 73.5 lb/ft^2 wing loading (tunnel test section ambient conditions). This wing loading value would decrease to 66 lb/ft^2 for typical atmospheric design conditions of 3000 ft/90°F. It can be seen from this figure that the transition speed range evaluated during BVWT 061 varied from

21 knots to 113 knots. Note that for C_{T_s} values greater than 0.70 (roughly 52 knots), the speed variation with C_{T_s} is basically the same for the three flight conditions shown; 10° climb angle, level flight and 10° descent angle.

Tunnel q was varied almost linearly with C_{T_s} for the constant propeller speed (RPM) type of testing utilized in BVWT 06&, as can be observed from the data presented in Figure 168. The minimum tunnel q that can be maintained in BVWT with reasonable accuracy is 1.0 lb/ft^2.This value fixes the maximum C_{T_s} that can be set up on Model VRO68Q for a given value of propeller RPM. With 6000 RPM a C_{T_s} of about .97 was achieved.

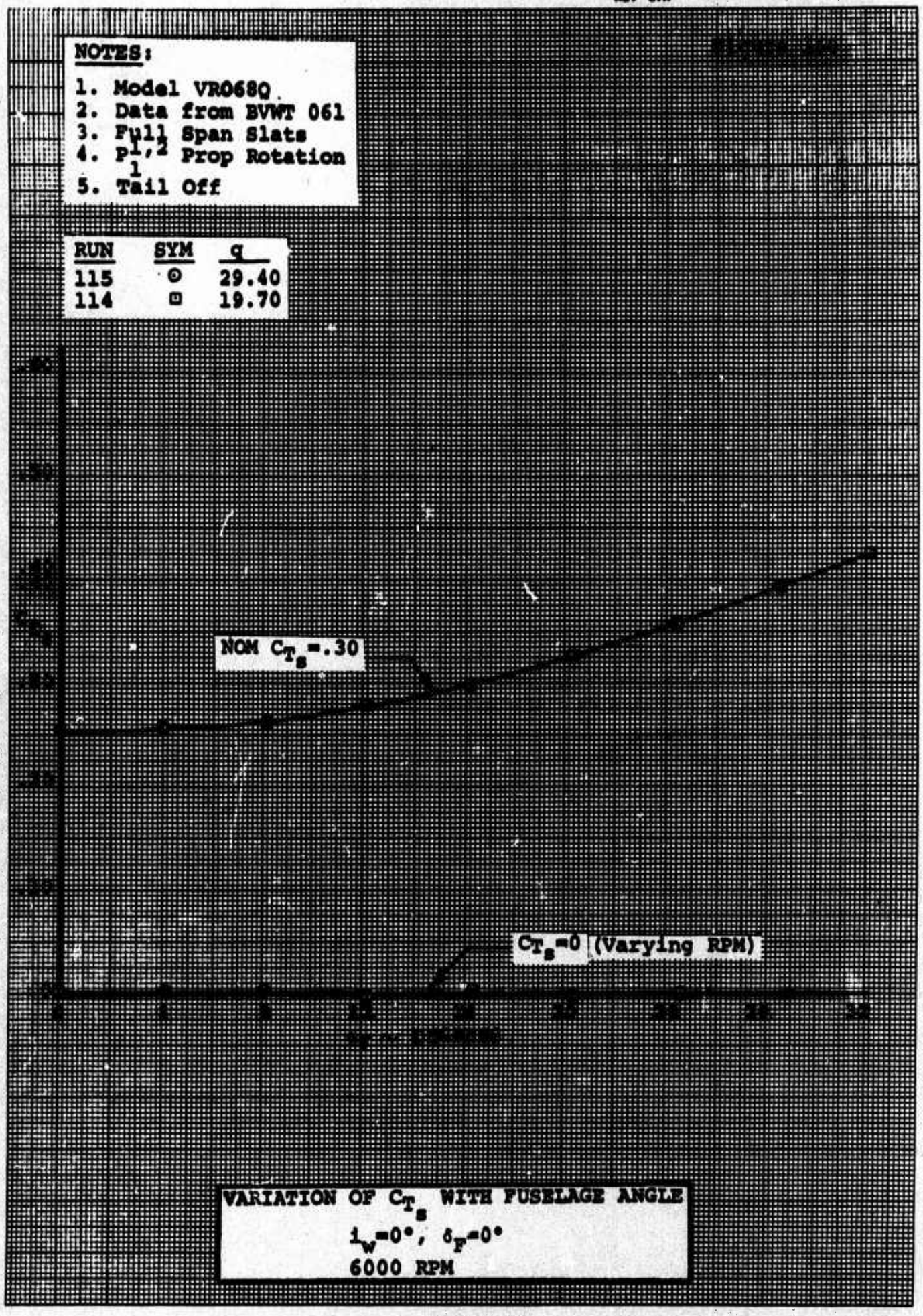

EUGENE DIETZGEN CO.
MADE IN U. S. A.
NO. 340R-MP DIETZGEN GRAPH PAPER
MILLIMETER

NOTES:

1. Model VRO68Q
2. Data from BVWT 061
3. Full Span Slats
4. p1,2 Prop Rotation
5. Tail Off

RUN	SYM	q
112	⊙	29.70
99	□	19.80
98	△	13.73

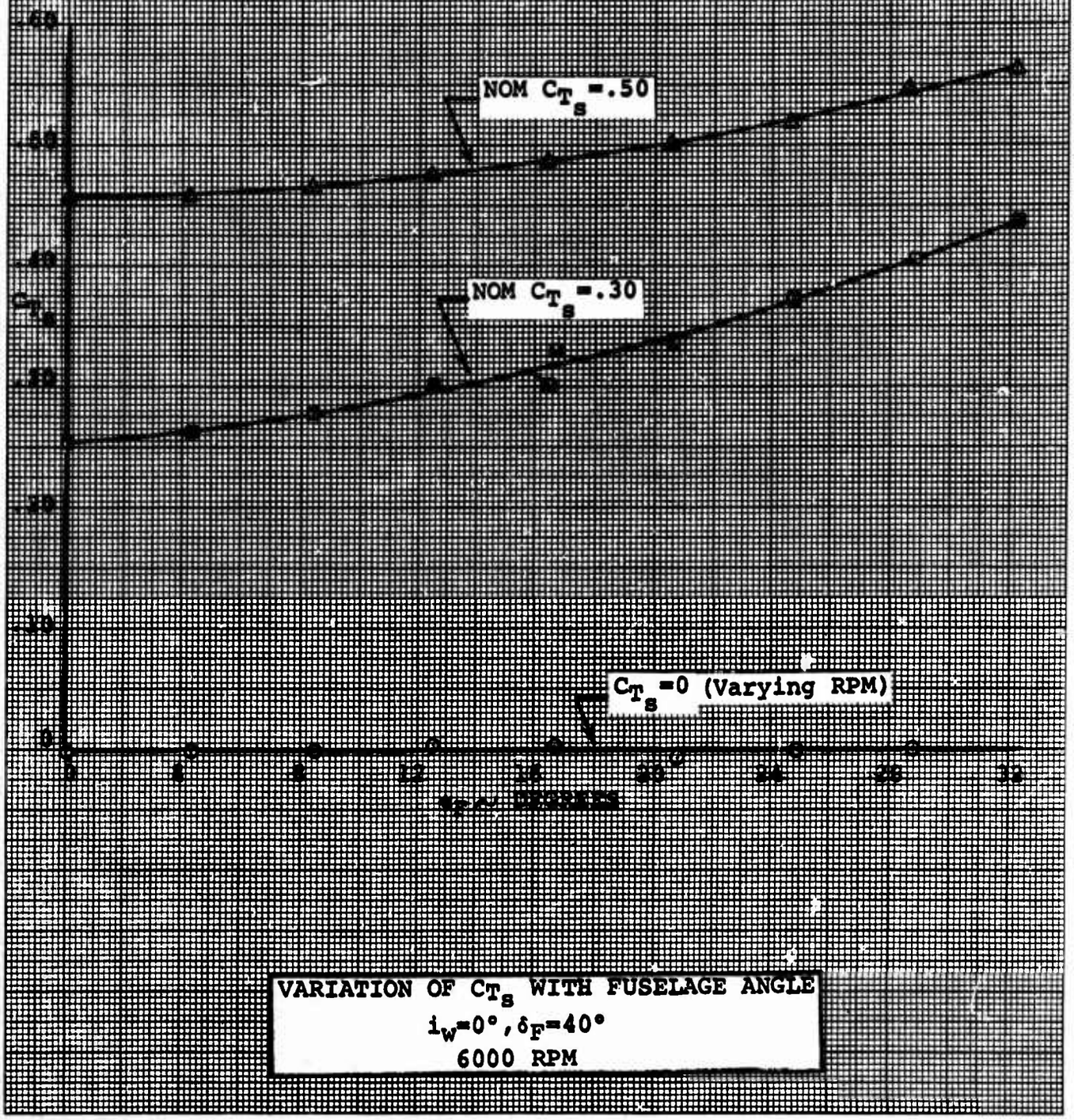

VARIATION OF C_{T_s} WITH FUSELAGE ANGLE
i_W=0°, δ_F=40°
6000 RPM

MADE IN U.S.A.
NO. 340R-MP DIETZGEN GRAPH PAPER MILLIMETER

NOT REPRODUCIBLE

RUN	SYM	q
82	⊡	27.81
81	△	19.30
80	◇	11.02

NOTES:
1. Model VRO68Q
2. Data from BVWT 061
3. Full Span Slats
4. $P_1^{1,2}$ Prop Rotation
5. Tail Off

Figure 362

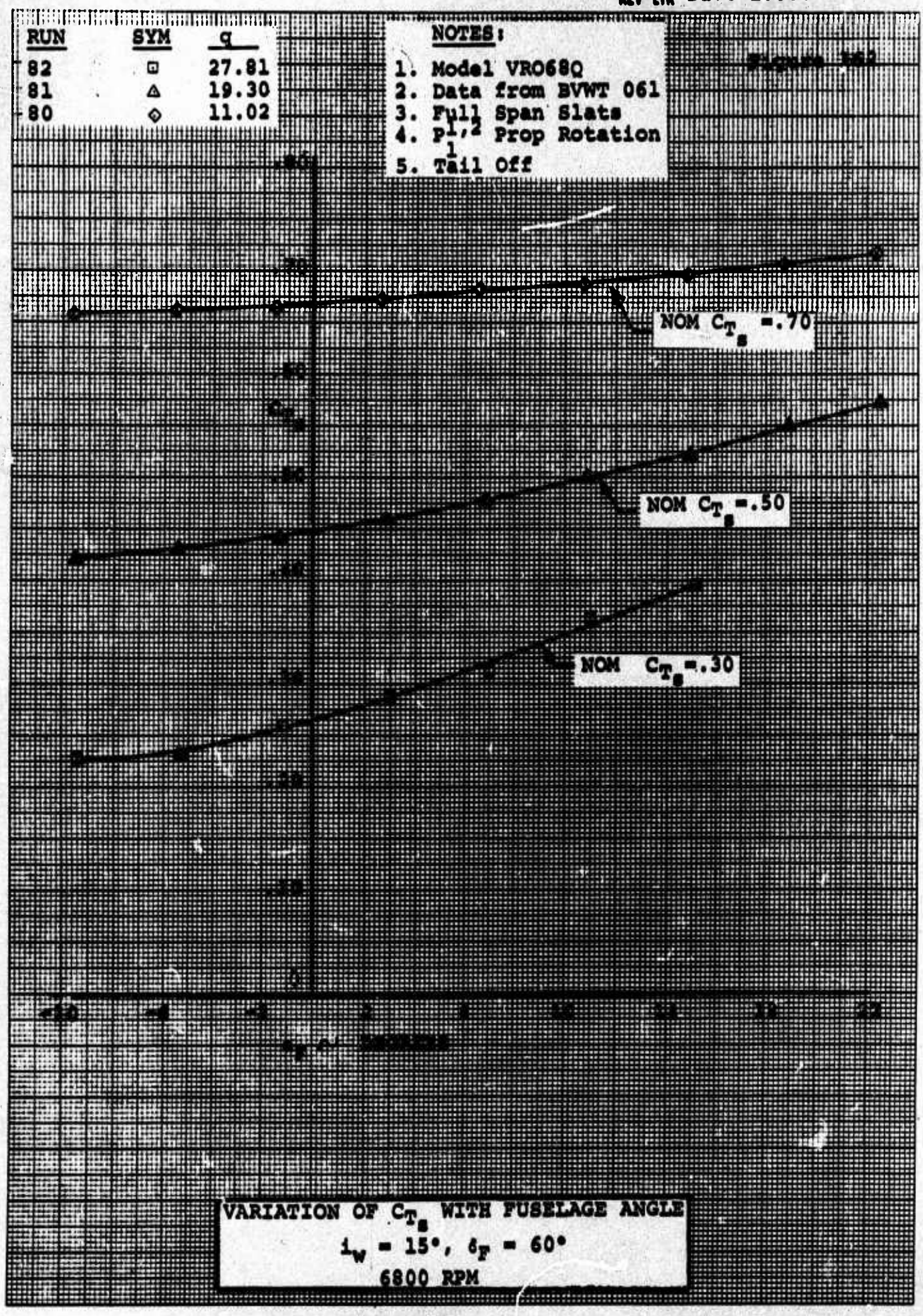

VARIATION OF C_{T_s} WITH FUSELAGE ANGLE
$i_w = 15°$, $\delta_F = 60°$
6800 RPM

EUGENE DIETZGEN CO. MADE IN U. S. A.
NO. 340R-HP DIETZGEN GRAPH PAPER MILLIMETER

NOTES:

1. Model VRO68Q
2. Data from BVWT 061
3. Full Span Slats
4. $P_1^{1,2}$ Prop Rotation
5. Tail Off

RUN	SYM	q
139	⊙	12.35
138	◇	8.08
137	△	5.08

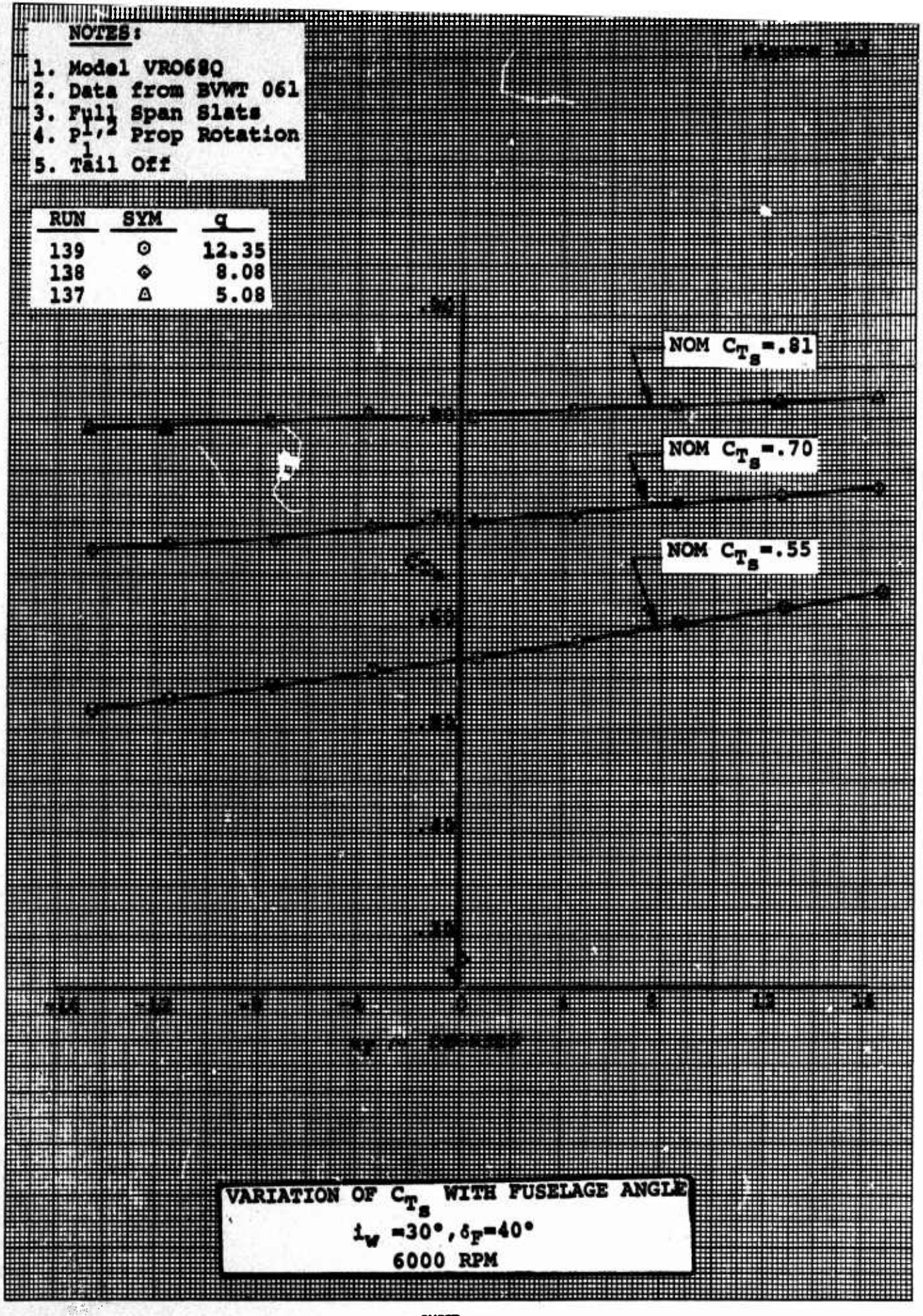

VARIATION OF C_{T_s} WITH FUSELAGE ANGLE
i_w =30°, δ_F=40°
6000 RPM

EUGENE DIETZGEN CO.
MADE IN U. S. A.
NO. 340R-MP DIETZGEN GRAPH PAPER
MILLIMETER

FIGURE 164

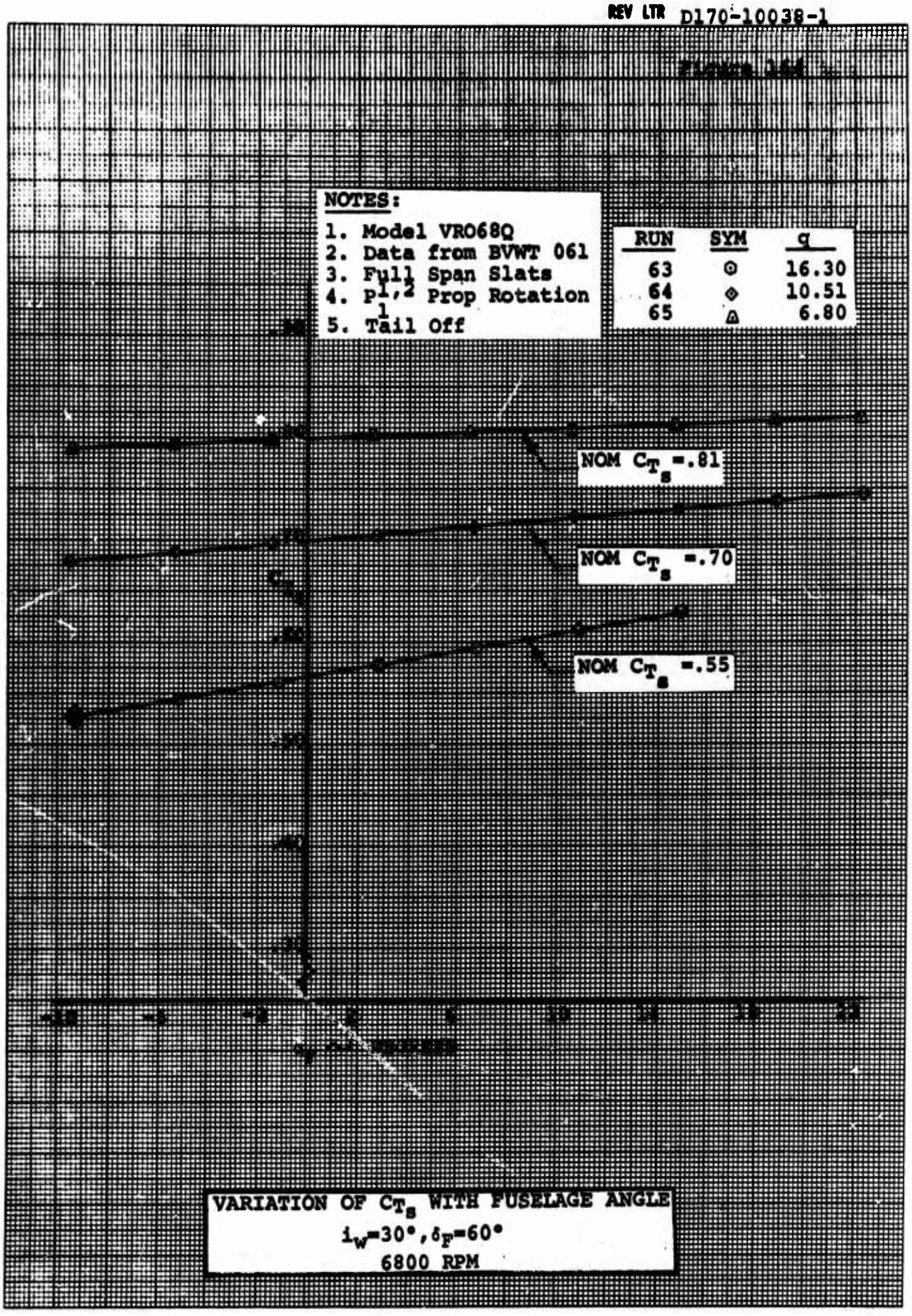

VARIATION OF C_{T_s} WITH FUSELAGE ANGLE
i_w=30°, δ_F=60°
6800 RPM

EUGENE DIETZGEN CO.
MADE IN U. S. A.
NO. 340R-HP DIETZGEN GRAPH PAPER
MILLIMETER

Figure 164

NOTES:
1. Model VR068Q
2. Data from BVWT 061
3. Full Span Slats
4. $P_{1,2}^{1}$ Prop Rotation
5. Tail Off

RUN	SYM	q
123	△	5.20
122	◁	2.20

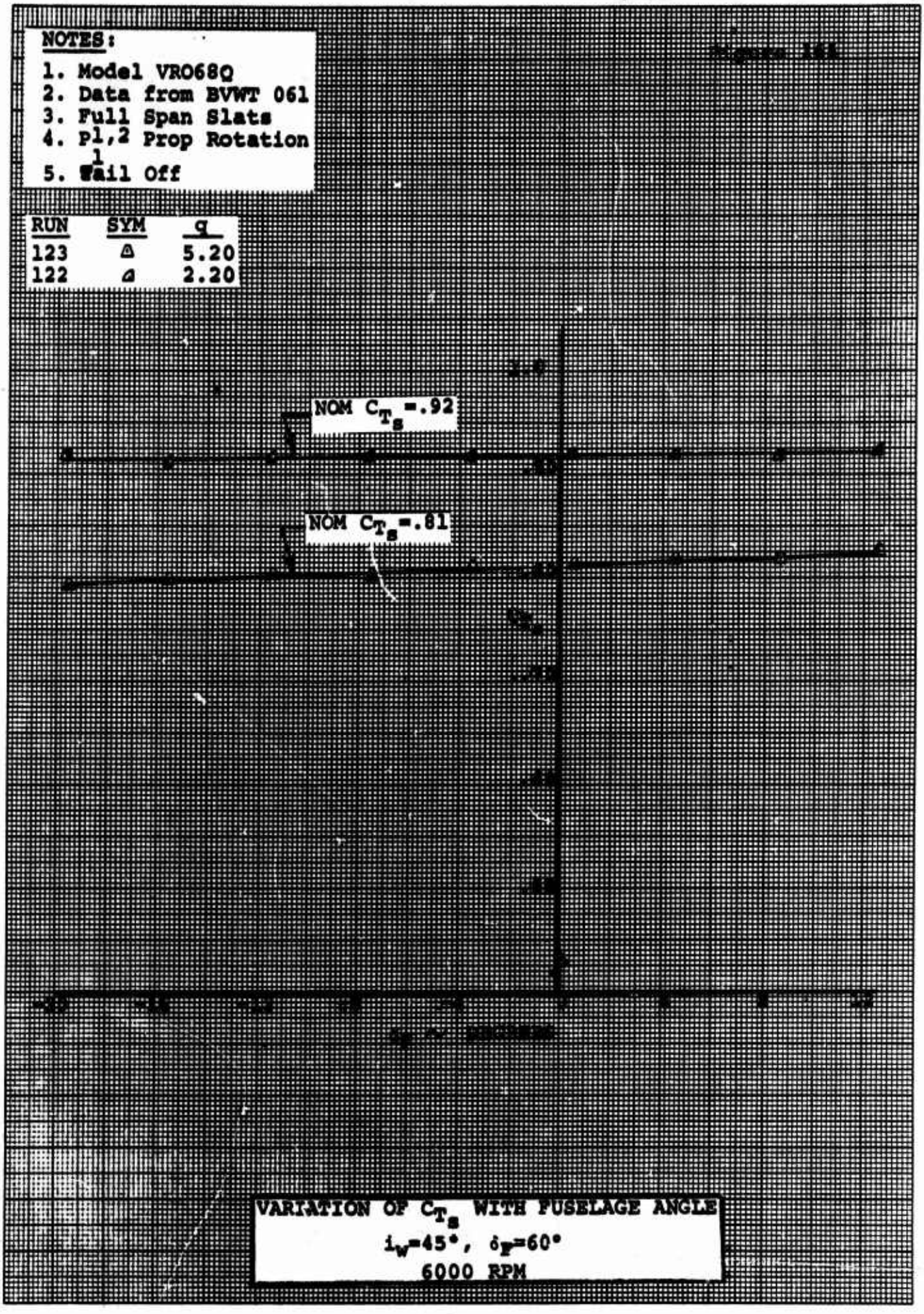

VARIATION OF C_{T_s} WITH FUSELAGE ANGLE
i_w=45°, δ_F=60°
6000 RPM

EUGENE DIETZGEN CO.
MADE IN U. S. A.
NO. 340R-MP DIETZGEN GRAPH PAPER
MILLIMETER

NOTES:
1. Model VR068Q
2. Data from BVWT 061
3. Full Span Slats
4. $P_{1,2}^{1}$ Prop Rotation
5. Tail Off

RUN	SYM	q	i_w	δ_F
132	+	1.57	55°	60°
135	∞	1.57	55°	40°
136	☆	1.0	70°	40°

VARIATION OF C_{T_s} WITH FUSELAGE ANGLE
i_w=55° & 70°, δ_F=40° & 60°
6000 RPM

EUGENE DIETZGEN CO.
MADE IN U. S. A.
NO. 340R-MP DIETZGEN GRAPH PAPER
MILLIMETER

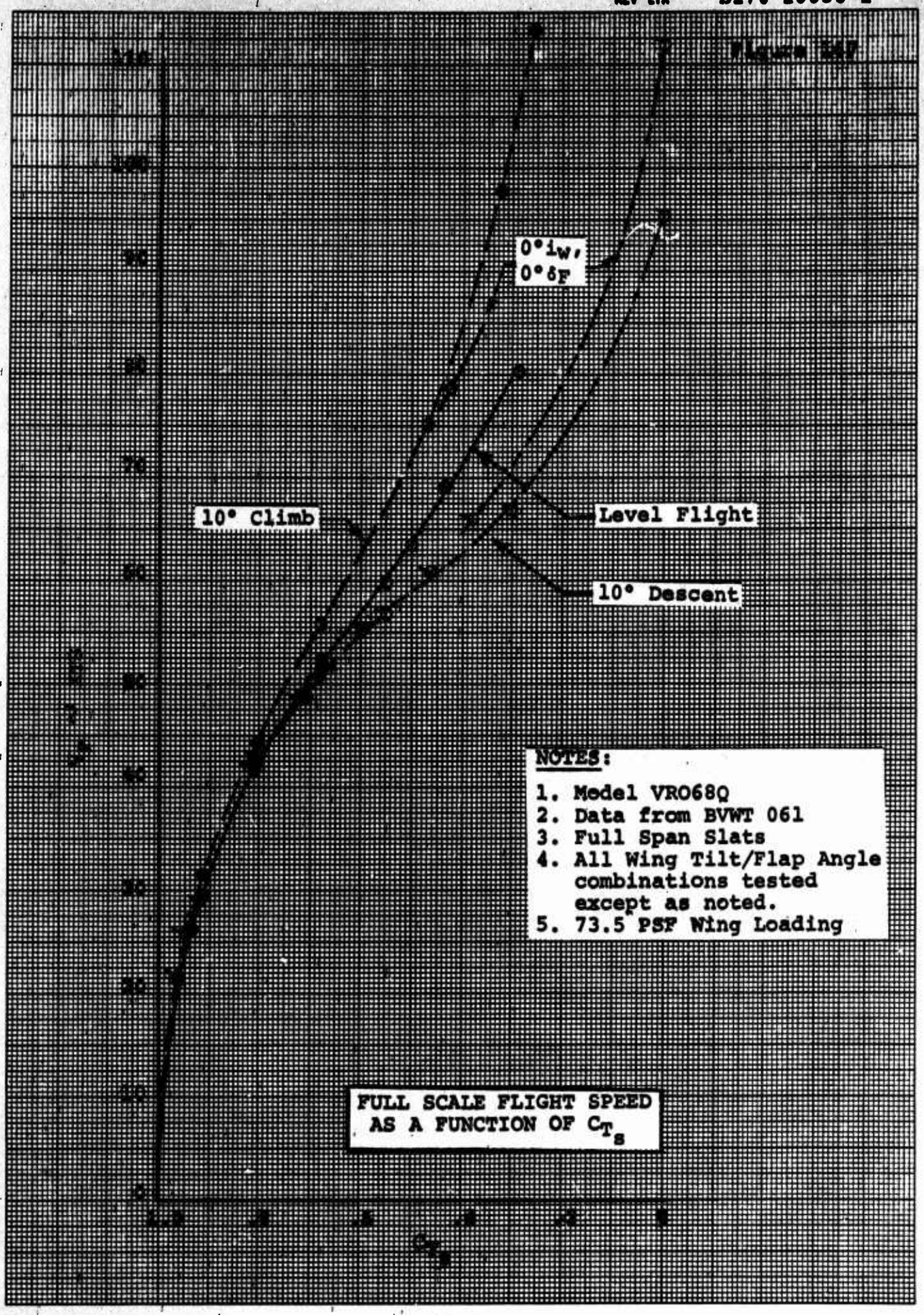

EUGENE DIETZGEN CO.
MADE IN U. S. A.
NO. 340R-MP DIETZGEN GRAPH PAPER
MILLIMETER

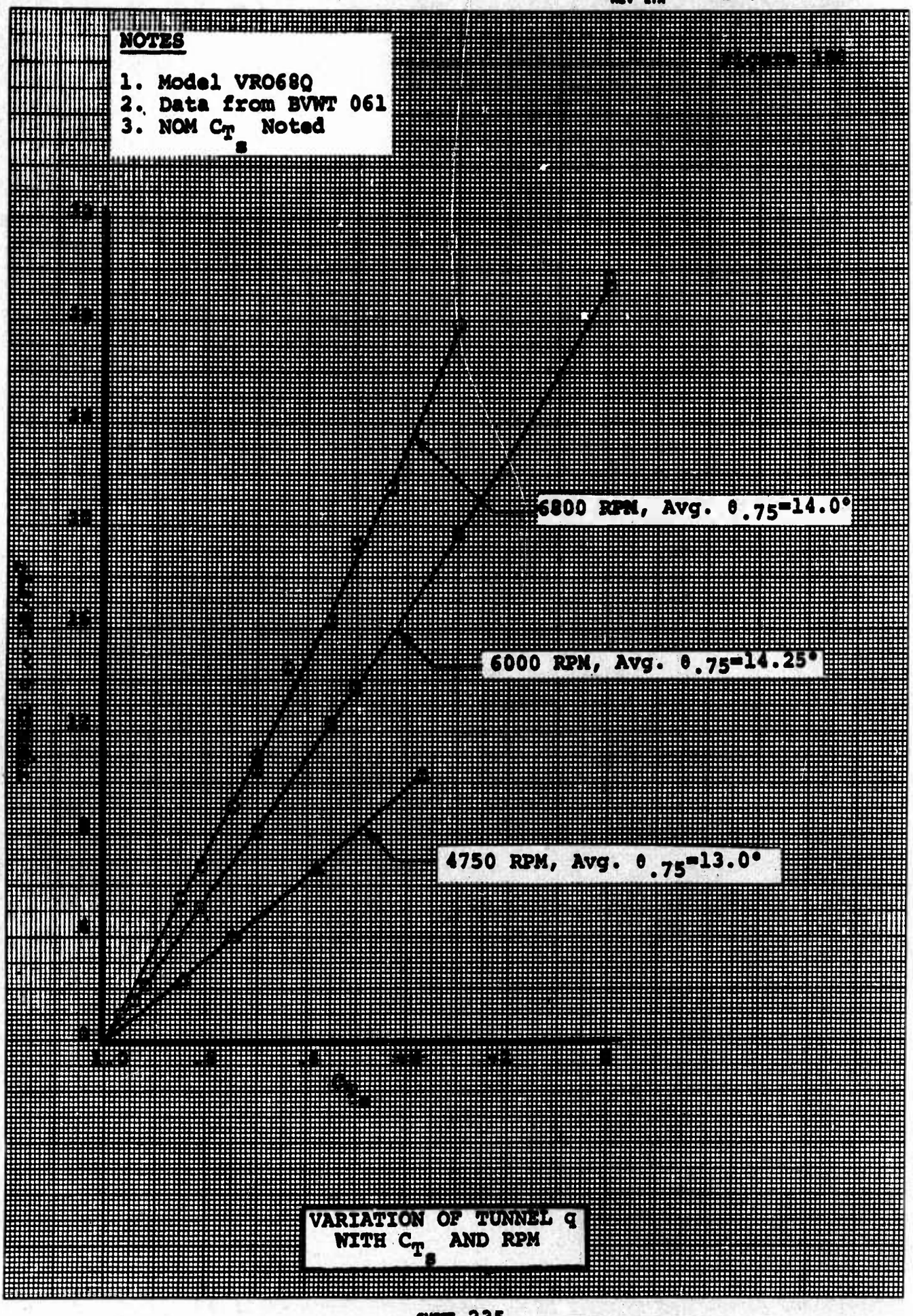

NO. 340R-MP DIETZGEN GRAPH PAPER
MILLIMETER
EUGENE DIETZGEN CO.
MADE IN U. S. A.

APPENDIX B - SHAFT TORQUE DURING JET THRUST CALIBRATION

The air motor jet thrust calibration discussed in Section 5.2 and presented in Figure 20 was conducted with a zero propeller thrust, cylindrical tube prop. In Figure 20, the jet thrust produced by each air motor is shown as a function of shaft torque. Of interest is the variation of shaft torque with RPM during the jet thrust calibration runs. Since the cylindrical tube prop operates in the static condition at basically a constant torque coefficient, the variation of shaft torque should be essentially linear with RPM^2. In addition as a result of utilizing the same tube prop for the various calibration runs, the same shaft torque should have been recorded at a particular RPM on each of the calibration runs. Figure 169 shows that this was the case.

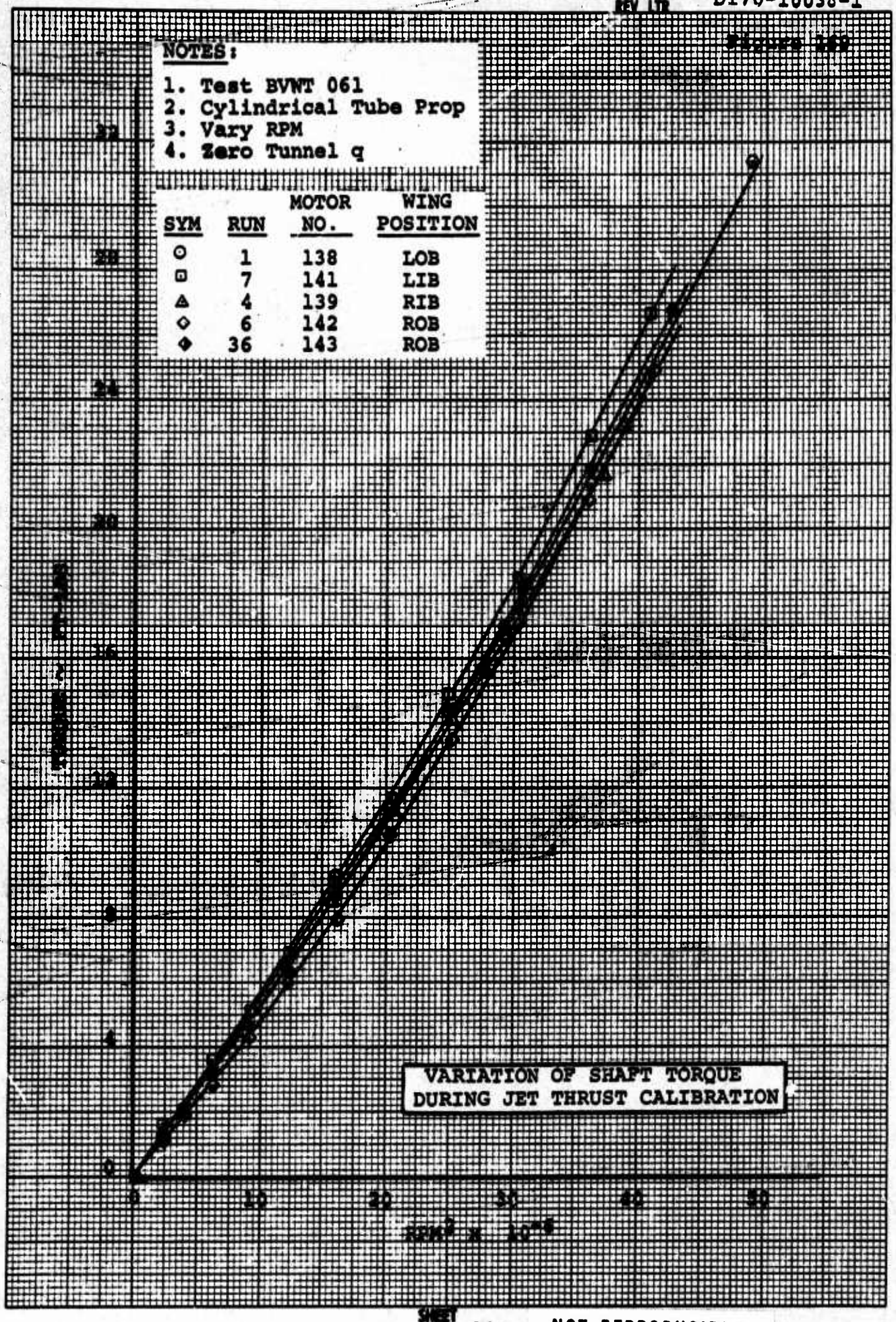

EUGENE DIETZGEN CO.
MADE IN U. S. A.
NO. 340R-20 DIETZGEN GRAPH PAPER
20 X 20 PER INCH

NOT REPRODUCIBLE